TECHNISCHE UNIVERSITÄT MÜNCHEN
FAKULTÄT FÜR MASCHINENWESEN
LEHRSTUHL FÜR MIKROTECHNIK UND MEDIZINGERÄTETECHNIK

Task-Based, Computer-Aided Kinematic Design of Spherically Constrained Kinematic Chains

Kassim Philipp Abdul-Sater

Vollständiger Abdruck der von der Fakultät für Maschinenwesen der Technischen Universität München zur Erlangung des akademischen Grades eines

Doktor-Ingenieurs

genehmigten Dissertation.

Vorsitzender:	Univ.-Prof. dr. ir. Daniel Rixen
Prüfer der Dissertation:	1. Univ.-Prof. Dr. rer. nat. Tim C. Lüth 2. Univ.-Prof. Dr.-Ing. Dr. h.c. Burkhard Corves, RWTH Aachen 3. apl. Prof. Dr. Johann Hartl

Die Dissertation wurde am 01.07.2015 bei der Technischen Universität München eingereicht und durch die Fakultät für Maschinenwesen am 25.01.2016 angenommen.

Für Lukas und Juliane

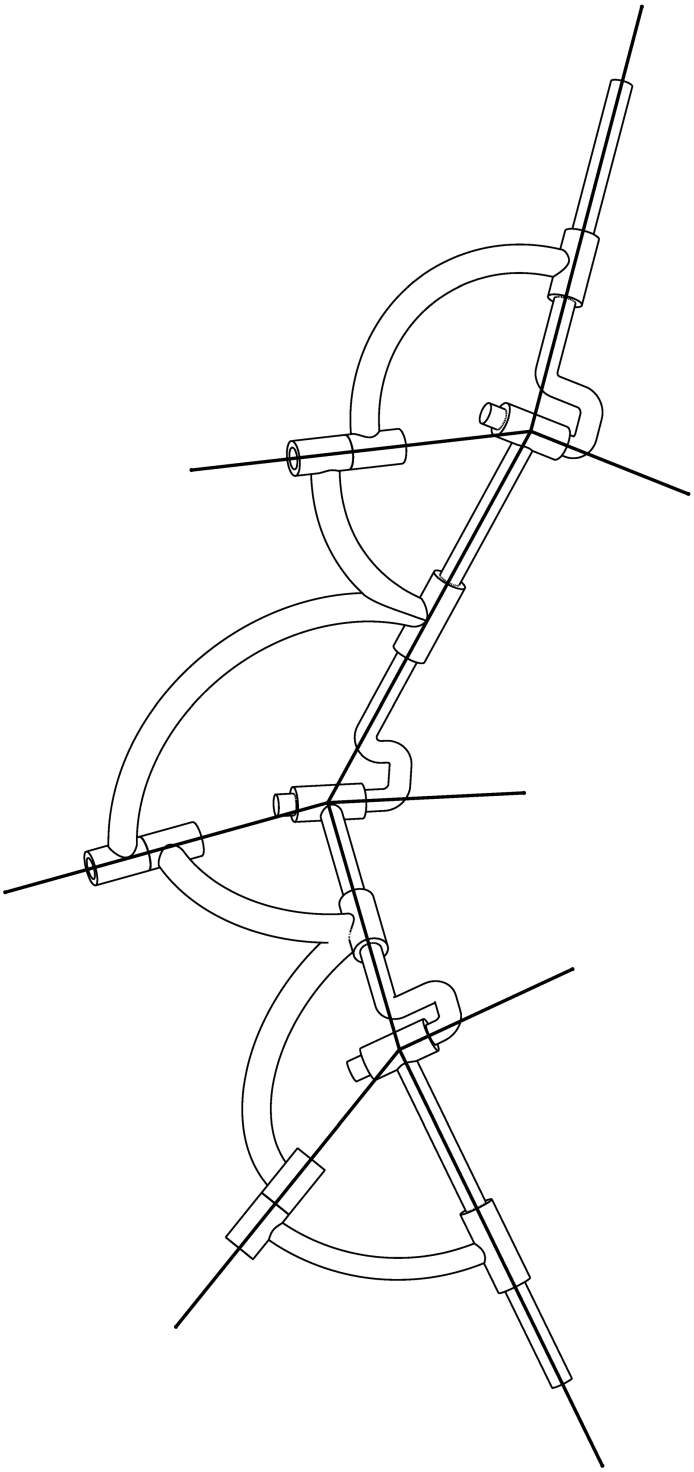

Acknowledgement

The research presented in this work has been influenced by many people I have met during my studies. However, first of all, my mother, my girlfriend and my loved little son deserve the warmest thanks for their continuous support and love over the years.

I wish to thank my colleagues at the institute of micro technology and medical device technology, where especially Dr. Thomas Ottnad and Dr. Franz Irlinger deserve my thanks for various fruitful discussions. I wish to thank professor Tim Christian Lüth who confided in me and enabled it to develop application-motivated research and teaching in kinematic design. It was furthermore a great pleasure, to supervise and to collaborate with my students Robert Bonifacic, Tobias Brockmeyer, Matthias Gehring, Martin Kamp, Jonas Koopmann, Simon Laudahn, Florian Pflügl, Martin Seidl and Manuel Winkler.

Although the todays major focus of the institute is on micro technology and medical device technology, it has an old and traditional relation with linkages and kinematics. There is still a considerable number of Reuleaux kinematic models available at the institute, bequeathed by professor Rudolf Beyer, who developed research and teaching in transmission systems and kinematics.

I furthermore want to thank the two further members of the committee of my doctoral thesis, professor Burkhard Corves from Aachen university and professor Johann Hartl from the faculty of mathematics here at TUM for their interest in my research and their useful remarks. Last but not least there are several people in the kinematics community I was able to meet on national and especially on international conferences, whose outstanding research motivated me to develop this work.

June, 2015,

Kassim Abdul-Sater

Publications

1. Abdul-Sater, K., Irlinger, F., and Lüth, T. C. (2012) "CAD-Integrierte Kinematische Auslegung Ebener Gelenkgetriebe". In: *VDI Bewegungstechnik*. VDI Verlag, ISBN 978318092 1754, pp. 225-241.

2. Abdul-Sater, K., Irlinger, F., and Lueth, T. C. (2013) "Two-Configuration Synthesis of Origami- Guided Planar, Spherical and Spatial Revolute-Revolute Chains". In: *ASME Journal of Mechanisms and Robotics* 5(3), DOI:10.1115/1.4024472, p. 10.

3. Abdul-Sater, K., Irlinger, F., and Lueth, T. C. (2014) "Four-Position Synthesis of Origami-Evolved, Spherically Constrained Planar RR Chains". In: *Interdisciplinary Applications of Kinematics*. Eds. A. Kecskemethy and F. Geu Flores. Springer, DOI 10.1007/978-3-319-10723-3_7, pp. 63-71.

4. Abdul-Sater, K., Lueth, T. C., and Irlinger, F. (2014) "Kinematic Design of Miura-Ori-Based Folding Structures Using the Screw Axis of a Relative Displacement". In: *Advances in Robot Kinematics*. Eds. J. Lenarcic and O. Khatib. Springer, DOI 10.1007/978-3-319-06698-1_25, pp. 233-241

5. Abdul-Sater, K., Lueth, T. C., and Irlinger, F. (2014) "Computer-Aided, Task-Based Kinematic Design of Linkages - A New Lecture for Engineering Students". In: *New Trends in Mechanism and Machine Science*. Eds. P. Flores and F. Viadero. Springer, DOI 10.1007/978-3-319-09411-3_93, pp. 891-899.

6. Kamp, M., Abdul-Sater, K., Irlinger, F., and Lueth, T. C. (2014) "Auslegung und Aufbau einer Sphärischen Parallel-Kinematik für Videoendoskope". In: *VDI Bewegungstechnik*. VDI Verlag, pp. 249-261.

7. D'Angelo, L. T., Abdul-Sater, K., Pfluegl, F. and Lueth, T. C. (2015) "Wheelchair Models With Integrated Transfer Support Mechanisms and Passive Actuation". In: *ASME Journal of Medical Devices* 9(1), DOI: 10.1115/1.4029507, p. 13

8. Abdul-Sater, K., Winkler, M. M., Irlinger, F., and Lueth (2015) "Three-Position Synthesis of Origami-Evolved, Spherically Constrained Spatial RR Chains ". In: *ASME Journal of Mechanisms and Robotics*, DOI: 10.1115/1.4030370, p. 14.

9. Abdul-Sater, K., Irlinger, F., and Lueth, T. C. (2015) "Three-Position Synthesis of Spherically Constrained Planar 3R Chains ". In: *ASME 2015 International Design Engineering Technical Conferences, 39th Mechanisms and Robotics Conference*. ASME, p. 8.

10. Abdul-Sater, K., Irlinger, F., and Lüth, T. C. (2015) "An Approach Towards Kinematic Multiposition / Multibody Synthesis". In: *1st IFToMM D-A-CH Konferenz*, DuEPublico, ISBN 978-3-940402-03-5, pp. 61-67.

11. Abdul-Sater, K., Laudahn, S., Winkler, M. M, Lüth, T.C., Irlinger, F. (2015) “Ein Beitrag zur Analyse Origami-Inspirierter, Sphärisch Zwangsgeführter RR-Ketten“. In: *11. Kolloquium Getriebetechnik*, Chapter: 8, Editors: Tim C. Lüth, Franz Irlinger, Kassim Abdul-Sater, pp.125-147 DOI: 10.14459/2015md1276132

Abstract

This dissertation presents a novel task-based approach towards computer-aided kinematic design of a spatially moveable class of linkages, called here spherically constrained kinematic chains. Based on a detailed review of the state of the art in theoretical kinematics, linkage design theory as well as computer-aided kinematic design new kinematic synthesis and analysis methods as well as a general CAD-integrated kinematic design process were developed, which also consider space requirements of a given engineering motion task. An example of a spatial kinematic motion task inspired from automotive engineering is used to demonstrate theory and methods.

Zusammenfassung

Die vorliegende Dissertation liefert einen neuartigen Ansatz zum aufgabenbasierten, computergestützten, kinematischen Design einer Klasse räumlich beweglicher Gelenkstrukturen, hier genannt sphärisch zwangsgeführte kinematische Ketten. Auf Basis des Standes der Forschung zur theoretischen Kinematik, Designtheorie von Mechanismen und dem rechner-gestützten kinematischen Design wurden neue kinematische Synthese- und Analysemethoden sowie ein allgemeiner CAD-integrierter kinematischer Designprozess erarbeitet. Die erarbeiteten Verfahren berücksichtigen auch gegebene Bauraumanforderungen einer vorliegenden Bewegungsaufgabe. Theorie und Methoden werden am Beispiel einer kinematisch räumlichen, Ingenieur- Bewegungsaufgabe aus dem Bereich Automotive demonstriert.

Contents

List of Figures

List of Tables

1. Introduction

The terminology *mechanical linkage design* refers to one of the most traditional and oldest disciplines in mechanical design engineering. It leads back to Franz Reuleaux, who derives a machine from a kinematic structure assembled from resistant bodies and joints that provides a well-defined mechanical movement. In his original treatise from 1875, [1], one may find the following definition:

Eine Maschine ist eine Verbindung widerstandsfähiger Körper, welche so eingerichtet ist, dass mittelst ihrer mechanische Naturkräfte genöthigt werden können, unter bestimmten Bewegungen zu wirken.

(English translation, see [2]: *A machine is a combination of resistant bodies so arranged that by their means the mechanical forces of nature can be compelled to do work accompanied by certain determinate motions.*)

Until today this is still an admirable definition, appropriately describing the task and meaning of current mechanical and mechatronic devices. Those range from classical mechanical low-degree-of-freedom (d.o.f.) linkage mechanisms to multi-d.o.f. robots, performing motion tasks in various different applications. On the one hand there are for instance tasks in the area of mechanical automotive engineering, where engineers design highly complex low-d.o.f. linkages consisting of numerous links and joints that define retractable tops of sports cars. On the other hand kinematic structures of multi-d.o.f. robots enable automated and flexible manufacturing processes. Furthermore, medical devices such as laparoscopic grippers, adjustable spinal implants or endoscope guidance devices require particularly moveable linkage structures. Other disciplines such as architecture, industrial design and even Nano-biology exist, where linkages are used to realize for instance transformable roofs or furniture or also to model hydrogen bonds of protein molecules.

1.1. Motivation and Problem Statement

The list of different existing examples where linkages are used to solve specific motion tasks is far from being complete and could be further continued. However, it may also be supplemented by the wealth of potential applications and motion tasks, that have not yet been explored to be solved by task-specific linkage structures. On the one hand there are clearly various tasks for multi-d.o.f. robotic linkage structures. However, on the other hand this is also particularly true for the class of low-d.o.f. linkages. Consider for instance a single-d.o.f. spatial orientation device, that guides solar panels along the sun's daily trajectory allowing it to reduce the number of actuators in common spatially orientable solar sun tracking systems. Another example is a car door that is guided along a spatial path upon the car top and hence eases getting into a car in cramped parking spots.

This list of potential applications is also far from being complete and specifically addresses the use of spatial low-d.o.f. linkage topologies in order to solve what may be called low-d.o.f. spatial motion tasks. In fact, there is wealth of spatial linkage topologies that could be used to solve motion tasks in various different applications by task-based kinematic designing

of linkages. This design process is particularly represented by what is known as kinematic dimensional synthesis, where kinematic dimensions measured between the different joints are calculated, such that the linkage provides the desired movement.

The circumstance that a variety of low-d.o.f. spatial linkage topologies is not yet used to solve motion tasks in practice first of all is based upon the complex nature of spatial dimensional synthesis. In order to somehow hide this fact from a designer appropriate computer-aided kinematic design approaches are required, which guide a designer through the process, [3]. This can be realized via specialized software tools or via computer-aided design methodologies, that integrate kinematic linkage design into other design software tools. Note that in this context we consider the kinematic design of linkages as a particular subdevelopment process, embedded into other larger computer-aided product development processes. Integration into existing design environments on the one hand particularly requires the development and implementation of proper kinematic design steps that combine appropriately with existing computer-aided design procedures. On the other hand computing methodologies in the sense of kinematic synthesis procedures are required, which allow systematic dimensional synthesis of task-specific kinematic dimensions of a given linkage topology. (Note that task-based structural synthesis, i.e. defining a task-specific linkage topology is clearly a concern, which, however was not the focus of this work.)

A second circumstance that exacerbates the use of a spatial linkage refers to the fact, that its joints are spatially located and oriented and can be useless, even though a structure obtained from synthesis solves the (kinematically) defined motion task. This is particularly the case, when synthesis results, i.e. kinematic dimensions dramatically violate space requirements of a given task (note that there are of course further requirements such as force transmission requirements, which, however, are not directly considered in this work). Such a space requirement is defined by obstacles in the configuration space and in fact always decides about whether synthesis results can be realized or not, so that we can conclude and identify the problem statement that defines the topics of this work:

What is needed in addition to computer-aided kinematic design methodologies are spatial linkage topologies, which can be synthesized compactly in order to solve spatial motion tasks in engineering design with respect to given space requirements.

Note that the objectives of this work are precisely defined in sect. 1.3. The relatively quick introduction to linkages given in the following should represent a sufficiently precise overview on linkages required to study this work.

1.2. Rigid Body Linkages

In this section a quick definition of linkages is given, which may also be found in detail in the numerous excellent literature on linkage design theory. Examples providing appropriate introductions are represented by Luck and Modler [4], Sandor and Erdman [5], Kerle et al. [6] or Uicker et al. [7] to name a few.

A mechanical linkage is known as a well ordered assembly of links and kinematic joints. The links are considered as rigid undeformable elements just representing Reuleaux's resistant bodies. In case that links and joints are assembled alternately in series the result is a *serial linkage topology*, see Fig. 1.1a). On the other hand, if a linkage consists of several serial chains, which form kinematic loops it is known as a *parallel kinematic linkage topology*, see

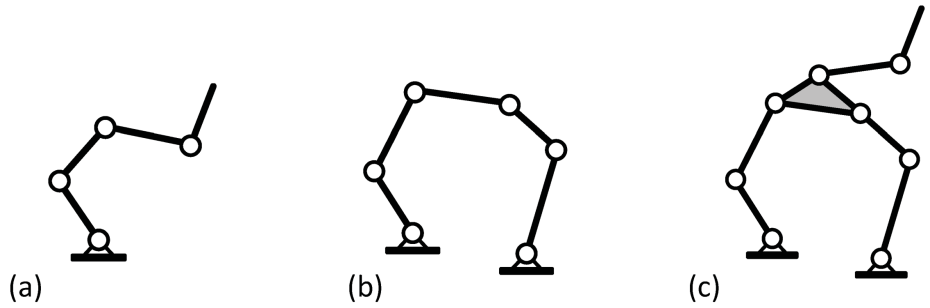

Figure 1.1.: Qualitative examples of a) serial, b) parallel and c) hybrid linkage topologies

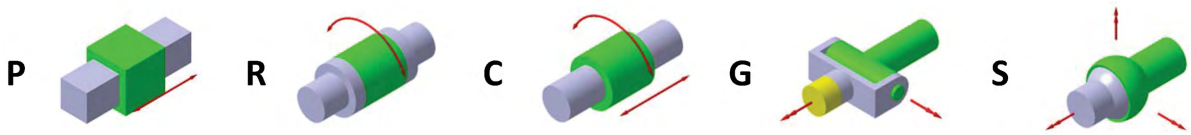

Figure 1.2.: Basic joint types: the prismatic (P) joint, the revolute (R) joint, the cylindric (C) joint, the universal or gimbal (G) joint, the ball or spherical (S) joint

figure b).

While the exemplary serial and parallel structure from Fig. 1.1 only consist of binary links, the hybrid linkage topology from figure c) also includes a ternary link, which is made up of three joints. This example introduces the type of links as another distinctive feature of linkages, which applies to *binary, ternary, quaternary links* and further types.

In order to classify the types of motion enabled by a specific serial or parallel topology, different possible kinematic pairs represented by the *kinematic joints* are considered. A pair can allow translational relative movement, rotational relative movement or either a combination of both. The relative movement may hence be a single-d.o.f. or either a multi-d.o.f. movement. An excerpt of the well-known lower kinematic pairs or joint types is shown in Fig. 1.2, which may be extended by various other types, see e.g. [4].

While the prismatic (P) and revolute (R) joint only allow single-d.o.f. relative movement between two consecutive links, the cylindrical (C) joint allows a combined slide and rotation. In fact, since rotation and translation are performed around and along the same axis this joint enables a screw motion between the different coupled links, which is a spatial movement. In contrast to C joints the gimbal (G) as well as the ball (S) joint allow pure spherical relative movement. The result is that C, G and S belong to the class of spatial joint types that are used to assemble spatially movable linkage structures, while P or R joints are also used in planar linkages.

Planar movable linkage topologies only consist of P joints whose joint axes lie in the plane and / or R joints whose axes are oriented perpendicular to the plane, where the motion takes place. In contrast to that spherical linkages can be viewed as only consisting of R joints, whose axes intersect at a specific point. This is known as the center of rotation of each of the links that make up the spherical structure. Finally, the class of spatially moveable structures is not restricted to have any particularly oriented joint axes and hence represents the most general class of linkage topologies. Figure 1.3 shows different examples of planar, spherical and also spatial linkage structures, which in fact are all single-d.o.f. structures.

In figure a1) the classical planar four-bar (or also 4R) linkage is shown, which has parallel

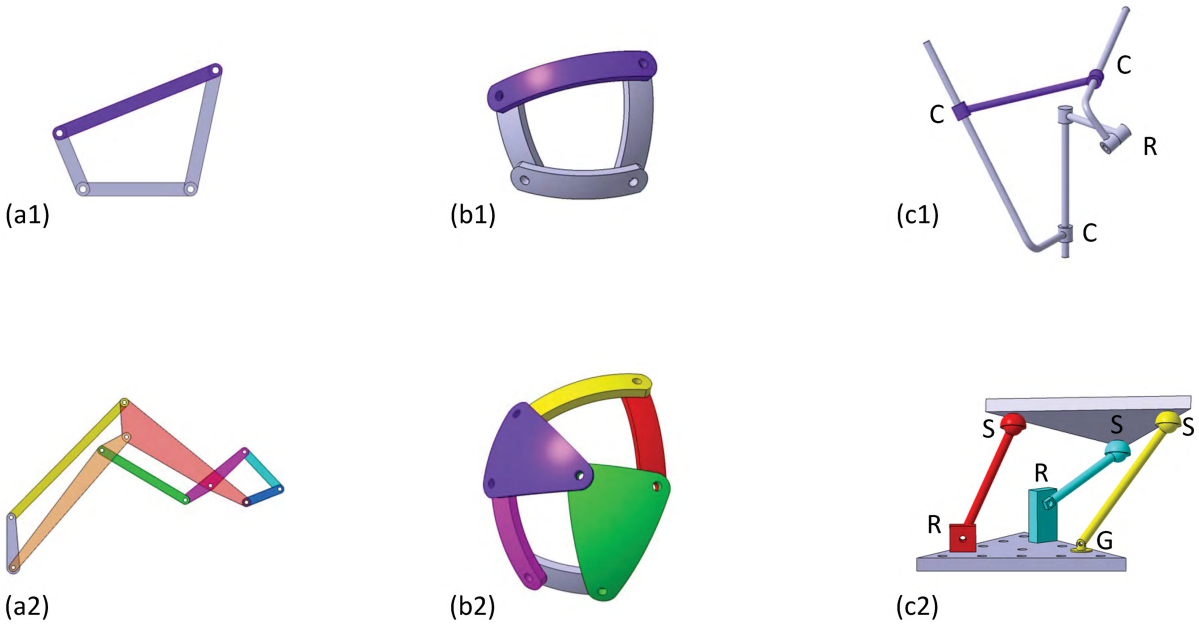

Figure 1.3.: Examples of planar, spherical and spatial linkage topologies with one single d.o.f. for arbitrary kinematic dimensions

joint axes that form a single kinematic loop. Three of these loops coupled in a specific way as shown in figure a2) form a multiloop 10R or eight-bar linkage, which consists of binary, ternary and also quaternary links. The basic concept also generalizes to spherical linkages with intersecting joint axes, where a spherical four-bar (4R) as well as a spherical six-bar (7R) is shown in Fig. 1.3 b). In case of spatial linkage topologies clearly also single and multiloop linkages exist as shown in figures c). On the one hand the RCCC single loop structure is shown in figure c1). On the other hand a so called spatial single-d.o.f. platform linkage is shown, which is known as the RSSR-GS multiloop linkage. This consists of a spatial RSSR four-bar linkage, which has an isolated d.o.f. due to the two spherical joints. Hence, in order to completely control the orientation of the moving platform another *building block chain* is used, which is a GS serial kinematic chain.

1.2.1. The Kinematic Linkage Design Process

The process of linkage design for a prescribed task includes various different steps and starts with the definition and classification of a motion task. This is followed by an appropriate selection of a linkage topology such as a serial or parallel linkage. Based on that, kinematic dimensional synthesis must be performed in order to obtain task specific kinematic dimensions. The resulting structure must next be analyzed in order to evaluate the performance as well as the feasibility of the system. The different steps form a specific stepwise process, that is called here the *task-based kinematic design process of linkages*.

The different steps surround a designer, who aims at solving a given motion task by designing a task specific mechanical or either mechatronic device. Figure 1.4 shows the steps of the process based on the simple qualitative example of a spherical guidance task for an endoscope. Endoscopes are often considered to be used in medical interventions, where spatially distinct perspectives from the inside of a patient are required, so that different spatial orientations of the device are required. An example of such an intervention is functional endoscopic sinus

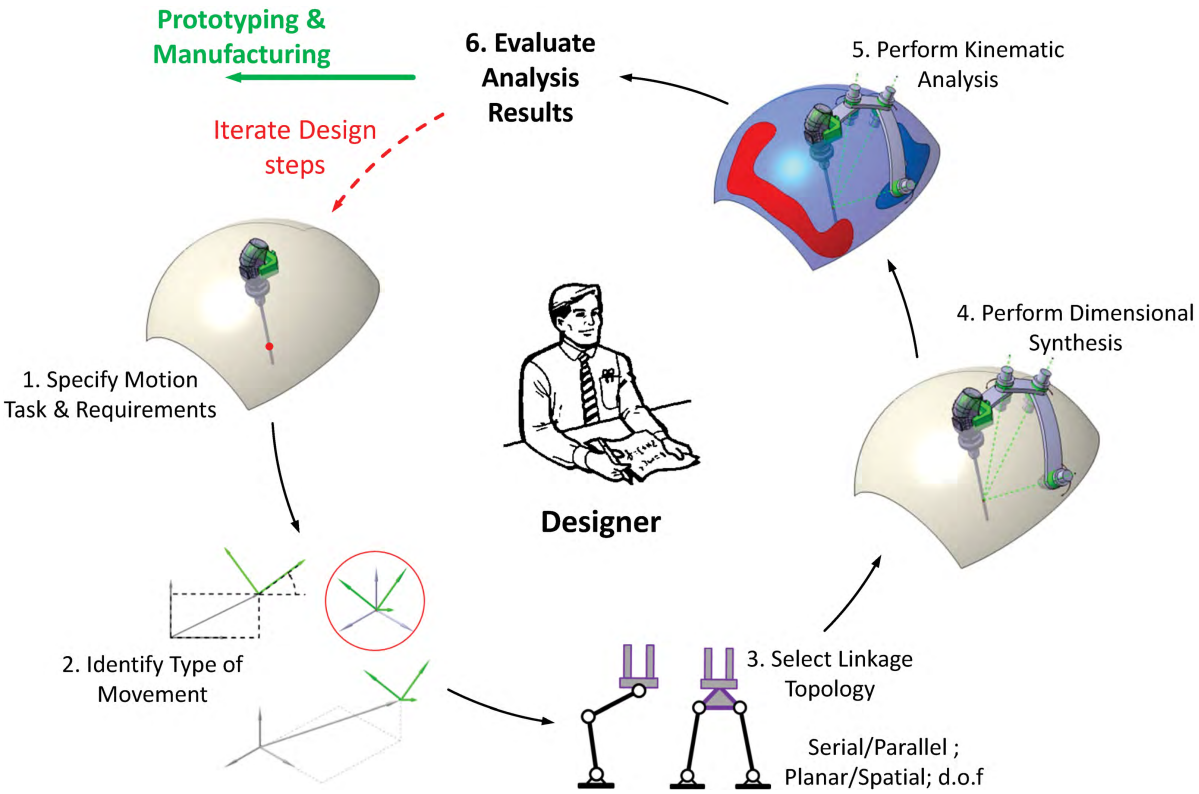

Figure 1.4.: Qualitative representation of a stepwise iterative kinematic design process of a linkage for a prescribed motion task

surgery (FESS), where drain and ventilation are rearranged at a patient's nose under endoscopic view, [8]. In order to support a surgeon in such interventions the development of task specific orientation devices is of interest, [9].

When a designer aims at finding a task specific linkage structure he needs to identify the types of motion associated with the endoscope guidance task. This is clearly a spherical movement, which hence also requires a spherical linkage topology. Within the set of spherical mechanisms the next step consists in selecting a topology with appropriate mobility. Since it might be required to orient the endoscope independently along longitude, latitude or also roll angles in order to obtain an adequate endoscopic view, a multi-d.o.f. structure such as a spherical serial 3R seems to be appropriate. Proper kinematic dimensions that allow the chain to reach any task position within a desired work space may then be found from dimensional synthesis procedures. Based on that, kinematic analysis must be performed in order to detect weak transmission properties of the structure. Furthermore, also collisions between the different links may be evaluated. Evaluation of the results then yields, whether the linkage design may be prepared for prototyping and manufacturing or whether another design iteration must be performed.

The different steps from Fig. 1.4 identify kinematic design as an iterative process, which, in the worst case, may require modifications of the definition of the task if design results do not match the given requirements. Then, also any further design steps could be affected from such modifications and may require another linkage topology with specific synthesis and analysis procedures. In another scenario, weak design results may directly require other selections of a linkage topology, which, however, will ask for other dimensional synthesis and analysis procedures. Finally, another scenario with, however, still perceptible impact on the effort for the designer may be iterations between synthesis and analysis. This may be performed by evalu-

ating free selectable parameters of dimensional synthesis or also those available in the specific geometric design of links.

In order to reduce iterations or to accelerate iteration steps in kinematic design processes various different computational approaches have been developed, which has led to what is called here *computer-aided kinematic design*. Then it is convenient to group different kinematic design steps in a way, that particularly regards their temporal sequence. Such a classification, that is also proposed by Corves and Niggemann [10], considers preprocessing, solving and postprocessing procedures in computer-aided kinematic design. Preprocessing includes the preparation and planning of the motion task, while solving includes any computational processes, such as synthesis and analysis calculations. Postprocessing on the other hand is defined by visualization and evaluation of design results.

In order to support these design steps a variety of software tools has been developed, where an excerpt will be discussed in sect. 2.4. On one hand there are standalone tools, that assist synthesis and analysis tasks. On the other hand also advanced CAD-add in tools exist, which integrate kinematic design into larger CAD-integrated product development processes. This latter approach is also considered in this work in order to provide a contribution towards CAD-integrated spatial linkage design.

1.2.2. Space Requirements

The different linkage examples from Fig. 1.3 in fact remain mobile for (almost) any chosen kinematic dimensions measured between the different joints. For the set of planar revolute jointed linkage topologies this means, that the locations of R joints may be varied in the plane where the motion takes place, while their direction must remain perpendicular to that plane. In case of spherical linkage topologies joint axes may be directed arbitrarily but must intersect at a common point. The examples of spatial linkage topologies from Fig. 1.3 c) obviously do not have the previously mentioned property of their planar and spherical counterparts. This means that joint axes or gimbal or ball joints may be varied arbitrarily without affecting the mobility of the structures. (Note that these considerations are clearly theoretical in character, based on the assumption of rigid links and ideal kinematic joints).

Kinematic dimensional synthesis methods for planar, spherical and spatial structures preserve the different basic properties of the three distinct topological classes (i.e. parallel, intersecting or skew axes). However, the 'feature of arbitrary kinematic dimensions' means that dimensional synthesis of a given linkage topology can produce dimensions that are completely useless in the sense that joint locations dramatically violate given *space requirements*. This is based on an inappropriately stated motion task which can yield joint locations that cannot be realized. An example is the synthesis of a linkage for a retractable top of a sports car, where an inappropriately stated task yields joints located outside the car. For the case of planar linkages Mlinar and Erdman [11] provide an introduction towards a theory that considers the dependencies between joint locations (synthesis results) and the parameters that define a motion task.

Because synthesis of planar linkages will only affect the joint locations, while the directions are not affected, planar synthesis results can usually be realized as a compact construction, which consists of a layered arrangement of thickened but approximately flat links. Observe that this property of 'flatness' is particularly important in real applications where other parts involved in the design task usually define a particularly small portion of space, where the linkage is allowed to move in. In case of spherical linkage topologies there is a similar situation, although joint axes intersect instead of being parallel. This is because the links always move on concentric spheres, which means that spherical linkages may always be designed compactly

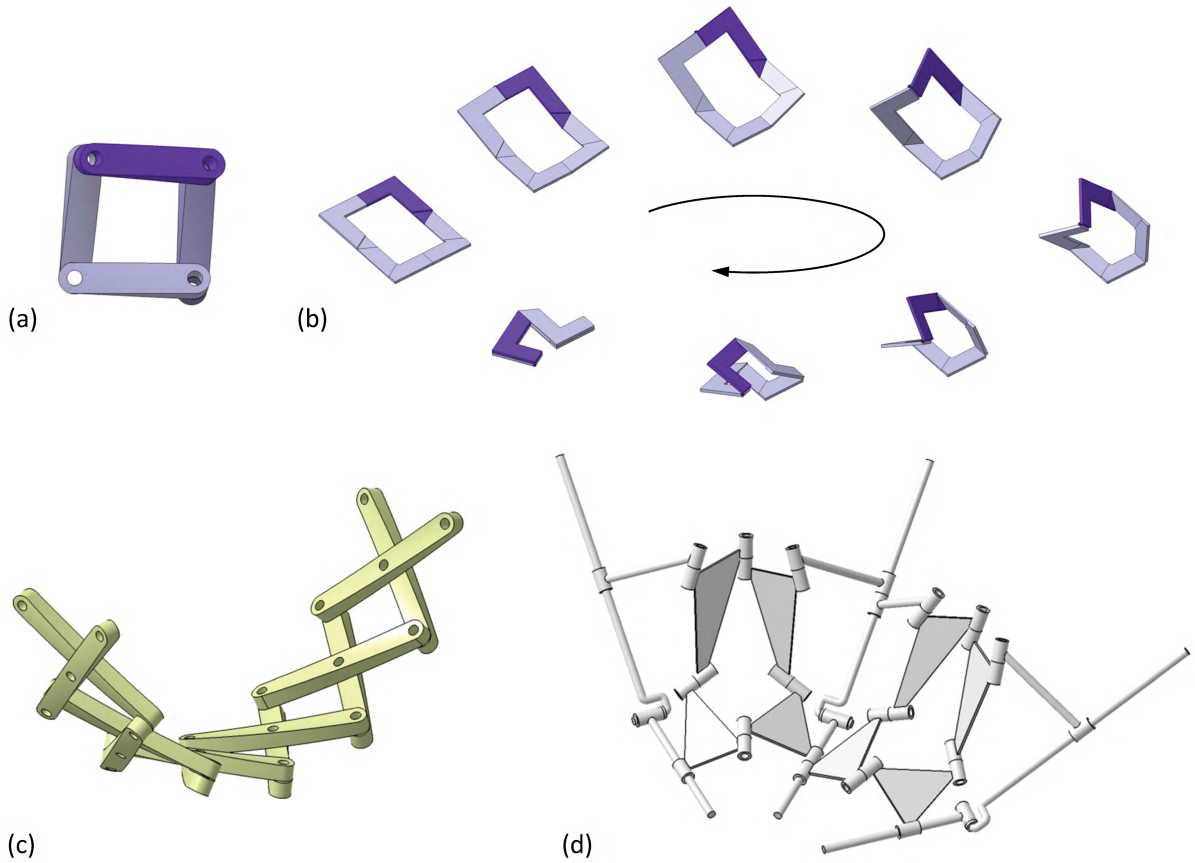

Figure 1.5.: Examples of spatially moveable overconstrained structures: a) Bennett's four-bar linkage. b) Another Bennett linkage with link geometry that allows collision-free folding into a compact state. c) A network of Bennett linkages. d) An origami-evolved linkage network consisting of several spherical substructures

around their center of rotation. These fundamental properties immanent to planar and spherical structures do not hold any longer for spatial linkage topologies and hence define the chances that a designer may synthesize a useful spatial linkage to be slim. However, another class of spatial linkage topologies exists, which is known for several examples having compact configurations. This is the class of *overconstrained spatial linkages*, which is introduced in the following.

1.2.3. Overconstrained Spatial Structures

Overconstrained spatial linkage topologies are those, whose mobility depends on special kinematic dimensions among the different joints, [12]. Figure 1.5 shows different examples of such linkages each of which moves with a single degree of freedom. Figure a) shows the well-known spatial Bennett four-bar or 4R mechanism [13], whose mobility depends on particular, symmetrically arranged revolute joint axes. However, it is important to note here, that there is not only a single set of kinematic dimensions that defines Bennett's linkage. Instead, an infinite number of four-bars exist, whose kinematic dimensions satisfy what is known as the Bennett conditions, also provided in the appendix. Such another example of Bennett's linkage is shown in figure b), where appropriately designed links allow a collision-free folding movement. Aside the Bennett four-bar a variety of further overconstrained single-loop structures exist such as those proposed by Delassus [14], Bricard [15], Myard [16], Goldberg [17] or - as one of the first - by Sarrus

[18].

While a single Bennett linkage is a single-loop linkage, also combinations or networks of Bennett linkages exist, which are coupled with particular respect to the overconstraining kinematic dimensions. Such networks are also of recent interest in kinematics and those will be discussed briefly in a subsection of sect. 2.3.6. An example of a Bennett network is shown in Fig. 1.5 c), which is a scissor mechanism that allows a compactly folded configuration and a circular deployment.

Origami-inspired linkages

In fact the property of foldability is a particular characteristic immanent to a variety of spatial overconstrained single-d.o.f. structures. An example of a linkage folding configuration is represented by joint axes that lie in a common plane. This may particularly also be observed at another class of network linkages which are known as the class of *rigid origami or origami-evolved linkage structures*. A rigid origami can also be assigned to the category of technical origami or origami-based engineering design, where specific engineering design problems are solved using the principles of the Japanese art of paper folding. Example applications are for instance transformable roofs in architecture, [19] , [20], or also deployable arrays of solid solar panels, [21]. However, origami-based engineering design has also yet been identified with further engineering design disciplines such as compliant mechanisms [22], meta materials [23], nano scaled DNA origami mechanisms [24], medical devices such as medical stents [25] as well as the design of mobile robots [26], [27].

A rigid origami is obtained by replacing the numerous creases and paper segments of an origami folding pattern by revolute joints and rigid panels, such that the resulting structure remains movable, see e.g. [28]. An example linkage network is shown in Fig. 1.5 d), which consists of several, highly symmetrical spherical sub-structures with intersecting joint axes, that introduce a high degree of overconstraint. Due to the fact, that a rigid origami originates from a crease pattern drawn on a continuous sheet of paper, there is usually no sliding along the joint axes, i.e. rigid origami are usually R jointed linkage topologies. Such structures also exhibit flat inflated as well as flat folded states, which, however depend on the thickness of the different parts that make up the structure.

1.2.4. Task-Based Dimensional Synthesis of Spatial Overconstrained Linkages

Even though various overconstrained spatial linkage topologies have the property of foldability and may hence be used to solve folding tasks, a particular problem may arise, if the structure should be used to realize a desired, pre-defined task-specific movement. This refers to the fact, that the mobility and hence also the motion capabilities rely on the special kinematic dimensions and will probably not directly match a task-specific, pre-defined trajectory in practice. However, in contrast to spatial linkages whose mobility doesn't depend on special kinematic dimensions, this means that the chances that a designer may find a useful linkage, which satisfies the requirements of a given motion task are outmost slim.

An example demonstrating that this is not necessarily always the case is the *finite position synthesis of Bennett's linkage*. This relies on the synthesis problem of spatial serial RR chains. An early result discovered by Tsai and Roth [29] in 1973 shows how to calculate or synthesize the kinematic dimensions of such a chain, such that its end link can reach three finitely separated and arbitrarily pre-defined spatial poses (Note, that we won't distinguish between the

words poses and positions in this work). In fact the algebraic calculation procedure yields two solutions, which represent two RR chains that form the Bennett linkage. However, this in turn means that one may always synthesize a Bennett 4R for three arbitrarily specified position.

When this fundamental result is considered in the context of linkage design in mechanical engineering the three poses can be used as the task positions, that define an engineering motion task. The result is that the finite position synthesis of an overconstrained linkage topology becomes available for task-based kinematic design in engineering.

While the initial result of Tsai and Roth has been reformulated and simplified, see e.g. Perez and McCarthy [30] or Brunnthaler, Schröcker and Husty [31], most recently Hegedüs, Schicho, and Schröcker [32] reported on the four-position synthesis of spatial 3R chains that can be used to form overconstrained 6R linkages. This gives hope that also further overconstrained linkages can be synthesized for engineering motion tasks.

1.3. Objectives

The results of this work shall address the problem statement from sect. 1.1. Hence, a computer-aided kinematic design approach will be developed, which allows the task-based design of spatial linkages for engineering motion problems. The approach should also take into account the problem of given space requirements, since those always decide about whether synthesis results can be realized or not. In order to meet the goal the following topics will be considered:

1. In order to solve motion tasks with challenging space requirements low-d.o.f. spatial linkage topologies will be considered, that have joint axes located relative to each other, such that a detailed design may have particularly slim shape.

2. In order to make practical use of the spatial topologies, kinematic synthesis and analysis techniques will be developed. This, on the one hand, will allow to calculate kinematic dimensions, such that the linkage can provide a desired movement. On the other hand analysis will allow to quantify 'the quality of the movement'.

3. In order to provide a kinematic design methodology also useful in engineering practice a methodology will be developed using commonly available computational as well as design environments.

4. In order to verify computational procedures as well as design methodologies a real engineering application will be considered, where a motion task must be solved. The task shall require spatial motion and needs to be characterized by particularly challenging space requirements.

1.4. Organization of the Work

The desired computer-aided kinematic design methodologies for spatial linkage topologies first of all require a detailed review of the state of the art in kinematic linkage design, which is provided in chapter 2. Section 2.1 provides essential foundations of *theoretical kinematics*, which yields the fundamental reference for kinematic analysis and synthesis of linkages, provided in sect. 2.2 and 2.3. These first three sections of the second chapter are additionally supported by the appendix, where further kinematics methods are derived. These also include algebraic solution procedures for synthesis problems, which were used throughout this work. Section 2.4 then

provides an overview on common computer-aided kinematic linkage design, which particularly include software tools commonly used to solve kinematic design problems.

Based on the state of the art a family of slim spatial linkages is developed in chapter 3, which belong to the class of overconstrained structures and which may be found from a specific rigid origami pattern. Synthesis procedures as well as analysis procedures of these structures are then derived in detail in chapter 4, which represents a major part of the work. When implemented into a commonly available computing environment the different procedures define the computational part in a computer-aided kinematic design process, which is performed within a design environment and which is based on a systematic kinematic design methodology. This methodology is derived in detail in chapter 5 and represents the second major part of the work. In chapter 6 the different results are evaluated using a suitable design engineering task. The computer-aided kinematic design methodology is used in order to synthesize a compact spatial linkage for a motion task with particularly challenging space requirements in order to evaluate and validate both synthesis and analysis procedures as well as the computer-aided kinematic design approach.

2. State-of-the-art

This chapter on the one hand provides the mathematical framework in rigid body kinematics, kinematic analysis as well as finite position dimensional synthesis of linkage building blocks required throughout the work. On the other hand the state-of-the-art in mechanically constrained serial kinematic chains as well as linkage design software is given.

2.1. Excerpts from Theoretical Kinematics of Rigid Motion

Theoretical kinematics aims at studying the fundamental properties of rigid motion and is based on the movement of points forming a rigid link or body. Starting from the group of *rigid displacements*, composed from a rotation and a translation, the section will derive the *velocity* of points using the *tangent operator* or *twist* of the motion group. This allows to identify the tangent operator as a 6-dimensional vector, also known as the *velocity screw*. Based on this, *lines* as special types of screws and the *spatial displacement of screws* are derived. In order to study line geometry the *dual vector algebra of screws* is introduced. A suitable reference for this section is [33].

More detailed derivations are given in appendix A, which may be consulted when required. These allow to study the *invariants of displacements*, particularly needed for linkage synthesis. Here also the linear combination of independent screws (*screw systems*) is identified in brief, that is used to analyze linkage structures.

2.1.1. The Motion Groups $\mathbf{SE}(3)$, $\mathbf{SO}(3)$ and $\mathbf{SE}(2)$

The points that form a rigid link K in a linkage can be measured in a Cartesian coordinate frame B, which shall be rigidly attached to K (see Fig. 2.1). Then an arbitrary point can be described in B using the vector ${}^{B}\bar{\mathbf{p}} = (u,\ v,\ w)^{T}$, where the left superscript denotes that ${}^{B}\bar{\mathbf{p}}$ is measured in B. The displaced coordinates of points are found in another frame W from the *displacement equation*

$$ {}^{W}\mathbf{p} = {}^{W}\mathbf{R}_{B} \cdot {}^{B}\bar{\mathbf{p}} + {}^{W}\mathbf{t}_{B}, \tag{2.1} $$

where the translation vector ${}^{W}\mathbf{t}_{B} \in \mathbb{R}^{3}$ points from the origin of W to that of B and is measured in W. Note that W-frame coordinates of points shall be denoted as ${}^{W}\mathbf{p} = (x,\ y,\ z)^{T}$ and we put the bar to ${}^{B}\bar{\mathbf{p}}$ because there are two different vectors describing the same point. ${}^{W}\mathbf{R}_{B}$ is a proper orthogonal 3×3 rotation matrix satisfying ${}^{W}\mathbf{R}_{B}({}^{W}\mathbf{R}_{B})^{T} = {}^{W}\mathbf{R}_{B}{}^{B}\mathbf{R}_{W} = \mathbf{E}$, which means that ${}^{W}\mathbf{R}_{B}$ represents an element of the *special orthogonal group* $SO(3)$ (here $\mathbf{E}$ is the 3×3 identity).

By adding a fourth vector component normalized to 1 the *homogeneous representation* of Eq. (2.1) is obtained:

$$ {}^{W}\mathbf{p} = \begin{pmatrix} {}^{W}\mathbf{R}_{B} & {}^{W}\mathbf{t}_{B} \\ \mathbf{0}^{T} & 1 \end{pmatrix} \cdot {}^{B}\bar{\mathbf{p}} = {}^{W}\mathbf{T}_{B} \cdot {}^{B}\bar{\mathbf{p}}. \tag{2.2} $$

Note that in this equation vectors take the form ${}^{W}\mathbf{p} = (x,\ y,\ z,\ 1)^{T}$ and ${}^{B}\bar{\mathbf{p}} = (u,\ v,\ w,\ 1)^{T}$. The 4×4 matrix ${}^{W}\mathbf{T}_{B}$ is called the *homogeneous transform* and represents an element of the *special Euclidean group* $SE(3)$ with properties:

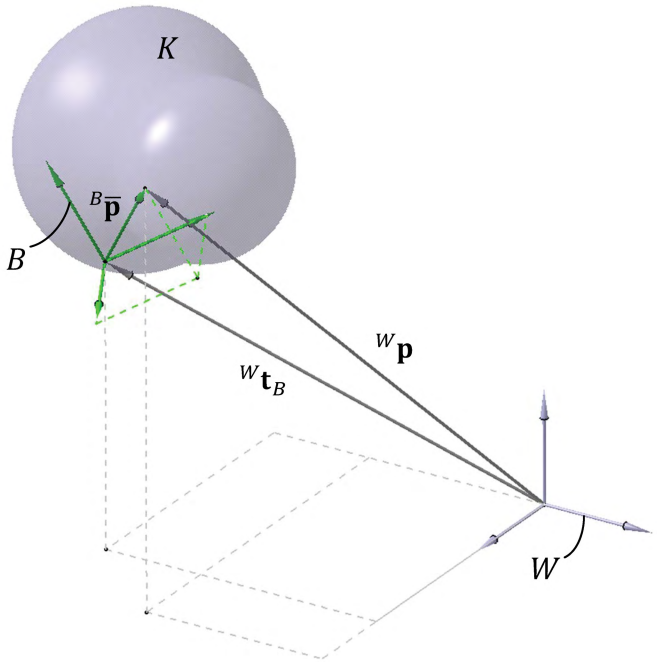

Figure 2.1.: Graphical representation of the displacement equation

1. ${}^W\mathbf{T}_{B2} = {}^W\mathbf{T}_{B1}\,{}^{B1}\mathbf{T}_{B2} = \begin{pmatrix} {}^W\mathbf{R}_{B1}\,{}^{B1}\mathbf{R}_{B2} & {}^W\mathbf{t}_{B1} + {}^W\mathbf{R}_{B1}\,{}^{B1}\mathbf{t}_{B2} \\ \mathbf{0}^T & 1 \end{pmatrix}$ (*composition of displacements*, with semi direct product acting on the translations). It is important to note here, that frames $B1$, $B2$, ..., indicated at the right subscript denote coordinate frames attached to different links $K1$, $K2$, ...

2. $({}^W\mathbf{T}_B)^{-1} = {}^B\mathbf{T}_W = \begin{pmatrix} {}^B\mathbf{R}_W & -{}^B\mathbf{R}_W\,{}^W\mathbf{t}_B \\ \mathbf{0}^T & 1 \end{pmatrix}$ (*inverse of a displacement*) and

3. $\mathbf{I} = \begin{pmatrix} \mathbf{E} & \mathbf{0} \\ \mathbf{0}^T & 1 \end{pmatrix}$ (*identity displacement*).

In the case that ${}^W\mathbf{R}_B$ is a proper 2×2 rotation matrix and ${}^W\mathbf{t}_B \in \mathbb{R}^2$ planar rigid motion can be embedded into 3×3 homogeneous transforms, which then form the group $SE(2)$. Considering the xy-plane of W and B being the plane where the motion takes place, this requires vectors ${}^W\mathbf{p} = (x,\, y,\, 1)^T$ and ${}^B\bar{\mathbf{p}} = (u,\, v,\, 1)^T$ in the planar version of Eq. (2.2). In what follows ${}^B\bar{\mathbf{p}}$ is considered to be rigid and hence independent of temporally and spatially different configurations of a link.

Relative displacements

A particular type of a composition of two displacements is termed *relative displacement*, which relates two general poses i and j of a frame B. These can be thought of as two temporally and spatially different poses of B, in the following also called *finitely separated poses*. Badging these configurations by another right superscript and using Eq. (2.2) yields ${}^W\mathbf{p}^i = {}^W\mathbf{T}^i_B \cdot {}^B\bar{\mathbf{p}}$ and ${}^W\mathbf{p}^j = {}^W\mathbf{T}^j_B \cdot {}^B\bar{\mathbf{p}}$ and eliminating ${}^B\bar{\mathbf{p}}$ yields the relative displacement equation

$$ {}^W\mathbf{p}^j = {}^W\mathbf{T}^j_B({}^W\mathbf{T}^i_B)^{-1} \cdot {}^W\mathbf{p}^i = \begin{pmatrix} {}^W\mathbf{R}^j_B\,{}^B\mathbf{R}^i_W & {}^W\mathbf{t}^j_B - {}^W\mathbf{R}^j_B\,{}^B\mathbf{R}^i_W \cdot {}^W\mathbf{t}^i_B \\ \mathbf{0}^T & 1 \end{pmatrix} \cdot {}^W\mathbf{p}^i. \tag{2.3} $$

Note that ${}^{B}\bar{\mathbf{p}}$ is considered to be rigid and hence independent of configuration i and j. Equation (2.3) is an expression only consisting of W-frame coordinates, transporting the points from configuration i to j. Hence, for relative displacements it is convenient to choose the following notation, which neglects the left superscript and uses the right lower index to denote the considered moving frame:

$$\mathbf{p}^j = \mathbf{T}_B^{ij} \cdot \mathbf{p}^i = \begin{pmatrix} \mathbf{R}_B^{ij} & \mathbf{t}_B^{ij} \\ \mathbf{0}^T & 1 \end{pmatrix} \cdot \mathbf{p}^i, \tag{2.4}$$

where $\mathbf{R}_B^{ij}$ and $\mathbf{t}_B^{ij}$ are the rotational and translational parts of the homogeneous transform from Eq. (2.3). Expanding Eq. (2.4) into the non-homogeneous representation of a displacement equation yield an expression consisting of usual 3×1 vectors:

$$\mathbf{p}^j = \mathbf{R}_B^{ij} \cdot \mathbf{p}^i + \mathbf{t}_B^{ij}. \tag{2.5}$$

Rotation matrices

A convenient way to describe or construct the spatial orientation of a link K or frame B is to perform a series of coordinate rotations. The well-known basic rotations about the x-, y- and z-axis of a certain coordinate frame are given as

$$\mathbf{R}_x = \begin{pmatrix} 1 & 0 & 0 \\ 0 & \mathrm{c}\phi & -\mathrm{s}\phi \\ 0 & \mathrm{s}\phi & \mathrm{c}\phi \end{pmatrix}, \quad \mathbf{R}_y = \begin{pmatrix} \mathrm{c}\phi & 0 & \mathrm{s}\phi \\ 0 & 1 & 0 \\ -\mathrm{s}\phi & 0 & \mathrm{c}\phi \end{pmatrix}, \quad \mathbf{R}_z = \begin{pmatrix} \mathrm{c}\phi & -\mathrm{s}\phi & 0 \\ \mathrm{s}\phi & \mathrm{c}\phi & 0 \\ 0 & 0 & 1 \end{pmatrix}, \tag{2.6}$$

where c and s denote the cosine and sine. Compositions of a certain combination of these rotations may then yield the desired spatial orientation of B with respect to another frame W. Within this work the z-x-z rotation sequence will mainly be used, because this is also provided by the CAD-system used for the kinematic design procedures:

$${}^{W}\mathbf{R}_B = \mathbf{R}_z(\psi)\mathbf{R}_x(\vartheta)\mathbf{R}_z(\varphi) = \begin{pmatrix} \mathrm{c}\psi\mathrm{c}\varphi - \mathrm{c}\vartheta\mathrm{s}\psi\mathrm{s}\varphi & -\mathrm{c}\psi\mathrm{s}\varphi - \mathrm{c}\vartheta\mathrm{c}\varphi\mathrm{s}\psi & \mathrm{s}\vartheta\mathrm{s}\psi \\ \mathrm{c}\varphi\mathrm{s}\psi + \mathrm{c}\vartheta\mathrm{c}\psi\mathrm{s}\varphi & \mathrm{c}\vartheta\mathrm{c}\psi\mathrm{c}\varphi - \mathrm{s}\psi\mathrm{s}\varphi & -\mathrm{c}\psi\mathrm{s}\vartheta \\ \mathrm{s}\vartheta\mathrm{s}\varphi & \mathrm{c}\varphi\mathrm{s}\vartheta & \mathrm{c}\vartheta \end{pmatrix}. \tag{2.7}$$

Another convenient way is to define rotations in terms of a rotation angle and rotation axis, as shown in sect. A.1.

Coordinate screw displacements

According to the previously described coordinate rotations, the 4×4 homogeneous transforms take a very simple form in the case of a slide s along and a rotation ϕ around the x-, y- or z-axis of a certain coordinate frame:

$$\mathbf{T}_x = \begin{pmatrix} 1 & 0 & 0 & s \\ 0 & \mathrm{c}\phi & -\mathrm{s}\phi & 0 \\ 0 & \mathrm{s}\phi & \mathrm{c}\phi & 0 \\ 0 & 0 & 0 & 1 \end{pmatrix}, \quad \mathbf{T}_y = \begin{pmatrix} \mathrm{c}\phi & 0 & \mathrm{s}\phi & 0 \\ 0 & 1 & 0 & s \\ -\mathrm{s}\phi & 0 & \mathrm{c}\phi & 0 \\ 0 & 0 & 0 & 1 \end{pmatrix}, \quad \mathbf{T}_z = \begin{pmatrix} \mathrm{c}\phi & -\mathrm{s}\phi & 0 & 0 \\ \mathrm{s}\phi & \mathrm{c}\phi & 0 & 0 \\ 0 & 0 & 1 & s \\ 0 & 0 & 0 & 1 \end{pmatrix}. \tag{2.8}$$

These matrices will also be denoted as $\mathbf{T}(\phi, s)$ and they are known as the *coordinate screw displacements*. Those are widely used in the analysis of spatial kinematic chains, see also sect. 2.2.2 and B.1.

2.1.2. Velocity and the Tangent Operator of $\mathbf{SE(3)}$

When a link in a linkage is considered to move smoothly through space from one pose to the next, the entries in ${}^W\mathbf{T}_B$ and ${}^W\mathbf{p}$ in Eq. (2.2) vary continuously with respect to time. Hence, considering these quantities as continuous functions in time and computing the derivative of Eq. (2.2) with respect to time yields: ${}^W\dot{\mathbf{p}} = {}^W\dot{\mathbf{T}}_B \cdot {}^B\bar{\mathbf{p}}$. Substituting ${}^B\bar{\mathbf{p}} = ({}^W\mathbf{T}_B)^{-1} \cdot {}^W\mathbf{p}$ into this expression then yields the *velocity* of the points forming the link:

$$ {}^W\dot{\mathbf{p}} = {}^W\dot{\mathbf{T}}_B({}^W\mathbf{T}_B)^{-1} \cdot {}^W\mathbf{p} = \begin{pmatrix} {}^W\dot{\mathbf{R}}_B{}^B\mathbf{R}_W & -{}^W\dot{\mathbf{R}}_B{}^B\mathbf{R}_W \cdot {}^W\mathbf{t}_B + \cdot{}^W\dot{\mathbf{t}}_B \\ \mathbf{0}^T & 0 \end{pmatrix} {}^W\mathbf{p}. \tag{2.9} $$

Equation (2.9) is an expression only consisting of W-frame coordinates, so that in the following indices indicating coordinate frames are neglected. Hence, after introducing the matrix $\Omega = \dot{\mathbf{R}}(\mathbf{R})^T$ and the vector $\mathbf{v} = -\Omega\mathbf{t} + \dot{\mathbf{t}}$ and assembling these into a 4×4 matrix Γ, Eq. (2.9) is written as:

$$ \dot{\mathbf{p}} = \Gamma \cdot \mathbf{p} = \begin{pmatrix} \Omega & \mathbf{v} \\ \mathbf{0}^T & 0 \end{pmatrix} \cdot \mathbf{p}. \tag{2.10} $$

The matrix Γ acts on the trajectories of points to yield their velocities and is also called the *tangent operator of* $SE(3)$. Another denotation of a tangent operator is *twist*, also used throughout the work.

Straight forward differentiation of $\mathbf{R}(\mathbf{R})^T = \mathbf{E}$ yields $\mathbf{R}(\dot{\mathbf{R}})^T = -\dot{\mathbf{R}}(\mathbf{R})^T$, which shows that Ω is skew symmetric. Hence, Ω may also be assembled from three parameters denoted as ω_x, ω_y and ω_z, which are nothing but the well-known angular velocity parameters. Assembling ω_x, ω_y and ω_z into a 3×1 vector $\vec{\omega}$ and using the common vector product allows to replace $-\Omega\mathbf{t}$ by $\mathbf{t} \times \vec{\omega}$, which yields $\mathbf{v} = \mathbf{t} \times \vec{\omega} + \dot{\mathbf{t}}$. The vector $\mathbf{v}$ is known as the linear or translational velocity. Using this, the matrix representation of the tangent operator reads

$$ \Gamma = \begin{pmatrix} \Omega & \mathbf{t} \times \vec{\omega} + \dot{\mathbf{t}} \\ \mathbf{0}^T & 0 \end{pmatrix}. \tag{2.11} $$

For a detailed derivation of tangent operators and their fundamental role as the elements of the Lie algebra $se(3)$ readers are referred to e.g. [34], pp. 29-35.

Twists in 6-vector representation

Since the sixteen elements of a tangent operator Γ only depend on six different parameters $\vec{\omega}$ and $\mathbf{v}$, these parameters can be assembled formally into a 6×1 vector. Such six-vectors are badged by a '^' throughout this work, which follows the notation also used by Beyer [35]:

$$ \hat{\mathbf{v}} = \begin{pmatrix} \vec{\omega} \\ \mathbf{t} \times \vec{\omega} + \dot{\mathbf{t}} \end{pmatrix}. \tag{2.12} $$

(Note that the role of a tangent operator in Eq. (2.10), i.e. relating the trajectory and velocity of points, shall be ignored for this purpose) A general six-vector $\hat{\mathbf{v}} = (\vec{\omega},\ \mathbf{v})^T$ satisfies $(\vec{\omega})^T\mathbf{v} \neq 0$ and is called a *screw*, first invented by Sir Robert Stawell Ball in his treatise *The Theory of Screws: A study in the dynamics of a rigid body* from 1876, [36].

2.1.3. Lines as Special Cases of Screws

The theory of screws provides a powerful tool since its elements - the screws - can be used to model several further quantities beside velocities that are of interest in the analysis and synthesis of linkages. A particular example are lines that are needed to model the axes of revolute

or cylindrical joints in a linkage. In order to see how to fit a line into a screw, consider the parameter form of a line:

$$\mathbf{r}(\lambda) = \mathbf{p} + \lambda \mathbf{h}, \quad \lambda \in \mathbb{R}, \tag{2.13}$$

where $\mathbf{h}$ is a (non-normalized) direction and $\mathbf{p}$ is an arbitrary point on the line . Now multiply on the right by $\times\mathbf{h}$ to obtain the fact, that any point on the line produces the same *moment of a line*:

$$\mathbf{r} \times \mathbf{h} = \mathbf{p} \times \mathbf{h}. \tag{2.14}$$

Hence, beside the parameter form, a line is also defined by its direction and moment, which together may be assembled into a 6×1 vector $(\mathbf{h},\ \mathbf{p} \times \mathbf{h})^T$. This has the from of a specific screw and the coordinates are also known as the *Plücker coordinates* of a line screw, named after Julius Plücker. However, this is not unique since any amount $|\mathbf{h}|$ may be used to define the line. Therefore, it may also be convenient to use a normalized direction $\mathbf{s} = \frac{\mathbf{h}}{|\mathbf{h}|}$. For a general line with direction $\mathbf{l}$ and location $\mathbf{p}$ the following notation is used within the work:

$$\hat{\mathbf{l}} = \begin{pmatrix} \mathbf{l} \\ \mathbf{p} \times \mathbf{l} \end{pmatrix}. \tag{2.15}$$

If a particular line or different lines $\hat{\mathbf{a}}$, $\hat{\mathbf{b}}$, ... need to be defined, the notation $\hat{\mathbf{a}} = (\mathbf{a},\ \mathbf{p}_a \times \mathbf{a})^T$, $\hat{\mathbf{b}} = (\mathbf{b},\ \mathbf{p}_b \times \mathbf{b})^T$, ... will be used to distinguish the lines.

2.1.4. Screw Transformations

The convenience of assembling the direction and moment of a line into a 6×1 vector can be seen by considering the spatial displacement of a line. This is easily constructed by considering the direction being written in terms of two vectors ${}^W\mathbf{p}$ and ${}^W\mathbf{q}$ both pointing from the origin of W to two corresponding points on the line:

$${}^W\hat{\mathbf{l}} = \left({}^W\mathbf{l},\ {}^W\mathbf{p} \times {}^W\mathbf{l}\right)^T = \left({}^W\mathbf{q} - {}^W\mathbf{p},\ {}^W\mathbf{p} \times ({}^W\mathbf{q} - {}^W\mathbf{p})\right)^T. \tag{2.16}$$

Now, since the line may be a part of a moving link (i.e. it may represent a revolute axis), the W-frame coordinates of $\mathbf{p}$ and $\mathbf{q}$ are obtained from Eq. (2.1) as ${}^W\mathbf{p} = {}^W\mathbf{R}_B \cdot {}^B\bar{\mathbf{p}} + {}^W\mathbf{t}_B$ and ${}^W\mathbf{q} = {}^W\mathbf{R}_B \cdot {}^B\bar{\mathbf{q}} + {}^W\mathbf{t}_B$ and assembling this into Eq. (2.16) and rearranging yields

$$\begin{aligned} {}^W\hat{\mathbf{l}} &= \begin{pmatrix} {}^W\mathbf{R}_B \cdot ({}^B\bar{\mathbf{q}} - {}^B\bar{\mathbf{p}}) \\ {}^W\mathbf{t}_B \times \left({}^W\mathbf{R}_B \cdot ({}^B\bar{\mathbf{q}} - {}^B\bar{\mathbf{p}})\right) + {}^W\mathbf{R}_B \cdot \left({}^B\bar{\mathbf{p}} \times ({}^B\bar{\mathbf{q}} - {}^B\bar{\mathbf{p}})\right) \end{pmatrix} = \\ &= \begin{pmatrix} {}^W\mathbf{R}_B \cdot {}^B\bar{\mathbf{l}} \\ {}^W\mathbf{t}_B \times \left({}^W\mathbf{R}_B \cdot {}^B\bar{\mathbf{l}}\right) + {}^W\mathbf{R}_B \cdot \left({}^B\bar{\mathbf{p}} \times {}^B\bar{\mathbf{l}}\right) \end{pmatrix}. \end{aligned} \tag{2.17}$$

Modelling the crossproduct ${}^W\mathbf{t}_B\times$ by introducing a skew symmetric matrix ${}^W\tilde{\mathbf{t}}_B$ assembled from the parameters of ${}^W\mathbf{t}_B$ allows to assemble the motion parameters in a 6×6 matrix ${}^W\hat{\mathbf{T}}_B$, that represents the *spatial displacement of a line*:

$$\underbrace{\begin{pmatrix} {}^W\mathbf{l} \\ {}^W\mathbf{p} \times {}^W\mathbf{l} \end{pmatrix}}_{{}^W\hat{\mathbf{l}}} = \underbrace{\begin{pmatrix} {}^W\mathbf{R}_B & \mathbf{0} \\ {}^W\tilde{\mathbf{t}}_B {}^W\mathbf{R}_B & {}^W\mathbf{R}_B \end{pmatrix}}_{{}^W\hat{\mathbf{T}}_B} \cdot \underbrace{\begin{pmatrix} {}^B\mathbf{l} \\ {}^B\bar{\mathbf{p}} \times {}^B\mathbf{l} \end{pmatrix}}_{{}^B\hat{\mathbf{l}}}. \tag{2.18}$$

Note that $\bar{\mathbf{l}} \equiv \mathbf{l}$ was taken into account here. Furthermore it can be shown, that the result also holds for general screws (see e.g. [33], pp. 292-293), which can be used to transform the

coordinates of a velocity screw. In order to describe the *relative displacement of a line* eliminate ${}^{B}\hat{\mathbf{l}}$ from ${}^{W}\hat{\mathbf{l}}^{i} = {}^{W}\hat{\mathbf{T}}^{i}_{B} \cdot {}^{B}\hat{\mathbf{l}}$ and ${}^{W}\hat{\mathbf{l}}^{j} = {}^{W}\hat{\mathbf{T}}^{j}_{B} \cdot {}^{B}\hat{\mathbf{l}}$ to obtain:

$$\hat{\mathbf{l}}^{j} = \hat{\mathbf{T}}^{ij}_{B} \cdot \hat{\mathbf{l}}^{i} = \begin{pmatrix} \mathbf{R}^{ij}_{B} & \mathbf{0} \\ \tilde{\mathbf{t}}^{ij}_{B}\mathbf{R}^{ij}_{B} & \mathbf{R}^{ij}_{B} \end{pmatrix} \cdot \hat{\mathbf{l}}^{i}. \tag{2.19}$$

2.1.5. Dual Vector Algebra of Screws

As one can see from Eq. (2.17) and (2.18) the structure of the screw transformation matrix ${}^{W}\hat{\mathbf{T}}_{B}$ yields that the direction of a line is only affected by rotations while the moment of a line is transformed by translational and rotational parts of the displacement. This and further properties of screws and the group of rigid motion allow to consider screws as elements of a specific algebra, called the *dual vector algebra of screws*, which preserves the algebraic properties. For a detailed introduction into this topic the reader is referred to Dimentberg [37] or also Beyer [35].

The construction of the dual algebra begins by defining the set of dual numbers $\hat{a} = a_1 + \sigma a_2$, where a_1 and a_2 are real numbers and the dual unit σ is manipulated as $\sigma^2 = 0$. Note that usually the symbol ε is used for the dual unit, which however is used throughout the work as specific angle, see chapter 4. Hence, we follow Rudolf Beyer, who used the symbol σ in [35].

The set of dual numbers forms a commutative ring on which (i) addition $\hat{a} + \hat{b} = a_1 + b_1 + \sigma(a_2 + b_2)$, (ii) subtraction $\hat{a} - \hat{b} = a_1 - b_1 + \sigma(a_2 - b_2)$ and (iii) a multiplication $\hat{a}\hat{b} = a_1 b_1 + \sigma(a_1 b_2 + b_1 a_2)$ (and (iv) a division, which is not needed here) among two elements is defined. If one allows vectors and matrices instead of real numbers, the result is a vector algebra, that represents a powerful tool to manipulate screws. An introductive example demonstrating this is the spatial displacement of a screw obtained from a multiplication of a screw by a screw transformation matrix, modelled as dual vector $\hat{\mathbf{v}} = \vec{\omega} + \sigma\mathbf{v}$ and a dual matrix $\hat{\mathbf{T}} = \mathbf{R} + \sigma\tilde{\mathbf{t}}\mathbf{R}$:

$$\hat{\mathbf{T}} \cdot \hat{\mathbf{v}} = \left(\mathbf{R} + \sigma\tilde{\mathbf{t}}\mathbf{R}\right)(\vec{\omega} + \sigma\mathbf{v}) = \mathbf{R} \cdot \vec{\omega} + \sigma\left(\tilde{\mathbf{t}}\mathbf{R} \cdot \vec{\omega} + \mathbf{R} \cdot \mathbf{v}\right). \tag{2.20}$$

When the screw represents a line, a comparison of this result with Eq. (2.17) or (2.18) shows that the multiplication of a line in dual vector form by a dual matrix assembled from the parameters of a screw transformation matrix yields the spatial displacement of the line.

Dual scalar product of two screws

The linearity of the scalar product of vectors allows the definition of the corresponding counter part in the dual vector algebra. Respecting $\sigma^2 = 0$ then yields the *dual scalar product*:

$$(\vec{\omega}_1 + \sigma\mathbf{v}_1) \cdot (\vec{\omega}_2 + \sigma\mathbf{v}_2) = (\vec{\omega}_1)^T \cdot \vec{\omega}_2 + \sigma\left((\vec{\omega}_1)^T \cdot \mathbf{v}_2 + (\mathbf{v}_1)^T \cdot \vec{\omega}_2\right). \tag{2.21}$$

Note that $\cdot$ among vectors denotes the scalar product so that the result ist a dual scalar composed from two real numbers.

Remark: Similarly a *dual vector product* can be defined as $(\vec{\omega}_1 + \sigma\mathbf{v}_1) \times (\vec{\omega}_2 + \sigma\mathbf{v}_2) = \vec{\omega}_1 \times \vec{\omega}_2 + \sigma(\vec{\omega}_1 \times \mathbf{v}_2 + \mathbf{v}_1 \times \vec{\omega}_2)$, where the result is another dual vector. An interesting aspect is that the dual vector product in fact represents the Lie product defined in the Lie algebra $se(3)$, which means that this Lie algebra represents the algebra of screws, called screw theory, see also [34], pp. 29-35.

Dual scalar product of two lines

If the screws in Eq. (2.21) represent two lines $\hat{\mathbf{a}} = (\mathbf{a},\ \mathbf{p}_a \times \mathbf{a})^T$ and $\hat{\mathbf{b}} = (\mathbf{b},\ \mathbf{p}_b \times \mathbf{b})^T$, where $\mathbf{a}$ and $\mathbf{b}$ are unit vectors, the dual scalar product yields

$$(\mathbf{a} + \sigma\mathbf{p}_a \times \mathbf{a}) \cdot (\mathbf{b} + \sigma\mathbf{p}_b \times \mathbf{b}) = (\mathbf{a})^T \cdot \mathbf{b} + \sigma \left((\mathbf{a})^T \cdot (\mathbf{p}_b \times \mathbf{b}) + (\mathbf{p}_a \times \mathbf{a})^T \cdot \mathbf{b} \right). \tag{2.22}$$

The real part of the resulting dual scalar clearly represents the cosine of the angle α enclosed by $\mathbf{a}$ and $\mathbf{b}$: $(\mathbf{a})^T \cdot \mathbf{b} = \cos\alpha$.

Since the triple products in (2.22) are invariant under a circular shift of the operators the dual part can be rearranged as:

$$\begin{aligned} (\mathbf{a})^T \cdot (\mathbf{p}_b \times \mathbf{b}) + (\mathbf{p}_a \times \mathbf{a})^T \cdot \mathbf{b} &= (\mathbf{p}_b)^T \cdot (\mathbf{b} \times \mathbf{a}) + (\mathbf{p}_a)^T \cdot (\mathbf{a} \times \mathbf{b}) = \\ &= (\mathbf{p}_a - \mathbf{p}_b)^T \cdot (\mathbf{a} \times \mathbf{b}). \end{aligned} \tag{2.23}$$

Next, consider $\mathbf{p}_a$ and $\mathbf{p}_b$ being points that define the intersections of the common normal line between $\hat{\mathbf{a}}$ and $\hat{\mathbf{b}}$ (Note that this definition is valid since Eq. (2.14) yielded that the choice of the point locating a line in space does not affect the moment of the line). Then vectors $(\mathbf{p}_a - \mathbf{p}_b)$ and $\mathbf{a} \times \mathbf{b}$ may be either parallel or antiparallel, which yields

$$\begin{aligned} (\mathbf{p}_a - \mathbf{p}_b)^T \cdot (\mathbf{a} \times \mathbf{b}) &= \pm|\mathbf{p}_a - \mathbf{p}_b||\mathbf{a} \times \mathbf{b}| = \\ &= \pm l \sin\alpha, \end{aligned} \tag{2.24}$$

where l represents the common normal distance between $\hat{\mathbf{a}}$ and $\hat{\mathbf{b}}$. Hence, the dual scalar product of two line screws yields

$$(\mathbf{a} + \sigma\mathbf{p}_a \times \mathbf{a}) \cdot (\mathbf{b} + \sigma\mathbf{p}_b \times \mathbf{b}) = \cos\alpha \pm \sigma l \sin\alpha, \tag{2.25}$$

which allows to study the relative location between two lines, e.g. whether they are parallel, intersect, etc.. In fact it can furthermore be shown, that the dual scalar product of two lines actually satisfies

$$(\mathbf{a} + \sigma\mathbf{p}_a \times \mathbf{a}) \cdot (\mathbf{b} + \sigma\mathbf{p}_b \times \mathbf{b}) = \cos\alpha - \sigma l \sin\alpha, \tag{2.26}$$

which may also be retraced from [35] pp. 74-77.

2.2. Kinematic Analysis of Linkages

Essential steps in the analysis of a kinematic chain with given kinematic dimensions are definition or determination of the movement of the chain. On the one hand, this refers to the *forward kinematics analysis problem* where it is the concern to find the spatial pose of a particular link or frame for given joint parameters. On the other hand, one has to deal with the *inverse kinematics analysis problem* where the goal is to find the joint parameters for a given spatial pose of a particular link or frame. Note that one may furthermore distinguish between analysis at the position, velocity, acceleration level or also higher levels of differentiation. The forward or inverse problem particularly differ for serial and parallel structures of different degrees of freedom. In order to determine this d.o.f. or mobility, a mobility analysis may be performed, where a classical approach is provided in brief in sect. 2.2.1.

In order to solve either the forward or inverse problem a mathematical description of the chain, known as the *kinematics equations of a chain*, is required, which captures the geometry

(kinematic dimensions) as well as the movement (joint parameters and link movement). A well known way to formulate kinematics equations is the *Denavit-Hartenberg convention*, which is given in sect. 2.2.2. This directly applies to planar, spherical and spatial serial structures and can also be used to state *kinematic constraint equations* of parallel structures. Cases exist, where such constraint equations can be solved in a unified manner. This is shown for the spherical four-bar in sect. 2.2.3, where the result is the solution of the forward analysis problem of spherical four-bars. This is also required for velocity considerations provided in sect. 2.2.4.

Analysis results of this section will be particularly required in sect. 4.1, where analysis procedures are presented for spherically constrained linkages.

2.2.1. The Mobility Formula

The question of whether a certain linkage topology consisting of a number of links and joints is actually mobile, leads to what is known as linkage mobility analysis. The goal is to determine the number of degrees of freedom (d.o.f.) of a given linkage structure. The mobility formula provides a counting formula to calculate the d.o.f. of a system consisting of n links. First neglecting the set of joints the d.o.f. is $M = 6n$, according to the three translational and three rotational d.o.f. each link has in space. Note that in the case of purely planar or spherically moveable systems the result is $M = 3n$, because of the three-parameter motion subgroups $SE(2)$ and $SO(3)$.

When the links are connected by g joints, each introducing c_i kinematic constraints, the d.o.f. of the system is reduced such that $M = 6n - \sum_{i=1}^{g} c_i$. Because it is more common to deal with a joint's d.o.f. than speaking of constraints, the freedom $f = 6 - c$ a joint allows is used to describe the mobility of the system. The result is $M = 6n - \sum_{i=1}^{g}(6 - f_i) = 6(n-g) + \sum_{i=1}^{g} f_i$, where f_i is the d.o.f. allowed by the i'th joint. Because at least one link of a linkage is always fixed, the number of moving links in fact is $n-1$, which yields

$$M = 6(n-1-g) + \sum_{i=1}^{g} f_i \text{ (space)} \quad \text{or} \quad M = 3(n-1-g) + \sum_{i=1}^{g} f_i \text{ (plane, sphere)} . \tag{2.27}$$

Equation (2.27) is known as the mobility formula, which yields the d.o.f. of a given structure. If for instance a given linkage structure yields $M = 1$, there is only one actuator required to perform a defined movement of the complete linkage.

In the case of spatial overconstrained linkages it happens that Eq. (2.27) yields a zero or negative mobility for a given structure, even though it is movable. An example is the spatial Bennett mechanism consisting of $n = 4$ links and $g = 4$ revolute joints. This yields $M = -2$ even though the system moves with mobility one, see also appendix C.3. In this case the structure contains some special kinematic dimensions such as symmetrically arranged hinges, which preserve the mobility. The total number of these dimensions is often written as a formal sum $\sum s$ so that it can be added to Eq. (2.27):

$$M = 6(n-1-g) + \sum_{i=1}^{g} f_i + \sum s . \tag{2.28}$$

In the case of overconstrained kinematic chains, as they will be introduced in chapter 3, calculating the correct mobility requires detailed considerations of special kinematic dimensions.

Beside the mobility formula also various other approaches exist, which allow to detect the mobility of a linkage. Here, for instance the so called *twist loop equations* of a structure may be used, which originate as specific linear combinations of screws from the time derivatives of

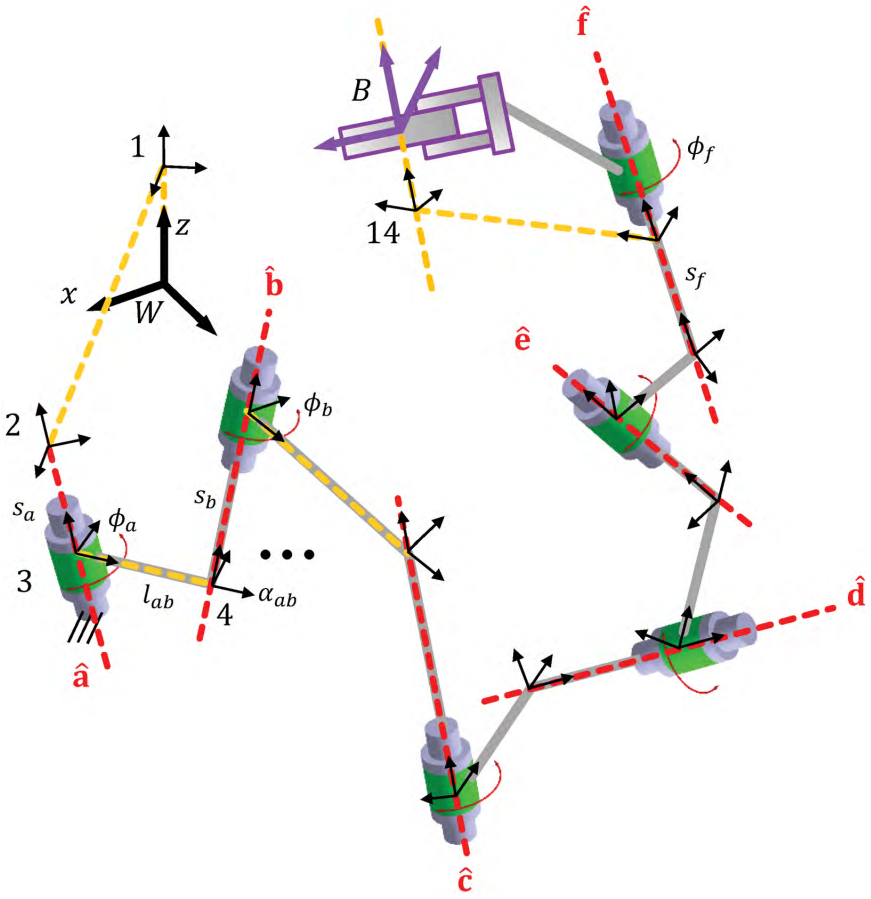

Figure 2.2.: The general spatial serial 6R chain with skew joint axes and coordinate frames associated with the Denavit-Hartenberg kinematics equations

the kinematics equations of the linkage. Then, the result is an instantaneous mobility analysis, see also [38], [39] or [40]. Further approaches consider connectivities and constraint analysis of building block chains of complex parallel kinematic chains, e.g. [41] or [42]. In [43] Stachel provides a detailed flexibility analysis of various overconstrained mechanisms. Flexible mechanisms are those, who are analytically able to change their spatial shape with respect to given input parameters. Examples are deployable polyhedral structures, linkage networks or also rigid origami folding patterns.

2.2.2. The Denavit-Hartenberg Kinematics Equations

In order to describe the geometry (kinematic dimensions) as well as the movement (joint parameters and link movement) of kinematic chains a mathematical description of the chain, known as the kinematics equations, is required. A well-known way to formulate kinematics equations is the Denavit-Hartenberg convention introduced in the following using the example of a general spatial 6R serial chain.

A general 6R chain with 6 d.o.f. (Fig. 2.2) can be viewed as a sequence of skew joint axes. A minimum set of parameters (the *Denavit-Hartenberg parameters*) consists of the kinematic dimensions as well as joint parameters and is represented by the angles and common normals among two consecutive joint axes as well as the angles and normal distances among each consecutive pair of the common normals.

A key feature of the Denavit-Hartenberg convention is that one may define the spatially displaced pose of a frame B, located somewhere in the end link of the chain by perfoming a composition of displacements only using screw coordinate displacements $\mathbf{T}_x$ and $\mathbf{T}_z$, introduced in section 2.1.1, Eq. (2.8). To retrace that, consider coordinate frames being attached along the normals of the chain as shown for the general 6R in Fig. 2.2. This allows to write the kinematics equations as an alternating composition of homogeneous transforms $\mathbf{T}_z$ and $\mathbf{T}_x$:

$$ {}^{W}\mathbf{T}_B = {}^{W}\mathbf{T}_{1,z}{}^{1}\mathbf{T}_{2,x}{}^{2}\mathbf{T}_{3,z}{}^{3}\mathbf{T}_{4,x}{}^{4}\mathbf{T}_{5,z}{}^{5}\mathbf{T}_{6,x}{}^{6}\mathbf{T}_{7,z}\ldots{}^{13}\mathbf{T}_{14,x}{}^{14}\mathbf{T}_{B,z}, \tag{2.29} $$

where the transformations ${}^{W}\mathbf{T}_2 = {}^{W}\mathbf{T}_{1,z}{}^{1}\mathbf{T}_{2,x}$ as well as ${}^{13}\mathbf{T}_B = {}^{13}\mathbf{T}_{14,x}{}^{14}\mathbf{T}_{B,z}$ describe the relative location between axis $\hat{\mathbf{a}}$ or $\hat{\mathbf{f}}$ and frame W or B. The remaining z-transformations capture the joint angles $\phi_a,\ldots,\phi_f$ around axes $\hat{\mathbf{a}},\ldots,\hat{\mathbf{f}}$ as well as the constant offsets $s_a,\ldots,s_f$. For instance s_a measures the distance between frames 2 and 3 along axis $\hat{\mathbf{a}}$. The remaining x-transformations in Eq. (2.29) include the constant angles $\alpha_{ab},\ldots,\alpha_{ef}$ and distances $l_{ab},\ldots,l_{ef}$ measured between the different joint axes. Using these parameters Eq. (2.29) can be rewritten as

$$ {}^{W}\mathbf{T}_B = {}^{W}\mathbf{T}_2{}^{2}\mathbf{T}_{3,z}(\phi_a,s_a){}^{3}\mathbf{T}_{4,x}(\alpha_{ab},l_{ab}){}^{4}\mathbf{T}_{5,z}(\phi_b,s_b)\cdots{}^{12}\mathbf{T}_{13,z}(\phi_f,s_f){}^{13}\mathbf{T}_B. \tag{2.30} $$

These are the Denavit-Hartenberg kinematics equations of the general 6R with arbitrarily located frames W and B. Note, that this view point is considered here, because it allows the derivation of relative kinematics equations, as shown in sect. B.1. For analysis it is convenient to consider W or B coinciding with frames 2 or 13 and the result is a more compact form of the kinematics equations.

Figure 2.2 will serve as certain 'general reference linkage' for the derivation of kinematics equations of simpler chains. This includes kinematics equations of spherical serial chains in the next section but also the matrix loop equation of a spherical four-bar, which is a parallel kinematic structure.

Kinematics Equations of Spherical Chains

An important special case is the class of spherical serial structures, which are able to produce movement within the three-parameter sub-group $SO(3)$. A chain whose end effector is able to perform an arbitrary motion in $SO(3)$ is the spherical 3R chain with intersecting joint axes. A 3R chain is obtained by cutting off joints $\hat{\mathbf{d}}$, $\hat{\mathbf{e}}$ and $\hat{\mathbf{f}}$ from the general 6R chain in Fig. 2.2. In order to state kinematics equations frames W and B are considered being located at the point of intersection of the joints and should have their z-axes coinciding with the directions of $\hat{\mathbf{a}}$ and $\hat{\mathbf{c}}$. The result are purely 'spherical' kinematics equations:

$$ {}^{W}\mathbf{R}_B = {}^{W}\mathbf{R}_{1,z}(\phi_a){}^{1}\mathbf{R}_{2,x}(\alpha_{ab}){}^{2}\mathbf{R}_{3,z}(\phi_b){}^{3}\mathbf{R}_{4,x}(\alpha_{bc}){}^{4}\mathbf{R}_{B,z}(\phi_c). \tag{2.31} $$

2.2.3. Forward Position Analysis of Spherical Four-Bars

As it is the case for serial structures, the forward kinematics problem of a parallel structure consists in determining movement of the chain for given joint parameters. However, compared to serial structures parallel systems always have kinematic loops and hence also have non-actuated passive joints, whose joint movement results from *loop-based kinematic constraints* in the structure. To determine the unknown joint movement a loop-based forward position analysis of parallel structures may be performed. This can be done using the *constraint equations of a loop*, which, can be derived using the Denavit-Hartenberg convention introduced in sect. 2.2.2.

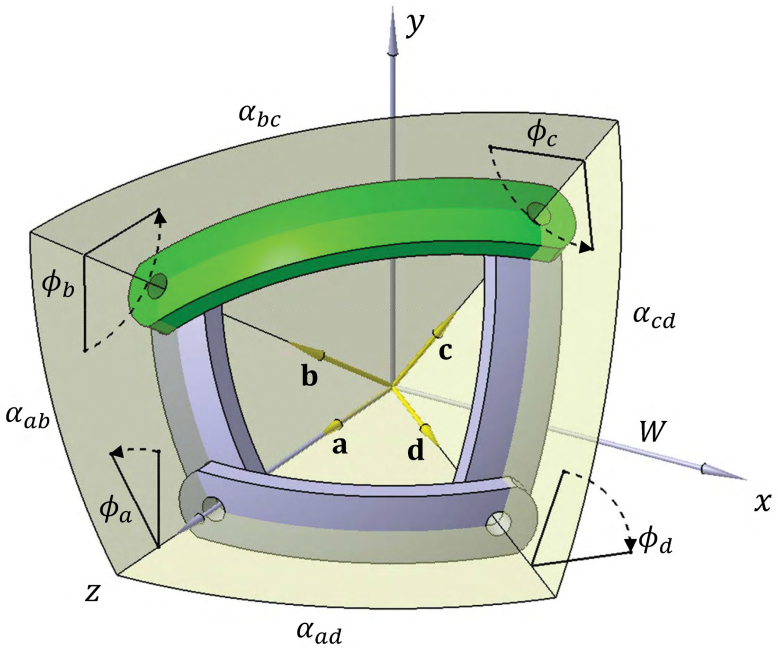

Figure 2.3.: The general spherical four-bar with angles and axes that allow to state matrix loop equations using the Denavit-Hartenberg kinematics equations

For parallel structures several solutions of the forward kinematics problem may exist, which yield different sets of passive joint parameter values for a given actuation. These result in different *assembly modes* and finding all such modes is a challenging part in forward position analysis of a parallel structure. A prominent example is the forward kinematic problem of the 6-SPS parallel structure (general Steward-Gough platform), which has been shown to have 40 different solutions at most (see e.g. [44]).

It can be shown that for specific types of parallel structures constraint equations of a loop can be transformed into a *standard form of a constraint equation*. This is shown for the spherical four-bar linkage from Fig. 2.3, that consist of a single loop and which is the building block of the systems analyzed in sect. 4.1. Based on *spherical Denavit-Hartenberg matrix loop equations* the standard form of a constraint equation is derived and it is shown that this can easily be solved using the well-known *tangent-half-angle solution formula*.

The matrix loop equation of spherical four-bars

A general spherical four-bar with angles $\phi_a,\ldots,\alpha_{ad}$ and directions $\mathbf{a},\ldots,\mathbf{d}$ is shown in Fig. 2.3 and allows to state the matrix loop equations. These are given by the following alternating composition of x- and z-rotations along the loop:

$$\begin{aligned} {}^{W}\mathbf{R}_{1,z}(\phi_a)\,{}^{1}\mathbf{R}_{2,x}(-\alpha_{ab})\,{}^{2}\mathbf{R}_{3,z}(\phi_b)\,{}^{3}\mathbf{R}_{4,x}(\alpha_{bc})\,{}^{4}\mathbf{R}_{5,z}(\phi_c) \\ {}^{5}\mathbf{R}_{6,x}(-\alpha_{cd})\,{}^{6}\mathbf{R}_{7,z}(-\phi_d)\,{}^{7}\mathbf{R}_{8,x}(-\alpha_{ad})\,{}^{8}\mathbf{R}_{W,z}(-\frac{\pi}{2}) = \mathbf{E}. \end{aligned} \tag{2.32}$$

Note that frame W is considered being located at the point of intersection, such that it has its z-axis aligned with direction $\mathbf{a}$ and its y-axis perpendicular to the plane spanned by $\mathbf{a}$ and $\mathbf{d}$. The remaining frames 1,...,8 are all located at the point of intersection and Fig 2.4 provides a graphical depiction of the matrix loop equation. The different signs arise from the definition of angles.

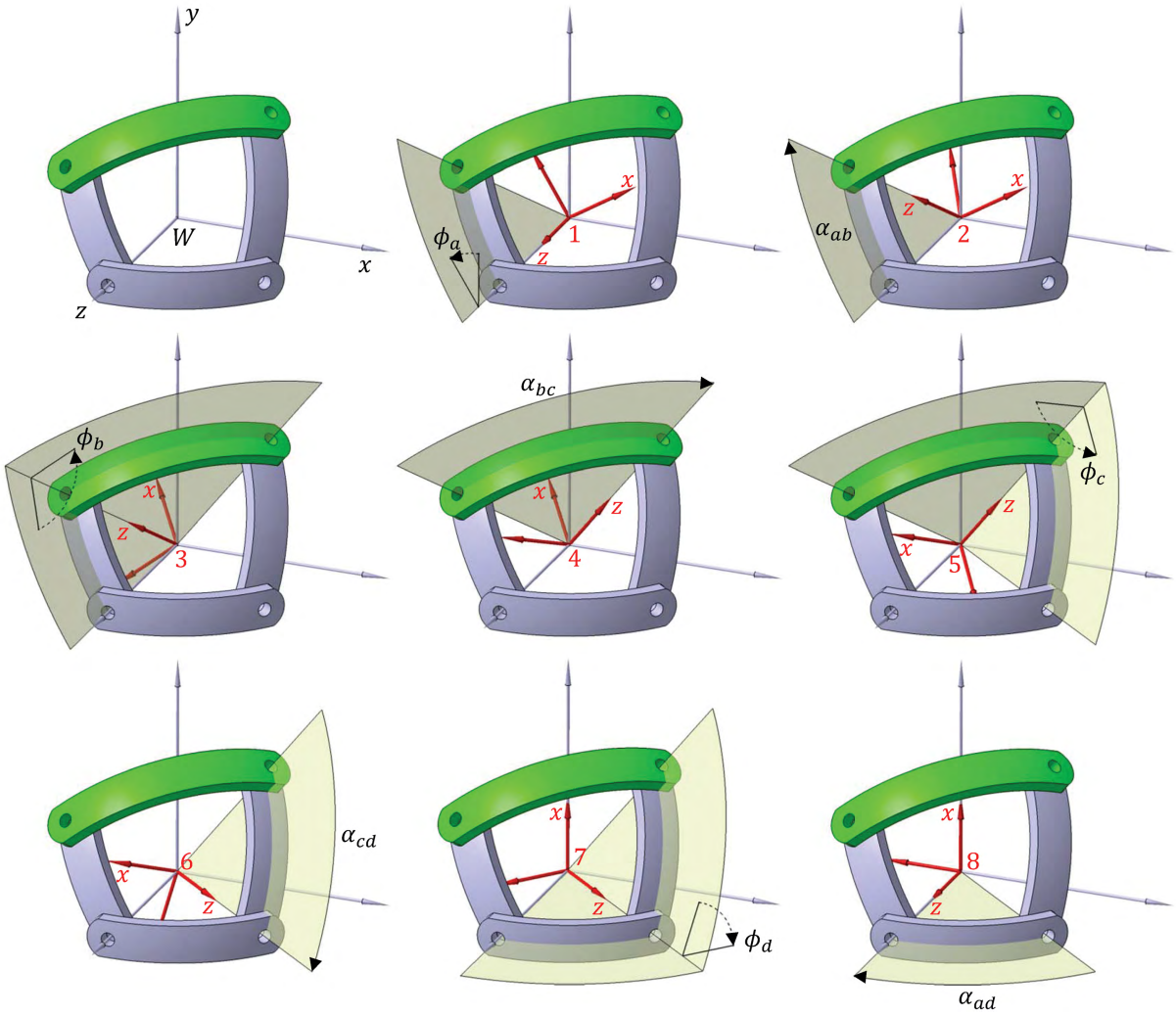

Figure 2.4.: Transformation sequence of coordinate frames along the spherical four-bar loop

Equation (2.32) can be verified using the following values, which belong to the structure from Fig. 2.3: $\phi_a = 32.020841$ deg, $\alpha_{ab} = 40$ deg, $\phi_b = 99.139761$ deg, $\alpha_{bc} = 70$ deg, $\phi_c = 87.383215$ deg, $\alpha_{cd} = 55$ deg, $\phi_d = 71.160834$ deg, $\alpha_{ad} = 50$ deg. Herein angles ϕ were measured in a CAD-system.

In a general analysis scenario dimensions α as well as one angle ϕ is known as a given input, while the remaining joint angles are unknown. Note that this is because the spherical four-bar moves with one single d.o.f.. Then Eq. (2.32) provides a set of non-linear equations, that can be solved to obtain the unknown joint angles. Further approaches towards solving matrix loop equations (also for multiloop structures) can be found in [33] or [45].

The constraint equation of a single loop

Another systematic approach to solve the forward position problem for the unknown joint angles of the four-bar uses the (normalized) directions $\mathbf{a},\ldots,\mathbf{d}$ in combination with rotation matrices from Eq. (2.32). Note, that axes $\mathbf{a}$ and $\mathbf{d}$ are known since they are considered to be fixed. If ϕ_a is considered to be given from an actuator one may write the following constraint equation for

the loop:

$$\left({}^{W}\mathbf{c}\right)^{T} \cdot {}^{W}\mathbf{d} = \cos\alpha_{cd}, \tag{2.33}$$

where

$$\begin{aligned} {}^{W}\mathbf{c} &= {}^{W}\mathbf{R}_{1,z}(\phi_a)\,{}^{1}\mathbf{R}_{2,x}(-\alpha_{ab})\,{}^{2}\mathbf{R}_{3,z}(\phi_b)\,{}^{3}\mathbf{R}_{4,x}(\alpha_{bc}) \cdot {}^{4}\mathbf{c} \\ {}^{W}\mathbf{d} &= \left({}^{7}\mathbf{R}_{8,x}(-\alpha_{ad})\,{}^{8}\mathbf{R}_{W,z}(-\frac{\pi}{2}))\right)^{T} \cdot {}^{7}\mathbf{d}. \end{aligned} \tag{2.34}$$

Observe that ${}^{4}\mathbf{c} = {}^{7}\mathbf{d} = (0\ 0\ 1)^{T}$. After inserting Eq. (2.34), Eq. (2.33) can be expanded and rearranged to yield the scalar standard form of a constraint equation as

$$\mathscr{A}_b(\phi_a)\cos\phi_b + \mathscr{B}_b(\phi_a)\sin\phi_b = \mathscr{C}_b(\phi_a), \tag{2.35}$$

where the parameters $\mathscr{A}$, $\mathscr{B}$ and $\mathscr{C}$ are given as

$$\begin{aligned} \mathscr{A}_b(\phi_a) &= \cos\alpha_{ad}\sin\alpha_{ab}\sin\alpha_{bc} + \cos\alpha_{ab}\sin\phi_a\sin\alpha_{bc}\sin\alpha_{ad} \\ \mathscr{B}_b(\phi_a) &= \cos\phi_a\sin\alpha_{bc}\sin\alpha_{ad} \\ \mathscr{C}_b(\phi_a) &= \cos\alpha_{cd} - \cos\alpha_{ab}\cos\alpha_{bc}\cos\alpha_{ad} + \\ &\quad + \cos\alpha_{bc}\sin\phi_a\sin\alpha_{ab}\sin\alpha_{ad}. \end{aligned} \tag{2.36}$$

An equation of the type $\mathscr{A}\cos\phi + \mathscr{B}\sin\phi = \mathscr{C}$ can be solved using tangent-half-angle substitutions for the sine and cosine to yield

$$\tan\frac{\phi}{2} = \frac{\mathscr{B} \pm \sqrt{\mathscr{A}^2 + \mathscr{B}^2 - \mathscr{C}^2}}{\mathscr{A} + \mathscr{C}}, \tag{2.37}$$

see e.g. [46], p. 296. Herein the two different solutions correspond to the *two different assembly modes of a four-bar* for a given input angle. Equation (2.37) is the well-known tangent-half-angle solution formula, which only has real solutions if

$$\mathscr{A}^2 + \mathscr{B}^2 \geq \mathscr{C}^2. \tag{2.38}$$

Then one may solve Eq. (2.37) for ϕ. In the specific case of Eq. (2.35) this yields the angular relationship $\phi_b(\phi_a)$, which represents the joint rotation of the joint axis **b**.

A particular linkage configuration is that, where $\mathscr{A}^2 + \mathscr{B}^2 = \mathscr{C}^2$, because this corresponds to the limit of an input angle ϕ, e.g. [33]. In fact, this configuration of the linkage is specifically singular in character and will be of particular interest in the later sections.

Instead of stating the constraint equation (2.33) one may also calculate

$$\left({}^{W}\mathbf{b}\right)^{T} \cdot {}^{W}\mathbf{c} = \cos\alpha_{bc} \tag{2.39}$$

for a given ϕ_a, where now

$$\begin{aligned} {}^{W}\mathbf{b} &= {}^{W}\mathbf{R}_{1,z}(\phi_a)\,{}^{1}\mathbf{R}_{2,x}(-\alpha_{ab}) \cdot {}^{2}\mathbf{b} \\ {}^{W}\mathbf{c} &= \left({}^{5}\mathbf{R}_{6,x}(-\alpha_{cd})\,{}^{6}\mathbf{R}_{7,z}(-\phi_d)\,{}^{7}\mathbf{R}_{8,x}(-\alpha_{ad})\,{}^{8}\mathbf{R}_{W,z}(-\frac{\pi}{2}))\right)^{T} \cdot {}^{5}\mathbf{c}, \end{aligned} \tag{2.40}$$

and ${}^{2}\mathbf{b} = {}^{5}\mathbf{c} = (0,\ 0,\ 1)^{T}$. This yields the standard form $\mathscr{A}_d(\phi_a)\cos\phi_d + \mathscr{B}_d(\phi_a)\sin\phi_d = \mathscr{C}_d(\phi_a)$. The result is the angular relationship $\phi_d(\phi_a)$ representing the joint rotation of the joint axis **d**.

The relations $\phi_b(\phi_a)$ and $\phi_d(\phi_a)$ together with the given input parameter ϕ_a, completely specify the movement of the three moving links of the four-bar. For this reason it is unnecessary to compute $\phi_c(\phi_a)$, which however may also be found from an appropriately stated constraint equation.

The procedure presented in this section may clearly also be executed for any input angle other that ϕ_a. The results are then different angular relations between angles and different limits on the input.

2.2.4. Twist-Loop Equations of Spherical Four-Bars

Particular configurations in a linkage occur when lines associated with the joint axes become linearly dependent. A physical interpretation of such situations is, that the mechanism loses its ability to resist external acting forces, even though there is an appropriately strong actuator. Such configurations are also termed singular configurations or singularities and are also the configurations where transmission properties become weak. See also see e.g. [47], [48] or [49] in the context.

In order to consider singularity aspects of the systems introduced in chapter 3, singularities of a spherical four-bar can be considered, which require the so called *twist loop equation of a spherical four-bar* introduced in the following.

Twist loop equations are obtained by studying the velocity properties of the four-bar using the matrix loop equation (2.32). Straight forward differentiating this equation with respect to time yields

$$\begin{aligned}\frac{\mathrm{d}}{\mathrm{d}t}\left(\mathbf{R}_z(\phi_a)\mathbf{R}_x(-\alpha_{ab})\ldots\mathbf{R}_z(-\frac{\pi}{2})\right) &= \dot{\mathbf{R}}_z(\phi_a,\dot{\phi}_a)\mathbf{R}_x(-\alpha_{ab})\ldots\mathbf{R}_z(-\frac{\pi}{2})+\\ &+\mathbf{R}_z(\phi_a)\ldots\dot{\mathbf{R}}_z(\phi_b,\dot{\phi}_b)\ldots\mathbf{R}_z(-\frac{\pi}{2})+\\ &+\mathbf{R}_z(\phi_a)\ldots\dot{\mathbf{R}}_z(\phi_c,\dot{\phi}_c)\ldots\mathbf{R}_z(-\frac{\pi}{2})+\\ &+\mathbf{R}_z(\phi_a)\ldots\dot{\mathbf{R}}_z(\phi_d,\dot{\phi}_d)\ldots\mathbf{R}_z(-\frac{\pi}{2})=\mathbf{0}. \quad (2.41)\end{aligned}$$

Note that the sub- and superscripts badging different coordinate frames were neglected here to keep overview in the equations. Multiplying this on the right by the inverse (transpose) of the left hand side of Eq. (2.32) yields

$$\begin{aligned}&\dot{\mathbf{R}}_z(\phi_a,\dot{\phi}_a)\left(\mathbf{R}_z(\phi_a)\right)^T+\mathbf{R}_z(\phi_a)\mathbf{R}_x(-\alpha_{ab})\dot{\mathbf{R}}_z(\phi_b,\dot{\phi}_b)\left(\mathbf{R}_z(\phi_b)\right)^T\left(\mathbf{R}_x(-\alpha_{ab})\right)^T\left(\mathbf{R}_z(\phi_a)\right)^T+\\ &\quad+\mathbf{R}_z(\phi_a)\ldots\dot{\mathbf{R}}_z(\phi_c,\dot{\phi}_c)\left(\mathbf{R}_z(\phi_c)\right)^T\ldots\left(\mathbf{R}_z(\phi_a)\right)^T+\\ &\quad+\mathbf{R}_z(\phi_a)\ldots\dot{\mathbf{R}}_z(\phi_d,\dot{\phi}_d)\left(\mathbf{R}_z(\phi_d)\right)^T\ldots\left(\mathbf{R}_z(\phi_a)\right)^T=\mathbf{0}. \quad (2.42)\end{aligned}$$

Herein the skew symmetric angular velocity matrices $\Omega_i=\dot{\mathbf{R}}_z(\phi_i,\dot{\phi}_i)\left(\mathbf{R}_z(\phi_i)\right)^T$ take the simple form

$$\Omega_i=\dot{\mathbf{R}}_z(\phi_i,\dot{\phi}_i)\left(\mathbf{R}_z(\phi_i)\right)^T=\dot{\phi}_i\begin{pmatrix}0&-1&0\\1&0&0\\0&0&0\end{pmatrix}. \quad (2.43)$$

Following sect. 2.1.2 and assembling the entries of a twist into a vector, here yields 3×1 angular velocity vectors $\vec{\omega}_i=\dot{\phi}_i(0,\,0,\,1)^T$. Note that these are measured in coordinate frames whose z-axes point along the directions **a**, **b**, **c** and **d**. However, pre- and post-multiplication by rotation matrices and their transpose in Eq. (2.42) is nothing but a transformation into W-frame

coordinates, so that the four angular velocity vectors measured in W are nothing but $\dot{\phi}_a{}^W\mathbf{a}$, $\dot{\phi}_b{}^W\mathbf{b}$, $\dot{\phi}_c{}^W\mathbf{c}$ and $\dot{\phi}_d{}^W\mathbf{d}$. Using this result, Eq. (2.42) can be written as

$$\dot{\phi}_a{}^W\mathbf{a} + \dot{\phi}_b{}^W\mathbf{b} + \dot{\phi}_c{}^W\mathbf{c} + \dot{\phi}_d{}^W\mathbf{d} = \mathbf{0}, \tag{2.44}$$

which is the vector notation of the *twist loop equation of a spherical four-bar*, used in sect. 4.1.3 to study transmission properties.

In the appendix, sect. A.2, Eq. (A.6) to Eq. (A.8), the standard form of a general screw is shown to have the form $\hat{\mathbf{v}} = \omega(\vec{v},\ \mathbf{p}_v \times \vec{v} + k\vec{v})^T$. When $k = 0$ this is a zero-pitch screw and the velocity is written in terms of the line $\hat{v} = (\vec{v},\ \mathbf{p}_v \times \vec{v})^T$ with direction $\vec{v}$, see sect. 2.1.3. When furthermore $\mathbf{p}_v$ is zero this line passes through the origin of a certain coordinate frame and the resulting velocity screw takes the form $\hat{\mathbf{v}} = \omega(\vec{v},\ \mathbf{0})^T$. This is just the case for the four velocities in Eq. (2.44), where the corresponding coordinate frame is W. Hence, Eq. (2.44) can be seen as a specific linear combination of line screws. See also sect. A.3 in the context, where screw systems are defined as linear combinations of independent screws). The result is, that studying the transmission properties in sect. 4.1.3 will be a line-based analysis of transmission properties.

2.3. Finite Position Dimensional Synthesis of Serial and Parallel Structures

This chapter provides different finite position dimensional synthesis approaches that will be used throughout the synthesis sections of the work, i.e. in sect. 4.2 and 4.3. The terminology 'finite position synthesis' (f.p.s.) was used by Roth [50] and it denotes a methodology, which allows to compute the kinematic dimensions of a linkage with given topology, such that it can be assembled in a prescribed finite number of task configurations. These configurations are given in terms of a discrete number of finitely separated task positions of specific links in a linkage, which corresponds to the number of unknown kinematic dimensions of the structure. This synthesis methodology is also called motion generation by Sandor and Erdman [5] or rigid body guidance by Suh [51].

Based on the simplest approach, which is the *synthesis of a single joint axis* connecting two links, the *constraint-based synthesis of planar spherical and spatial RR chains* as well as of *spatial GS and SS chains* is given. These serial kinematic chains are the building blocks of complex multilink mechanisms and are made up from three links, which are coupled by two joints. While the spatial SS chain uses two spherical or ball joints, the GS chain uses a gimbal and a spherical joint. Planar, spherical and spatial RR chains have revolute joints and either the property of parallel, intersecting or skew joint axes. The derivation of the synthesis equations of the SS and GS as well as of planar and spherical RR chains aims at providing one single synthesis equation, that can be used for each of these chains. This equation is based on the study of geometric constraints and may also be found in [52].

In order to synthesize complex multilink mechanisms different synthesis solutions of the building block chains introduced above can be joined together in a systematic way. This may be termed the *constraint-based synthesis of linkages* and is also the approach followed in the synthesis sections of this work. Here a specific approach is the *synthesis of mechanically constrained serial kinematic chains*, where the state of the art is given in sect. 2.3.6. Beside the constraint-based synthesis further f.p.s. methods such as the loop equation-based methods, e.g. [53], [54], [55], [56], dual quaternion synthesis, e.g. [57], [58], or also factorization methods e.g. [32] exist, which will not be used in this work, however.

2.3.1. Synthesis Using Finite Displacement Invariants

The simplest dimensional f.p.s. approach consists in finding a single joint axis for a given finite displacement task. In fact this can be done only for two finitely separated poses 1 and 2 and leads to calculation of an invariant line - namely the *screw axis of a relative displacement*. The approach is introduced in the appendix, sect. A.4 and A.5.

In the case of a general spatial displacement $\mathbf{T}_B^{12}$ this may yield a slide $s^{12} \neq 0$ (see sect. A.5), which means that the resulting screw axis corresponds to a cylindrical joint. In the case that $\mathbf{T}_B^{12}$ yields $s^{12} = 0$ the resulting screw axis corresponds to a revolute joint. This latter case may correspond to a planar or either a spherical relative displacement, which is discussed in the following.

Pole-based planar two-position synthesis of revolute joints

In the case that the task is planar, let's say the motion takes place in the *xy*-plane of W (or planes parallel to that), the entries in a 4×4 matrix $\mathbf{T}_B^{12}$ satisfy $\mathbf{t}_B^{12} = (x_t^{12},\, y_t^{12},\, 0)^T$ and $\mathbf{R}_B^{12} = \mathbf{R}_z(\phi^{12})$, where $\phi^{12} = \phi^2 - \phi^1$. Then the solution of Eq. (A.10) for a specific line screw $\hat{\mathbf{s}}$ will always yield a direction $\mathbf{s} = (0,\, 0,\, 1)^T$, a location $\mathbf{p}_s = (x_{p_s},\, y_{p_s},\, 0)^T$ and a slide $s^{12} = 0$. Hence, the result is a revolute joint located in and directed perpendicular to the *xy*-plane of W. This is uniquely determined by the point $\mathbf{p}_s$, which is known as the *pole of a planar relative displacement*.

Rotation axis-based spherical two-position synthesis of revolute joints

In the case that a given task is spherical in character, it is clear that task poses of the link may be defined using coordinate frames whose origins remain coincident. Then the task consists of $\mathbf{t}_B^{12} = \mathbf{0}$ and general 3×3 rotation matrices and the result for $\hat{\mathbf{s}}$ is a general direction $\mathbf{s} = (x_s,\, y_s,\, z_s)^T$, where $|\mathbf{s}| = 1$ and a location $\mathbf{p}_s = \mathbf{0}$. The slide again satisfies $s^{12} = 0$ because $\mathbf{t}_B^{12} = \mathbf{0}$ (origins of coordinate frames remain coincident) and the result is a revolute joint passing through the origin of W and B, which is identical to the *rotation axis of a relative rotation*.

However, another example of a spherical movement can be constructed, where the origins of coordinate frames are not attached to each other, i.e. where translations are not equal to zero. However, then it is required that $(\mathbf{t}_B^{12})^T \cdot \mathbf{s} = 0$, which provides a condition for the translations. The result is a revolute joint axis, which has $\mathbf{p}_s \neq \mathbf{0}$.

2.3.2. Constraint-Based Synthesis of Planar RR Chains

The general planar RR chain is a serial chain that consists of three planar movable links *Ka*, *Kb* and *Kc* and two parallel revolute joints. Links *Ka* and *Kc* shall have two rigidly attached frames *Ba* and *Bc* required for synthesis. Note that the frame *Bb* is not of importance, because the movement of the corresponding link is never involved in the synthesis of the RR chain. The motion of the different links shall take place in the *xy*-plane of a fixed frame W so the revolute joints coupling the links have their directions pointing along the *z*-axis of W. Since *z*-coordinates will not be affected from planar motion, the synthesis problem only affects the locations of the R joints, which can be defined in the *xy*-plane and shall be represented by two vectors $\mathbf{p}_a$ and $\mathbf{p}_b$ measured in W.

Fig. 2.5 shows the general planar RR chain in a linkage configuration i. Using the relative displacement equation (2.4) allows to describe any configuration i of $\mathbf{p}_a$ and $\mathbf{p}_b$ in terms of a

reference configuration 1: $\mathbf{p}_b^i = \mathbf{T}_{Bc}^{1i} \cdot \mathbf{p}_b^1$ and $\mathbf{p}_a^i = \mathbf{T}_{Ba}^{1i} \cdot \mathbf{p}_a^1$. This expands to yield

$$\mathbf{p}_b^i = \mathbf{R}_{Bc}^{1i} \cdot \mathbf{p}_b^1 + \mathbf{t}_{Bc}^{1i} \quad \text{and} \quad \mathbf{p}_a^i = \mathbf{R}_{Ba}^{1i} \cdot \mathbf{p}_a^1 + \mathbf{t}_{Ba}^{1i}, \tag{2.45}$$

where $i = 2, \ldots, n$. The translations are of type $\mathbf{t}_B^{1i} = (x_t^{1i},\ y_t^{1i},\ 0)^T$ and the rotations may be written as $\mathbf{R}_B^{1i} = \mathbf{R}_z(\phi^{1i})$ (see Eq. (2.6)), where $\phi^{1i} = \phi^i - \phi^1$. Aside Eq. (2.45) $\mathbf{p}_a$ and $\mathbf{p}_b$ must satisfy a constraint equation of the planar RR chain, which describes the constant distance l among the R joints in each configuration i of the chain:

$$(\mathbf{p}_b^i - \mathbf{p}_a^i)^T \cdot (\mathbf{p}_b^i - \mathbf{p}_a^i) = l^2, \quad i = 1, \ldots, n. \tag{2.46}$$

Subtracting the first equation from the remaining ones eliminates the parameter l and substituting Eq. (2.45) allows to describe $\mathbf{p}_b^i$ and $\mathbf{p}_a^i$ in terms of $\mathbf{p}_b^1$, $\mathbf{p}_a^1$ as well as the pre-defined task position data. After some rearranging the result is the set of *bilinear scalar design or synthesis equations*:

$$(\mathbf{p}_b^1)^T \cdot \mathbf{M}^{1i} \cdot \mathbf{p}_a^1 + (\vec{\lambda}^{1i})^T \cdot \mathbf{p}_b^1 + (\vec{\mu}^{1i})^T \cdot \mathbf{p}_a^1 + \delta^{1i} = 0, \quad i = 2, \ldots, n, \tag{2.47}$$

where $\mathbf{M}^{1i} = \mathbf{E} - (\mathbf{R}_{Bc}^{1i})^T \mathbf{R}_{Ba}^{1i}$, $(\vec{\lambda}^{1i})^T = (\mathbf{t}_{Bc}^{1i} - \mathbf{t}_{Ba}^{1i})^T \cdot \mathbf{R}_{Bc}^{1i}$, $(\vec{\mu}^{1i})^T = (\mathbf{t}_{Ba}^{1i} - \mathbf{t}_{Bc}^{1i})^T \cdot \mathbf{R}_{Ba}^{1i}$ and $\delta^{1i} = \frac{1}{2}(\mathbf{t}_{Bc}^{1i})^T \cdot \mathbf{t}_{Bc}^{1i} - (\mathbf{t}_{Ba}^{1i})^T \cdot \mathbf{t}_{Bc}^{1i} + \frac{1}{2}(\mathbf{t}_{Ba}^{1i})^T \cdot \mathbf{t}_{Ba}^{1i}$.

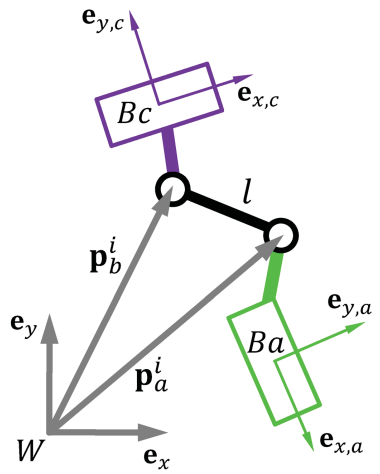

Figure 2.5.: The planar RR chain

The maximum number of task positions is $n = 5$, since then there are four equations in the four unknown W-frame coordinates $x_{p_a}^1$, $y_{p_a}^1$ and $x_{p_b}^1$, $y_{p_b}^1$ of the locations $\mathbf{p}_b^1$ and $\mathbf{p}_a^1$. However, the bilinear structure does not allow a direct solution for the unknowns but requires an *algebraic elimination procedure* that can be found in [33], pp. 108-109. The solution of Eq. (2.47) immediately becomes simpler for underspecified problems where $n = 4$, $n = 3$ or $n = 2$ and will be discussed in later chapters when required. Note that the solution procedure for $n = 4$ is given in detail in sect. C.1.

2.3.3. Constraint-Based Synthesis of Spatial GS and SS Chains

The general spatial SS chain also consists of three moving links Ka, Kb and Kc with rigidly attached frames Ba and Bc required for synthesis, Fig. 2.6. However, it differs from the planar RR in the sense that links may perform spatial motion and that spherical joints allow spherical movement between the different links. Never the less, letting two three dimensional vectors $\mathbf{p}_b$ and $\mathbf{p}_b$, measured in a fixed frame W, describe the center points of the S joints, the geometric constraint of a SS chain may be written as

$$(\mathbf{p}_b^i - \mathbf{p}_a^i)^T \cdot (\mathbf{p}_b^i - \mathbf{p}_a^i) = l^2, \quad i = 1, \ldots, n, \tag{2.48}$$

which is identical to that of the planar RR chain. Since a gimbal or G joint is also completely described by its center point, i.e. the point of intersection between its two R joints (see also Fig. 1.2), Eq. (2.48) also holds for the GS chain.

Using the relative displacement equation (2.4) for general spatial displacements allows to describe the movement of $\mathbf{p}_b$ and $\mathbf{p}_b$ as $\mathbf{p}_b^i = \mathbf{T}_{Bc}^{1i} \cdot \mathbf{p}_b^1$ and $\mathbf{p}_a^i = \mathbf{T}_{Ba}^{1i} \cdot \mathbf{p}_a^1$, which expands to yield

$$\mathbf{p}_b^i = \mathbf{R}_{Bc}^{1i} \cdot \mathbf{p}_b^1 + \mathbf{t}_{Bc}^{1i} \quad \text{and} \quad \mathbf{p}_a^i = \mathbf{R}_{Ba}^{1i} \cdot \mathbf{p}_a^1 + \mathbf{t}_{Ba}^{1i}. \tag{2.49}$$

Compared to the planar case, the translations are of type $\mathbf{t}_B^{1i} = (x_t^{1i},\, y_t^{1i},\, z_t^{1i})^T$ and the 3×3 rotation matrices $\mathbf{R}_{Ba}^{1i}$ and $\mathbf{R}_{Bc}^{1i}$ describe general spatial relative orientations. However, as in the planar case, subtracting the first equation from the remaining ones eliminates the parameter l and substituting relative displacements allows to describe $\mathbf{p}_b^i$ and $\mathbf{p}_a^i$ in terms of $\mathbf{p}_b^1$, $\mathbf{p}_a^1$ as well as the pre-defined task position data and yields, after some rearranging, the set of *bilinear scalar design or synthesis equations*:

$$(\mathbf{p}_b^1)^T \cdot \mathbf{M}^{1i} \cdot \mathbf{p}_a^1 + (\vec{\lambda}^{1i})^T \cdot \mathbf{p}_b^1 + (\vec{\mu}^{1i})^T \cdot \mathbf{p}_a^1 + \delta^{1i} = 0, \quad i = 2, \ldots, n, \tag{2.50}$$

where $\mathbf{M}^{1i} = \mathbf{E} - (\mathbf{R}_{Bc}^{1i})^T \mathbf{R}_{Ba}^{1i}$, $(\vec{\lambda}^{1i})^T = (\mathbf{t}_{Bc}^{1i} - \mathbf{t}_{Ba}^{1i})^T \cdot \mathbf{R}_{Bc}^{1i}$, $(\vec{\mu}^{1i})^T = (\mathbf{t}_{Ba}^{1i} - \mathbf{t}_{Bc}^{1i})^T \cdot \mathbf{R}_{Ba}^{1i}$ and $\delta^{1i} = \frac{1}{2}(\mathbf{t}_{Bc}^{1i})^T \cdot \mathbf{t}_{Bc}^{1i} - (\mathbf{t}_{Ba}^{1i})^T \cdot \mathbf{t}_{Bc}^{1i} + \frac{1}{2}(\mathbf{t}_{Ba}^{1i})^T \cdot \mathbf{t}_{Ba}^{1i}$.

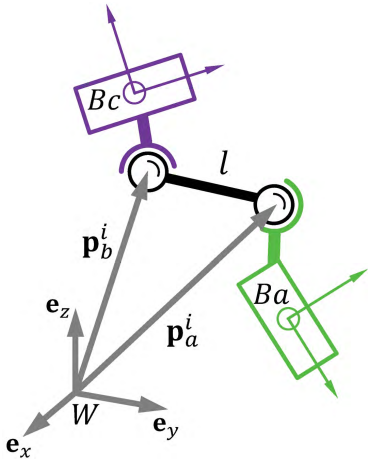

Figure 2.6.: The spatial SS chain

Since now there are six unknown W-frame coordinates $x_{p_a}^1$, $y_{p_a}^1$, $z_{p_a}^1$ and $x_{p_b}^1$, $y_{p_b}^1$, $z_{p_b}^1$ of the locations $\mathbf{p}_a^1$ and $\mathbf{p}_b^1$ the maximum number of task positions is $n = 7$. However, the bilinear structure does not allow a direct solution for the unknowns but requires an *algebraic elimination procedure*, derived by Innocenti [59]. The solution of Eq. (2.50) immediately becomes simpler for underspecified problems where $n = 4$, $n = 3$ or $n = 2$ and will be discussed in later chapters when required.

2.3.4. Constraint-Based Synthesis of Spherical RR Chains

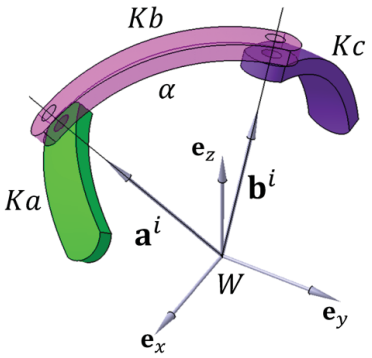

Figure 2.7.: The spherical RR chain

The spherical RR chain has intersecting axes and each of the links Ka to Kc perform pure rotational movement about the point of intersection. Hence, the finite position synthesis problem is conveniently studied in frames that are located at this point. The benefit is that translations equal zero and the synthesis equations of a spherical RR chain simply originate from a constraint equation, describing the constant angle α enclosed by the directions of the revolute joints in each configuration i of the chain (see Fig. 2.7):

$$(\mathbf{a}^i)^T \cdot \mathbf{b}^i = |\mathbf{a}^i||\mathbf{b}^i| \cos\alpha, \quad i = 1, \ldots, n \tag{2.51}$$

(Note that the frames that correspond to Ka and Kc are not shown here to keep clarity in the figure, while that corresponding to Kb is not shown since this link is never involved in the constraint-based synthesis of the RR chain). Subtracting the first equation from the remaining ones eliminates the right hand side and after substituting relative rotations $\mathbf{b}^i = \mathbf{R}_{Bc}^{1i} \cdot \mathbf{b}^1$ and $\mathbf{a}^i = \mathbf{R}_{Ba}^{1i} \cdot \mathbf{a}^1$ with pre-defined rotation matrices the design problem takes the simple form:

$$(\mathbf{b}^1)^T \cdot \mathbf{M}^{1i} \cdot \mathbf{a}^1 = 0, \, i = 2, \ldots, n, \tag{2.52}$$

where $\mathbf{M}^{1i} = \mathbf{E} - (\mathbf{R}_{Bc}^{1i})^T \mathbf{R}_{Ba}^{1i}$. Compared to the planar RR chain the bilinear polynomial design equations consist of six unknown coordinates $\mathbf{a}^1 = (x_a^1, y_a^1, z_a^1)^T$ and $\mathbf{b}^1 = (x_b^1, y_b^1, z_b^1)^T$. However, the design equation is homogeneous in character since expansion of (2.52) yields that each

monomial is of order three. This means that only four of the six unknowns are independent. In other words, one may choose i.e. $z_a^1 = z_b^1 = 1$ to obtain a design equation that has the same structure as the one discussed for the planar RR chain (section 2.3.2). The result is that the maximum number of task positions is again $n = 5$ and the bilinear structure does not allow a direct solution for the unknowns but requires an algebraic elimination procedure, see e.g. [33], pp. 108-109. The solution of Eq. (2.52) immediately becomes simpler for underspecified problems where $n = 4$, $n = 3$ or $n = 2$ and will be discussed in later chapters when required. Note that the solution procedure for $n = 4$ is given in detail in sect. C.2.

2.3.5. Constraint-Based Synthesis of Spatial RR Chains

While the synthesis problem of planar and spherical RR chains as well as that of spatial SS chains was relatively easy to state when taking into account the particular geometry of these chains, the spatial generalization is of significantly higher complexity due to skew joint axes that allow spatial motion. In contrast to the previously described chains, the synthesis of the spatial RR will be studied in the following by considering one of the end links being fixed.

The set of design equations

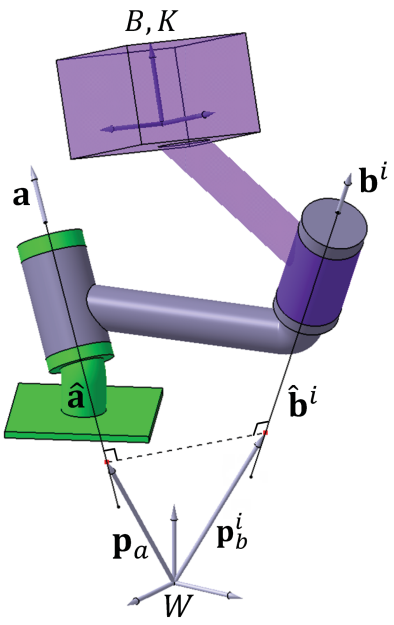

Figure 2.8.: The spatial RR chain

Research on the design problem of spatial RR chains dates back to 1967, where Roth [50] described the application of finite position theory to mechanism synthesis. In the same year Veldkamp [60] studied the spatial RR synthesis for three instantaneous spatial poses of the end link of the chain. In 1969 Suh [61] discovered that RR chains always exist in pairs in the case of three finitely separated spatial poses. A broad description of the design equations of various chains including the spatial RR was reported by Tsai and Roth in 1972, who then, in 1973, used these equations to solve the RR synthesis algebraically for a maximum number of three poses [29]. A particular result was, that there exist two solutions of the design equations, representing two RR chains, which together may be used to form a Bennett linkage, already found by Bennett in 1901, [13]. This closed loop linkage is known as the spatial four-bar with special, symmetric kinematic dimensions that provide mobility. In 1996 Huang reported, that the screw axes of the movement of Bennett's linkage always form a specific surface in space, known as the cylindroid or Plücker conoid (see also [62]). This result is also considered in brief in sect. C.3 and it motivated Perez and McCarthy [30] to associate the cylindroid with the synthesis problem of RR chains. The result was a synthesis, with particularly simplified design equations, which are also used in this work. Later then in 2005, Brunnthaler, Schröcker and Husty [31] reformulated and solved the problem by using the Study quadric, a specific projective space particularly suitable to study spatial motion.

In what follows, the design equations of the spatial RR chain based on geometric constraints are revisited. Note that deriving these equations here requires dual vector algebra introduced in

brief in sect. 2.1.5.

Figure 2.8 shows a spatial RR chain together with the different geometric parameters, needed to describe the geometric constraints. Note that the link that includes axis $\hat{\mathbf{a}}$ shall be fixed here, which reduces the number of moving frames involved in the synthesis to a single frame B, located somewhere in the end link K.

When the chain moves through n configurations, the first constraint is that the revolute axes must preserve a constant angle α and distance l. This can be formulated using the dual scalar product between the dual vectors $\hat{\mathbf{a}} = (\mathbf{a},\ \mathbf{p}_a \times \mathbf{a})^T$ and $\hat{\mathbf{b}}^i = (\mathbf{b}^i,\ \mathbf{p}_b^i \times \mathbf{b}^i)^T$, derived in section 2.1.5, Eq. (2.26):

$$\hat{\mathbf{a}} \cdot \hat{\mathbf{b}}^i = \cos\alpha - \sigma l \sin\alpha, \quad i = 1,\ldots,n, \tag{2.53}$$

where $\hat{\mathbf{a}}$ and $\hat{\mathbf{b}}^i$ shall be measured in a fixed frame W. Subtracting the first equation from the remaining ones eliminates the right hand side of this equation. Next, using the relative displacement of a line allows to describe $\hat{\mathbf{b}}^i$ in terms of $\hat{\mathbf{b}}^1$, $\hat{\mathbf{b}}^i = \hat{\mathbf{T}}_B^{1i} \cdot \hat{\mathbf{b}}^1$. Note that the screw transformation matrix shall be a dual matrix, such that $\hat{\mathbf{T}}_B^{1i} = \mathbf{R}_B^{1i} + \sigma\tilde{\mathbf{t}}_B^{1i}\mathbf{R}_B^{1i}$. The position data of frame B will be given, so rearranging and substituting the relative displacement yields

$$\begin{aligned} \hat{\mathbf{a}} \cdot \hat{\mathbf{b}}^1 - \hat{\mathbf{a}} \cdot \hat{\mathbf{b}}^i &= \hat{\mathbf{a}} \cdot \left(\hat{\mathbf{b}}^1 - \hat{\mathbf{b}}^i\right) = \\ &= \hat{\mathbf{a}} \cdot \left(\hat{\mathbf{b}}^1 - \hat{\mathbf{T}}_B^{1i} \cdot \hat{\mathbf{b}}^1\right) = \\ &= \hat{\mathbf{a}} \cdot \left(\mathbf{E} - \hat{\mathbf{T}}_B^{1i}\right) \cdot \hat{\mathbf{b}}^1 = 0, \quad i = 2,\ldots,n. \end{aligned} \tag{2.54}$$

The matrix has the form $(\mathbf{E} - \hat{\mathbf{T}}_B^{1i}) = \mathbf{E} - \mathbf{R}_B^{1i} - \sigma\tilde{\mathbf{t}}_B^{1i}\mathbf{R}_B^{1i}$ and expansion of (2.54) yields a real and dual part equal to zero:

$$(\mathbf{a})^T \cdot \left(\mathbf{E} - \mathbf{R}_B^{1i}\right) \cdot \mathbf{b}^1 = 0 \qquad \text{and} \tag{2.55}$$

$$(\mathbf{a})^T \cdot \left(\mathbf{E} - \mathbf{R}_B^{1i}\right) \cdot \left(\mathbf{p}_b^1 \times \mathbf{b}^1\right) + (\mathbf{p}_a \times \mathbf{a})^T \cdot \left(\mathbf{E} - \mathbf{R}_B^{1i}\right) \cdot \mathbf{b}^1 - (\mathbf{a})^T \cdot \tilde{\mathbf{t}}_B^{1i}\mathbf{R}_B^{1i} \cdot \mathbf{b}^1 = 0, \quad i = 2,\ldots,n. \tag{2.56}$$

These equations are often called the direction and moment constraints, which describe a constant angle and distance between $\hat{\mathbf{a}}$ and $\hat{\mathbf{b}}$ in each configuration. While Eq. (2.55) is nothing but the design equation of the spherical RR chain with one fixed link a particular property of the moment constraint is that it can be simplified by considering the geometry of an RR chain in combination with the screw axis of $\hat{\mathbf{T}}_B^{1i}$. The result is that Eq. (2.56) can be replaced by the simpler equation

$$(\mathbf{s}^{1i})^T \cdot \left(\mathbf{p}_a - \mathbf{p}_b^1\right) - \frac{s^{1i}}{2} = 0 \quad i = 2,\ldots,n, \tag{2.57}$$

where $\mathbf{s}^{1i}$ and s^{1i} are the normalized direction of and the slide along the screw axes $\hat{\mathbf{s}}^{1i}$, see also appendix A, sect. A.5. This equation is obtained from insight in the so called screw triangles spanned by the axes $\hat{\mathbf{a}}$, $\hat{\mathbf{b}}^1$ and $\hat{\mathbf{s}}^{1i}$, see e.g. [63].

However, direction and moment constraint do not take into account whether line $\hat{\mathbf{a}}$ and $\hat{\mathbf{b}}$ perform a sliding when the RR chain moves, which would amount to a movement of $\mathbf{p}_a$ and $\mathbf{p}_b^i$ along $\hat{\mathbf{a}}$ and $\hat{\mathbf{b}}$. This can be suppressed by forcing that $\mathbf{p}_a$ and $\mathbf{p}_b^i$ remain on the common normal between $\hat{\mathbf{a}}$ and $\hat{\mathbf{b}}$ (dashed line in Fig. 2.8). This is expressed by two further constraints:

$$(\mathbf{a})^T \cdot \left(\mathbf{p}_a - \mathbf{p}_b^i\right) = 0 \qquad \text{and} \qquad (\mathbf{b}^i)^T \cdot \left(\mathbf{p}_a - \mathbf{p}_b^i\right) = 0, \quad i = 1,\ldots,n. \tag{2.58}$$

Since it is known from a spatial displacement of lines that $\mathbf{b}^i = \mathbf{R}_B^{1i} \cdot \mathbf{b}^1$ and from a spatial displacement of points that $\mathbf{p}_b^i = \mathbf{R}_B^{1i} \cdot \mathbf{p}_b^1 + \mathbf{t}_B^{1i}$ one may substitute this into (2.58) to obtain

$$(\mathbf{a})^T \cdot \left(\mathbf{p}_a - \mathbf{R}_B^{1i} \cdot \mathbf{p}_b^1 + \mathbf{t}_B^{1i}\right) = 0 \quad \text{and} \quad (\mathbf{b}^1)^T \cdot \left((\mathbf{R}_B^{1i})^T \cdot \mathbf{p}_a - (\mathbf{R}_B^{1i})^T \cdot \mathbf{t}_B^{1i} - \mathbf{p}_b^1\right) = 0, \quad i = 1,\ldots,n. \tag{2.59}$$

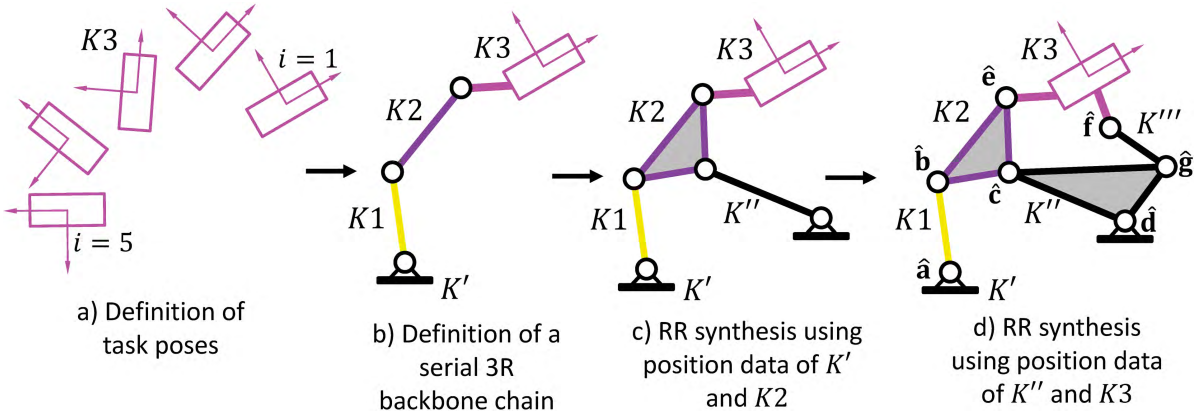

Figure 2.9.: Qualitative representation of a stepwise finite position synthesis procedure of a Watt-1 linkage topology

Equations (2.55), (2.57) and (2.59) represent the set of *bilinear scalar design or synthesis equations* in the ten independent unknown W-frame coordinates x_a, y_a, x_b^1, y_b^1, x_{p_a}, y_{p_a}, z_{p_a}, $x_{p_b}^1$, $y_{p_b}^1$ and $z_{p_b}^1$. Hence, the maximum number of task poses that can be predefined for the end link is $n = 3$, since then there are ten equations in these unknowns.

As already mentioned in the introduction of this section Perez and McCarthy [30] associate the cylindroid with the three task positions, which allows to simplify the design equations. In particular this means, that if Eq. (2.55), (2.57) and (2.59) are stated in a specific coordinate frame associated with the cylindroid Eq. (2.59) is identically satisfied so that the number of equations reduces to four. This corresponds to the fact, that the ten design parameters x_a, y_a, x_b^1,...,$z_{p_b}^1$ can be replaced by an equivalent set of four design parameters. The coordinate frame is the *principal axis frame* of the cylindroid and it can be determined from the three task position of the synthesis problem, as shown in [30]. Different relations between a three-position task, the associated cylindroid with principal axis frame as well as the spatial Bennett four-bar linkage are roughly described in the appendix, sect. C.3, since it is required in one of the major synthesis procedures of this work, see sect. 4.3.4.

2.3.6. Building-Block-Based Synthesis Procedures for Multiloop Linkages

In order to compute the kinematic dimensions of a linkage with given topology, such that specific links can reach a finite number of prescribed task poses, different linkage building block chains such as planar spherical or spatial RR chains as well as spatial GS or SS chains can be assembled in a systematic manner. This leads to what may be denoted as *synthesis procedures of a linkage*, where an example is the synthesis of a 5-SS platform linkage, [64]. A further specific approach is to systematically constrain a serial kinematic chain, that guides a specific link through a finite number of task poses by adding building blocks in a systematic manner. The basic approach is shown in Fig. 2.9 for a Watt-1 linkage topology, see also [65].

A Watt linkage topology consists of six links K', K'', K''', $K1$, $K2$ and $K3$ and seven joints or joint axes $\hat{\mathbf{a}}$, $\hat{\mathbf{b}}$, $\hat{\mathbf{c}}$, $\hat{\mathbf{d}}$, $\hat{\mathbf{e}}$, $\hat{\mathbf{f}}$ and $\hat{\mathbf{g}}$ and is essentially characterized by two consecutively hinged ternary links $K2$ and K''. When a binary link, such as K' is considered as the fixed link the linkage is called a Watt-1 topology, otherwise, i.e. a ternary link is fixed, a Watt-2 topology. In the case that the different joints are revolute, the mechanism may be termed as Watt's 7R

linkage.

When such revolute jointed Watt linkages have parallel joint axes each of the links move in planes parallel to each other and the resulting structure is a planar linkage. Then, the synthesis procedures based on building block chains require the synthesis equations (2.47) of planar RR chains. The second case is spherical Watt linkages with intersecting R joints, which then require the synthesis equations (2.52) of spherical RR chains. In both cases applying the mobility formula to this type of linkage yields the d.o.f. $M = 1$. Due to the fact that the planar and spherical RR synthesis problems both are limited to a maximum number of five task poses, also the synthesis procedures of complete Watt topologies is restricted to five poses.

The synthesis procedure of a Watt-1 linkage begins with the definition of n planar or spherical task poses of link $K3$, i.e. a frame $B3$, where $2 \leq n \leq 5$ (Fig. 2.9a)). In a second step a planar or spherical serial 3R chain is defined, which can reach the prescribed task poses of $K3$. Note that the dimensions of the planar and spherical motion sub groups $SE(2)$ and $SO(3)$ are 3, which means that a planar or spherical 3R chain (with appropriate kinematic dimensions) with d.o.f. equal to three is always able to reach each of the given poses. Fig. 2.9b) shows such a 3R chain formed by links K', $K1$, $K2$ and $K3$. Inverse kinematics calculations of the 3R next allow to determine poses of the link $K2$ in configurations where $K3$ reaches the initially specified task poses. This allows to synthesize a RR chain among $K2$ and the fixed link K', so that the result is another link K'' and a four-bar loop formed by K', $K1$, $K2$ and K'' (Fig. 2.9c)). Analysis of this four-bar yields the finitely separated poses of K'' that correspond to the initial task poses of $K3$ and a final RR synthesis among links K'' and $K3$ yields the remaining link K''' and completes the Watt-1 synthesis procedure.

The synthesis procedure described above has also been developed for planar single-d.o.f. six-bar mechanisms which consist of PRR or RPR guiding chains instead of a 3R chain, [66], [67]. The synthesis procedure from above for a spherical Watt-1 linkage may be found for instance in [68]. Another synthesis procedure where spatial GS chains are used to constrain a spatial TRS guiding chain is presented in [69]. Due to the GS synthesis problem the result is a seven-position synthesis which yields a spatial 2-d.o.f. eight-bar linkage. In [70] the idea of mechanically constrained serial chains based on cable drives instead of systematically added RR chains is presented. Beside the approach of constraining serial chains the synthesis of planar and spherical eight-bar linkages can also be performed by systematically adding linkage building blocks to a parallel kinematic loop, [71], [72].

The synthesis of spatial kinematic chains based on geometric constraints is more multifarious due to the larger set of different joint types. Beside the R, G and S joints also building block chains with cylindrical (C) joints exist. However, here also synthesis procedures exist, e.g. [73]. Synthesis procedures based on building block chains with different joint types such as a RC chain introduce asymmetry, which requires specific attention, as shown recently in [74].

Finite Position Synthesis of Overconstrained Linkages

Another class of linkages, where synthesis is performed are the overconstrained spatial linkage topologies, already introduced in sect. 1.2.3. (See e.g. [75, 76, 77, 78, 79] for further studies on the class of overconstrained linkages). However, since the mobility of these structures particularly depends on special kinematic dimensions usually finite position synthesis based on prescribed task positions is not possible. Example where this is usually true for large scale linkage networks [80] or also deployable polyhedral structures [81], [41].

Furthermore, also the class of rigid origami (see also sect. 1.2.3) usually resists successful application of f.p.s. An example approach that may be assigned to a certain dimensional synthesis

of origami structures is given by Tachi [82].

The reason why f.p.s. is hard to apply to overconstained topologies may be ascribed to the typically high degree of overconstraint. However, as already mentioned in the introduction, the finite position synthesis can be applied for certain overconstrained linkage topologies. This on the one hand was shown to be possible for the Bennett linkage, see sect. 2.3.5. In addition to this early result further other synthesis results exist such as the f.p.s. of RPRP and RCCR single loops reported by Perez [83] and Batbold et al. [84]. Furthermore, recently Hegedüs, Schicho and Schröcker [32] report on the four-position synthesis of angle-symmetric 6R linkages.

2.4. Computer-Aided Linkage Design

In order to support a designer along the different steps of a kinematic design process from Fig. 1.4 various different software and computational approaches have been developed or used, where an overview is provided in the following. A first large field of linkage design software is represented by specialized, standalone linkage design software, which is available commercially and as research software code. However, since linkage design is also oftentimes considered as a sub-development process embedded into larger CAD-integrated product development processes also CAD-systems are used for kinematic design. Herein the designer may perform kinematic preprocessing as well as postprocessing, i.e. he may specify the motion task using available parts of a virtual CAD product or may evaluate linkage design solutions. On the other hand general mathematical computing environments are available that allow for the implementation of kinematic solvers.

2.4.1. Overview of Standalone Linkage Design Software Tools

In the area of standalone software for kinematic or linkage design various tools have been implemented that support different design steps. For instance the program Symeku [85] represents a standalone tool, which enables dimensional synthesis of multilink planar single-d.o.f.-structures. The program GENESYS (Getriebe-Entwurfs- und Entwicklungs-System, [86, 87]) represents another multifarious standalone tool, which provides dimensional synthesis, kinematic and kinetostatic analysis as well as optimization procedures of various linkage and mechanism topologies. This includes planar linkages as well as planar and spatial cams and gear trains. Furthermore, the designer may also specify his motion task based on CAD geometries of different links and parts.

While Symeku and GENESYS represent non-commercial software tools, also other commercially available standalone tools for planar linkage design exist, such as for instance SAM, ASOM or Optimus Motus. Functionalities of these tools are described at the dmglib-web platform, which is a digital mechanism library [88].

In [89] Ruth et al. describe the standalone tool 'SphinxPC', which can be used for finite position synthesis as well as kinematic analysis of spherical four-bars. Another non-commercial tool with name 'Spades' (SPAtial mechanism DESign) [90] allows to synthesize spatial 4C mechanisms. The program SYNTHETICA [91] represents an extensive standalone tool that enables the synthesis of several spatial linkage topologies ranging from serial to different parallel structures. Other computational tools such as DARWIN2K also consider synthesis and analysis procedures for robotic multi-d.o.f. structures as multicriteria optimization problems, where automated evolutionary optimization approaches are used to solve design problems [92].

Apart from standalone linkage analysis and synthesis software also interactive geometry software provides functionalities that provide powerful visualization for kinematic synthesis and hence may provide support in a kinematic design process. Examples of such tools are 'GeoGebra', 'Cinderella' or 'GEONExT', whose functionalities are compared and discussed for instance in [93].

2.4.2. Mathematical Computing Environments

Mathematical computing environments such as MATLAB, Mathematica or Maple (to name a few) provide numerical and algebraic solver modules that allow to manipulate and solve systems of equations as those arising in kinematic synthesis and analysis. As it was shown in sect. 2.3 synthesis problems essentially represent polynomial systems of equations whose solutions are linkage structures, which satisfy a finite position task. Since a maximum number of alternative linkage solutions are of interest the complete set of solutions of the equations should be found, which requires appropriate numerical solvers. These are provided in computational environments using polynomial homotopy approaches, which allow to search for several solutions. See for instance [94] and [95], where polynomial continuation is used to solve kinematic synthesis problems. A MATLAB add-in for polynomial homotopy is described in [96].

In addition to solver modules particularly suitable to solve polynomial systems computing environments also provide other modules for general nonlinear systems of equations or optimization problems. When kinematic analysis solving processes are a concern the solution of nonlinear loop equations may be performed using Newton-Raphson solvers, which are are commonly available. For optimization problems gradient-based methods solvers such as Levenberg-Marquard algorithms as well as evolutionary genetic algorithms are commonly available. An example showing optimization-based kinematic design processes using MATLAB optimization solvers is demonstrated in [97]. Solvers may also be realized as individualized standalone executable solver code.

2.4.3. CAD-Integrated Kinematics Software Tools

A particular characteristic the software tools from sect. 2.4.1 have in common is that they represent standalone programs with specific graphical user interfaces. Even though some of the tools provide an interface to CAD-systems, they do not provide extensive integration into such tools. However, kinematic design can be considered as a subdevelopment process, which takes place in an early stage of larger virtual product development processes. Hence, CAD-integrated design represents an advantageous linkage design approach. This is also particularly true because kinematic design may directly fade into a detailed CAD-design of links and parts of the mechanism. Furthermore actual CAD-systems provide powerful kinematic solver modules for simulation and partially also advanced kinematic as well as dynamic analysis.

The state-of-the-art in CAD-integrated kinematic design software on the one hand includes graphical constructions, see e.g. [98, 99, 100]. Based on macro-controlled execution of CAD-functionalities synthesis results are obtained from automated graphical synthesis. Here Corves et al. [10] provide a CAD-integrated synthesis approach for cam mechanisms, which is described in detail in the following.

Aside CAD-integrated kinematic design based on graphical constructions also the approach of a combination of CAD-environments and computing environments exists. This is based on an executable kinematic solver, which performs analysis and synthesis calculations using methods such as those introduced in sect. 2.2 and 2.3. The solver is connected to the CAD-system,

which is used to visualize synthesis results. This yields CAD-integrated pre- and postprocessing and kinematic solving, which is performed within the computing environment (see again sect. 1.2.1 for a few introductory words describing pre- and postprocessing as well as solving). An example towards CAD-integrated kinematic design is shown in [101], where a CAD add-in for the synthesis of a spatial RSSR linkage is described. Another commercially available program is the CAD add-in Mechanism Generator, which allows the f.p.s. of several linkage topologies. The performance of this software package is demonstrated in [68] and is also described in the following.

CADiS

The CAD-add in software package CADiS (CAD-integrierte Synthese), see Corves et al. [10], assists a designer in synthesizing planar, spherical and spatial cam mechanisms.

An essential feature of CADiS is that pre- and postprocessing as well as solving procedures are integrated into the CAD-system 'Mechanical Desktop'. This means that CADiS particularly controls different CAD-construction steps, which can be operated via graphical user interfaces. Postprocessing functionalities include colored graphics and animations for evaluation. Additional solver modules also allow optimization of cam mechanisms.

Mechanism generator

The program demonstrated by Sonawale et al. [68] is denoted as Mechanism Generator or MechGen and allows the f.p.s. of several planar and spherical linkages. MechGen is based on a kinematic solver, which is implemented using the Mathematica computing environment and it is a so called partner product of SolidWorks.

The solver focuses on synthesis procedures based on RR building block chains with a maximum number of prescribed task positions. That way the synthesis of a spherical six-bar requires an input of five task positions. Since this number strongly reduces the chances to find real solutions in RR synthesis the program iterates task position data within specified tolerance zones. The result is particularly increased chances to find useful synthesis solutions.

Own approaches

In [102] the author presents a CAD-integrated kinematic design tool for planar four-bar and six-bar linkages, which is also based on CAD-integrated preprocessing and postprocessing and external kinematic solving. However, in contrast to any other available approach the software allows to specify task positions for two distinct parts or links of the linkage topologies. The preprocessing and postprocessing is performed using CATIA V5, while the kinematic solver is implemented and compiled as a dynamic link library (dll data format) using the MATLAB computing environment.

The program allows to design linkages for two- and three-position tasks of up to two links. However, because also the synthesis of planar RR chains is involved this leads to underspecified synthesis problems, where free design parameters must be evaluated efficiently. This is achieved by evaluating user-defined regions, where joints are allowed to be located. This increases the chances to find useful synthesis solutions, but represents an alternative approach to other programs. While there the terminology 'useful linkage' first of all refers to a kinematically useful linkage, the consideration of allowed regions for joints considers the feasibility of a linkage in connection to space requirements of a given task.

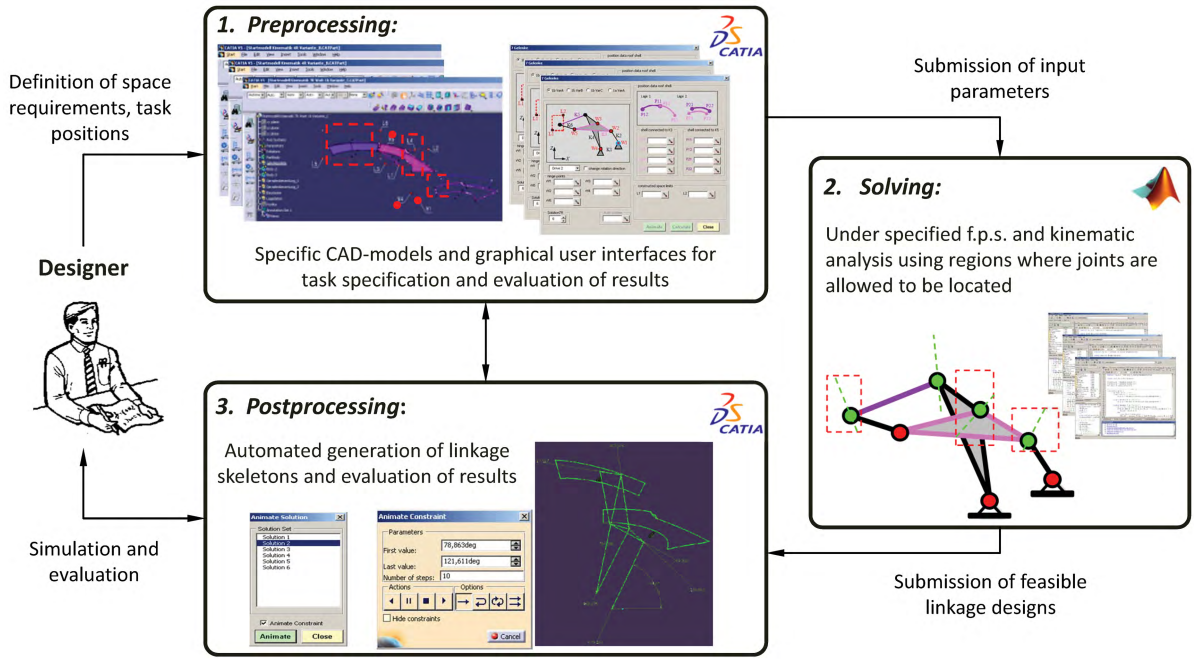

Figure 2.10.: Graphical depiction of a CAD-integrated kinematic design process with external solving processes, hidden from a designer

The basic concept of the software is shown in Fig. 2.10, where a designer specifies the motion task in terms of finite positions of desired parts as well as in terms of additional parts that define a portion of space, where the linkage is allowed to move in. This is done using specifically defined CAD-models, that contain different initially given geometric information on the type of linkage as well as synthesis procedure. Graphical user interfaces allow to extract required input parameters in the CAD-system and transmit it to the kinematic solver, which evaluates linkage designs in the given allowed space. Valid solutions are next re-submitted to the CAD-system, where simple skeletons of the linkage are generated automatically. Postprocessing includes the evaluation of results using kinematic simulation functionalities available in the CAD-System. An automated switching between different linkage solutions is also realized via specific graphical user interfaces. The different CAD-integrated GUIs are controlled via VBA macro programming, which is available in todays CAD-systems.

The automation approach provides various different synthesis strategies for four-bar and six-bar linkage topologies. This yields a flexible design approach, since four-bars occur as sub-structures in six-bar linkages and hence allow a combination of design strategies. Furthermore, automated CAD-integrated generation of linkage skeletons finally allow a quick evaluation of the feasibility of a given linkage.

Further approaches

Further approaches towards CAD-integrated kinematic design are described at the dmg-lib digital mechanism library, [88]. Here for instance the commercially available CAD add-in 'induDrive' for synthesis of cam mechanisms and the design of servo motors is presented, which is a partner product of SolidWorks and Autodesk. Other software packages are represented by 'BMX - Behavioural Modelling eXtensions', 'EasyEvoOpt-3D' and 'EvoCAT', which provide optimization-based design procedures.

3. Spherically Constrained Serial Revolute Jointed Chains

As already stated in sect. 2.3.6 low-d.o.f. linkages, that result from joining together different linkage building blocks (e.g. planar or spatial RR chains) in a way that the movement of a serial kinematic chain is constrained are termed mechanically constrained serial chains. However, when performing dimensional synthesis this approach typically yields a multiloop linkage with several joints, which may be located far from each other. In applications with space requirements this can yield an unfeasible mechanism as it violates the given requirements. Hence, an alternative way to constrain the movement of different serial revolute jointed chains is developed in the following, which was initially inspired from the *Miura-ori origami folding pattern*.

Substantial ideas of the following sections have also already been considered in [103] and were also partially published in [104] and [105].

3.1. The Rigid Foldable Miura-ori Origami Pattern

Origami is known to be the Japanese art of paper folding, where two- or three-dimensional objects such as animals or figures are folded from a crease pattern drawn on a single sheet of paper. While generally twisting as well as bending of the sheet is allowed to obtain a desired object, the subcategory *rigid origami* deals with patterns that remain movable even if the numerous creases and paper segments are replaced by kinematic revolute joints and rigid plates.

Rigid origami represent highly overconstrained spatially foldable linkages consisting of numerous symmetrically arranged links and joints, which allow mobility. A prominent example is the Miura-ori pattern shown in Fig. 3.1 (a). It has the specific geometric characteristic that it is assembled from a symmetrical, recurring arrangement of four intersecting joint axes, that form a plane symmetric spherical building block four-bar. This is known as the rigid origami mechanism equivalent of the Miura-ori building block vertex and is formed by four links $K1$,...,$K4$, Fig. 3.1 (b). The whole rigid foldable Miura pattern may then be called a system of spherical mechanisms following Bowen et al. [106], who identify further spherical mechanisms in various origami structures.

3.1.1. The Kinematically Equivalent Spherical Building Block Four-Bar

The two halfs of the plane-symmetric Miura-building block four-bar perform identical movement, when the linkage is considered to move as shown in Fig. 3.1 (b). However, this allows to replace one half of the structure by two new links K' and K'', which play the role of the line of symmetry in the original Miura-building block four-bar. The result is another kinematically equivalent spherical four-bar, Fig. 3.1 (c), which was also found by Wei et al. [107] as a subsystem of the mechanism equivalent of a folded carton box. Note that plate-like segments $K1$ and $K2$ were replaced here by circular curved, tube-like links commonly used for spherical mechanisms.

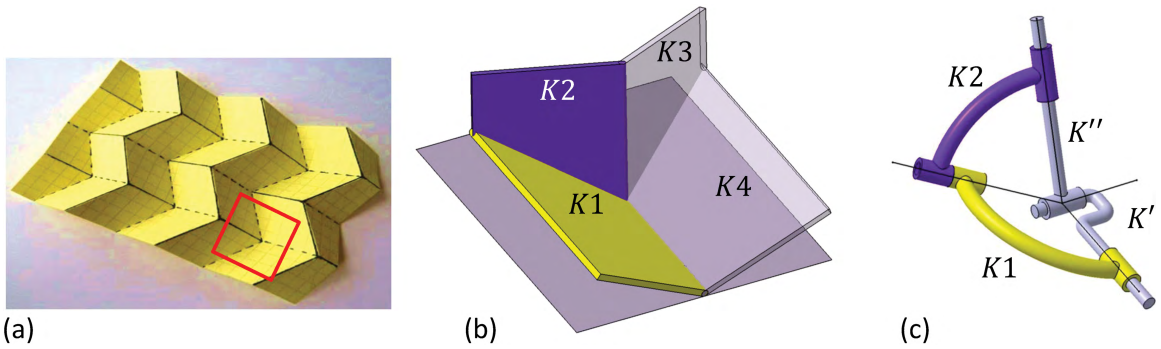

Figure 3.1.: The Rigid Foldable Miura-ori Pattern a) consisting of numerous plane symmetric spherical building block four-bars b). Replacing one half of the linkage by two new links yields a kinematically equivalent spherical building block four-bar c)

3.2. Spherically Constrained Chains with Mobility 1

The following section shows how to couple several of the kinematically equivalent spherical four-bar from Fig. 3.1 (c). Due to the fact that this moves with one single d.o.f., the coupled systems will also have mobility 1. The result is a family of mechanisms, which are called *spherically constrained, revolute-jointed serial chains* here and which have a naturally given slim and compact shape. This is because the spherical vertices, i.e. spherical four-bars can be designed compactly around their center of rotation.

3.2.1. Spherically Constrained Planar, Spherical and Spatial RR Chains

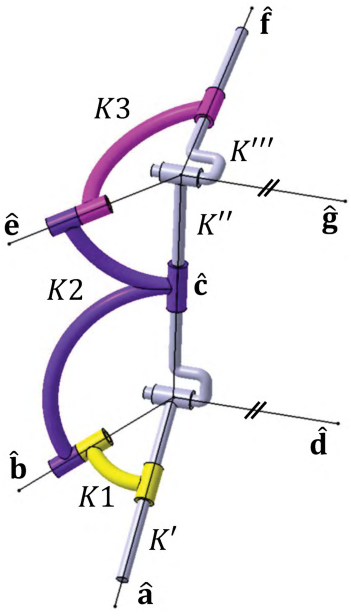

Figure 3.2.: The spherically constrained planar RR chain

A coupling of two of the kinematically equivalent spherical four-bar from Fig. 3.1 (c) yields a linkage that contains two displaced vertices, which share a common joint axis denoted as $\hat{\mathbf{c}}$, see Fig 3.2. This yields an overconstrained linkage consisting of $n = 6$ links and $g = 7$ revolute joints with axes $\hat{\mathbf{a}},\ldots,\hat{\mathbf{g}}$. Observe that this includes a planar RR chain formed by axes $\hat{\mathbf{d}}$ and $\hat{\mathbf{g}}$. We call this linkage the origami-evolved, spherically constrained planar RR chain (see also [105]) or simply spherically constrained RR chain and applying Eq. (2.27) yields

$$M = 6(n-1-g)+\sum_{i=1}^{g} f_i = 6(6-1-7)+7 = -5\,, \quad (3.1)$$

which shows that this is an overconstrained linkage. Note that K' was considered here as fixed link, so that $K3$ performs spatial movement allowing the application of the spatial mobility formula. Never-the-less, 1-d.o.f. mobility of the structure is ensured because the link K'' connecting the revolute axes of the planar RR chain provides the hinge of $K2$ which preserves each of the vertices formed by the spherical building block four-bars.

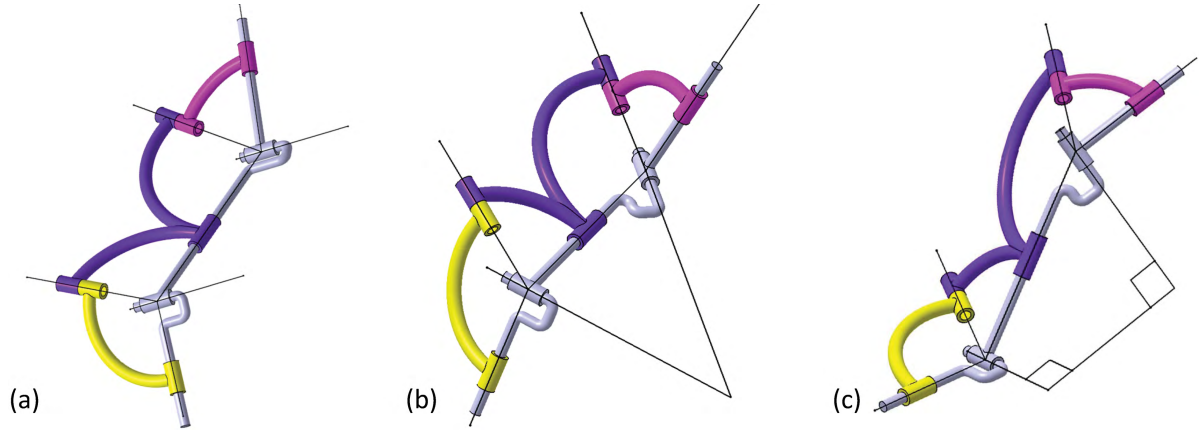

Figure 3.3.: The family of 1-d.o.f. spherically constrained planar, spherical and spatial RR chains

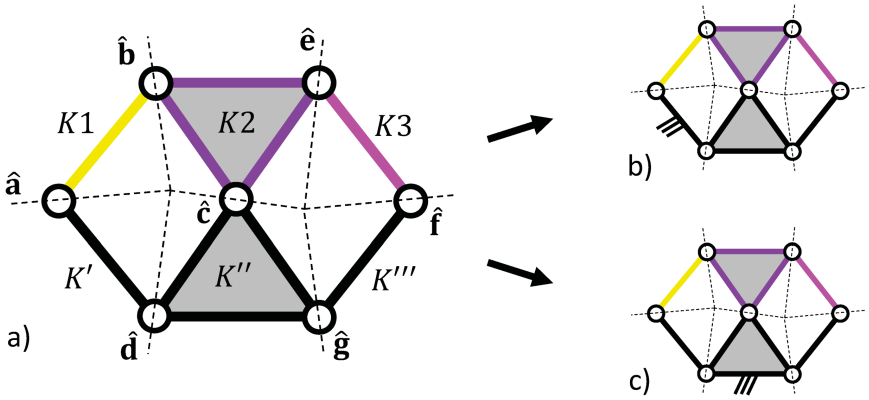

Figure 3.4.: Spherically constrained RR chains as Watt-related linkage topologies with two consecutively hinged ternary links

The mobility of the origami-evolved mechanism remains 1 even when the kinematic dimensions are modified. Note that such modifications must preserve the different vertices. On the one hand this may yield further constrained planar RR chains, Fig. 3.3 (a). On the other hand the axes $\hat{\mathbf{d}}$ and $\hat{\mathbf{g}}$ may also form a spherical or spatial RR chain, Fig. 3.3 (b) and (c). This classification follows the common distinction of planar, spherical and spatial systems, which is useful, when the family of spherically constrained RR chains is considered to solve either planar, spherical or spatial motion tasks.

It is noteworthy, that removing the joint connecting $K2$ and K'' in a spherically constrained RR chain yields what is known as the overconstrained double-spherical 6R single loop mechanism, see e.g. [108], which performs identical movement. However, the seventh R joint provides additional stiffness in the linkage, which is of particular importance for accuracy in real applications.

Spherically constrained RR chains as Watt-related linkage topolgies

From a topological view point, the class of spherically constrained RR chains with six bars and seven revolute joints have two ternary links $K2$ and K'' that are hinged consecutively, while

the remaining links are binary cranks. Hence, a simplified graph of the chain may be drawn as shown Fig. 3.4a), where the spherical sub-four-bars are marked by intersecting lines, representing joint axes. However, this representation directly evolves from Watt's kinematic chain, which is also defined as a six-bar chain with seven joints and two consecutive ternary links. If either a binary or a ternary link is considered as the fixed ground the Watt-1 or the Watt-2 linkage is obtained from Watt's kinematic chain (see also Fig. 2.9d)). These cases are also possible for the spherically constrained RR chains as shown in Fig. 3.4b) and c), so that the spherically constrained RR chains may also be considered as the Watt-related linkage topologies.

Spherically constrained RR chains as a particular RCC-C-CCC linkage topology

A RCCC linkage is usually defined as a spatial linkage with skew joint axes, see Fig. 1.3 c3). However, it is known that this transforms into a spherical four-bar (where no sliding along the axes is observed), if the four axes intersect at a common point [109], p. 270. In other words the common normal distances must be equal to zero. When two spherical four-bars are coupled to yield a spherically constrained RR chain, this means that one may also think of a coupling of two corresponding RCCC linkages. However, since there are only seven joints one of the R joint vanishes.

Elimination of a R joint instead of a C joint is considered because it eliminates the overconstraining property of a spherically constrained RR chain. To see this apply Eq. (2.27), which yields:

$$M = 6(n-1-g) + \sum_{i=1}^{g} f_i = 6\,(6-1-7) + 13 = 1. \tag{3.2}$$

The result is that a spherically constrained RR chain may also be seen as a RCC-C-CCC linkage topology, where the axes form two displaced, spherically moveable vertices that share a common C joint. This is useful, when kinematic CAD-models of spherically constrained RR chains should be assembled, see also sect. 5.4. In the following another approach is presented, which considers the normal distances among the different joint axes in order to show 1-d.o.f. mobility of spherically constrained nR chains.

3.2.2. Spherically Constrained nR Chains

It is obvious that also a larger number of spherical building block four-bars (Fig. 3.1 (c)) can be coupled in the way presented in the previous sections. Recall that such a coupling must preserve the different vertices of the building block four-bars. An example of such a coupling of three four-bars is shown in Fig. 3.5, which results in a general spherically constrained 3R chain.

In order to see, that the mobility of an arbitrary number of coupled spherical building block four-bars is always 1, the number of links and joints can be expressed in terms of a general number of vertices k:

$$n = 4 + 2\,(k-1) = 2\,(k+1) \qquad \text{and} \qquad g = \sum_{i=1}^{g} f_i = 3k+1, \quad k \geq 2 \tag{3.3}$$

Note that $k \geq 2$ to obtain a spatial linkage. Next, following Eq. (2.28) a number of conditions can be added as a formal sum $\sum s$ to Eq. (3.3) and considering $M = 1$ yields:

$$1 = 6\,(2\,(k+1) - 1 - (3k+1)) + (3k+1) + \sum s \qquad \Rightarrow \sum s = 3k \tag{3.4}$$

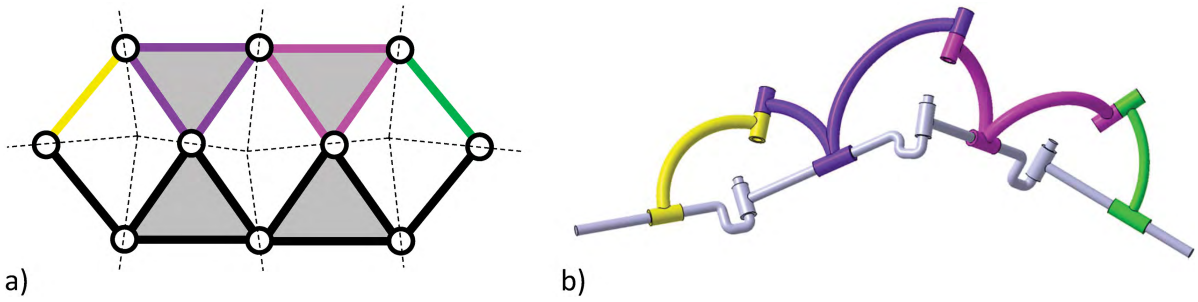

Figure 3.5.: The general spherically constrained 3R chain

This number of conditions needs to be satisfied for a spherically constrained, revolute-jointed serial chain consisting of k vertices. However, it is easy to see that the number δ of zero-common normal distances required to preserve the different vertices simply also increases in such a way that $\delta = 3k$. Hence, there are always as many zero common normal distances as are required from Eq. (3.4), so a spherically constrained nR chain also performs 1-d.o.f. motion. Note that the considerations of this section may also be found in [104].

3.3. Concepts of Spherically Constrained Chains with mobility > 1

The family of spherically constrained RR, 3R,...,nR chains presented in the previous sections were single-d.o.f. structures, which hence, belong to the class of classical mechanical linkages. However, as it will be shown in this section also different further spherically constrained kinematic chains with d.o.f. > 1 can be found. On the one hand spherically constrained 2-d.o.f. RR chains can be considered. On the other hand also multi-d.o.f. chains based on a particular coupling of Cardan chains can be found, which essentially are nothing but numerous coupled spherical four-bar linkages. The result is a demonstration of a variety of different spherically constrained multi-d.o.f. chains that may represent the kinematic architectures in robotic devices.

3.3.1. Spherically Constrained RR Chains with Mobility 2

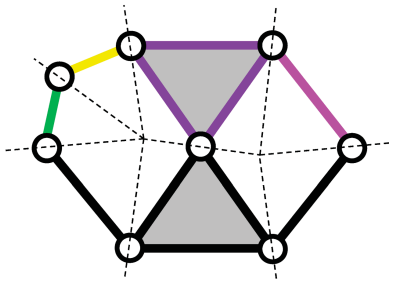

Figure 3.6.: A spherically constrained RR chain with mobility 2

Planar, spherical or either spatial RR chains can also be constrained in the spherical manner, such that the result is 2-d.o.f. structure. A qualitative representation of such a chain is shown in Fig. 3.6, which essentially represents the coupling of a spherical five-bar with a spherical four-bar. As already described in sect. 3.2.1 the joint connecting the two ternary links may be neglected, which results in what is termed a 2-d.o.f. overconstrained double-spherical 7R mechanism by Kiper et al. [110].

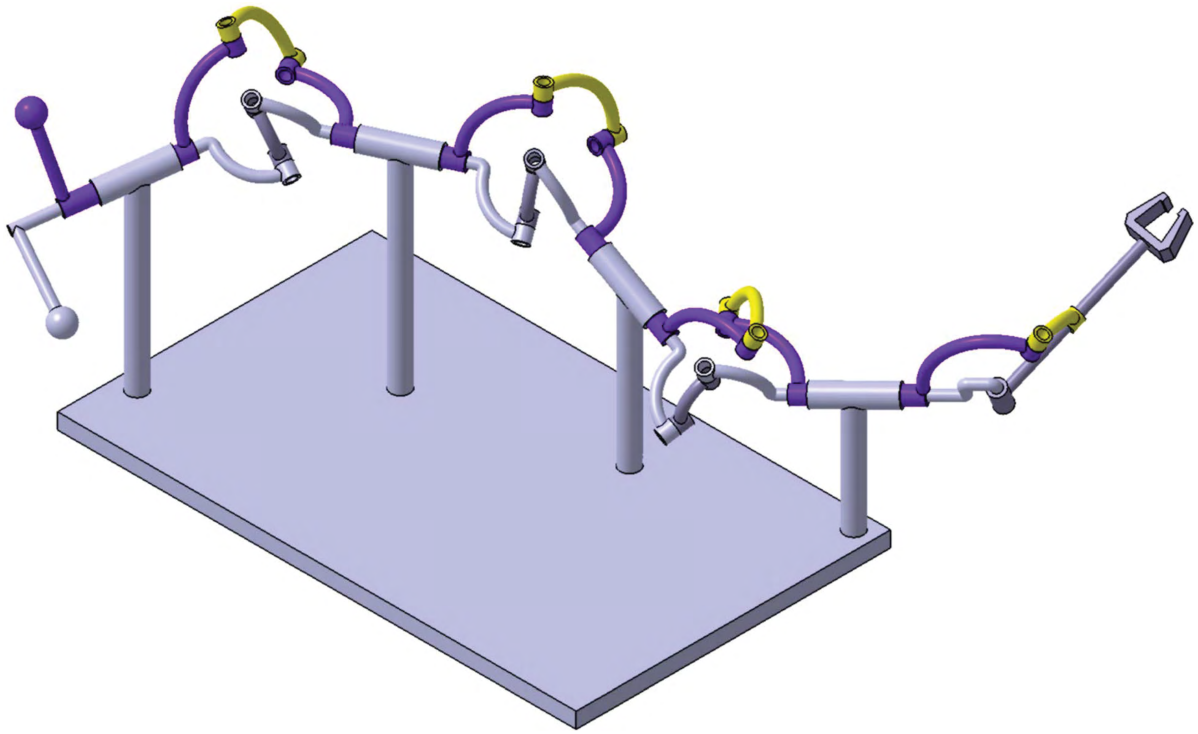

Figure 3.7.: Two coupled Cardan chains resulting in a 2-d.o.f. spherically constrained structure, which allows to actuate and re-orient a spherical four-bar

3.3.2. Coupled Cardan Chains with Mobility 2

Figure 3.7 shows another spherically constrained 2-d.o.f. structure essentially consisting of two specific overlayed Cardan kinematic chains. One of these chains enables a changing of the orientation of joint that connects for instance a gripper to the chain. Observe, that the number of Cardan vertices is not limited to three but may also be increased depending on the requirements of a specific task. The end links of the second Cardan chain then combine with the end links of the first Cardan chain to yield a spherical four-bar. The two combined Cardan chains have two degrees of freedom but may be considered as a reconfigurable structure, which allows to orient and actuate a spherical four-bar. In fact various further configurations may be achieved by changing the location and orientation of the different fixed joints connected to the platform. The result is a flexible reconfigurable and also slim structure, when made up of compactly designed spherical vertices.

The concept of coupled Cardan chains may also be extended by simply overlying another such chain. The result is another degree of freedom available at the end of the chain. One may then connect a spherical five-bar instead of a four-bar and use two d.o.f. as the input and the third one to control the orientation of the five-bar.

4. Kinematic Design Processes for Spherically Constrained Linkages

This section presents different kinematic analysis as well as finite position synthesis procedures and methodologies for different types of spherically constrained linkages. When considered as the computational part in a computer-aided kinematic design process these procedures are implemented and executed using a computing environment.

The kinematic analysis and synthesis methodologies provided in sect. 4.1.1 and 4.2 were already partially considered in [103] and [104], and have been precisely specified in [111]. The second synthesis approach derived in sect. 4.3 follows [105] and [112].

4.1. Kinematic Analysis of Origami-Evolved Linkages

Analysis provided in this section includes position analysis based on sect. 2.2.3 as well as line-based analysis of transmission properties using twist loop equations (sect. 2.2.4). Position analysis yields insight in the angular relations of the Miura-ori origami building block 4-bar from sect. 3.1 as well as spherically constrained RR chains, which is required for f.p.s. in sect. 4.2.4. Line-based analysis provides insight in the stability properties of the structure, which will be of particular importance in the application scenario, sect. 6.3.

4.1.1. Position Analysis of the Kinematically Equivalent Miura-ori Building Block 4-Bar

The structure under consideration is shown in Fig. 4.1. Recall from sect. 3.1.1 that this is kinematically equivalent to the original building block four-bar from Fig. 3.1b). In order to analyze the angular relations of the structure frames $B1$, $B2$ and B'' (not shown, to keep overview in the figure) are considered, whose origins shall coincide with that of W. $B1$ describes the movement of link $K1$, which shall have it's xz-plane coinciding with the plane spanned by $\mathbf{a}$ and $\mathbf{b}$. The x-axis of $B1$ should point along the x-axis of W, while the y-axis of $B1$ should point along $\mathbf{b} \times \mathbf{a}$. Using this its easy to see that the $B1$ performs a simple x-rotation, so that its movement can be written as ${}^{W}\mathbf{R}_{B1} = \mathbf{R}_x(\phi_a)$. Similarly $B2$ describes the movement of link $K2$, which shall have its xz-plane coinciding with the plane spanned by $\mathbf{b}$ and $\mathbf{c}$. The x-axis coincides with direction $\mathbf{c}$ and the y-axis points along $\mathbf{c} \times \mathbf{b}$. Then a pose of $B2$ measured in W is given by the composition

$$ {}^{W}\mathbf{R}_{B2} = \mathbf{R}_z(\phi_d)\mathbf{R}_x(-\phi_c) = \begin{pmatrix} \cos\phi_d & -\cos\phi_c \sin\phi_d & -\sin\phi_d \sin\phi_c \\ \sin\phi_d & \cos\phi_d \cos\phi_c & \cos\phi_d \sin\phi_c \\ 0 & -\sin\phi_c & \cos\phi_c \end{pmatrix}. \tag{4.1} $$

Using ${}^{W}\mathbf{R}_{B1}$, ${}^{W}\mathbf{R}_{B2}$ as well as the direction $\mathbf{b}$ allows to determine the relation between ϕ_a and ϕ_c. To see this, consider the flat unfolded configuration of the four-bar, where each direction vector

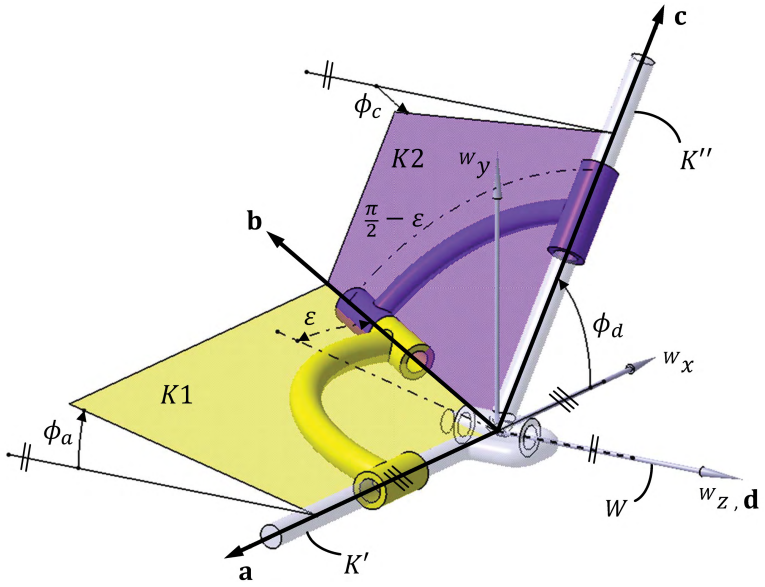

Figure 4.1.: Quantities for the position analysis of the mechanism equivalent of the Miura-ori building block four-bar

lies in the xz-plane of W and all frames are aligned. Note that this corresponds to the unfolded case of the Miura-ori pattern. In this configuration one has ${}^{B1}\mathbf{b} = {}^{B2}\mathbf{b} = (\sin\varepsilon,\ 0,\ -\cos\varepsilon)^T$ and calculating the W-frame coordinates yields

$$\begin{aligned} {}^{W}\mathbf{b} &= {}^{W}\mathbf{R}_{B1} \cdot {}^{B1}\mathbf{b} = {}^{W}\mathbf{R}_{B2} \cdot {}^{B2}\mathbf{b} = \\ &= \begin{pmatrix} \sin\varepsilon \\ \sin\phi_a \cos\varepsilon \\ -\cos\phi_a \cos\varepsilon \end{pmatrix} = \begin{pmatrix} \cos\phi_d \sin\varepsilon + \sin\phi_d \sin\phi_c \cos\varepsilon \\ \sin\phi_d \sin\varepsilon - \cos\phi_d \sin\phi_c \cos\varepsilon \\ -\cos\phi_c \cos\varepsilon \end{pmatrix}. \end{aligned} \tag{4.2}$$

Comparing the z-coordinates in Eq. (4.2) yields $\cos\phi_a = \cos\phi_d$, which suggests that the four-bar satisfies $\phi_a = \phi_c$. However, in fact the result is

$$\phi_a = -\phi_c \tag{4.3}$$

because of the matrix $\mathbf{R}_x(-\phi_c)$ in Eq. (4.1). Equation (4.3) states that the opening angles of the four-bar from Fig. 4.1 only differ in signs for any given angle ε. Due the fact that this four-bar was kinematically equivalent to the original Miura-ori folding pattern (see sect. 3.1.1) this also holds for the structure from Fig. 3.1b). Equation (4.3) is of particular importance for the two-configuration synthesis of Miura-ori-based folding structures presented in sect. 4.2.

The second important relation is the transmission angle $\phi_d(\phi_a)$. This is easily found using the constraint equation

$$\left({}^{W}\mathbf{b}\right)^T \cdot {}^{W}\mathbf{c} = \cos\left(\frac{\pi}{2} - \varepsilon\right) = \sin\varepsilon, \tag{4.4}$$

see also Eq. (2.33). ${}^{W}\mathbf{b}$ is already known from ${}^{W}\mathbf{R}_{B1} \cdot {}^{B1}\mathbf{b}$ and ${}^{W}\mathbf{c}$ is easily found as ${}^{W}\mathbf{c} = (\cos\phi_d,\ \sin\phi_d,\ 0)^T$, so that the standard form of Eq. (4.4) is easily found after expanding and rearranging as

$$\cos\phi_d + k\sin\phi_a \sin\phi_d = 1, \qquad k = \cot\varepsilon. \tag{4.5}$$

Using the tangent-half-angle formula from Eq. (2.37) with coefficients $\mathscr{A}_d = 1$, $\mathscr{B}_d = k\sin\phi_a$ and $\mathscr{C}_d = 1$ yields

$$\tan\frac{\phi_d}{2} = k\sin\phi_a. \tag{4.6}$$

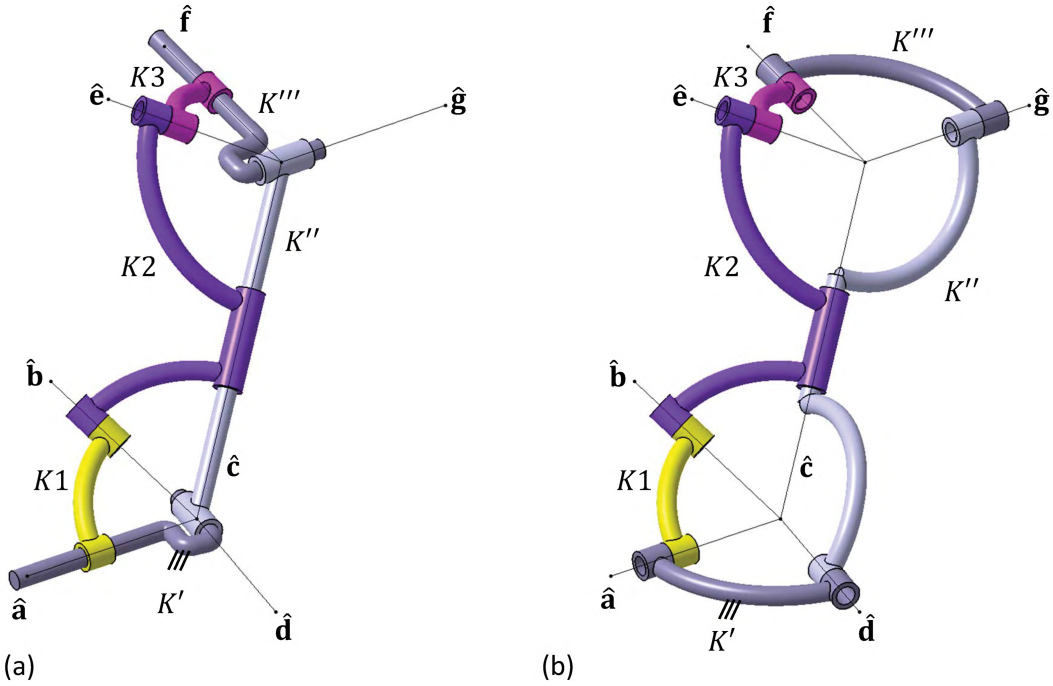

Figure 4.2.: Two kinematically equivalent representations of a general spherically constrained RR chain

The $\phi_d(\phi_a)$ is also used for the two-configuration synthesis of Miura-ori-based folding structures and is hence required in sect. 4.2.

4.1.2. Position Analysis of Spherically Constrained RR Chains

In this section the goal is to determine kinematics relations in a general spherically constrained RR chain. Recall that the most general linkage is the spherically constrained spatial RR chain as shown in Fig. 4.2a). This is essentially nothing but two specifically coupled general spherical four-bars, which is why the familiar geometric shape of four-bars is considered in the following, see Fig. 4.2b).

In order to analyze the spherically constrained spatial RR chain angles ϕ and α are introduced in Fig. 4.3, where the notation $\phi_a,\ldots,\phi_g$ and $\alpha_{ab},\ldots,\alpha_{fg}$ directly follows Fig. 2.3 and 2.4 from sect. 2.2.3. A suitable reference frame for the following vector calculations is B'', which is rigidly attached to link K''. B'' is located at the first vertex, has its z-axis aligned with axis $\hat{\mathbf{c}}$ and has its yz-plane coinciding with the plane spanned by $\hat{\mathbf{c}}$ and $\hat{\mathbf{d}}$. Following sect. 2.2.3 transformations about x- and z-axes are used in order to derive the constraint equations of the two displaced spherical loops.

In the application scenario discussed in chapter 6 a spherically constrained spatial RR chain is considered to be actuated, such that the input angle of the mechanism is ϕ_d. Hence, this is also considered here as input and the goal is to obtain the angular relationships $\phi_c(\phi_d)$ and $\phi_g(\phi_d)$ from the constraint equations. These relations can then be used to describe the movement of all joint axes of the linkage, which is required for line-based analysis of transmission properties in sect. 4.1.3.

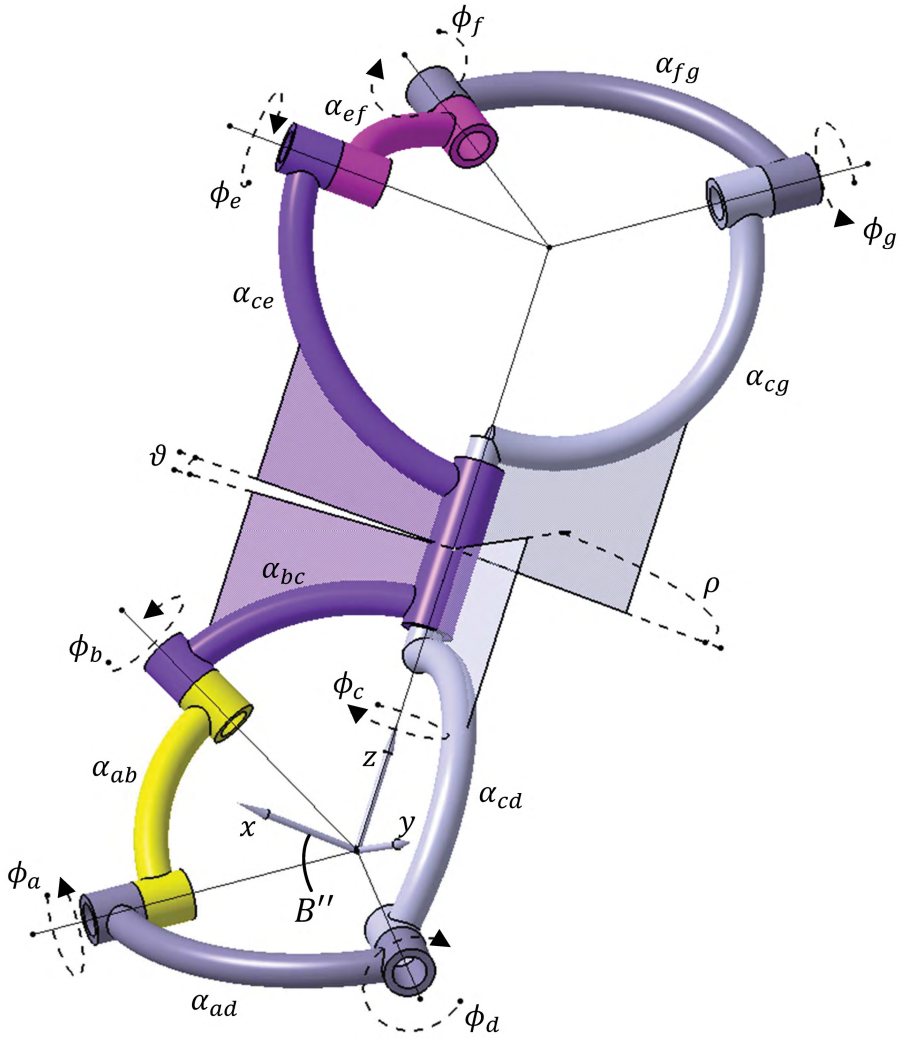

Figure 4.3.: Angles, frames and planes for position analysis of spherically constrained spatial RR chains

Angular relationship $\phi_c(\phi_d)$

The angular relationship $\phi_c(\phi_d)$ is easily obtained from the following kinematic constraint equation

$$\left({}^{B''}\mathbf{a}\right)^T \cdot {}^{B''}\mathbf{b} = \cos\alpha_{ab}, \tag{4.7}$$

where $\mathbf{a}$ and $\mathbf{b}$ are the directions of axes $\hat{\mathbf{a}}$ and $\hat{\mathbf{b}}$. The coordinates of vectors measured in B'' can be found from two transformations ${}^{B''}\mathbf{a} = {}^{B''}\mathbf{R}_{B'} \cdot {}^{B'}\mathbf{a}$ and ${}^{B''}\mathbf{b} = {}^{B''}\mathbf{R}_{B2} \cdot {}^{B2}\mathbf{b}$. For analysis purposes frame B' shall have its z-axis aligned with $\hat{\mathbf{a}}$ and its x-axis pointing along $\mathbf{a} \times \mathbf{d}$. $B2$ shall have its z-axis aligned with $\hat{\mathbf{b}}$ and its x-axis pointing along $\mathbf{c} \times \mathbf{b}$. The result for the coordinates of direction vectors is ${}^{B'}\mathbf{a} = {}^{B2}\mathbf{b} = (0,\ 0,\ 1)^T$. The corresponding coordinate transforms are then found as:

$$\begin{aligned} {}^{B''}\mathbf{R}_{B'} &= \mathbf{R}_x(-\alpha_{cd})\mathbf{R}_z(-\phi_d)\mathbf{R}_x(-\alpha_{ad}) \\ {}^{B''}\mathbf{R}_{B2} &= \mathbf{R}_z(\phi_c)\mathbf{R}_x(\alpha_{bc}). \end{aligned} \tag{4.8}$$

Using this, Eq. (4.7) can be expanded and rearranged to yield the scalar standard form of a constraint equation as

$$\mathscr{A}_c(\phi_d)\cos\phi_c + \mathscr{B}_c(\phi_d)\sin\phi_c = \mathscr{C}_c(\phi_d), \tag{4.9}$$

where the parameters $\mathscr{A}_c$, $\mathscr{B}_c$ and $\mathscr{C}_c$ are obtained as

$$\begin{aligned}
\mathscr{A}_c(\phi_d) &= -\sin\alpha_{bc}(\cos\alpha_{ad}\sin\alpha_{cd} + \cos\alpha_{cd}\cos\phi_d\sin\alpha_{ad}) \\
\mathscr{B}_c(\phi_d) &= \sin\phi_d\sin\alpha_{ad}\sin\alpha_{bc} \\
\mathscr{C}_c(\phi_d) &= \cos\alpha_{ab} - \cos\alpha_{bc}(\cos\alpha_{cd}\cos\alpha_{ad} - \cos\phi_d\sin\alpha_{cd}\sin\alpha_{ad}).
\end{aligned} \tag{4.10}$$

Applying the tangent-half-angle solution formula (2.37) to Eq. (4.9) yields

$$\phi_c(\phi_d) = 2\arctan\left(\frac{\mathscr{B}_c \pm \sqrt{\mathscr{A}_c^2 + \mathscr{B}_c^2 - \mathscr{C}_c^2}}{\mathscr{A}_c + \mathscr{C}_c}\right), \tag{4.11}$$

which has real solutions only if

$$\mathscr{A}_c^2 + \mathscr{B}_c^2 \geq \mathscr{C}_c^2. \tag{4.12}$$

However, even if Eq. (4.12) is satisfied for a given angle ϕ_d, the second four-bar defined by links K'', K''', $K2$ and $K3$ may be in a configuration where it cannot be assembled. Hence, the next step is to derive a similar condition for the second four-bar, which is obtained after determining $\phi_g(\phi_d)$.

Angular relationship $\phi_g(\phi_d)$

In order to obtain $\phi_g(\phi_d)$ it is important to see, that the angle $\phi_c(\phi_d)$, given by Eq. (4.11), represents the input parameter of the second four-bar. Then, the desired relation can be found by considering the constant dual scalar product from sect. 2.1.5, Eq. (2.26), using the lines $\hat{\mathbf{e}}$ and $\hat{\mathbf{f}}$, measured in B'':

$${}^{B''}\hat{\mathbf{e}} \cdot {}^{B''}\hat{\mathbf{f}} = \left({}^{B''}\mathbf{e} + \sigma\,{}^{B''}\mathbf{p}_e \times {}^{B''}\mathbf{e}\right) \cdot \left({}^{B''}\mathbf{f} + \sigma\,{}^{B''}\mathbf{p}_f \times {}^{B''}\mathbf{f}\right) = \cos\alpha_{ef} - \sigma l_{ef}\sin\alpha_{ef}, \tag{4.13}$$

To obtain $\hat{\mathbf{e}}$ and $\hat{\mathbf{f}}$, measured in B'' the coordinate transforms (4.8) of directions are extended to those of line screws using screw transformation matrices $\hat{\mathbf{T}}$, introduced in sect. 2.1.4 Eq. (2.18). Following the Denavit-Hartenberg methodology by only using transformations about x- and z-axes, requires screw transformation matrices of the form

$$\hat{\mathbf{T}}_x(\alpha, l) = \begin{pmatrix} \mathbf{R}_x(\alpha) & \mathbf{0} \\ \tilde{\mathbf{t}}_x(l)\mathbf{R}_x(\alpha) & \mathbf{R}_x(\alpha) \end{pmatrix} \quad \text{and} \quad \hat{\mathbf{T}}_z(\phi, s) = \begin{pmatrix} \mathbf{R}_z(\phi) & \mathbf{0} \\ \tilde{\mathbf{t}}_z(s)\mathbf{R}_z(\phi) & \mathbf{R}_z(\phi) \end{pmatrix}, \tag{4.14}$$

where $\tilde{\mathbf{t}}_x(l)$ and $\tilde{\mathbf{t}}_z(s)$ are skew symmetric matrices assembled from translation vectors $\mathbf{t}_x = (l,\, 0,\, 0)^T$ and $\mathbf{t}_z = (0,\, 0,\, s)^T$.

The B''-frame coordinates of axis $\hat{\mathbf{e}}$ are found from the screw transformation ${}^{B''}\hat{\mathbf{e}} = {}^{B''}\hat{\mathbf{T}}_{\bar{B}2} \cdot {}^{\bar{B}2}\hat{\mathbf{e}}$, where frame $\bar{B}2$ is rigidly attached to $B2$ from the previous section but is located at the new vertex, defined by axes $\hat{\mathbf{c}}$, $\hat{\mathbf{e}}$, $\hat{\mathbf{f}}$ and $\hat{\mathbf{g}}$. The z-axis of $\bar{B}2$ is aligned with $\hat{\mathbf{e}}$ while its x-axis should point along $\mathbf{e} \times \mathbf{c}$. Note that in the context of screw transformations $\hat{\mathbf{e}}$ is considered as a 6×1 vector instead of a dual vector. In frame $\bar{B}2$ $\hat{\mathbf{e}}$ then takes the simple form ${}^{\bar{B}2}\hat{\mathbf{e}} = (0,\, 0,\, 1,\, 0,\, 0,\, 0)^T$ and using the matrices introduced in Eq. (4.14) the corresponding screw transformation can be found as

$${}^{B''}\hat{\mathbf{T}}_{\bar{B}2} = \hat{\mathbf{T}}_z(\phi_c(\phi_d) + \vartheta, r)\hat{\mathbf{T}}_x(\pi - \alpha_{ce}, 0). \tag{4.15}$$

Herein the constant angle ϑ is measured between two planes in $K2$. The first one is spanned by the directions of $\hat{\mathbf{b}}$ and $\hat{\mathbf{c}}$, the second one is spanned by the directions of $\hat{\mathbf{c}}$ and $\hat{\mathbf{e}}$. r denotes the constant distance between the two displaced vertices, which may be measured along axis $\hat{\mathbf{c}}$.

In a similar fashion the B''-frame coordinates of axis $\hat{\mathbf{f}}$ are found from the screw transformation ${}^{B''}\hat{\mathbf{f}} = {}^{B''}\hat{\mathbf{T}}_{B'''}{}^{B'''} \cdot \hat{\mathbf{f}}$, where now frame B''' moves with link K''' and is located at the vertex, defined by axes $\hat{\mathbf{c}}$, $\hat{\mathbf{e}}$, $\hat{\mathbf{f}}$ and $\hat{\mathbf{g}}$. For analysis purposes the z-axis of this frame is aligned with the direction of $\hat{\mathbf{f}}$ while its x-axis points along $\mathbf{g} \times \mathbf{f}$. In B''' also $\hat{\mathbf{f}}$ takes the simple form ${}^{B'''}\hat{\mathbf{f}} = (0,\ 0,\ 1,\ 0,\ 0,\ 0)^T$ and using the matrices from Eq. (4.14) yields

$$ {}^{B''}\hat{\mathbf{T}}_{B'''} = \hat{\mathbf{T}}_z(\rho, r)\hat{\mathbf{T}}_x(-(\pi - \alpha_{cg}), 0)\hat{\mathbf{T}}_z(-\phi_g, 0)\hat{\mathbf{T}}_x(\alpha_{fg}, 0), \tag{4.16} $$

where the constant angle ρ is measured between two planes in K''. The first one is spanned by the directions of $\hat{\mathbf{d}}$ and $\hat{\mathbf{c}}$, the second one is spanned by the directions of $\hat{\mathbf{g}}$ and $\hat{\mathbf{c}}$.

In order to expand Eq. (4.13) the different lines ${}^{B''}\hat{\mathbf{e}}$ and ${}^{B''}\hat{\mathbf{f}}$ are written as dual vectors. Then the real part in Eq. (4.13) reads

$$ \left({}^{B''}\mathbf{e}\right)^T \cdot {}^{B''}\mathbf{f} = \cos\alpha_{ef}, \tag{4.17} $$

while the dual part is identically satisfied. This shows, that the angular relation $\phi_g(\phi_d)$ is only defined by the real part of the dual scalar product. The result is, that analysis of angular relations may also be performed by considering the two spherical four-bars being located at one common vertex. This reduces the calculation efforts to a purely spherical analysis.

Eq. (4.17) is also known as the spherical image of the dual scalar product since it represents nothing but a constraint equation of a spherical four-bar. This expands to yield the standard form

$$ \mathscr{A}_g(\phi_c(\phi_d))\cos\phi_g + \mathscr{B}_g(\phi_c(\phi_d))\sin\phi_g = \mathscr{C}_g(\phi_c(\phi_d)), \tag{4.18} $$

where the parameters $\mathscr{A}_g$, $\mathscr{B}_g$ and $\mathscr{C}_g$ are obtained as

$$ \begin{aligned} \mathscr{A}_g(\phi_c(\phi_d)) &= -\cos\alpha_{ce}\sin\alpha_{cg}\sin\alpha_{fg} - \cos(\phi_c(\phi_d)+\vartheta)\cos\alpha_{cg}\sin\alpha_{ce}\sin\alpha_{fg}\cos\rho - \\ &\quad \sin(\phi_c(\phi_d)+\vartheta)\cos\alpha_{cg}\sin\alpha_{ce}\sin\alpha_{fg}\sin\rho \\ \mathscr{B}_g(\phi_c(\phi_d)) &= \cos(\phi_c(\phi_d)+\vartheta)\sin\alpha_{ce}\sin\alpha_{fg}\sin\rho - \sin(\phi_c(\phi_d)+\vartheta)\sin\alpha_{ce}\sin\alpha_{fg}\cos\rho \\ \mathscr{C}_g(\phi_c(\phi_d)) &= \cos\alpha_{ef} - \cos\alpha_{ce}\cos\alpha_{cg}\cos\alpha_{fg} + \\ &\quad \cos(\phi_c(\phi_d)+\vartheta)\cos\alpha_{fg}\sin\alpha_{ce}\sin\alpha_{cg}\cos\rho + \\ &\quad \sin(\phi_c(\phi_d)+\vartheta)\cos\alpha_{fg}\sin\alpha_{ce}\sin\alpha_{cg}\sin\rho. \end{aligned} \tag{4.19} $$

Applying the tangent-half-angle solution formula (2.37) to Eq. (4.19) yields

$$ \phi_g(\phi_c(\phi_d)) = 2\arctan\left(\frac{\mathscr{B}_g \pm \sqrt{\mathscr{A}_g^2 + \mathscr{B}_g^2 - \mathscr{C}_g^2}}{\mathscr{A}_g + \mathscr{C}_g}\right), \tag{4.20} $$

which has real solutions if $\mathscr{A}_g^2 + \mathscr{B}_g^2 \geq \mathscr{C}_g^2$. This combines with Eq. (4.12) of the 'first' four-bar and yields the following condition for two coupled spherical four-bars to have a valid assembly mode for a given angular value ϕ_d:

$$ \mathscr{A}_c^2 + \mathscr{B}_c^2 \geq \mathscr{C}_c^2 \qquad \wedge \qquad \mathscr{A}_g^2 + \mathscr{B}_g^2 \geq \mathscr{C}_g^2. \tag{4.21} $$

The angular relations $\phi_c(\phi_d)$ and $\phi_g(\phi_c(\phi_d))$ from Eq. (4.11) and (4.20) allow to determine the location and orientation of each axis of the spherically constrained spatial RR chain. On the one

hand axes ${}^{B''}\hat{\mathbf{a}}$, ${}^{B''}\hat{\mathbf{b}}$ and ${}^{B''}\hat{\mathbf{d}}$ can be found in the lower four-bar (see again Fig. 4.2 or 4.3). On the other hand ${}^{B''}\hat{\mathbf{e}}$, ${}^{B''}\hat{\mathbf{f}}$ and ${}^{B''}\hat{\mathbf{g}}$ can be found in the upper four-bar. The complete set of formulas that allow the calculation of the current location and orientation of lines is given as

$$
\begin{aligned}
{}^{B''}\hat{\mathbf{a}} &= {}^{B''}\hat{\mathbf{T}}_{B'}{}^{B'} \cdot \hat{\mathbf{a}} & {}^{B''}\hat{\mathbf{T}}_{B'} &= \hat{\mathbf{T}}_x(-\alpha_{cd},0)\hat{\mathbf{T}}_z(-\phi_d,0)\hat{\mathbf{T}}_x(-\alpha_{ad},0),\\
{}^{B''}\hat{\mathbf{b}} &= {}^{B''}\hat{\mathbf{T}}_{B2}{}^{B2} \cdot \hat{\mathbf{b}} & {}^{B''}\hat{\mathbf{T}}_{B2} &= \hat{\mathbf{T}}_z(\phi_c(\phi_d),0)\hat{\mathbf{T}}_x(\alpha_{bc},0),\\
{}^{B''}\hat{\mathbf{d}} &= {}^{B''}\hat{\mathbf{T}}_{\bar{B}'}{}^{\bar{B}'} \cdot \hat{\mathbf{d}} & {}^{B''}\hat{\mathbf{T}}_{\bar{B}'} &= \hat{\mathbf{T}}_x(-\alpha_{cd},0),\\
{}^{B''}\hat{\mathbf{e}} &= {}^{B''}\hat{\mathbf{T}}_{\bar{B}2}{}^{\bar{B}2} \cdot \hat{\mathbf{e}} & {}^{B''}\hat{\mathbf{T}}_{\bar{B}2} &= \hat{\mathbf{T}}_z(\phi_c(\phi_d)+\vartheta,r)\hat{\mathbf{T}}_x(\pi-\alpha_{ce},0),\\
{}^{B''}\hat{\mathbf{f}} &= {}^{B''}\hat{\mathbf{T}}_{B'''}{}^{B'''} \cdot \hat{\mathbf{f}} & {}^{B''}\hat{\mathbf{T}}_{B'''} &= \hat{\mathbf{T}}_z(\rho,r)\hat{\mathbf{T}}_x(-(\pi-\alpha_{cg}),0)\hat{\mathbf{T}}_z(-\phi_g,0)\hat{\mathbf{T}}_x(\alpha_{fg},0),\\
{}^{B''}\hat{\mathbf{g}} &= {}^{B''}\hat{\mathbf{T}}_{\bar{B}''}{}^{\bar{B}''} \cdot \hat{\mathbf{g}} & {}^{B''}\hat{\mathbf{T}}_{\bar{B}''} &= \hat{\mathbf{T}}_z(\rho,r)\hat{\mathbf{T}}_x(-(\pi-\alpha_{cg}),0),
\end{aligned}
\tag{4.22}
$$

where ${}^{B'}\hat{\mathbf{a}} = {}^{B2}\hat{\mathbf{b}} = {}^{\bar{B}'}\hat{\mathbf{d}} = {}^{\bar{B}2}\hat{\mathbf{e}} = {}^{B'''}\hat{\mathbf{f}} = {}^{\bar{B}''}\hat{\mathbf{g}} = (0,\ 0,\ 1,\ 0,\ 0,\ 0)^T$. Note that one may directly specify ${}^{B''}\hat{\mathbf{c}} = (0,\ 0,\ 1,\ 0,\ 0,\ 0)^T$.

Example

As a quick example the analytical relationships $\phi_c(\phi_d)$ and $\phi_g(\phi_d)$ from Eq. (4.11) and (4.20) were calculated for the linkage from Fig. 4.3. The kinematic dimensions of the linkage are given as $\alpha_{ab} = 65.97$ deg, $\alpha_{bc} = 60.46$ deg, $\alpha_{cd} = 120.69$ deg, $\alpha_{ad} = 81.2$ deg, $r = 186.14$ mm, $\vartheta = 19.94$ deg, $\rho = 83.9$ deg, $\alpha_{ce} = 91.3$ deg, $\alpha_{ef} = 62.71$ deg, $\alpha_{cg} = 123.78$ deg and $\alpha_{fg} = 91.52$ deg. The input angle is defined as a simple linear function in time: $\phi_d(t) = t$ within a motion range of 55 deg $\leq \phi_d \leq$ 200 deg. Fig. 4.4 shows the resulting relations. Note that angles measured at the kinematic CAD-model of the spherically constrained RR chain were in perfect accordance with the relations shown in the figure.

Numerical solution approach

Due to the fact that multiloop linkages can also yield constraint equations, which cannot be solved analytically and independently as shown above, also another numerical solution approach is briefly sketched here. The approach aims at using the Newton-Raphson algorithm (see e.g. [6], pp. 100-106 for details about the Newton-Raphson method in the context of numerical linkage analysis) and hence requires a nonlinear system of equations. This is given by Eq. (4.9) and (4.18) and may be written as

$$
\mathbf{z}(\phi_c,\phi_g) = \begin{pmatrix} z_1(\phi_c,\phi_g) \\ z_2(\phi_c,\phi_g) \end{pmatrix} = \begin{pmatrix} \mathscr{A}_c(\phi_d)\cos\phi_c + \mathscr{B}_c(\phi_d)\sin\phi_c - \mathscr{C}_c(\phi_d) \\ \mathscr{A}_g(\phi_c)\cos\phi_g + \mathscr{B}_g(\phi_c)\sin\phi_g - \mathscr{C}_g(\phi_c) \end{pmatrix} = \begin{pmatrix} 0 \\ 0 \end{pmatrix},
\tag{4.23}
$$

where ϕ_d is the given input. Note that in contrast to Eq. (4.18) z_2 is considered here only as a function of ϕ_c. Applying the Newton-Raphson formula yields

$$
\begin{pmatrix} \phi_c \\ \phi_g \end{pmatrix}^{i+1} = \begin{pmatrix} \phi_c \\ \phi_g \end{pmatrix}^{i} - \underbrace{\begin{pmatrix} \frac{\partial z_1}{\partial \phi_c} & \frac{\partial z_1}{\partial \phi_g} \\ \frac{\partial z_2}{\partial \phi_c} & \frac{\partial z_2}{\partial \phi_g} \end{pmatrix}^{-1}}_{(\mathbf{J}^i)^{-1}} \cdot \begin{pmatrix} z_1 \\ z_2 \end{pmatrix}^{i},
\tag{4.24}
$$

where $\mathbf{J}$ is a Jacobian matrix. A convenient set of starting values ϕ_c^1, ϕ_g^1 may be found from a synthesis solution of a linkage in a reference configuration. Implementing the algorithm yields the angular relations $\phi_c(\phi_d)$ and $\phi_g(\phi_d)$, where the second relation will yield the same result as $\phi_g(\phi_c(\phi_d))$ from Eq. (4.20).

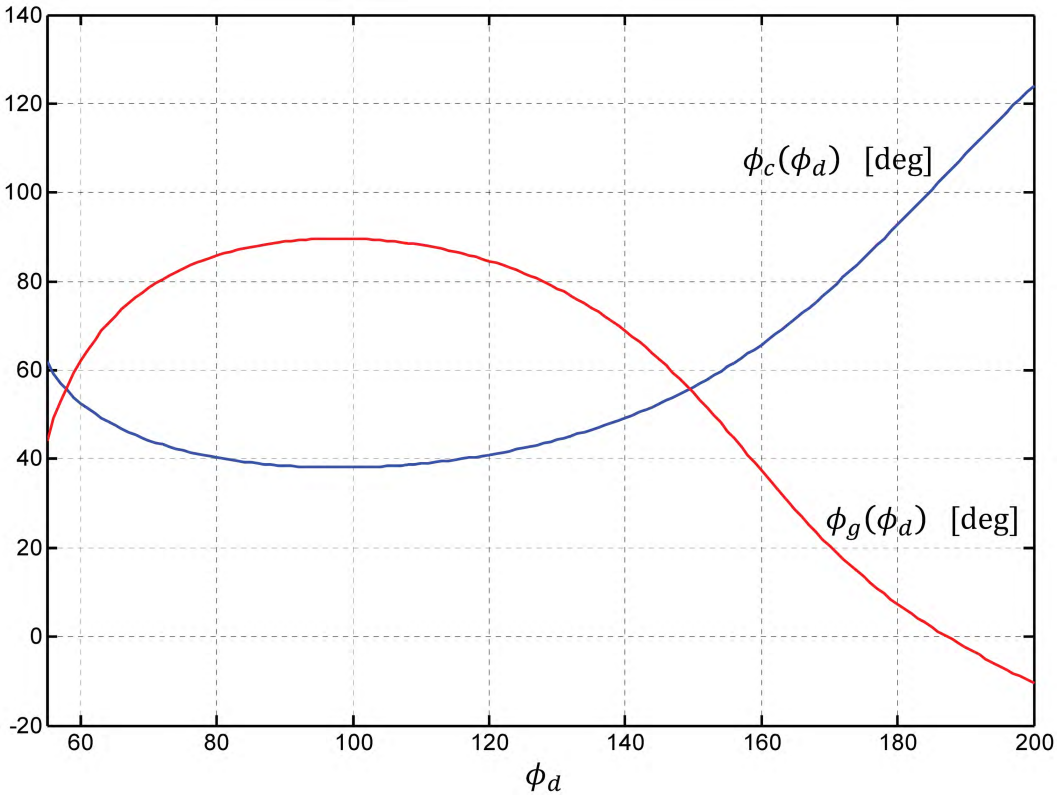

Figure 4.4.: Angular relations $\phi_c(\phi_d)$ and $\phi_g(\phi_d)$ of a spherically constrained RR chain for the input range 55 deg $\leq \phi_d \leq$ 200 deg

Modifications for spherically constrained, spherical RR chains

In the case that axes $\hat{\mathbf{d}}$ and $\hat{\mathbf{g}}$ form a spherical RR chain, they intersect at a certain point (see, sect. 3.2.1 Fig. 3.3b). Another way of saying this is that $\hat{\mathbf{d}}$ and $\hat{\mathbf{g}}$ lie in one plane, which means that the angle ρ equals zero in the analysis of a spherically constrained, spherical RR chain.

Modifications for spherically constrained, planar RR chains

In the case that axes $\hat{\mathbf{d}}$ and $\hat{\mathbf{g}}$ form a planar RR chain, they are parallel to each other (see, sect. 3.2.1 Fig. 3.2 and 3.3a). As it was the case for the spherical RR chain, this means that the angle ρ equals zero. However, in addition to that, the angle α_{cg} satisfies the relation $\alpha_{cg} = \pi - \alpha_{cd}$ in the analysis of a spherically constrained, planar RR chain.

4.1.3. Line-Based Analysis of Transmission Properties of a Single Spherical Four-Bar

Line-based singularities of a linkage were introduced in sect. 2.2.4 as configurations, where joint axes become linearly dependent. Even though this text does not aim at providing a complete analysis or list of line-based singularities, the goal of this section is to provide at least a little study on such configurations in spherically constrained RR chains. Since this type of linkage is nothing but two specifically coupled spherical four-bars, the study requires a line-based analysis of a spherical four-bar. This is provided in a general manner in the following and leads to what is called here a line-based analysis of transmission properties.

Line-based identification of the limits on input and output angles

In order to perform a line-based analysis of a spherical four-bar, the directions ${}^W\mathbf{a}$, ${}^W\mathbf{b}$, ${}^W\mathbf{c}$ and ${}^W\mathbf{d}$ of the screw system from Eq. (2.44) are considered to be known from a position analysis. When $\phi_a = \phi_a(t)$ is considered to be the given time dependent input also $\dot{\phi}_a$ is known and ${}^W\mathbf{a}$, ${}^W\mathbf{b}$, ${}^W\mathbf{c}$ and ${}^W\mathbf{d}$ move within the limits of the input angle ϕ_a. On the other hand $\dot{\phi}_b$, $\dot{\phi}_c$ and $\dot{\phi}_d$ are unknown and Eq. (2.44) can be rearranged as

$$\underbrace{\left({}^W\mathbf{b}\;{}^W\mathbf{c}\;{}^W\mathbf{d}\right)}_{\mathbf{J}_{bcd}} \cdot \underbrace{\begin{pmatrix} \dot{\phi}_b \\ \dot{\phi}_c \\ \dot{\phi}_d \end{pmatrix}}_{\dot{\mathbf{q}}_{bcd}} = -\underbrace{\dot{\phi}_a\,{}^W\mathbf{a}}_{\vec{\omega}_a}. \tag{4.25}$$

This linear system of equations only has a solution if $\det(\mathbf{J}_{bcd}) \neq 0$, i.e. if the three directions **b**, **c** and **d** are linearly independent. In turn, $\det(\mathbf{J}_{bcd}) = 0$ yields linear dependent joint axes, which means that **b**, **c** and **d** lie in the same plane. The four-bar is said to be in a singular configuration, which can be detected by tracing the determinant:

$$\det(\mathbf{J}_{bcd}) \begin{cases} = 0 & \mathbf{J}_{bcd} \text{ is singular} \\ \neq 0 & \mathbf{J}_{bcd} \text{ is regular.} \end{cases} \tag{4.26}$$

In fact, there are two cases where $\det(\mathbf{J}_{bcd}) = 0$, which correspond to the *lower and upper limits of the input*[1] (see e.g. [33] pp. 31-33 and pp. 165-167 for the definition of input limits of planar and spherical four-bars). The physical interpretation of the configurations defined by Eq. (4.26) is, that the four-bar allows a small amount of rotations $\mathrm{d}\mathbf{q}_{bcd} = (\mathrm{d}\phi_b,\, \mathrm{d}\phi_c,\, \mathrm{d}\phi_d)^T$ about the axes **b**, **c** and **d** although the actuation is blocked. In a real linkage with structural elasticity and joint clearance as well as external forces acting on the different links the result is a mechanism configuration that will provide significant mobility and cannot be controlled by the actuator.

The matrix $\mathbf{J}_{bcd}$ can be seen as a *Jacobian of a spherical four-bar*. However, instead of assembling **J** from **b**, **c** and **d** one may also define three other criteria, which correspond to lower and upper limits of angles ϕ_b, ϕ_c and ϕ_d:

$$\det(\mathbf{J}_{acd}) = 0, \qquad \det(\mathbf{J}_{abd}) = 0, \qquad \det(\mathbf{J}_{abc}) = 0. \tag{4.27}$$

Since $\phi_a = \phi_a(t)$ is still considered as the input angle here, the three angles ϕ_b, ϕ_c and ϕ_d represent *output angles of the linkage* and the geometric meanings of the criteria in Eq. (4.27) are:

1. $\det(\mathbf{J}_{acd}) = 0$: In a configuration defined by a value $\phi_a(t)$ the output about **b** doesn't change, i.e. $\mathrm{d}\phi_b = 0$ or $\dot{\phi}_b = 0$.

2. $\det(\mathbf{J}_{abd}) = 0$: In a configuration defined by a value $\phi_a(t)$ the output about **c** doesn't change, i.e. $\mathrm{d}\phi_c = 0$ or $\dot{\phi}_c = 0$.

3. $\det(\mathbf{J}_{abc}) = 0$: In a configuration defined by a value $\phi_a(t)$ the output about **d** doesn't change, i.e. $\mathrm{d}\phi_d = 0$ or $\dot{\phi}_d = 0$.

[1] It is crucial to mention here, that only two cases exist in the absence of special kinematic dimensions. If a linkage has for instance dimensions that allow a configuration where all joint axes lie in a common plane it can happen that further cases must be taken into account.

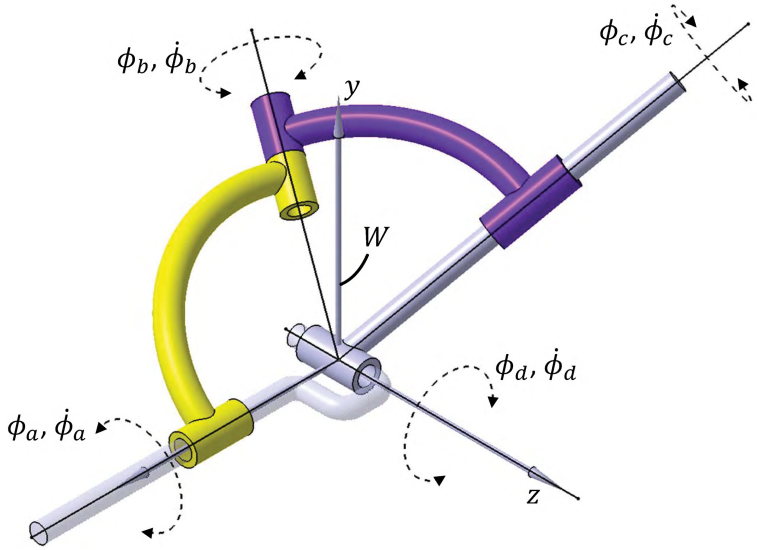

Figure 4.5.: Example four-bar for line-based analysis of transmission properties

In an application, where it is for instance the goal to make use of a $\dot{\phi}_d \neq 0$ over a specified input range of ϕ_a, the criterion $\det(\mathbf{J}_{abc}) = 0$ may be used to check whether the considered four-bar actually realizes the desired goal. Another scenario may be a moment, trying to induce $\mathrm{d}\phi_d$ at the four-bar. However, if $\det(\mathbf{J}_{abc}) = 0$ the result is $\mathrm{d}\phi_d = 0$ for any given input $\phi_a(t)$, which in turn means that no movement can be, induced by the torque.

A weighted Frobenius condition number as singularity measure

Another approach to detect the singular configurations in a numerical analysis is to consider ill-conditioned cases of a Jacobian $\mathbf{J}$. A suitable measure to consider such cases is the condition number

$$\kappa(\mathbf{J}) = |\mathbf{J}||\mathbf{J}^{-1}|, \tag{4.28}$$

where $|\mathbf{J}|$ is a matrix norm of $\mathbf{J}$. As stated by Angeles and Park [113], p. 236 or also in [114] in particular a *weighted Frobenius norm* defined as

$$|\mathbf{J}|_F = \sqrt{\frac{1}{n}\mathrm{tr}\,(\mathbf{J}(\mathbf{J})^T)} \tag{4.29}$$

is a suitable norm, where the weight $\frac{1}{n}$ shall be $\frac{1}{3}$ because $\mathbf{J}$ is a 3×3 matrix for four-bar analysis. This yields the weighted Frobenius condition number

$$\kappa_F(\mathbf{J}) = \frac{1}{3}\sqrt{\mathrm{tr}\,(\mathbf{J}(\mathbf{J})^T)}\sqrt{\mathrm{tr}((\mathbf{J}(\mathbf{J})^T)^{-1})}, \tag{4.30}$$

where tr() is the trace of a matrix. The linkage is said to be in or close to a singular configuration when $\kappa_F(\mathbf{J}) >> 1$. Beside Eq. (4.26) this provides another condition to trace singularities.

Example

The determinant $\det(\mathbf{J})$ as well as the weighted Frobenius condition number $\kappa_F(\mathbf{J})$ were calculated for an exemplary spherical four-bar formed by directions $\mathbf{a}$, $\mathbf{b}$, $\mathbf{c}$ and $\mathbf{d}$, and with dimensions $\alpha_{ab} = 115$ deg, $\alpha_{bc} = 70$ deg, $\alpha_{cd} = 70$ deg and $\alpha_{ad} = 90$ deg. Figure 4.5 shows the four-bar in a reference configuration, where ${}^W\mathbf{a} = (1,\ 0,\ 0)^T$ and ${}^W\mathbf{d} = (0,\ 0,\ 1)^T$. -147.5 deg $<$

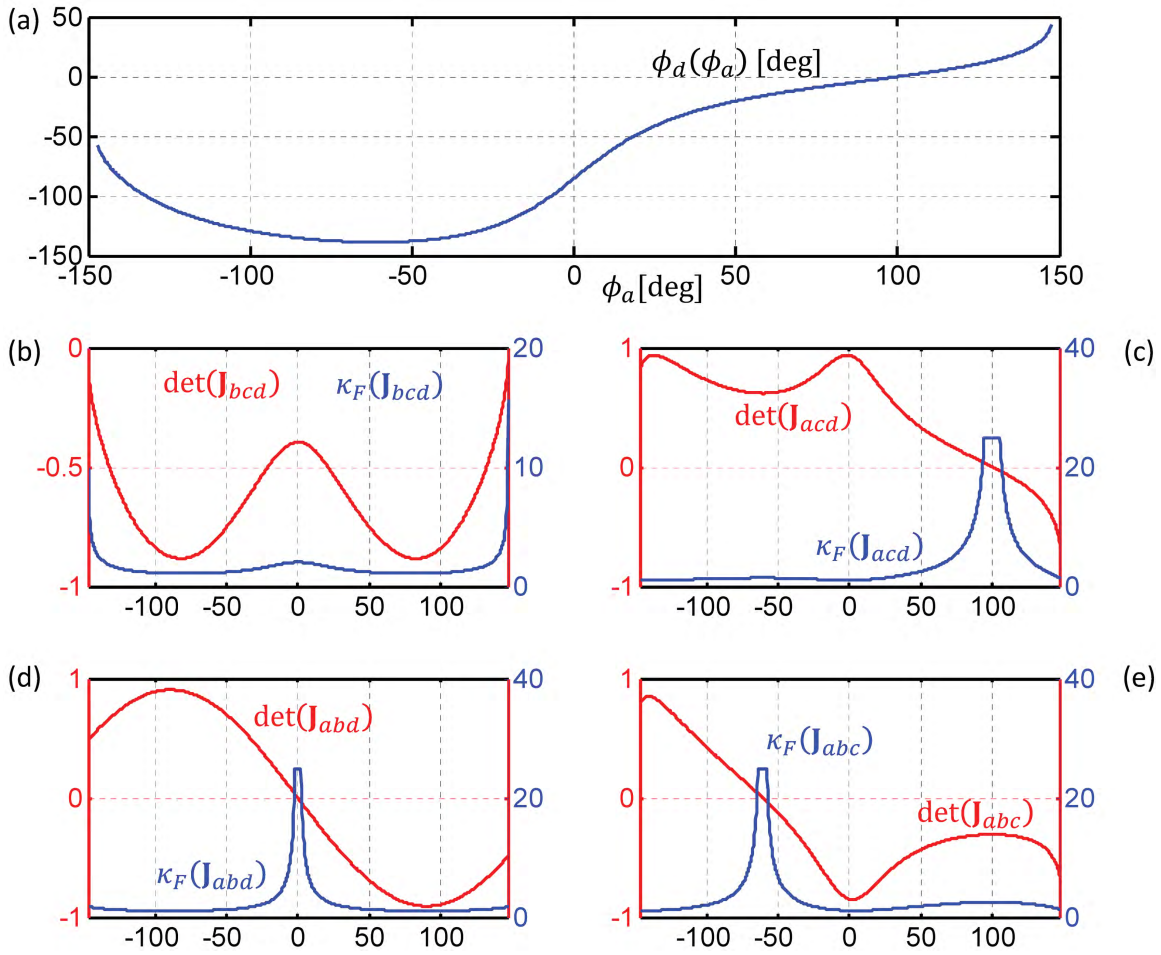

Figure 4.6.: Angular relation $\phi_d(\phi_a)$ within the input range -147.5 deg $< \phi_a <$ 147.5 deg as well as singular configurations of the four-bar

$\phi_a <$ 147.5 deg shall represent the given range of the input angle ϕ_a, which is used to determine the current orientation of the moving direction ${}^W\mathbf{b}$. Based on a forward position analysis the angular relation $\phi_d(\phi_a)$ is found, which is then used to obtain the current orientation of the second moving direction ${}^W\mathbf{c}$.

The relation $\phi_d(\phi_a)$ is shown in Fig. 4.6a), which shows a continuous function over the range -147.5 deg $< \phi_a <$ 147.5 deg. In order to determine singular configurations that belong to the limits of input angles, the following quantities were evaluated:

$$\det(\mathbf{J}_{bcd}(\phi_a)) \qquad \text{and} \qquad \kappa_F(\mathbf{J}_{bcd}(\phi_a)), \tag{4.31}$$

where κ_F is the weighted Frobenius condition number from Eq. (4.30). The results are shown in Fig. 4.6b), where the determinant or the condition number tend to zero or to infinity at the starting and ending configuration of the linkage. In fact, these are nothing but the (approximate) limits of the input angle ϕ_a.

In order to determine configurations that belong to the limits of output angles within the input range, the following quantities were evaluated:

$$\det(\mathbf{J}_{acd}(\phi_a)) \qquad \text{and} \qquad \kappa_F(\mathbf{J}_{acd}(\phi_a)), \tag{4.32}$$

$$\det(\mathbf{J}_{abd}(\phi_a)) \qquad \text{and} \qquad \kappa_F(\mathbf{J}_{abd}(\phi_a)), \tag{4.33}$$

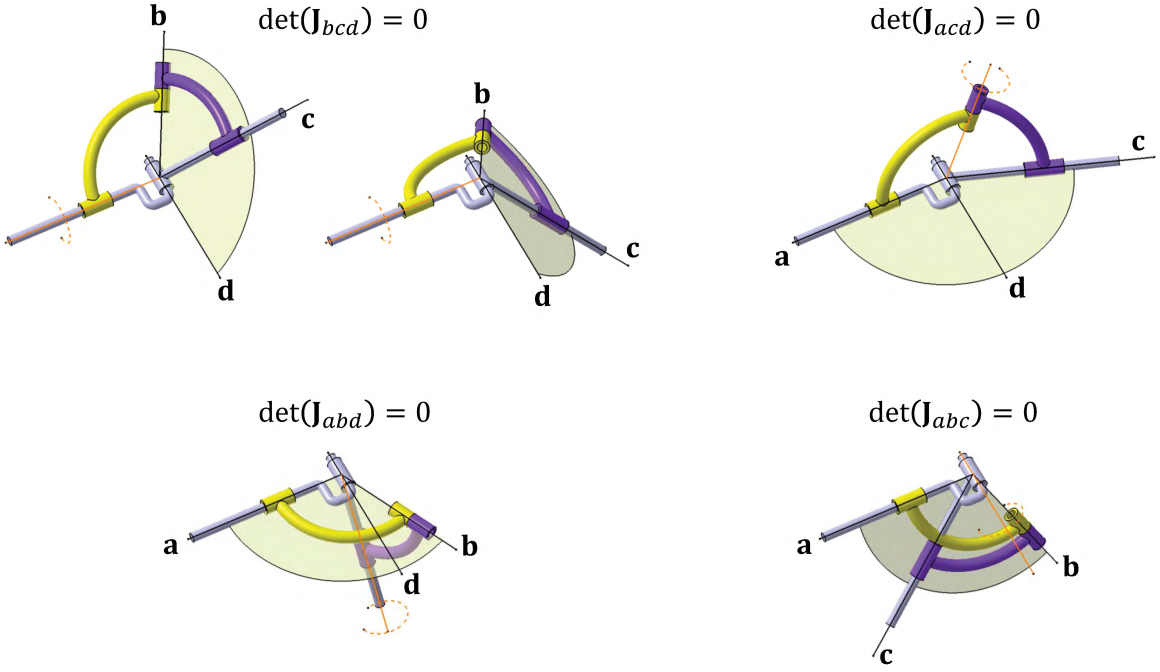

Figure 4.7.: Line-based analysis results that correspond to the limits of input and output angles

$$\det(\mathbf{J}_{abc}(\phi_a)) \qquad \text{and} \qquad \kappa_F(\mathbf{J}_{abc}(\phi_a)), \tag{4.34}$$

The results are shown in Fig. 4.6c) to e), where limits of outputs were found for each of these cases. Equation (4.32) is satisfied at $\phi_a \approx 100$ deg, while (4.33) and (4.34) are at $\phi_a \approx 0$ deg and $\phi_a \approx -61$ deg respectively. The corresponding linkage configurations are shown in Fig. 4.7.

As one can see $\det(\mathbf{J})$ varies within the range of $(1,-1)$, while $\kappa_F(\mathbf{J})$ tends to very large values when angular limits are reached. For this reason $\kappa_F(\mathbf{J})$ is cut here at a maximum value of 25. Thus, different characteristics can be observed, so that both measures will be considered within this work.

4.1.4. Line-Based Analysis of Transmission Properties of Two Coupled Spherical Four-Bars

In the case of a spherically constrained RR chain there are two coupled spherical four-bars, see e.g. Fig. 4.2 or 4.3. Due to the coupling, the actuation between these four-bars interact, which has just been shown in sect. 4.1.2. Here ϕ_d was considered as the input of the first four-bar, which resulted in $\phi_c(\phi_d)$ as the input for the second four-bar. A configuration in a spherically constrained RR chain, which corresponds to a limit in the inputs then means

1. the input ϕ_d of the first four-bar cannot sufficiently resist angular changes

$$\mathrm{d}\mathbf{q}_{abc} = (\mathrm{d}\phi_a,\, \mathrm{d}\phi_b,\, \mathrm{d}\phi_c)^T, \qquad \text{or} \tag{4.35}$$

2. the input $\phi_c(\phi_d)$ of the second four-bar cannot sufficiently resist angular changes

$$\mathrm{d}\mathbf{q}_{efg} = (\mathrm{d}\phi_e,\, \mathrm{d}\phi_f,\, \mathrm{d}\phi_g)^T. \tag{4.36}$$

The corresponding conditions allowing it to detect these cases are hence

$$\det(\mathbf{J}_{abc}(\phi_d)) \qquad \text{and} \qquad \kappa_F(\mathbf{J}_{abc}(\phi_d)) \tag{4.37}$$

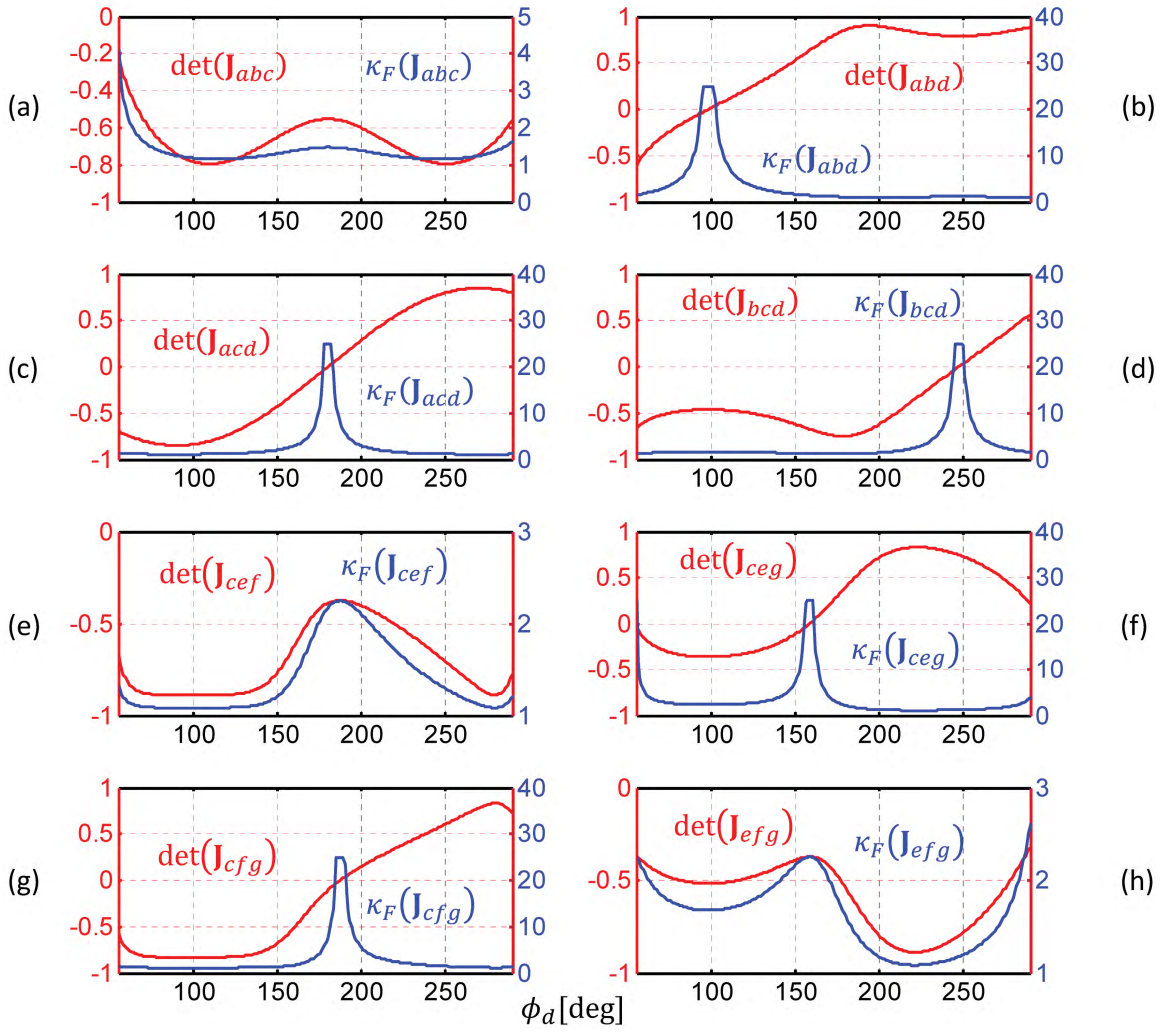

Figure 4.8.: Singular configurations of the two coupled four-bars from Fig. 4.3 within an input range 55 deg $< \phi_d <$ 290 deg

and

$$\det(\mathbf{J}_{efg}(\phi_c(\phi_d))) \qquad \text{and} \qquad \kappa_F(\mathbf{J}_{efg}(\phi_c(\phi_d))). \tag{4.38}$$

However, beside limits of the inputs, also limits on the outputs may occur, which can be detected by tracing the determinant or the condition number of Jacobians assembled from any other possible combination of joint axes (directions) of the two different four-bars.

Figure 4.8 shows the determinants as well as the condition numbers of the spherically constrained RR chain from Fig. 4.3 over the input ϕ_d, where here the motion range has been enlarged, such that 55 deg $< \phi_d <$ 290 deg. Note that the current orientation of joint axes may be found from Eq. (4.22). Then coordinates are consistently measured in frame B'', which, however, does not affect the calculation of determinants or condition numbers.

Figure 4.8a) to d) correspond to Jacobians, which are assembled from directions **a**, **b**, **c** and **d** that make up the 'first' four-bar. As one can see from figure a), $\det(\mathbf{J}_{abc}(\phi_d = 55 \text{ deg}))$ or $\kappa_F(\mathbf{J}_{abc}(\phi_d = 55 \text{ deg}))$ tends to zero or to values $>> 1$, which means that the first four-bar is close to a limit on the input in this configuration. On the other hand figures b), c) and d) show, that there are limits of the output angles ϕ_a, ϕ_b and ϕ_c at input values of $\phi_d \approx 247$ deg, $\phi_d \approx 180$ deg and $\phi_d \approx 98$ deg.

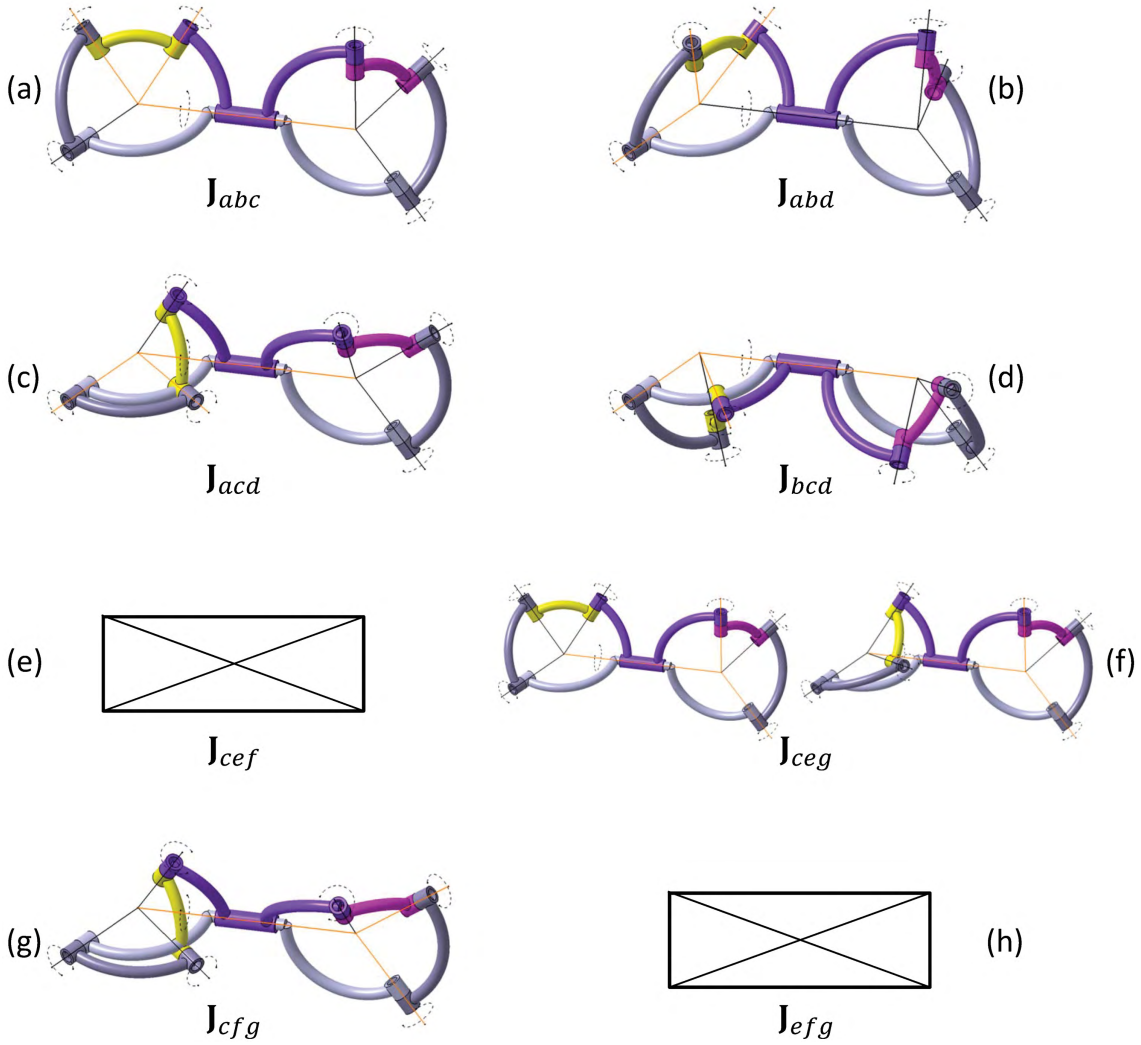

Figure 4.9.: Graphical depiction of the singular configurations of the two coupled four-bars from Fig. 4.3 within an input range 55 deg $< \phi_d <$ 290 deg

Figures e) to h) belong to Jacobians of the 'second' four-bar, assembled from directions **c**, **e**, **f** and **g**. Since here $\phi_c(\phi_d)$ is the corresponding input, limits of this input are detected when $\det(\mathbf{J}_{efg}(\phi_c(\phi_d))) = 0$ or $\kappa_F(\mathbf{J}_{efg}(\phi_c(\phi_d))) >> 1$. However, as one can see, this is not the case in figure h), which means that the 'second' four-bar does not reach any input limits within 55 deg $< \phi_d <$ 290 deg. Similarly one can see from figure e), that this is also the case for the output angle ϕ_g. However, the two remaining outputs possess two limits within the input range. On the one hand there is ϕ_e, which reaches a limit at $\phi_d \approx 187$ deg, see figure g). On the other hand there is ϕ_f, which in fact reaches a limit at $\phi_d = 55$ deg and another one at $\phi_d \approx 158$ deg.

Even though the input $\phi_c(\phi_d)$ of the 'second' four-bar itself does not reach any input limits within the range of ϕ_d, $\phi_c(\phi_d)$ was the output of the 'first' four-bar, which reached its limit at $\phi_d \approx 247$ deg. Hence, in this configuration no motion is transmitted into the 'second' four-bar, which in turn also represents a certain limitation on the input of the 'second' four-bar.

Figure 4.9 provides the graphical depiction of the different configurations of the spherically constrained RR chain. Note that axes are highlighted, which are lying in a plane, i.e. which define a limit on an input or output. At figure f) one can see, that the two different singular situations of $\mathbf{J}_{ceg}$ at $\phi_d = 55$ deg and at $\phi_d \approx 158$ deg actually correspond to the same configuration

of the 'second' four-bar but to two different configurations of the 'first' four-bar.

4.2. Two-Configuration Synthesis Procedures

For the f.p.s. of spherically constrained linkages a *two-configuration synthesis* is developed in this section, which allows it to compute joint axes of a linkage, such that each link in a linkage can reach two prescribed planar, spherical or either spatial poses. Beside spherically constrained linkages the methodology also applies to all other types of linkages that consist of R and/or C joints and may be particularly helpful when two distinct configurations (e.g. compact, stowed configurations) of a system are a concern.

Detailed solution procedures to solve the synthesis equations derived here are given in the appendix, sect. A.4 and may be consulted when required. Note that the general method has also been considered in [103] and [104], and has been specified precisely in [111]

4.2.1. The General Spatial Two-Configuration Synthesis Method

Two-configuration synthesis evolves from considering two poses of two consecutive links Ka and Kb of the linkage. Those are described by two frames Ba and Bb, rigidly attached to the consecutive links. Ba and Bb shall be displaced by two pre-defined 4×4 homogeneous transforms $({}^W\mathbf{T}^i_{Ba}, {}^W\mathbf{T}^j_{Ba})$ and $({}^W\mathbf{T}^i_{Bb}, {}^W\mathbf{T}^j_{Bb})$, where $\mathbf{T}\in SE(3)$. Using Eq. (2.3) yields the relative displacements $\mathbf{T}^{ij}_{Ba}$ and $\mathbf{T}^{ij}_{Bb}$.

Next, the Plücker coordinates $\hat{\mathbf{l}} = (\mathbf{l},\ \mathbf{p}_l \times \mathbf{l})^T$ of either a R or C joint axis are considered, which couples the different links. The coupling implies that $\hat{\mathbf{l}}$ must satisfy $\mathbf{T}^{ij}_{Ba}$ and $\mathbf{T}^{ij}_{Bb}$, which means that $\hat{\mathbf{l}}$ must satisfy two different relative displacement equations of a line:

$$\hat{\mathbf{l}}^j = \hat{\mathbf{T}}^{ij}_{Ba}\cdot\hat{\mathbf{l}}^i \qquad \text{and} \qquad \hat{\mathbf{l}}^j = \hat{\mathbf{T}}^{ij}_{Bb}\cdot\hat{\mathbf{l}}^i, \tag{4.39}$$

see Eq. (2.19). Recall here, that relative displacements are completely measured in W. Subtracting and rearranging yields $(\hat{\mathbf{T}}^{ij}_{Ba} - \hat{\mathbf{T}}^{ij}_{Bb})\cdot\hat{\mathbf{l}}^i = \hat{\mathbf{0}}$ and multiplication on the left by $(\hat{\mathbf{T}}^{ij}_{Ba})^{-1}$ results in

$$(\hat{\mathbf{E}} - \underbrace{(\hat{\mathbf{T}}^{ij}_{Ba})^{-1}\hat{\mathbf{T}}^{ij}_{Bb}}_{\hat{\mathbf{T}}^{ij}_{Ba|Bb}})\cdot\hat{\mathbf{l}}^i = \hat{\mathbf{0}}, \tag{4.40}$$

where

$$\hat{\mathbf{T}}^{ij}_{Ba|Bb} = \begin{pmatrix} (\mathbf{R}^{ij}_{Ba})^T\mathbf{R}^{ij}_{Bb} & \mathbf{0} \\ (\mathbf{R}^{ij}_{Ba})^T\left((\tilde{\mathbf{t}}^{ij}_{Ba})^T + \tilde{\mathbf{t}}^{ij}_{Bb}\right)\mathbf{R}^{ij}_{Bb} & (\mathbf{R}^{ij}_{Ba})^T\mathbf{R}^{ij}_{Bb} \end{pmatrix}. \tag{4.41}$$

Notice that multiplication by $(\hat{\mathbf{T}}^{ij}_{Bb})^{-1}$ yields a similar result as $\hat{\mathbf{T}}^{ij}_{Bb|Ba} = (\hat{\mathbf{T}}^{ij}_{Bb})^{-1}\hat{\mathbf{T}}^{ij}_{Ba}$. To see that $\hat{\mathbf{T}}^{ij}_{Ba|Bb}$ actually represents a spatial relative displacement of a line introduce the matrix $\mathbf{R}^\star = (\mathbf{R}^{ij}_{Ba})^T\mathbf{R}^{ij}_{Bb}$. Rearranging, so that $\mathbf{R}^{ij}_{Bb} = \mathbf{R}^{ij}_{Ba}\mathbf{R}^\star$ and re-substituting into the left lower submatrix in Eq. (4.41) yields $\tilde{\mathbf{t}}^\star\mathbf{R}^\star$, where

$$\tilde{\mathbf{t}}^\star = (\mathbf{R}^{ij}_{Ba})^T\left((\tilde{\mathbf{t}}^{ij}_{Ba})^T + \tilde{\mathbf{t}}^{ij}_{Bb}\right)\mathbf{R}^{ij}_{Ba} \tag{4.42}$$

is a skew symmetric matrix. This is easily verified by showing that $(\tilde{\mathbf{t}}^\star)^T = -\tilde{\mathbf{t}}^\star$:

$$\left((\mathbf{R}^{ij}_{Ba})^T\left((\tilde{\mathbf{t}}^{ij}_{Ba})^T + \tilde{\mathbf{t}}^{ij}_{Bb}\right)\mathbf{R}^{ij}_{Ba}\right)^T = (\mathbf{R}^{ij}_{Ba})^T\left((\tilde{\mathbf{t}}^{ij}_{Ba})^T + \tilde{\mathbf{t}}^{ij}_{Bb}\right)^T\mathbf{R}^{ij}_{Ba} = -(\mathbf{R}^{ij}_{Ba})^T\left((\tilde{\mathbf{t}}^{ij}_{Ba})^T + \tilde{\mathbf{t}}^{ij}_{Bb}\right)\mathbf{R}^{ij}_{Ba}. \tag{4.43}$$

Table 4.1.: Arbitrarily chosen task position for an exemplary two-configuration synthesis

	ψ	ϑ	φ	${}^W\mathbf{t}_B$
Ba^1	130.0 deg	−15.0 deg	10.0 deg	$(\ 50.0 \quad -55.0 \quad 65.0\ )^T$
Ba^2	5.0 deg	30.0 deg	−35.0 deg	$(\ -120.0 \quad -50.0 \quad 150.0\ )^T$
Bb^1	30.0 deg	0.0 deg	0.0 deg	$(\ -50.0 \quad -150.0 \quad 100.0\ )^T$
Bb^2	−30.0 deg	45.0 deg	0.0 deg	$(\ -120.0 \quad 50.0 \quad 70.0\ )^T$

Table 4.2.: Axis coordinates of a C joint calculated from two-configuration synthesis example

	Direction $\mathbf{l}^1$	Location $\mathbf{p}_l^1$
$\hat{\mathbf{l}}^1$	$\left(\ 0.1285 \quad 0.0453 \quad 0.9907\ \right)^T$	$\left(\ -18.8700 \quad -76.4786 \quad 5.9425\ \right)^T$

The result is that $\hat{\mathbf{T}}^{ij}_{Ba|Bb}$ represents a spatial relative displacement of a line for any specified $\mathbf{T}^{ij}_{Ba}$ and $\mathbf{T}^{ij}_{Bb}$ and hence comparing the situation with Eq. (A.10) from sect. A.4 shows, that Eq.(4.40) is nothing but the equation of the screw axis of finite rigid motion. This means that $\hat{\mathbf{l}}^i$ may either be interpreted as the screw axis of the relative displacement $\hat{\mathbf{T}}^{ij}_{Ba|Bb}$ or as the joint axis in configuration i, that satisfies $\mathbf{T}^{ij}_{Ba}$ and $\mathbf{T}^{ij}_{Bb}$. Following the discussion provided in sect. A.5 and 2.3.1 it can be specified, whether the line $\hat{\mathbf{l}}$ represents a R or a C joint. This is done by considering the slide along $\hat{\mathbf{l}}$, which is found as

$$s^{ij} = (\mathbf{t}^\star)^T \cdot \mathbf{l}, \tag{4.44}$$

where $\mathbf{t}^\star$ is the vector assembled from the parameters of the skew symmetric translational matrix $\tilde{\mathbf{t}}^\star$. The result are again the cases

1. $s^{ij} \neq 0$: The spatial displacements $\mathbf{T}^{ij}_{Ba}$ and $\mathbf{T}^{ij}_{Bb}$ lead to a rotation around and the slide along $\hat{\mathbf{l}}^i$, so that $\hat{\mathbf{l}}^i$ corresponds to a C joint.
2. $s^{ij} = 0$: The spatial displacements $\mathbf{T}^{ij}_{Ba}$ and $\mathbf{T}^{ij}_{Bb}$ only lead to a rotation around $\hat{\mathbf{l}}^i$, so that $\hat{\mathbf{l}}^i$ corresponds to a R joint.

Example

The results of a numerical example based on position data given in table 4.1 are shown in Fig. 4.10. Note that angles ψ, ϑ and φ correspond to Euler angles, introduced in sect. 2.1. Table 4.2 lists the corresponding calculated set of axis coordinates, i.e. the normalized direction $\mathbf{l}^1$ and the location $\mathbf{p}_l^1$, both measured in W. The slide between frames Ba and Bb from configuration 1 to 2 was calculated as $s^{12} = (\mathbf{t}^\star)^T \cdot \mathbf{l}^1 = 141.044$, where $\mathbf{t}^\star$ is assembled from the parameters of $\tilde{\mathbf{t}}^\star = (\mathbf{R}^{12}_{Ba})^T \left((\tilde{\mathbf{t}}^{12}_{Ba})^T + \tilde{\mathbf{t}}^{12}_{Bb}\right) \mathbf{R}^{12}_{Ba}$. Hence, the line $\hat{\mathbf{l}}^1$ corresponds to a C joint in configuration 1.

A spherical version of two-configuration synthesis

In the case of a spherical linkage two poses of two arbitrary (consecutive) links Ka and Kb may be described using displacements $({}^W\mathbf{T}^i_{Ba}, {}^W\mathbf{T}^j_{Ba})$ and $({}^W\mathbf{T}^i_{Bb}, {}^W\mathbf{T}^j_{Bb})$, with translations satisfying

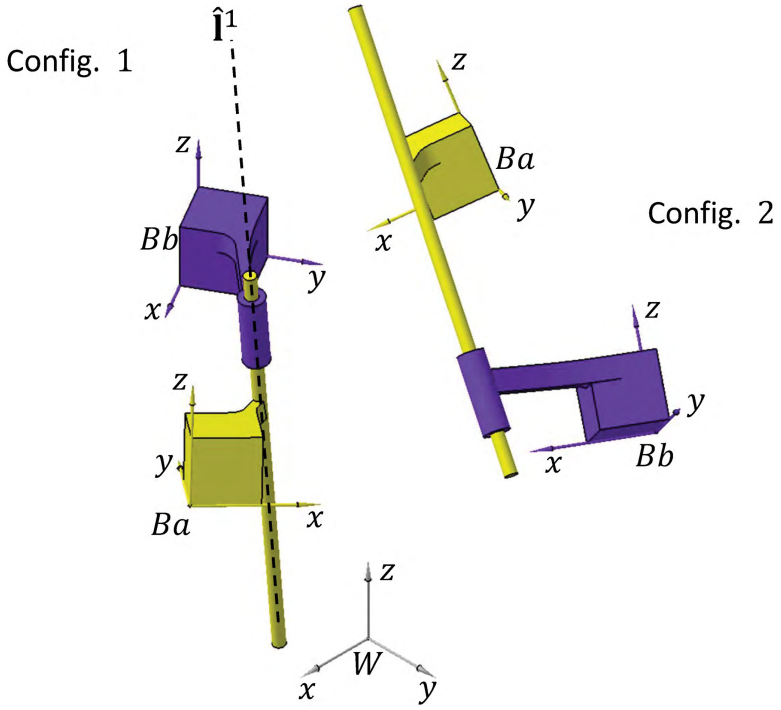

Figure 4.10.: C joint, which allows the assembly of two links in two prescribed spatial positions

${}^{W}\mathbf{t}^{i}_{Ba} = {}^{W}\mathbf{t}^{j}_{Ba} = {}^{W}\mathbf{t}^{i}_{Bb} = {}^{W}\mathbf{t}^{j}_{Bb} = \mathbf{0}$. This results in a pure spherical version of Eq. (4.41) as

$$\hat{\mathbf{T}}^{ij}_{Ba|Bb} = \begin{pmatrix} \mathbf{R}^{\star} & \mathbf{0} \\ \mathbf{0} & \mathbf{R}^{\star} \end{pmatrix} = \begin{pmatrix} (\mathbf{R}^{ij}_{Ba})^{T}\mathbf{R}^{ij}_{Bb} & \mathbf{0} \\ \mathbf{0} & (\mathbf{R}^{ij}_{Ba})^{T}\mathbf{R}^{ij}_{Bb} \end{pmatrix}. \tag{4.45}$$

Substituting $\hat{\mathbf{T}}^{ij}_{Ba|Bb}$ and afterwards expanding Eq. (4.40) yields two equations that correspond to those two from Eq. (A.11)

$$(\mathbf{E} - \mathbf{R}^{\star}) \cdot \mathbf{l}^{i} = \mathbf{0} \quad \text{and} \quad (\mathbf{E} - \mathbf{R}^{\star}) \cdot \left(\mathbf{p}^{i}_{l} \times \mathbf{l}^{i}\right) = \mathbf{0}. \tag{4.46}$$

As described in sect. A.4 the first equation may be solved using Cayley's formula from sect. A.1, which yields the direction of the axis $\hat{\mathbf{l}}^{i}$. However, this means that $\mathbf{p}^{i}_{l} = \mathbf{0}$ in order to have a meaningful solution for the second equation. The result is the line $\hat{\mathbf{l}}^{i} = (\mathbf{l}^{i}\ \mathbf{0})^{T}$ which passes through the origin of W. Furthermore, translations equal to zero yield $s^{ij} = 0$, see Eq. (4.44), which shows that $\hat{\mathbf{l}}$ corresponds to the axis of a revolute joint.

A planar version of two-configuration synthesis

In the case of a planar linkage that moves in the xy-plane (or in a plane parallel to that) two poses of two arbitrary (consecutive) links Ka and Kb may be described using 3×3 homogeneous transforms $({}^{W}\mathbf{T}^{i}_{Ba}, {}^{W}\mathbf{T}^{j}_{Ba})$ and $({}^{W}\mathbf{T}^{i}_{Bb}, {}^{W}\mathbf{T}^{j}_{Bb})$, which are transformed into relative displacement data $\mathbf{T}^{ij}_{Ba}$ and $\mathbf{T}^{ij}_{Bb}$. A revolute joint, that couples the two links may simply be described as a point in the xy-plane. When a homogeneous 3×1 vector $\mathbf{p}$ with a third component normalized to 1 describes the location of the R joint, the coupling implies that $\mathbf{p}$ must satisfy the following relative displacement equation

$$\mathbf{p}^{j} = \mathbf{T}^{ij}_{Ba} \cdot \mathbf{p}^{i} \qquad \text{and} \qquad \mathbf{p}^{j} = \mathbf{T}^{ij}_{Bb} \cdot \mathbf{p}^{i}. \tag{4.47}$$

Subtracting and rearranging eliminates $\mathbf{p}^j$ and yields an equation for $\mathbf{p}^i$:

$$(\mathbf{E} - \underbrace{(\mathbf{T}_{Ba}^{ij})^{-1}\mathbf{T}_{Bb}^{ij}}_{\mathbf{T}_{Ba|Bb}^{ij}}) \cdot \mathbf{p}^i = \mathbf{0}, \tag{4.48}$$

where $\mathbf{E}$ is a 3×3 identity and

$$\mathbf{T}_{Ba|Bb}^{ij} = \begin{pmatrix} (\mathbf{R}_{Ba}^{ij})^T\mathbf{R}_{Bb}^{ij} & (\mathbf{R}_{Ba}^{ij})^T \cdot (\mathbf{t}_{Bb}^{ij} - \mathbf{t}_{Ba}^{ij}) \\ 0 \quad 0 & 1 \end{pmatrix}. \tag{4.49}$$

Herein $\mathbf{R}_B^{ij}$ and $\mathbf{t}_B^{ij}$ are the 2×2 rotational and 2×1 translational sub-components of $\mathbf{T}_{Ba}^{ij}$ and $\mathbf{T}_{Bb}^{ij}$. Using this transformation data one may expand and rearrange Eq. (4.48) to obtain

$$\mathbf{p}^i = (\mathbf{E} - (\mathbf{R}_{Ba}^{ij})^T\mathbf{R}_{Bb}^{ij})^{-1}(\mathbf{R}_{Ba}^{ij})^T \cdot (\mathbf{t}_{Bb}^{ij} - \mathbf{t}_{Ba}^{ij}), \tag{4.50}$$

where now $\mathbf{p}^i$ is a common 2×1 coordinate vector. This is the equation of the pole of the displacement defined by $\mathbf{T}_{Ba|Bb}^{ij}$, which has a solution as long as $\mathbf{E} \neq (\mathbf{R}_{Ba}^{ij})^T\mathbf{R}_{Bb}^{ij}$. In the context of two-configuration synthesis $\mathbf{p}^i$ defines the location of a R joint in configuration i, which satisfies two arbitrary planar poses of two consecutive links Ka and Kb.

4.2.2. Two-Configuration Synthesis of Spherical Four-Bars

The method described in the previous section shall be applied here to a spherical four-bar. The resulting procedure is also part of [104] and yields a linkage, whose links can be assembled in two prescribed task orientations. Such an approach may particularly important in applications, where two distinct configurations of each link of the linkage are of interest. Examples are foldable four-bars as substructures of transformable furniture or retractable tops of sports cars, where the generation of two significant configurations is of particular importance.

Table 4.3 list the orientation data of three moving frames $B1$, $B2$ and B'', that correspond to three links $K1$, $K2$ and K''. Note that angles ψ, ϑ and φ correspond to Euler angles, introduced in sect. 2.1. Figure 4.11a) provides a corresponding graphical depiction of $K1$, $K2$ and K'' in two configurations 1 and 2. A fixed base link K' of the four-bar is associated with the reference frame W. To obtain four directions $\mathbf{a}$, $\mathbf{b}$, $\mathbf{c}$ and $\mathbf{d}$ of a spherical four-bar that reaches the given orientations, Eq. (4.40) must be solved for appropriately stated matrices $\hat{\mathbf{T}}_{Ba|Bb}^{12}$, see Eq. (4.41). However, due to a purely spherical task, where translations are equal to zero, Eq. (4.41) becomes

$$\hat{\mathbf{T}}_{Ba|Bb}^{12} = \begin{pmatrix} (\mathbf{R}_{Ba}^{12})^T\mathbf{R}_{Bb}^{12} & \mathbf{0} \\ \mathbf{0} & (\mathbf{R}_{Ba}^{12})^T\mathbf{R}_{Bb}^{12} \end{pmatrix}. \tag{4.51}$$

This leads to nothing but the spherical version of two-configuration synthesis, see Eq. (4.45), which means that the axis, obtained from the solution of Eq. (4.40) passes through the origin of frame W. The result is, that only the direction equation needs to be solved, which yields

$$(\mathbf{E} - \underbrace{(\mathbf{R}_{Ba}^{12})^{-1}\mathbf{R}_{Bb}^{12}}_{\mathbf{R}_{Ba|Bb}^{12}}) \cdot \mathbf{l}^1 = \mathbf{0}. \tag{4.52}$$

To obtain the four directions $\mathbf{a}$, $\mathbf{b}$, $\mathbf{c}$ and $\mathbf{d}$ in configuration 1 the following equations need to be stated and solved using the solution procedure, provided in sect. A.4:

$$\begin{aligned} (\mathbf{E} - \mathbf{R}_{W|B1}^{12}) \cdot \mathbf{a}^1 &= \mathbf{0} \qquad & (\mathbf{E} - \mathbf{R}_{B1|B2}^{12}) \cdot \mathbf{b}^1 &= \mathbf{0} \\ (\mathbf{E} - \mathbf{R}_{B2|B''}^{12}) \cdot \mathbf{c}^1 &= \mathbf{0} \qquad & (\mathbf{E} - \mathbf{R}_{B''|W}^{12}) \cdot \mathbf{d}^1 &= \mathbf{0} \end{aligned} \tag{4.53}$$

Table 4.3.: Exemplary task orientations for two-configuration synthesis of a spherical four-bar

Bi	ψ	ϑ	ϕ	${}^W\mathbf{t}^i_{Bi}$
$B1^1$	0.0 deg	20.0 deg	0.0 deg	$(\ 0.0\ \ 0.0\ \ 0.0\ )^T$
$B1^2$	0.0 deg	60.0 deg	0.0 deg	$(\ 0.0\ \ 0.0\ \ 0.0\ )^T$
$B2^1$	40.0 deg	−10.0 deg	0.0 deg	$(\ 0.0\ \ 0.0\ \ 0.0\ )^T$
$B2^2$	120.0 deg	−70.0 deg	0.0 deg	$(\ 0.0\ \ 0.0\ \ 0.0\ )^T$
B''^1	40.0 deg	0.0 deg	0.0 deg	$(\ 0.0\ \ 0.0\ \ 0.0\ )^T$
B''^2	120.0 deg	0.0 deg	0.0 deg	$(\ 0.0\ \ 0.0\ \ 0.0\ )^T$

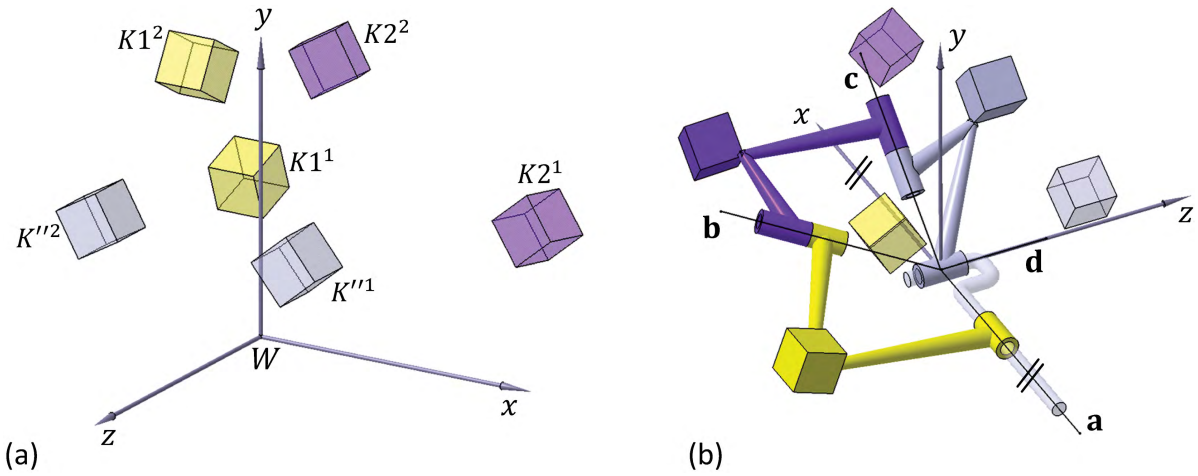

Figure 4.11.: Task orientations and corresponding spherical four-bar synthesized using the two-configuration synthesis approach

Note, that in the equations for **a** and **d** the rotations of the fixed frame W is included as $\mathbf{R}^{12}_W = \mathbf{E}$. Hence, these equations may also be written neglecting index 1 at vectors, since these directions also belong to the fixed frame W. Solving Eq. (4.53) yields the values for the different directions listed in table 4.4. Figure 4.11b) shows a CAD design of the four-bar, assembled in configuration 1, which can also reach the prescribed configurations 2, see Fig. 4.12.

4.2.3. Transformation of G- or S-Jointed Kinematic Chains Using Two-Configuration Synthesis

In this section the two-configuration synthesis approach is used to transform specific kinematic chains consisting of gimbal and / or spherical joints into revolute-jointed chains. This is shown for the spatial GS chain with one fixed end link, where the result is a spatial RR chain, that reaches two configurations. Note that this is also part of [104]. The configurations are defined by the two moving links of the GS chain and the synthesis procedure on the one hand requires the GS synthesis equations (2.50) for two prescribed spatial poses of one of the end links. On the other hand the inverse kinematics of the synthesized GS chain is required in order to prescribe poses of another moving link. Throughout the procedure the G joint is considered to be the fixed joint.

In order to synthesize a GS chain defined by three links K', K'' and K''', two spatial poses of

Table 4.4.: Directions **a**, **b**, **c** and **d** in configuration i

	Direction
a	$\begin{pmatrix} 1.0 & 0.0 & 0.0 \end{pmatrix}^T$
$\mathbf{b}^1$	$\begin{pmatrix} -0.3834 & -0.3384 & 0.8594 \end{pmatrix}^T$
$\mathbf{c}^1$	$\begin{pmatrix} 0.7660 & 0.6428 & 0.0 \end{pmatrix}^T$
d	$\begin{pmatrix} 0.0 & 0.0 & 1.0 \end{pmatrix}^T$

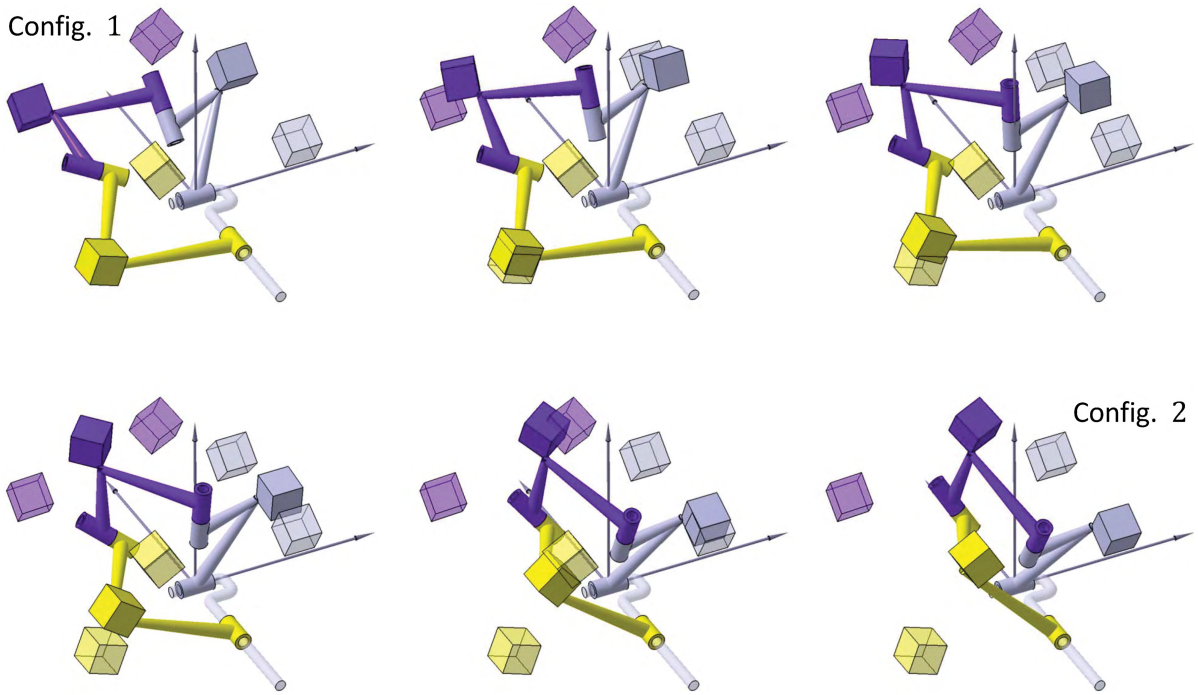

Figure 4.12.: Spherical four-bar reaching the two configurations

the moving end link K''' are considered. Those are prescribed using a corresponding frame B''' and are measured with respect to another fixed reference frame W, associated with K'. Table 4.5 lists the arbitrarily chosen position data, where angles ψ, ϑ and φ correspond to Euler angles, introduced in sect. 2.1. The position data is used to assemble the bilinear scalar design or synthesis equations from sect. 2.3.3 for a two-position task:

$$(\mathbf{p}_b^1)^T \cdot \mathbf{M}^{12} \cdot \mathbf{p}_a + (\vec{\lambda}^{12})^T \cdot \mathbf{p}_b^1 + (\vec{\mu}^{12})^T \cdot \mathbf{p}_a + \delta^{12} = 0. \tag{4.54}$$

Due to the fact that there is one fixed end link in the chain the parameters containing position data take the simple form $\mathbf{M}^{12} = \mathbf{E} - (\mathbf{R}_{B'''}^{12})^T$, $(\vec{\lambda}^{12})^T = (\mathbf{t}_{B'''}^{12})^T \cdot \mathbf{R}_{B'''}^{12}$, $(\vec{\mu}^{12})^T = -(\mathbf{t}_{B'''}^{12})^T$ and $\delta^{12} = \frac{1}{2}(\mathbf{t}_{B'''}^{12})^T \cdot \mathbf{t}_{B'''}^{12}$. Note that the right superscript vanishes at $\mathbf{p}_a$, because this should describe the center point of the fixed G joint.

Since now there is only one single scalar equation, five of the six W-frame coordinates x_{p_a}, y_{p_a}, z_{p_a} and $x_{p_b}^1$, $y_{p_b}^1$, $z_{p_b}^1$ represent free design parameters and may hence be chosen arbitrarily. When for instance five W-frame coordinates are chosen as $x_{p_b}^1 = -21.6987$, $y_{p_b}^1 = -99.0192$, $z_{p_b}^1 = 30.0$, $x_{p_a} = 20.0$ and $y_{p_a} = 0.0$, the remaining parameter is easily found after rearranging

Table 4.5.: Task poses for two-position synthesis of a spatial GS chain

	ψ	ϑ	φ	${}^W\mathbf{t}^i_{B'''}$
B'''^1	30.0 deg	0.0 deg	0.0 deg	$(\ -50.0 \quad -150.0 \quad 100.0\ )^T$
B'''^2	-30.0 deg	45.0 deg	0.0 deg	$(\ -120.0 \quad 50.0 \quad 70.0\ )^T$

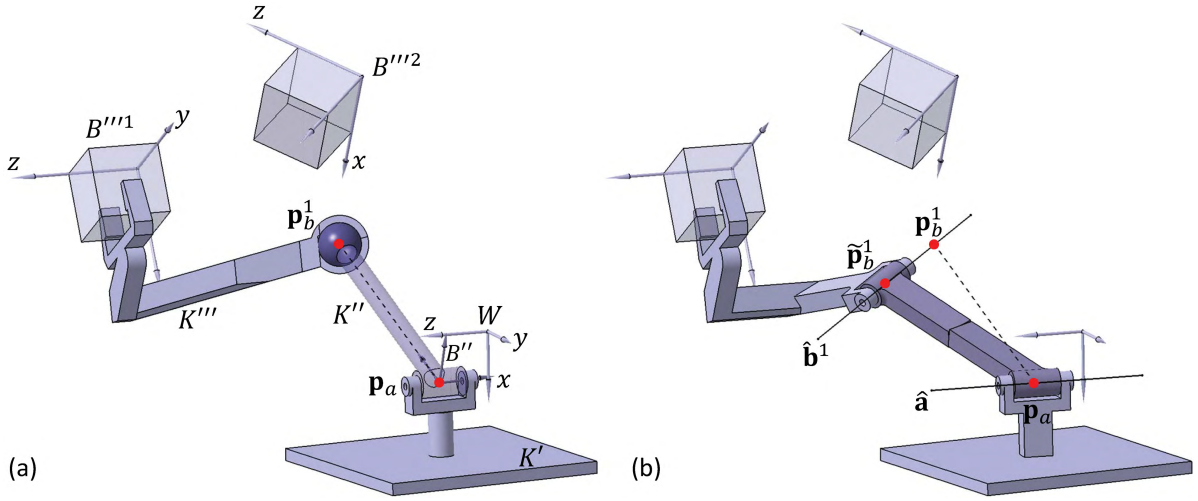

Figure 4.13.: a) A spatial GS chain in reference configuration 1 obtained from two-position synthesis using coordinate frame B'''. b) A spatial RR chain obtained from transforming the GS chain using two-configuration synthesis

the linear design equation as $z_{p_a} = 21.1883$.

Figure 4.13a) shows a detailed CAD design of the GS chain in reference configuration 1 together with the poses of the cube-like link K''' and corresponding frame B'''. The chain can also be assembled in configuration 2, defined by B'''^2. In order to connect the moving S joint, defined by $\mathbf{p}_b$, to the cube in configuration 1 a gripper was designed, which, as a consequence also belongs to K'''.

To transform the GS chain into the desired spatial RR chain, Eq. (4.40) must be solved for appropriately stated matrices $\hat{\mathbf{T}}^{12}_{Ba|Bb}$. Since there are three links K', K'' and K''', this can be achieved by assembling $\hat{\mathbf{T}}^{12}_{W|B''}$ and $\hat{\mathbf{T}}^{12}_{B''|B'''}$ using the frames W, B'' and B'''. While position data of W and B''' is already given (W performs the identity displacement) that of B'' must be calculated and it is convenient for this purpose, to consider this frame being defined as shown in Fig. 4.13a). B'' shall be located at the previously determined fixed pivot defined by $\mathbf{p}_a$. In order to define the orientation of the frame using z-x-z-Euler angles, introduced in sect. 2.1 its z-axis shall point along a direction, defined as $\mathbf{c} = \frac{\mathbf{p}^i_b - \mathbf{p}_a}{|\mathbf{p}^i_b - \mathbf{p}_a|}$. This allows to obtain the desired orientation data from the following inverse kinematics calculations:

$$\psi^i_{B''} = \arctan\left(\frac{x^i_c}{\sqrt{(y^i_c)^2 + z^i_c)^2}}\right) \qquad \text{and} \qquad \vartheta^i_{B''} = \arctan\left(\frac{y^i_c}{z^i_c}\right), \tag{4.55}$$

where $i = 1,2$. Using the numerical values from GS synthesis, this yields $\psi^1_{B''} = 157.1601$ deg, $\psi^2_{B''} = 35.43$ deg as well as $\vartheta^1_{B''} = -85.3001$ deg, $\vartheta^2_{B''} = -79.02$ deg, which, together with

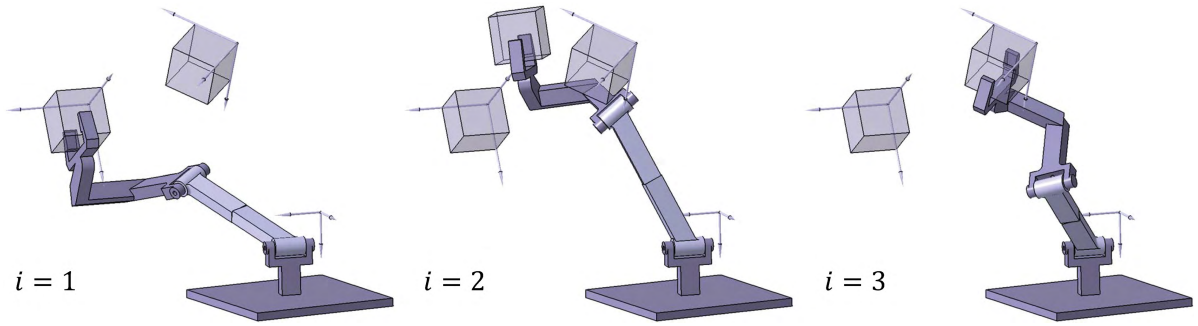

Figure 4.14.: Starting, intermediate and ending configuration of the spatial RR chain obtained from two-configuration synthesis

${}^{W}\mathbf{t}^{i}_{B''} = \mathbf{p}_a$ allows to define the desired position data of frame B''. Hence, matrices $\hat{\mathbf{T}}^{12}_{W|B''}$ and $\hat{\mathbf{T}}^{12}_{B''|B'''}$ can be assembled, which yields:

$$\hat{\mathbf{T}}^{12}_{W|B''} = \begin{pmatrix} \mathbf{R}^{12}_{B''} & \mathbf{0} \\ \tilde{\mathbf{t}}^{12}_{B''}\mathbf{R}^{12}_{B''} & \mathbf{R}^{12}_{B''} \end{pmatrix} \tag{4.56}$$

(note that $\mathbf{R}^{12}_{W} = \mathbf{E}$ and $\tilde{\mathbf{t}}^{12}_{W} = \mathbf{0}$ from the identity displacement) and

$$\hat{\mathbf{T}}^{12}_{B''|B'''} = \begin{pmatrix} (\mathbf{R}^{12}_{B''})^T\mathbf{R}^{12}_{B'''} & \mathbf{0} \\ (\mathbf{R}^{12}_{B''})^T\left((\tilde{\mathbf{t}}^{12}_{B''})^T + \tilde{\mathbf{t}}^{12}_{B'''}\right)\mathbf{R}^{12}_{B'''} & (\mathbf{R}^{12}_{B''})^T\mathbf{R}^{12}_{B'''} \end{pmatrix}. \tag{4.57}$$

Next, solving the equations

$$(\hat{\mathbf{E}} - \hat{\mathbf{T}}^{12}_{W|B''}) \cdot \hat{\mathbf{a}} = \hat{\mathbf{0}} \qquad \text{and} \qquad (\hat{\mathbf{E}} - \hat{\mathbf{T}}^{12}_{B''|B'''}) \cdot \hat{\mathbf{b}}^1 = \hat{\mathbf{0}} \tag{4.58}$$

using the solution procedure provided in sect. A.4 yields two joint axes $\hat{\mathbf{a}}$ and $\hat{\mathbf{b}}^1$. These actually belong to two revolute joints, because the calculation of slides s^{12} using Eq. (4.44) along $\hat{\mathbf{a}}$ and $\hat{\mathbf{b}}^1$ yields zero slides.

Figure 4.13b) shows the CAD-model of the RR chain in reference configuration 1, which in fact is a spatial RR chain, because one can measure a non-zero common normal distance as well as a non-zero angle between $\hat{\mathbf{a}}$ and $\hat{\mathbf{b}}^1$ (Note that this can also be verified using the dual scalar product from Eq. (2.26)). The angle is indicated at the connecting rectangular rod between $\hat{\mathbf{a}}$ and $\hat{\mathbf{b}}^1$ by an angular offset. Furthermore, as one can see, the moving R joint is designed at some other point $\tilde{\mathbf{p}}^1_b$ than the previously determined center point $\mathbf{p}^1_b$ of the S joint. Note that this is possible, because both points lie on $\hat{\mathbf{b}}^1$.

Figure 4.14 shows the starting, an intermediate and the ending configuration of the chain, where the intermediate state of the cube, i.e. K''', was chosen arbitrarily. When this intermediate pose would represent another task position in a three-position synthesis approach of a spatial RR chain (see sect. 2.3.5) the result would be two RR synthesis solutions, out of which one would exactly represent the chain, obtained here from two-configuration synthesis.

Another idea is to compare a two-position RR synthesis approach using the design equations from sect. 2.3.5 with the approach presented here. A two-position task of link K''' yields underspecified design equations (2.55), (2.57) and (2.59) since then there are only six equations in the ten W-frame coordinates x_a, y_a, x^1_b, y^1_b, x_{p_a}, y_{p_a}, z_{p_a}, $x^1_{p_b}$, $y^1_{p_b}$ and $z^1_{p_b}$. Hence, four of these parameters may be pre-defined with respect to certain other requirements of the task such as given

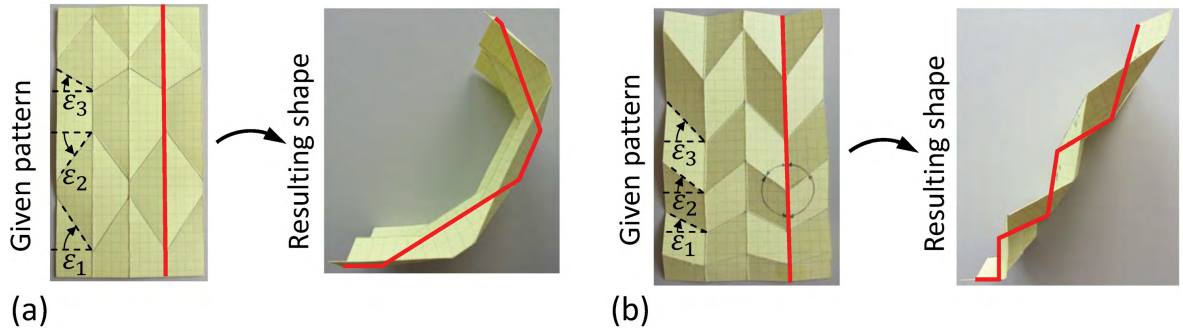

Figure 4.15.: Two examples of modified Miura patterns differently chosen angles ε, which result in different folded configurations: a) Configuration characterized by a convex shape of a polyline. b) Configuration characterized by a zig-zag shape of a polyline

space requirements. However, due to the fact that the two-configuration synthesis approach made use of the underspecified synthesis equation of GS or SS chains, here the result were five free design parameters. While these five parameters are restricted to be location parameters, the four paramters from Eq. (2.55), (2.57) and (2.59) may also be direction coordinates.

4.2.4. Two-Configuration Synthesis of Miura-Ori-Based Folding Structures

As shown in the previous sections two-configuration synthesis may be used to design linkages, such that they can be assembled in two different configurations, prescribed in terms of two spatial poses of each link that make up the structure. However, in the case of spatial (overconstrained) linkages this can be a challenging task, because special kinematic dimensions must be taken into account, which preserve the mobility of the systems. Another way of saying this is, that there is particularly strong dependency between kinematic dimensions and the movement of the linkage. Hence, using two-configuration synthesis to obtain the kinematic dimensions of an overconstrained linkage requires essential information on the movement of the desired structure.

In what follows, two-configuration synthesis of overconstrained systems based on the Miura-ori folding pattern are presented. This becomes possible through the kinematic analysis results from sect. 4.1.1, where the transmission properties in the Miura-ori building block four-bar have been identified. The result is the two-configuration synthesis of Miura-ori-based folding structures which is also presented in [111]. The corresponding configurations are defined in terms of two configurations of a polyline, which is a particular part of the pattern.

Folding structures with flat unfolded configuration

A particular result from sect. 4.1.1 is that the opening angle of a Miura-ori building block four-bar satisfies $\phi_a = -\phi_c$ for any given angle ε, see Eq. (4.3) as well as Fig. 4.1. Furthermore, Eq. (4.6) provides another transmission relation as $\tan\frac{\phi_d}{2} = \cot\varepsilon\sin\phi_a$. Writing this in terms of two configurations 1 and 2 yields

$$\phi_a^i = -\phi_c^i \qquad \text{and} \qquad \tan\frac{\phi_d^i}{2} = \cot\varepsilon\sin\phi_a^i, \qquad i = 1,2, \tag{4.59}$$

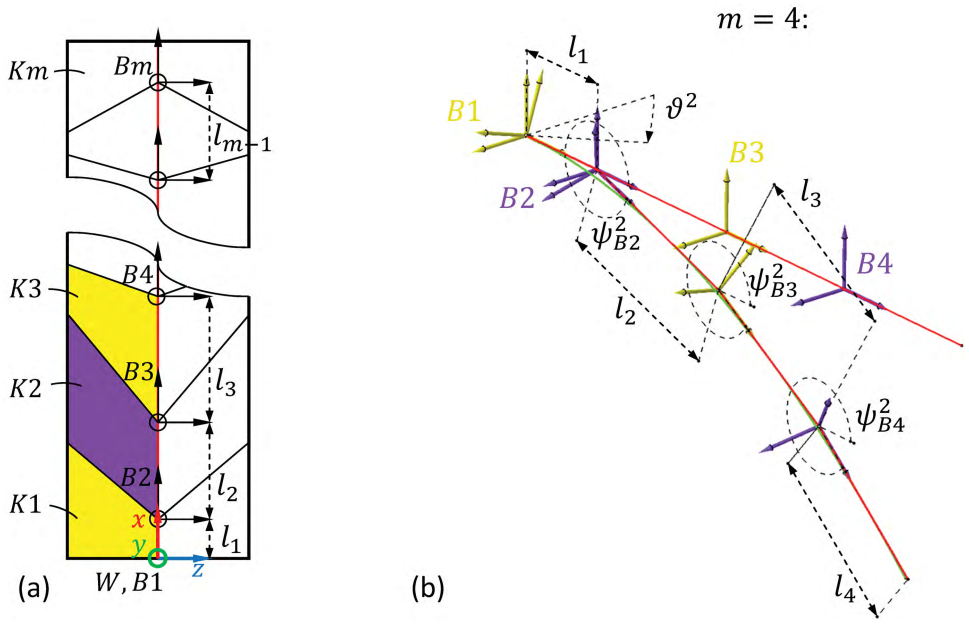

Figure 4.16.: a) Frames defined along one plane symmetric half of a serial assembly of Miura building block four-bars. b) Example configurations of a polyline for synthesis: Unfolded flat line and line segments, defined as tangents to a parabola.

where the first equation simply states the equality of the amount of opening angles in any configuration of the four-bar and is independent of any kinematic dimensions. When analysis is a concern and ϕ_a^i or ϕ_d^i is considered to be a given input parameter, the second equation may easily be solved for ϕ_d^i or ϕ_a^i. However, in case of synthesis ε represents the unknown parameter and the second equation represents a system of two linear equations in the parameter $k = \cot\varepsilon$. This will generally not yield a valid ε for two general configurations, which means that no two arbitrary configurations of a building block four-bar can be pre-defined. However, when configuration 1 represents the flat unfolded state the result is $\phi_d^1 = \phi_a^1 = 0$ and the second equation of Eq. (4.59) is identically satisfied. Then $\tan\frac{\phi_d^2}{2} = \cot\varepsilon\sin\phi_a^2$ can be solved for ε, for any given ϕ_d^2 and ϕ_a^2.

For this reason, a Miura-ori folding pattern consisting of numerous building block four-bars can also be modified in various ways as shown in Fig. 4.15, where the result are different folded configurations. The particular difference can be characterized by the shape of a certain polyline, which is found as a straight vertical line of symmetry in the unfolded flat configuration. On the one hand, if directions of angles ε alternate along this line the result is a convex shape. On the other hand, if directions of angles ε remain the same along the line the result is a zig-zag folded shape.

Instead of choosing a set of angles ε and observing the resulting shape of the polyline one may ask for the angles ε, such that the polyline of the pattern can reach a certain pre-defined shape. This problem can be solved by applying two-configuration synthesis to one single stripe of the pattern, using the flat unfolded as well as a certain folded configuration. Several of such identical stripes may then be assembled right next to each other, to form a complete modified Miura-ori pattern.

Figure 4.16a) shows a plane symmetric unfolded flat stripe, which is also called a serial assembly of Miura-ori building block four-bars in the following. Due to the symmetry only one

Table 4.6.: Position data of frames $B1$ to $B4$, which correspond to one half of a serial assembly of Miura building blocks that approximates the shape of a parabola (angles measured in [deg])

	ϑ^1	ϑ^2	ψ^1	ψ^2	${}^W\mathbf{t}_B^1$	${}^W\mathbf{t}_B^2$
$B1$	0.0	-17.5	0.0	0.0	$(\ 0.0 \quad 0.0 \quad 0.0\ )^T$	$(\ 0.0 \quad 0.0 \quad 0.0\ )^T$
$B2$	0.0	17.5	0.0	340.9352	$(\ 30.0 \quad 0.0 \quad 0.0\ )^T$	$(\ 30.0 \quad 0.0 \quad 0.0\ )^T$
$B3$	0.0	-17.5	0.0	329.0854	$(\ 85.0 \quad 0.0 \quad 0.0\ )^T$	$(\ 81.9832 \quad -17.965 \quad 0\ )^T$
$B4$	0.0	17.5	0.0	319.9781	$(\ 135.0 \quad 0.0 \quad 0.0\ )^T$	$(\ 124.8799 \quad -43.653 \quad 0\ )^T$

Table 4.7.: Axis coordinates of joints, connecting the different links in one half of a serial assembly of Miura building blocks

	Direction	Location
$\hat{\mathbf{a}}^1$	$(\ 0.8731 \quad 0.0000 \quad -0.4876\ )^T$	$(\ 7.1315 \quad 0.0000 \quad 12.7705\ )^T$
$\hat{\mathbf{b}}^1$	$(\ -0.9453 \quad 0.0000 \quad -0.3262\ )^T$	$(\ 9.0466 \quad 0.0000 \quad -26.213\ )^T$
$\hat{\mathbf{c}}^1$	$(\ 0.9667 \quad 0.0000 \quad -0.256\ )^T$	$(\ 8.8494 \quad 0.0000 \quad 33.4119\ )^T$

half of the pattern needs to be synthesized, and the complete plane symmetric serial assembly may afterwards be found as a mirrored counterpart. One such half of the pattern shall have links $K1,\ldots,Km$, which shall move with respect to another fixed link, not shown in the figure. Note that $m > 2$, in order to consider a spatial linkage with at least two vertices.

To describe the movement of links corresponding frames $B1,\ldots,Bm$ are considered to be located along the polyline, such that their xz-planes coincide with the flat panels. Another frame W, associated with the fixed link, is located at the lower bound of the pattern, having its origin coinciding with that of $B1$. The x- axes of frames shall be aligned with the different segments of the polyline, which are characterized by arbitrary lengths $l_1,\ldots,l_m$. These definitions allow to describe a spatial configuration of a certain frame Bj using Euler angles, introduced by Eq. (2.7) as well as the different segments of the polyline:

$$ {}^W\mathbf{R}_{Bj} = \mathbf{R}_z(\psi_{Bj})\mathbf{R}_x(\vartheta_{B(j-1)}), \qquad {}^W\mathbf{t}_{Bj} = {}^W\mathbf{t}_{B(j-1)} + l_{j-1}\begin{pmatrix} \cos\psi_{B(j-1)} \\ \sin\psi_{B(j-1)} \\ 0 \end{pmatrix}. \tag{4.60} $$

Note that $j = 2,\ldots,m$ to have a consistent description. Furthermore, the result from sect. 4.1.1, Eq. (4.3), must be added as $\vartheta_{B(j-1)} = -\vartheta_{Bj}$ in order to have this formula actually describing the considered half of a serial assembly of Miura building blocks.

Equation (4.60) can be retraced using the example shown in Fig. 4.16b), where the number of segments of the polyline is $m = 4$. Configuration 1 of the polyline corresponds to the flat unfolded pattern. Configuration 2 is defined, such that the different line segments define tangents to a parabola.

The lengths of the different segments may be chosen arbitrarily and are defined here as $l_1 = 30$, $l_2 = 55$, $l_3 = 50$ and $l_4 = 50$. Furthermore, respecting Eq. (4.3), the amount of the angle ϑ^2 can be chosen arbitrarily, which corresponds to the opening angle of the considered serial assembly of Miura-ori building block four-bars. Note that $\vartheta^1 = 0$ is required in order

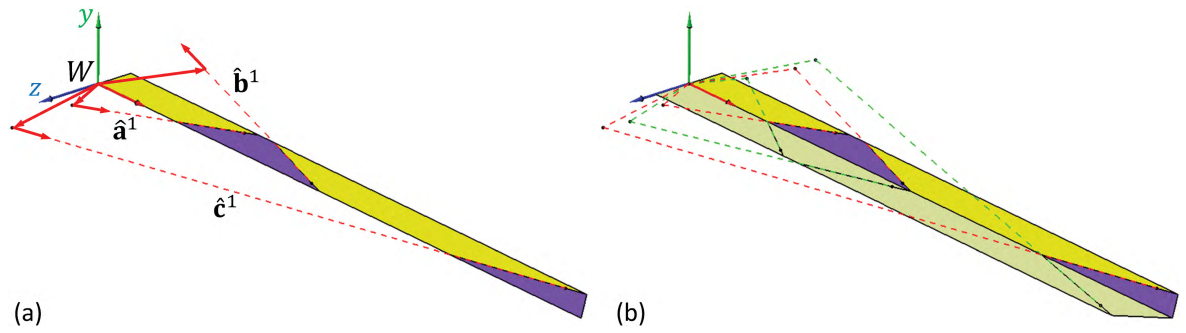

Figure 4.17.: a) Two-configuration synthesis results of one half of the plane symmetric serial assembly of Miura building block four-bars. b) Complete serial assembly

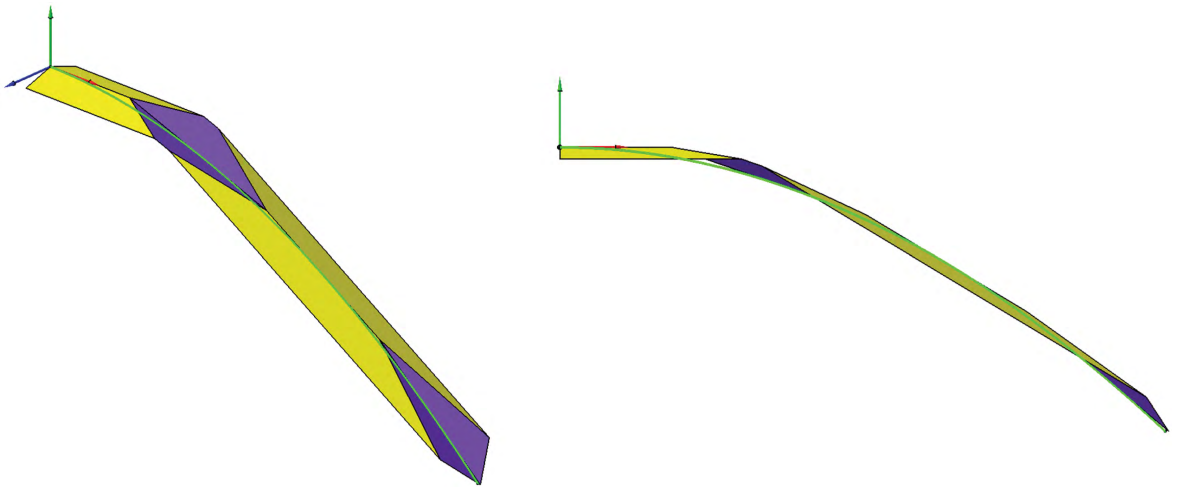

Figure 4.18.: Complete serial assembly reaching a folded configuration, defined in terms of a parabola

to prescribe the flat unfolded configuration. Next, angle ψ^2 can be prescribed at the different vertices of the polyline. The result is the position data, listed in table 4.6 that corresponds to the example from Fig. 4.16b). Recall that odd values of ψ result from the fact, that the different segments of the polyline are tangent to the arbitrarily prescribed parabola. Using this position data in combination with Eq. (4.60) allows to calculate the relative displacements $\mathbf{T}_{Bi}^{12}$, $i = 1,\ldots,4$, whose entries can then be assembled into corresponding 6×6 screw transformation matrices

$$\hat{\mathbf{T}}_{Bi}^{12} = \begin{pmatrix} \mathbf{R}_{Bi}^{12} & \mathbf{0} \\ \tilde{\mathbf{t}}_{Bi}^{12}\mathbf{R}_{Bi}^{12} & \mathbf{R}_{Bi}^{12} \end{pmatrix}, \qquad i = 1,\ldots,4. \tag{4.61}$$

Afterwards computing $\hat{\mathbf{T}}_{B(j-1)|Bj}^{12} = (\hat{\mathbf{T}}_{B(j-1)}^{12})^{-1}\hat{\mathbf{T}}_{Bj}^{12}$, $j = 2,\ldots,4$, using Eq. (4.41) allows to state two-configuration synthesis equations as

$$(\hat{\mathbf{E}} - \hat{\mathbf{T}}_{B(j-1)|Bj}^{12})\cdot\hat{\mathbf{l}}^1 = \hat{\mathbf{0}}, \qquad j = 2,\ldots,4, \tag{4.62}$$

where $\hat{\mathbf{l}}^1$ is a joint axis in configuration 1 that connects two consecutive links $K(j-1)$ and Kj.

Using the position data from table 4.6 Eq. (4.62) can be solved using the solution procedure presented in sect. A.4. The result are three joint axes $\hat{\mathbf{a}}^1$, $\hat{\mathbf{b}}^1$ and $\hat{\mathbf{c}}^1$, measured in W whose axes parameters are listed in table 4.7. The y-components of the vectors are equal to zero, which

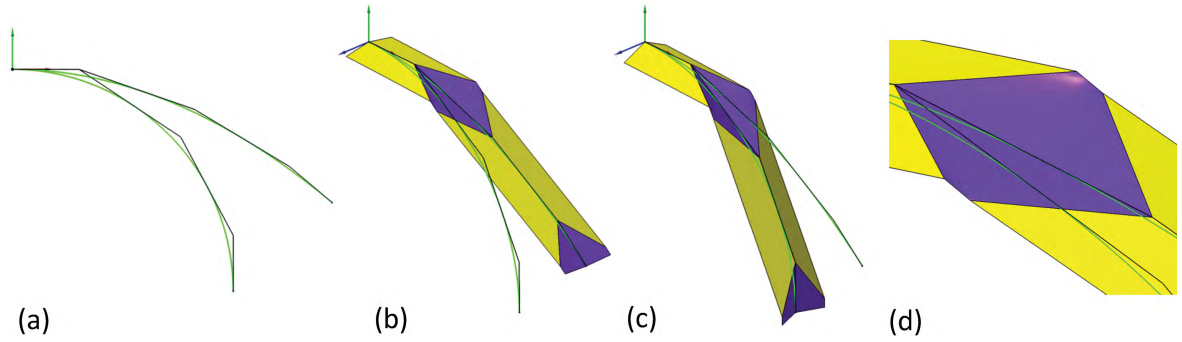

Figure 4.19.: A Miura-ori-based serial assembly of non-flat four-bars reaching folded configurations, defined in terms of a circle and a parabola

corresponds to the unfolded configuration 1 of the pattern. Using Eq. (4.44) in order to classify the slide along axes $\hat{\mathbf{a}}$, $\hat{\mathbf{b}}$ and $\hat{\mathbf{c}}$ yielded a zero sliding for each axis, which shows that those correspond to revolute joints. Figure 4.17a) shows the resulting plane symmetric half of the serial assembly in configuration 1. The mirrored counterpart of the structure is shown in figure b), which completes the serial assembly of Miura building block four-bars. Figure 4.18 shows the folded configuration of the structure, where the polyline touches the parabola.

Folding structures without flat unfolded configuration

Another interesting design case is to consider two different shapes of the polyline in a serial assembly of Miura-ori building block four-bars. This amounts to two different sets of angles $\vartheta^1, \vartheta^2 \neq 0$ and $\psi^1, \psi^2 \neq 0$ in each building block four-bar. Following Eq. (4.6) these angles satisfy

$$\begin{aligned} \tan\frac{\psi^1}{2} &= k\sin\vartheta^1 \\ \tan\frac{\psi^2}{2} &= k\sin\vartheta^2. \end{aligned} \tag{4.63}$$

However, when synthesis is a concern Eq. (4.63) represents overdetermined linear system in the unknown dimensional parameter $k = \cot\varepsilon$. This in turn means, that a serial assembly of Miura-ori building block four-bars will not be able to reach the two desired configurations of the polyline. However, straight forward application of the two-configuration synthesis procedure yields another serial assembly of four-bars, which may reach the prescribed configurations but has no flat inflatable state. Those may be called Miura-based serial assemblies due to a certain similarity to the previous patterns that have a flat unfolded state.

The synthesis approach basically follows the same design idea as shown before. However, now a polyline is attached to two different curves, as shown in Fig. 4.19a). This yields sets of angles $\psi^1, \psi^2 \neq 0$ at each vertex along the polyline, where afterwards a set of opening angles $\vartheta^1, \vartheta^2 \neq 0$, identical for each vertex along the line may be prescribed. Using Eq. (4.60) and (4.61) then allows to define relative displacements and again solving Eq. (4.62) for each reasonable combination of frames yields joint axes of Miura-based serial assemblies of of non-flat inflatable four-bars. An example is shown in Fig. 4.19, where a polyline is defined to touch a parabola in configuration 1 and a circle in configuration 2. Figure 4.19d) shows non-flat panels, which result from joint axes that do not lie in one single plane at one segment. Finally, using

Eq. (4.44) in order to classify the slide along axes yielded a zero sliding for each axis, which shows that those correspond to revolute joints.

Applications of the folding structures presented here could be transformable roofs in architecture or also robotic grasping devices.

4.3. Constraint-Based Synthesis of Spherically Constrained RR Chains

This section presents f.p.s. procedures of the structures introduced in sect. 3.2.1. Compared to the previous section, where two-configuration synthesis is a concern, the procedures presented here require the synthesis equations of planar, spherical and spatial RR chains, introduced in sect. 2.3.2, 2.3.4 and 2.3.5. The result is a general design procedure, which can be used to synthesize spherically constrained planar, spherical and spatial RR chains for a prescribed set of task positions of the end link of a RR guiding chain.

The procedure essentially requires the definition of specific coordinate frames in order to perform synthesis. Using these frames, examples are provided showing four- and three-position synthesis procedures of a spherically constrained planar as well as a spatial RR chain, which can also be found in [105] and [112]. These procedures also make use of the algebraic solution procedures of planar, spherical and spatial RR chains, given in detail in the appendix, sect. C.1, C.2 and C.3.

4.3.1. Specification of Coordinate Frames for Synthesis

Figure 4.20 shows a general spherically constrained spatial RR chain. Recall here, that this is the most general case, which may always be transformed into the planar or spherical types. A fixed frame W shall be associated with the fixed link K'. The moving frames $B2$ and B''' correspond to the moving links $K2$ and K''' and are required for synthesis. While W and B''' can be located arbitrarily somewhere in K' and K''', frame $B2$ is required to have its z-axis parallel to axis $\hat{\mathbf{c}}$.

The location and orientation of $\hat{\mathbf{c}}$ can be defined by the location of R joints at axes $\hat{\mathbf{d}}$ and $\hat{\mathbf{g}}$. This is equivalent to saying, that the z-axis of $B2$ may be defined by a constant angle β, which is measured in a plane spanned by the directions of $\hat{\mathbf{c}}$ and $\hat{\mathbf{d}}$. When the linkage moves, $B2$ performs spherical movement about the fixed vertex, defined by axes $\hat{\mathbf{a}}$, $\hat{\mathbf{b}}$, $\hat{\mathbf{c}}$ and $\hat{\mathbf{d}}$, which is a composition of rotations around $\hat{\mathbf{c}}$ and $\hat{\mathbf{d}}$ by angles ϕ_c and ϕ_d. These angles, axes and frames serve as a certain reference for the following synthesis procedure and may be used in the design of constrained planar, spherical or either spatial RR chains.

4.3.2. General Synthesis Steps for Spherically Constrained RR Chains

Before providing synthesis procedures in detail it is convenient to consider essential design steps, similar in the design of spherically constrained planar, spherical or either spatial RR chains:

1. The first step in the synthesis procedure consists in defining a finite number of task poses of link K''' using frame B''' whose location and orientation is measured with respect to the fixed frame W. Those may be defined using homogeneous transforms, introduced by Eq. (2.2), which allow to compute relative displacements using Eq. (2.3).

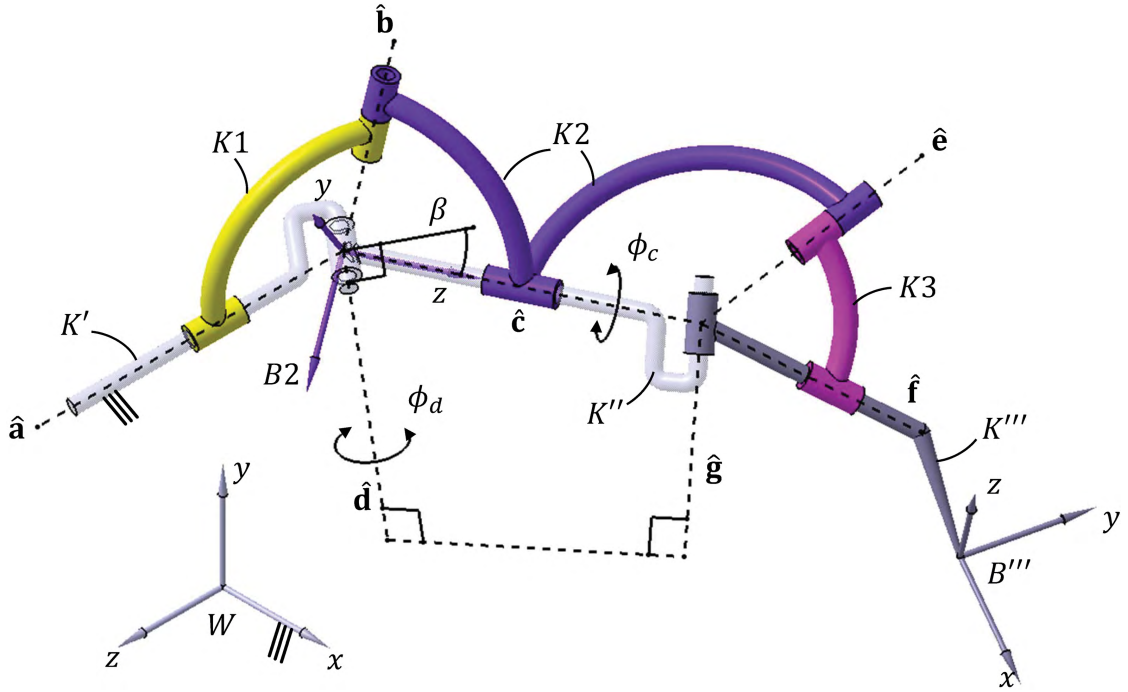

Figure 4.20.: Axes, links and frames of a general spherically constrained RR chain, required for constraint-based synthesis

2. The next step consists in synthesizing a RR guiding chain for the previously prescribed finite set of task poses. This RR chain is formed by the links K', K'' and K''' in a spherically constrained RR chain. The case of a planar or spherical RR guiding chain requires the design equations (2.47) or (2.52) from sect. 2.3.2 or 2.3.4. Note that synthesis equations must be adopted appropriately since here one end link is considered to be fixed. The case of a spatial RR chain requires the design equations (2.55), (2.57) and (2.59) from sect. 2.3.5. The result of synthesis calculations are the axes $\hat{\mathbf{d}}$ and $\hat{\mathbf{g}}$, which are parallel, intersect or are either skew.

3. Based on the synthesized RR guiding chain, the next step is to prescribe finitely separated poses of link $K2$ using frame $B2$. Those must be compositions of rotations around axes $\hat{\mathbf{c}}$ and $\hat{\mathbf{d}}$ by angles ϕ_c and ϕ_d at the synthesized RR guiding chain. On the one hand this requires the definition of $\hat{\mathbf{c}}$ by choosing R joints at the previously determined axes $\hat{\mathbf{d}}$ and $\hat{\mathbf{g}}$. On the other hand an inverse kinematic analysis of the guiding RR chain is required.

4. The final synthesis step consists in applying spherical RR synthesis to obtain the remaining links $K1$ and $K3$ in a spherically constrained RR chain. This again requires the design equations (2.52) from sect. 2.3.4 and yields the remaining axes $\hat{\mathbf{a}}$, $\hat{\mathbf{c}}$, $\hat{\mathbf{e}}$ and $\hat{\mathbf{f}}$ at the fixed and moving vertex.

The different steps are visualized qualitatively in Fig. 4.21, where a general spherically constrained RR chain is drawn using the linkage graph introduced in Fig. 3.4.

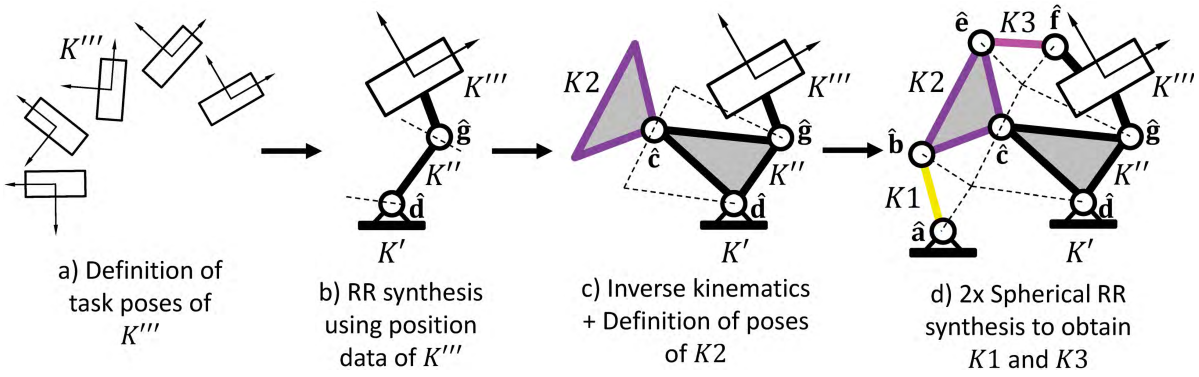

Figure 4.21.: Qualitative representation of the stepwise constraint-based finite position synthesis procedure of spherically constrained RR chains

4.3.3. Four-Position Synthesis of Spherically Constrained Planar RR Chains

The synthesis of spherically constrained planar RR chains is considered in the following for four prescribed planar poses of link K'''. Note that essential steps may also be found in [105]. This follows straight forward execution of the previously synthesis steps and particularly and requires synthesis equations (2.47) and (2.52) of planar and spherical RR chains. Since these can be solved for up to five finitely separated task poses, the procedures may also be extended into a five-position synthesis procedure, which however has not been examined here.

Prescribing task poses and planar RR synthesis

Figure 4.22a) shows four finitely separated task poses of frame B'''. Note that the motion shall take place in the xy-plane of W, such that the z-axes of B''' and W are parallel. The different poses correspond to the position data, listed in table 4.8 and using Eq. (2.2) this can be assembled into planar homogeneous transforms that take the form

$$ {}^{W}\mathbf{T}^{i}_{B'''} = \begin{pmatrix} {}^{W}\mathbf{R}^{i}_{B'''} & {}^{W}\mathbf{t}^{i}_{B'''} \\ 0 \;\; 0 & 1 \end{pmatrix} = \begin{pmatrix} \cos\varphi^{i} & -\sin\varphi^{i} & x^{i}_{t} \\ \sin\varphi^{i} & \cos\varphi^{i} & y^{i}_{t} \\ 0 & 0 & 1 \end{pmatrix}, \qquad i = 1,\ldots,4. \tag{4.64} $$

Since the synthesis equations of the planar RR guiding chain require relative displacements this is transformed into

$$ \mathbf{T}^{1i}_{B'''} = {}^{W}\mathbf{T}^{i}_{B'''}({}^{W}\mathbf{T}^{1}_{B'''})^{-1} = \begin{pmatrix} \mathbf{R}^{1i}_{B'''} & \mathbf{t}^{1i}_{B'''} \\ 0 \;\; 0 & 1 \end{pmatrix}, \qquad i = 2,3,4, \tag{4.65} $$

using Eq. (2.3). The rotations $\mathbf{R}^{1i}_{B'''}$ and translations $\mathbf{t}^{1i}_{B'''}$ represent the input parameters of the planar RR synthesis equations (2.47), which, however, are stated in sect. 2.3.2 for two moving end links of the chain. Since one of these links is the fixed link K' here, one needs to insert $\mathbf{R}^{1i}_{B'} = \mathbf{E}$ and $\mathbf{t}^{1i}_{B'} = \mathbf{0}$, which, after writing in terms of $\mathbf{p}_d$ and $\mathbf{p}^{1}_{g}$, yields the simplified planar RR synthesis equations as

$$ (\mathbf{p}^{1}_{g})^{T}\cdot\mathbf{M}^{1i}\cdot\mathbf{p}_d + (\vec{\lambda}^{\,1i})^{T}\cdot\mathbf{p}^{1}_{g} + (\vec{\mu}^{\,1i})^{T}\cdot\mathbf{p}_d + \delta^{1i} = 0, \qquad i = 2,3,4, \tag{4.66} $$

Herein the motion parameters take the simple form $\mathbf{M}^{1i} = \mathbf{E} - (\mathbf{R}^{1i}_{B'''})^{T}$, $(\vec{\lambda}^{\,1i})^{T} = (\mathbf{t}^{1i}_{B'''})^{T}\cdot\mathbf{R}^{12}_{B'''}$, $(\vec{\mu}^{\,1i})^{T} = -(\mathbf{t}^{1i}_{B'''})^{T}$ and $\delta^{1i} = \frac{1}{2}(\mathbf{t}^{1i}_{B'''})^{T}\cdot\mathbf{t}^{1i}_{B'''}$ and $\mathbf{p}_d$ and $\mathbf{p}^{1}_{g}$ represent the unknown locations of

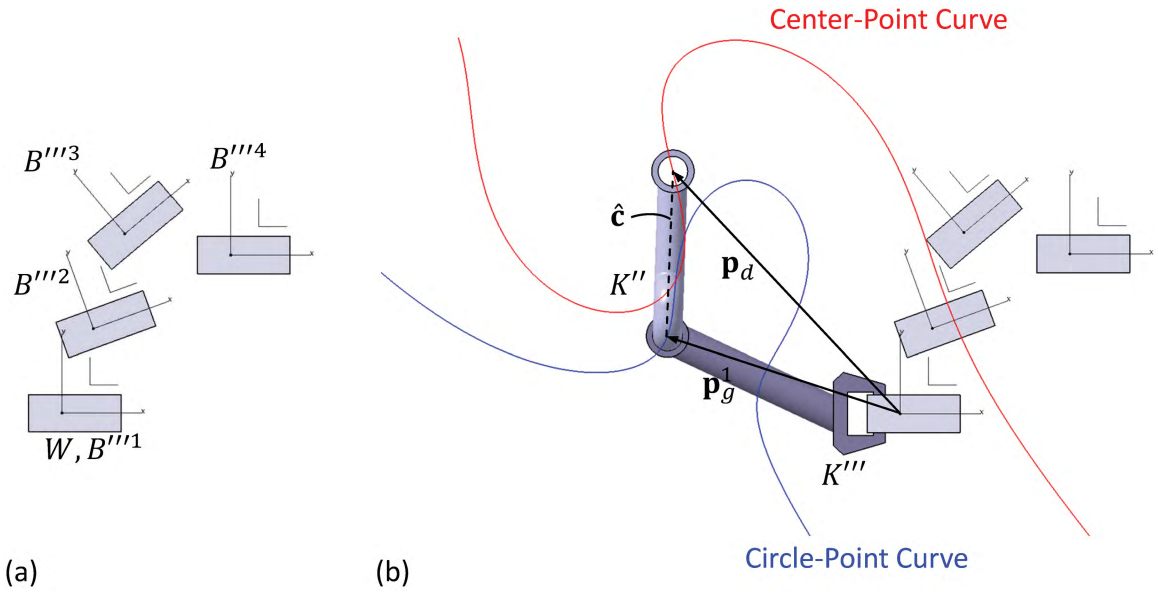

Figure 4.22.: a) Four planar task poses for a planar RR chain. b) center-point and circle-point curve that correspond to the four poses and a planar RR chain

Table 4.8.: Task poses for four-position synthesis of a planar RR chain

	B'''^1	B'''^2	B'''^3	B'''^4
φ^i	0.0 deg	20.0 deg	40.0 deg	0.0 deg
${}^W\mathbf{t}_B^i$	$(\ 0.0 \quad 0.0 \ )^T$	$(\ 7.5 \quad 20.0 \ )^T$	$(\ 15.0 \quad 42.5 \ )^T$	$(\ 40.0 \quad 37.5 \ )^T$

the parallel axes $\hat{\mathbf{d}}$ and $\hat{\mathbf{g}}$ of the planar RR chain. Equation (4.66) represents the set of three bilinear scalar synthesis equations, that can be solved for $\mathbf{p}_d$ and $\mathbf{p}_g^1$ using the algebraic solution procedure developed in detail in the appendix, sect. C.1. The result is that $\mathbf{p}_d$ and $\mathbf{p}_g^1$ can be selected at specific planar curves, known as the center-point and circle-point curve. Figure 4.22b) shows these curves, where a specific $\mathbf{p}_d$ and $\mathbf{p}_g^1$ is chosen in order to design a planar RR chain.

Inverse kinematics of the planar RR chain and definition of orientations of K2

Following the third step from sect. 4.3.2, inverse kinematics calculations are required in order to define orientation data of link $K2$. Recall here from Fig. 4.20, that the movement of this link is conveniently described using frame $B2$, that may be considered as being located at $\mathbf{p}_d$ having its z-axis pointing along axis $\hat{\mathbf{c}}$ of a spherically constrained RR chain. Hence, the next step is to define axis $\hat{\mathbf{c}}$, which can be done for each configuration i using the previously determined locations $\mathbf{p}_d$ and $\mathbf{p}_g^1$:

$$\hat{\mathbf{c}}^i = \begin{pmatrix} \mathbf{c}^i \\ \mathbf{p}_c^i \times \mathbf{c}^i \end{pmatrix}, \quad i = 1,\ldots,4 \qquad \mathbf{c}^i = \frac{\mathbf{p}_g^i - \mathbf{p}_d}{|\mathbf{p}_g^i - \mathbf{p}_d|}, \quad \mathbf{p}_c^i = \mathbf{p}_d. \tag{4.67}$$

Due to the fact, that $\mathbf{p}_d$ and $\mathbf{p}_g^1$ are considered as planar vectors in Eq. (4.66), both lying in the xy-plane of W, this definition of $\hat{\mathbf{c}}$ yields the angle $\beta = 0$ (see again Fig. 4.20). However, by

simply adding a third vector component to $\mathbf{p}_d$ and $\mathbf{p}_g^1$ other than zero, also angles $\beta \neq 0$ may be produced. This yields differently placed R joints along axes $\hat{\mathbf{d}}$ and $\hat{\mathbf{g}}$. Note that such a definition is valid, because no additional constraints are added to the planar RR chain. Never the less this section continues discussing the case of $\beta = 0$, because $\beta \neq 0$ will be retraced in sect. 4.3.4.

When $\beta = 0$, the movement of frame $B2$ is simply a composition of a z- and x-rotation, by angles ϕ_d and ϕ_c:

$$ {}^W\mathbf{R}_{B2}^i = \mathbf{R}_z(\phi_d^i)\mathbf{R}_x(\phi_c^i) = \begin{pmatrix} \cos\phi_d & -\cos\phi_c\sin\phi_d & \sin\phi_d\sin\phi_c \\ \sin\phi_d & \cos\phi_d\cos\phi_c & -\cos\phi_d\sin\phi_c \\ 0 & \sin\phi_c & \cos\phi_c \end{pmatrix}^i, \quad i = 1,\ldots,4. \tag{4.68} $$

Note that the movement of K'' may be described by ${}^W\mathbf{R}_{B''}^i = \mathbf{R}_z(\phi_d^i)$. Since ϕ_d simply measures the angle around the fixed axes $\hat{\mathbf{d}}$ of the planar RR chain it may easily be found from following inverse kinematics calculations as

$$ \phi_d^i = \arctan\left(\frac{y_c^i}{x_c^i}\right), \qquad i = 1,\ldots,4, \tag{4.69} $$

where y_c^i and x_c^i are W-frame coordinates of direction $\mathbf{c}^i$. For the x-rotation, angles ϕ_c^i may be specified arbitrarily, because no additional constraints are added to the planar RR chain. For the example shown in Fig. 4.22 angles were calculated as $\phi_d^1 = 268.122$ deg, $\phi_d^2 = 274.889$ deg, $\phi_d^3 = 292.534$ deg and $\phi_d^4 = 358.172$ deg using Eq. (4.69). Angle ϕ_c was chosen arbitrarily as $\phi_c^1 = 0.0$ deg, $\phi_c^2 = 20.0$ deg, $\phi_c^3 = 40.0$ deg and $\phi_c^4 = 120.0$ deg. Using this data, allows to calculate the following relative rotations, which represents an essential input for the synthesis of spherical RR chains in the final design step in the next section:

$$ \mathbf{R}_{B2}^{1i} = {}^W\mathbf{R}_{B2}^i({}^W\mathbf{R}_{B2}^1)^{-1}, \quad i = 2,3,4. \tag{4.70} $$

Four-position synthesis of spherical RR chains

In order to complete the spherically constrained planar RR chain the remaining links $K1$ and $K3$ must be found, such that the resulting linkage reaches the four poses of K'''. This is done using Eq. (2.52) and synthesizing two spherical RR chains. The first one is formed by links K', $K1$ and $K2$, while the second one is formed by links $K2$, $K3$ and K'''. Because K' is a fixed link this yields $\mathbf{R}_W^{1i} = \mathbf{E}$ and $\mathbf{a}^1 = \mathbf{a}$ and the result are the following synthesis equations for the first RR chain

$$ (\mathbf{b}^1)^T \cdot \mathbf{M}^{1i} \cdot \mathbf{a} = 0,\ i = 2,\ldots,4, \quad \text{where} \quad \mathbf{M}^{1i} = \mathbf{E} - (\mathbf{R}_{B2}^{1i})^T. \tag{4.71} $$

Note, that $\mathbf{R}_{B2}^{1i}$ is given from the previous section.

It's important to recall here, that the spherical synthesis problem only includes information about the orientation of frames, while their locations are not of interest. For this reason the different locations of W and $B2$ shown in Fig. 4.20 do not affect the spherical RR synthesis and Eq. (4.71) may be solved without considering the aspect.

The spherical algebraic four-position RR synthesis procedure parallels that of planar RR chains and yields what is known as the center-axis and circling-axis cones. These cones are ruled surfaces of order three, passing through the fixed vertex formed by axes $\hat{\mathbf{a}}$, $\hat{\mathbf{b}}$, $\hat{\mathbf{c}}$ and $\hat{\mathbf{d}}$ and contain the directions $\mathbf{a}$ and $\mathbf{b}^1$. Due to relative orientations $\mathbf{R}_{B2}^{1i}$, these are measured in W.

The algebraic four-position synthesis procedure towards center-axis and circling-axis cones is provided in the appendix, sect. C.2 and also holds for the case of two moving end links in a spherical RR chain. This is just the case for the chain formed by links $K2$, $K3$ and K''' at the

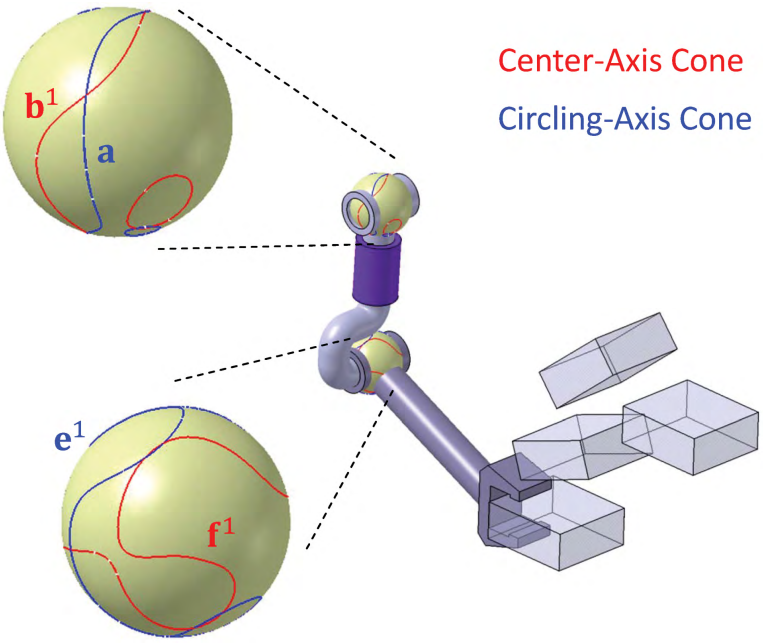

Figure 4.23.: Center-axis and circling-axis cones obtained from four-orientation synthesis of spherical RR chains

moving vertex defined by axes $\hat{\mathbf{c}}$, $\hat{\mathbf{e}}$, $\hat{\mathbf{f}}$ and $\hat{\mathbf{g}}$. The corresponding synthesis equations may be written as

$$(\mathbf{f}^1)^T \cdot \mathbf{M}^{1i} \cdot \mathbf{e}^1 = 0,\ i = 2,\ldots,4, \quad \text{where} \quad \mathbf{M}^{1i} = \mathbf{E} - (\mathbf{R}^{1i}_{B'''})^T \mathbf{R}^{1i}_{B2}, \tag{4.72}$$

where $\mathbf{R}^{1i}_{B'''} = {}^W\mathbf{R}^i_{B'''}({}^W\mathbf{R}^1_{B'''})^{-1}$ is the rotation matrix from Eq. (4.65), which contains the planar rotation data from table 4.8. However, due to the fact that $\mathbf{R}^{1i}_{B2}$ is a 3×3 matrix, $\mathbf{R}^{1i}_{B'''}$ must represent a 3×3 matrix as well, which is easily arranged by defining

$${}^W\mathbf{R}^i_{B'''} = \begin{pmatrix} \cos\varphi^i & -\sin\varphi^i & 0 \\ \sin\varphi^i & \cos\varphi^i & 0 \\ 0 & 0 & 1 \end{pmatrix}, \qquad i = 1,\ldots,4. \tag{4.73}$$

Equation (4.72) may also be solved to obtain a center-axis and circling-axis cone using the algebraic four-position synthesis procedure provided in the appendix, sect. C.2. Hence, there are two center-axis and circling-axis cones, one located at the fixed vertex formed by axes $\hat{\mathbf{a}}$, $\hat{\mathbf{b}}$, $\hat{\mathbf{c}}$ and $\hat{\mathbf{d}}$ and another one located at the moving vertex defined by axes $\hat{\mathbf{c}}$, $\hat{\mathbf{e}}$, $\hat{\mathbf{f}}$ and $\hat{\mathbf{g}}$. Intersecting these cones with spheres yields spherical curves of intersection. Such curves are shown in Fig. 4.23 for the different center-axis and circling-axis cones determined before and may be seen as the analogue, spherical versions of center-point and circle-point curves of planar RR chains. At these curves a suitable $\mathbf{a}$, $\mathbf{b}^1$, $\mathbf{f}^1$ and $\mathbf{e}^1$ may be chosen in order to complete the four-position synthesis of a spherically constrained planar RR chain.

Example design of a spherically constrained planar RR chain

Figure 4.24 shows the animation of a detailed CAD-model that reaches the four initially prescribed poses of link K'''. Based on a parametrized CAD-model of the chain with simplified link geometry (see sect. 5.2) the detailed design was carried out, which allows collision-free movement of the linkage.

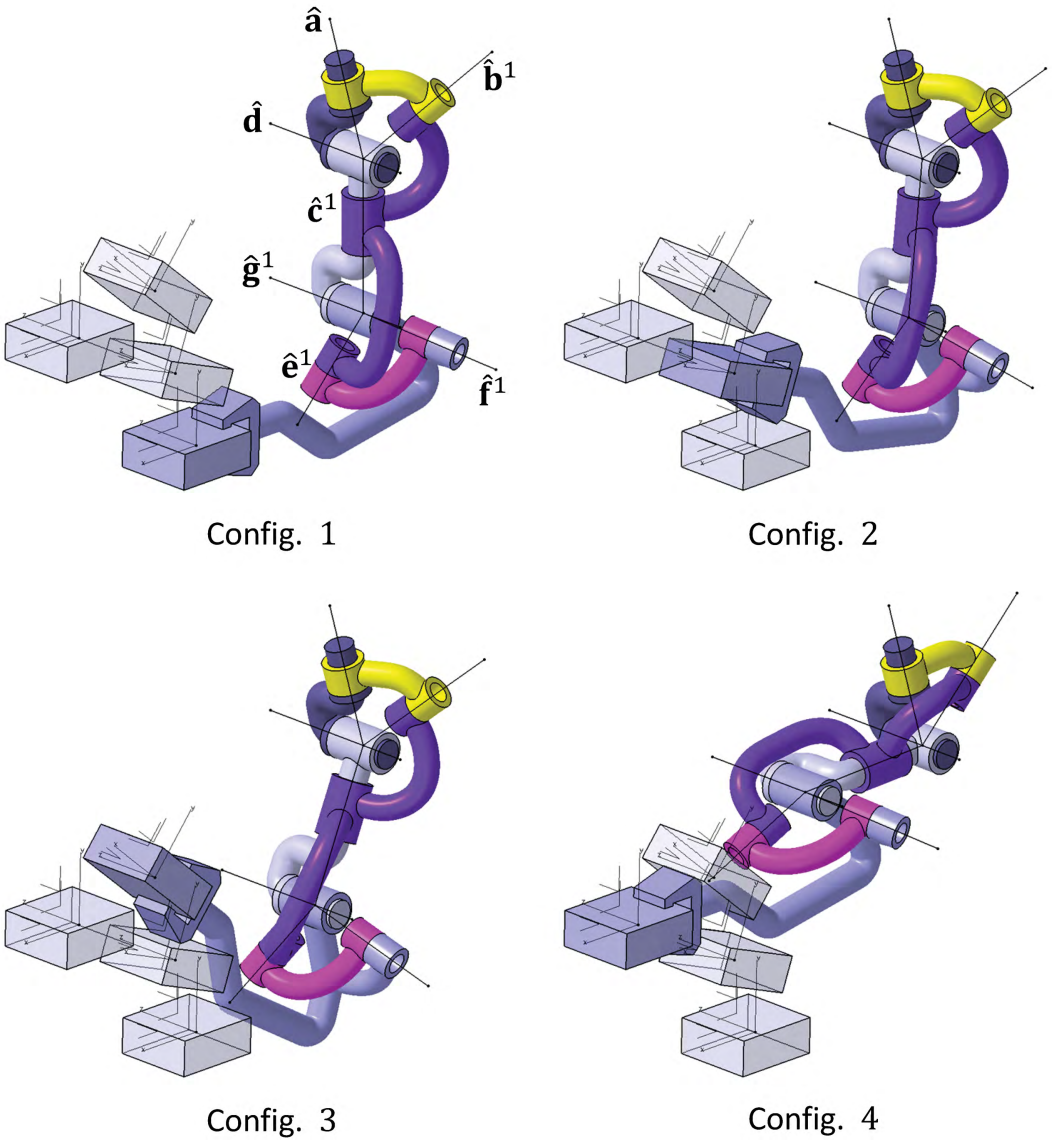

Figure 4.24.: Detailed kinematic CAD-model reaching the four planar poses of link K'''

4.3.4. Three-Position Synthesis of Spherically Constrained Spatial RR Chains

This section describes a synthesis procedure of spherically constrained spatial RR chains for three prescribed spatial poses of link K'''. Note that essential steps of the following remarks may also be found in [112]. The procedure requires synthesis equations of spatial and spherical RR chains. Recall from sect. 2.3.5 that three is the maximum number of poses for spatial RR synthesis. Hence, spherical RR synthesis is also performed for three positions only, even though the problem can also be solved for up to five positions. The result is an underspecified spherical synthesis which provides free parameters that can be specified with respect to further requirements of the task.

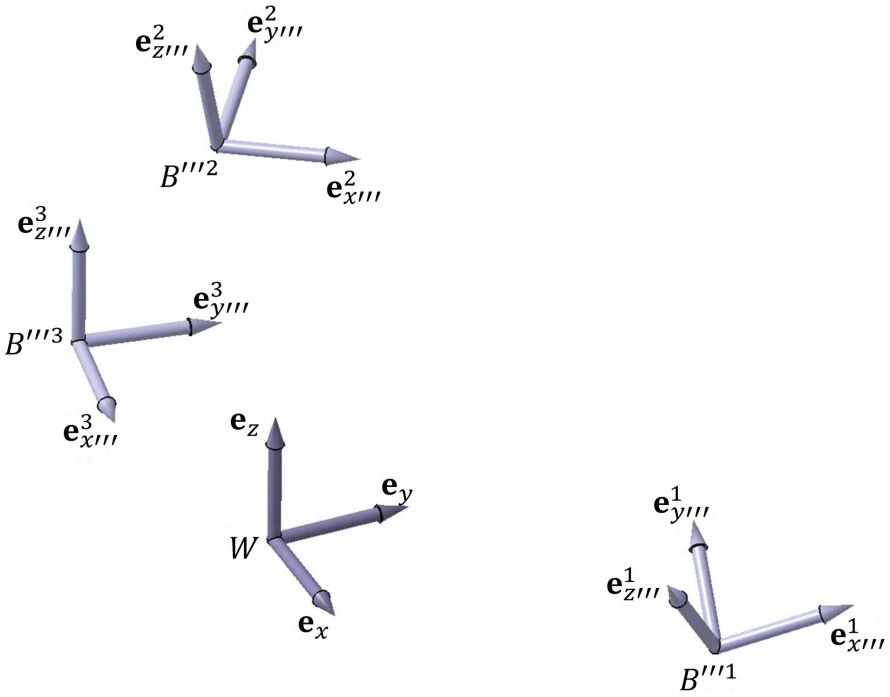

Figure 4.25.: Three finitely separated task positions of frame B''' and a fixed reference frame W for three-position synthesis of a spherically constrained spatial RR chain.

Table 4.9.: Three task positions of frame B''' for spatial RR synthesis

	ψ	ϑ	φ	${}^W\mathbf{t}^i_{B'''}$
$B'''1$	30.0 deg	35.0 deg	40.0 deg	$(\ 90.0 \quad 65.0 \quad 10.0\ )^T$
$B'''2$	30.0 deg	15.0 deg	20.0 deg	$(\ -10.0 \quad -10.0 \quad 100.0\ )^T$
$B'''3$	0.0 deg	0.0 deg	-10.0 deg	$(\ -60.0 \quad -20.0 \quad 20.0\ )^T$

Prescribing task poses and spatial RR synthesis equations

Figure 4.25a) shows three finitely separated spatial task poses of frame B'''. The different poses correspond to the position data, listed in table 4.9, where the orientation of frames is defined with respect to the fixed reference frame W using the z-x-z-Euler transformation from Eq. (2.7). Using Eq. (2.2) this can be assembled into 4×4 homogeneous transforms as

$$ {}^W\mathbf{T}^i_{B'''} = \begin{pmatrix} & {}^W\mathbf{R}^i_{B'''} & & {}^W\mathbf{t}^i_{B'''} \\ 0 & 0 & 0 & 1 \end{pmatrix}, \qquad i = 1,2,3. \tag{4.74} $$

Since the synthesis equations of the spatial RR chain require relative displacements this is transformed into

$$ \mathbf{T}^{1i}_{B'''} = {}^W\mathbf{T}^i_{B'''}({}^W\mathbf{T}^1_{B'''})^{-1} = \begin{pmatrix} & \mathbf{R}^{1i}_{B'''} & & \mathbf{t}^{1i}_{B'''} \\ 0 & 0 & 0 & 1 \end{pmatrix}, \qquad i = 2,3, \tag{4.75} $$

using Eq. (2.3). The rotations $\mathbf{R}^{1i}_{B'''}$ and translations $\mathbf{t}^{1i}_{B'''}$ represent the input parameters of Eq. (2.55), (2.56) and (2.59). When furthermore stated in terms of the axes $\hat{\mathbf{d}} = (\mathbf{d},\ \mathbf{p}_d \times \mathbf{d})^T$ and

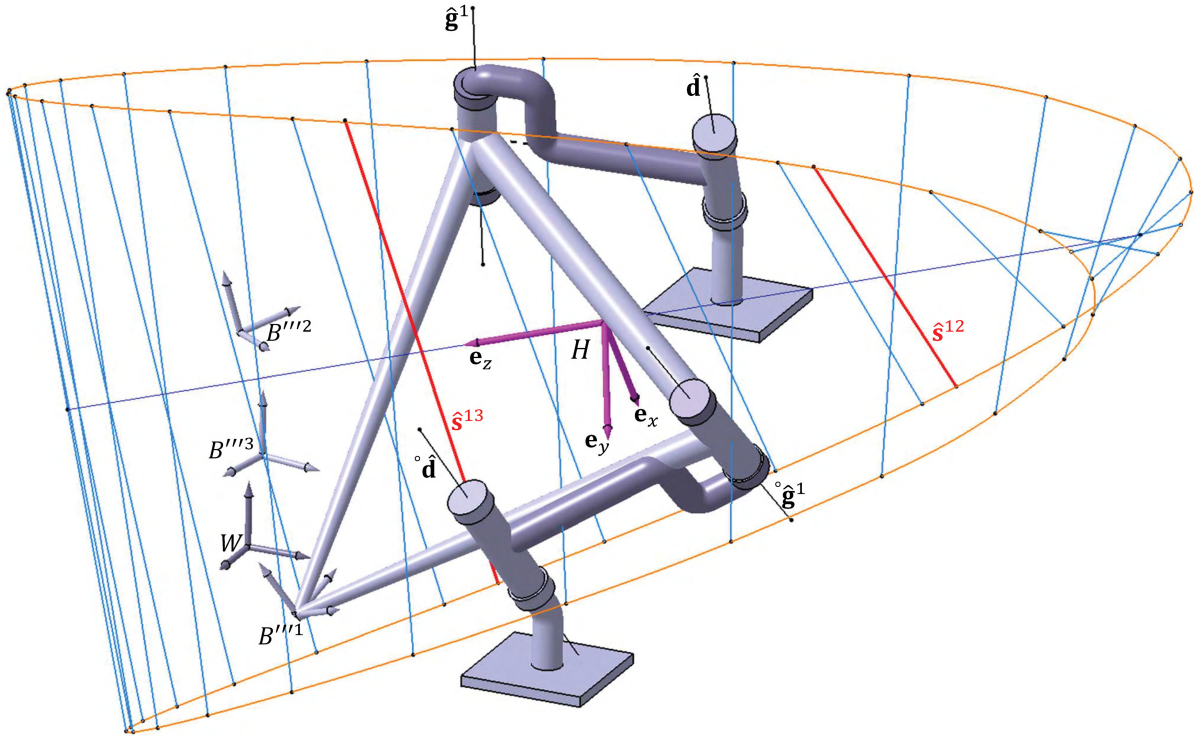

Figure 4.26.: The cylindroid generated from the three position task (table 4.9), which includes the relative screw axes $\hat{\mathbf{s}}^{12}$ and $\hat{\mathbf{s}}^{13}$

$\hat{\mathbf{g}}^1 = (\mathbf{g}^1,\ \mathbf{p}_g^1 \times \mathbf{g}^1)^T$, measured in W these equations take the form

$$(\mathbf{d})^T \cdot \left(\mathbf{E} - \mathbf{R}_{B'''}^{1i}\right) \cdot \mathbf{g}^1 = 0, \tag{4.76}$$

$$(\mathbf{d})^T \cdot \left(\mathbf{E} - \mathbf{R}_{B'''}^{1i}\right) \cdot \left(\mathbf{p}_g^1 \times \mathbf{g}^1\right) + (\mathbf{p}_d \times \mathbf{d})^T \cdot \left(\mathbf{E} - \mathbf{R}_{B'''}^{1i}\right) \cdot \mathbf{g}^1 - (\mathbf{d})^T \cdot \tilde{\mathbf{t}}_{B'''}^{1i} \mathbf{R}_{B'''}^{1i} \cdot \mathbf{g}^1 = 0, \quad i = 2,3. \tag{4.77}$$

and

$$(\mathbf{d})^T \cdot \left(\mathbf{p}_d - \mathbf{R}_{B'''}^{1i} \cdot \mathbf{p}_g^1 + \mathbf{t}_{B'''}^{1i}\right) = 0 \text{ and } (\mathbf{g}^i)^T \cdot \left((\mathbf{R}_{B'''}^{1i})^T \cdot \mathbf{p}_d - (\mathbf{R}_{B'''}^{1i})^T \cdot \mathbf{t}_{B'''}^{1i} - \mathbf{p}_g^1\right) = 0, \quad i = 1,2,3. \tag{4.78}$$

As already described in sect. 2.3.5, Eq. (4.77) can be replaced by the following simpler equation

$$(\mathbf{s}^{1i})^T \cdot \left(\mathbf{p}_d - \mathbf{p}_g^1\right) - \frac{s^{1i}}{2} = 0 \quad i = 2,3, \tag{4.79}$$

where $\mathbf{s}^{1i}$ is the direction of the screw axes $\hat{\mathbf{s}}^{1i}$ associated with the relative displacement $\mathbf{T}_{B'''}^{1i}$ and s^{1i} is the slide along $\mathbf{s}^{1i}$. See also sect. A.4 and A.5 to see how to determine these quantities.

Synthesis of a Bennett linkage using the principal axis frame of the cylindroid

As described in sect. C.3 the screw axes $\hat{\mathbf{s}}^{12}$ and $\hat{\mathbf{s}}^{13}$ associated with $\mathbf{T}_{B'''}^{12}$ and $\mathbf{T}_{B'''}^{13}$ are involved in finding the principal axis frame H of a cylindroid (see [115]). The benefit of knowing the location and orientation of H is that Eq. (4.78) is identically satisfied , when measured in H. Furthermore, the ten unknown W-frame coordinates x_d, y_d, x_g^1, y_g^1, x_{p_d}, y_{p_d}, z_{p_d}, $x_{p_g}^1$, $y_{p_g}^1$ and $z_{p_g}^1$ can then be replaced by four equivalent parameters that define coordinates of vectors in H.

Table 4.10.: Synthesized axis parameters, measured in the principal axis frame H, of two spatial RR chains forming Bennett's linkage in configuration $i = 1$

	Direction	Location
${}^{H}\hat{\mathbf{d}}$	$(0.9819 \quad -0.1061 \quad 0.1570)^T$	$(8.7136 \quad -80.6060 \quad -54.4861)^T$
${}^{H}\hat{\mathbf{g}}^1$	$(0.9724 \quad 0.1051 \quad 0.2082)^T$	$(-11.6684 \quad -107.9391 \quad 54.4861)^T$
${}^{H\circ}\hat{\mathbf{d}}$	$(0.9724 \quad 0.1051 \quad -0.2082)^T$	$(11.6684 \quad 107.9391 \quad 54.4861)^T$
${}^{H\circ}\hat{\mathbf{g}}^1$	$(0.9819 \quad -0.1061 \quad -0.1570)^T$	$(-8.7136 \quad 80.6060 \quad -54.4861)^T$

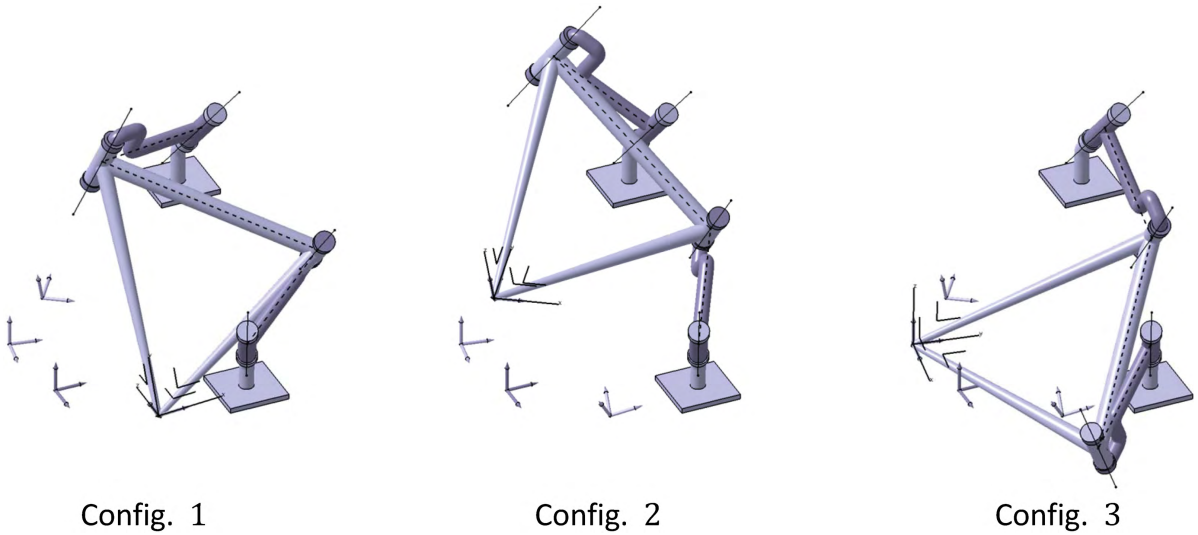

Figure 4.27.: Synthesized Bennett linkage reaching the three positions from table 4.9

The complete procedure is shown in detail in [30] together with an algebraic solution of Eq. (4.76) and (4.79), that yields two RR chains that can be assembled to form a Bennett linkage. This procedure is used here in order to determine the axis parameters $\mathbf{d}$, $\mathbf{p}_d$, $\mathbf{g}^1$ and $\mathbf{p}_g^1$ of a RR chain, measured in H. To distinguish H-frame parameters in this section from the usual W-frame coordinates they are denoted as ${}^{H}\mathbf{d}$, ${}^{H}\mathbf{p}_d$, ${}^{H}\mathbf{g}^1$ and ${}^{H}\mathbf{p}_g^1$ here.

Using the screw axes $\hat{\mathbf{s}}^{12}$ and $\hat{\mathbf{s}}^{13}$ associated with the position data from table 4.9 and following [115] and [30] yields the desired principal axis frame as well as the RR synthesis solutions forming a Bennett linkage. Figure 4.26 shows the Bennett linkage as well as the cylindroid generated following sect. C.3, which includes $\hat{\mathbf{s}}^{12}$ and $\hat{\mathbf{s}}^{13}$. Table 4.10 lists the coordinates of axes measured in H. The results show a certain symmetry, which results from the particular relative location and orientation between the Bennett linkage and the principal axis frame. This is a particular feature of the geometry of Bennett's linkage and the principal axis frame, discussed in detail in [116]. The synthesis solution actually satisfies the three positions as shown in Fig. 4.27.

Transformation into W-frame coordinates

In order to continue the synthesis procedure of the spherically constrained spatial RR chain, the transformation of the different axis coordinates into W-frame coordinates is required. This is because further synthesis calculations are conveniently performed in frame W. Based on the calculations of the previous section the transformation between H and W was found as

$$ {}^{W}\mathbf{T}_{H} = \begin{pmatrix} {}^{W}\mathbf{R}_{H} & {}^{W}\mathbf{t}_{H} \\ 0\ \ 0\ \ 0 & 1 \end{pmatrix} = \begin{pmatrix} -0.5736 & 0.7617 & 0.3012 & -15.4284 \\ 0.0119 & 0.3755 & -0.9268 & 170.7447 \\ -0.8191 & -0.5280 & -0.2245 & 134.9617 \\ 0 & 0 & 0 & 1 \end{pmatrix}. \tag{4.80} $$

Using this numerical data in combination with that from table 4.9, the W-frame coordinates $\mathbf{d}$, $\mathbf{p}_d$, $\mathbf{g}^1$ and $\mathbf{p}_g^1$ from table 4.10 are found as:

$$ \mathbf{d} = {}^{W}\mathbf{R}_{H} \cdot {}^{H}\mathbf{d} \qquad \mathbf{p}_d = {}^{W}\mathbf{R}_{H} \cdot {}^{H}\mathbf{p}_d + {}^{W}\mathbf{t}_{H} \tag{4.81} $$

and

$$ \mathbf{g}^1 = {}^{W}\mathbf{R}_{H} \cdot {}^{H}\mathbf{g}^1 \qquad \mathbf{p}_g^1 = {}^{W}\mathbf{R}_{H} \cdot {}^{H}\mathbf{p}_g^1 + {}^{W}\mathbf{t}_{H}. \tag{4.82} $$

Inverse kinematics of the spatial RR chain and definition of orientations of K2

The parameters obtained from Eq. (4.81) and (4.82) form the axes of the spatial RR chain that is used as the guiding chain in the spherically constrained linkage. Based on that the next step in the synthesis procedure is to define three finitely separated poses of the link $K2$. Retrace in Fig. 4.20 that this is a composition of the rotations about $\hat{\mathbf{d}}$ and $\hat{\mathbf{c}}^i$ by angles ϕ_d^i and ϕ_c^i, for each configuration $i = 1,2,3$ of the chain. Because $\hat{\mathbf{d}}$ is already known from spatial RR synthesis, the first step towards a definition of poses of $K2$ is to determine $\hat{\mathbf{c}}^i$. In fact, this axis can be defined using two points $\tilde{\mathbf{p}}_d = \mathbf{p}_d + \lambda_d \mathbf{d}$ and $\tilde{\mathbf{p}}_g^i = \mathbf{p}_g^i + \lambda_g \mathbf{g}^i$, where λ_d and λ_g are arbitrary real constants, which define a Plücker coordinate vector $\hat{\mathbf{c}}^i$, measured in W:

$$ \hat{\mathbf{c}}^i = \begin{pmatrix} \mathbf{c}^i \\ \mathbf{p}_c^i \times \mathbf{c}^i \end{pmatrix}, \quad \mathbf{c}^i = \frac{\tilde{\mathbf{p}}_g^i - \tilde{\mathbf{p}}_d}{|\tilde{\mathbf{p}}_g^i - \tilde{\mathbf{p}}_d|}, \quad \mathbf{p}_c^i = \tilde{\mathbf{p}}_d. \tag{4.83} $$

The next step is to determine the angle ϕ_d^i in each configuration $i = 1,2,3$ of the spatial RR chain. However, since axis $\hat{\mathbf{d}}$ may have arbitrary spatial orientation in W it is convenient to introduce a coordinate transformation between W and another fixed frame $\tilde{W}$, which has its x-axis parallel to the direction of $\hat{\mathbf{d}}$:

$$ {}^{W}\mathbf{R}_{\tilde{W}} = \mathbf{R}_y(-\xi)\mathbf{R}_z(\zeta) = \begin{pmatrix} \cos\zeta\cos\xi & -\sin\zeta\cos\xi & \sin\xi \\ \sin\zeta & \cos\zeta & 0 \\ \cos\zeta\sin\xi & -\sin\zeta\sin\xi & \cos\xi \end{pmatrix}, \tag{4.84} $$

This is a composition of coordinate rotations about y- and z-axes, where the constant angles can be calculated from the direction $\mathbf{d}$ as

$$ \xi = \begin{cases} \arctan\left(\frac{z_d}{x_d}\right): & \{x_d, z_d\} > 0;\ x_d > 0,\ z_d < 0 \\ \arctan\left(\frac{z_d}{x_d}\right) - \pi: & x_d < 0,\ z_d < 0 \\ \arctan\left(\frac{z_d}{x_d}\right) + \pi: & x_d < 0,\ z_d > 0 \end{cases}. \tag{4.85} $$

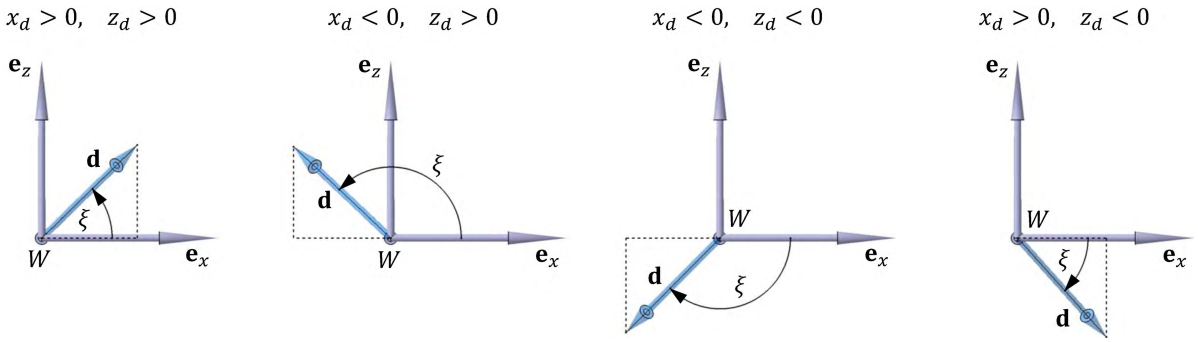

Figure 4.28.: Four different cases, which define the calculation of ξ from Eq. (4.85). Note that the direction of the rotation corresponds to $\mathbf{R}_y(-\xi)$

and

$$\zeta = \arctan\left(\frac{y_d}{\sqrt{(x_d)^2 + (z_d)^2}}\right). \tag{4.86}$$

Herein parameters x_d, y_d and z_d define the direction $\mathbf{d}$. Retrace the geometric meaning of the different cases from Fig. 4.28. Eq. (4.84) allows to obtain the $\tilde{W}$-frame coordinates of the direction $\mathbf{c}^i$ as

$$^{\tilde{W}}\mathbf{c}^i = {}^{\tilde{W}}\mathbf{R}_W \cdot \mathbf{c}^i, \quad i = 1,2,3, \tag{4.87}$$

which in turn allow to calculate ϕ_d^i as

$$\phi_d^i = \begin{cases} \arctan\left(\frac{^{\tilde{W}}y^i}{^{\tilde{W}}z^i}\right): & \{^{\tilde{W}}y^i, {}^{\tilde{W}}z^i\} > 0;\ {}^{\tilde{W}}y^i < 0,\ {}^{\tilde{W}}z^i > 0 \\ \arctan\left(\frac{^{\tilde{W}}y^i}{^{\tilde{W}}z^i}\right) - \pi: & {}^{\tilde{W}}y^i < 0,\ {}^{\tilde{W}}z^i < 0 \\ \arctan\left(\frac{^{\tilde{W}}y^i}{^{\tilde{W}}z^i}\right) + \pi: & {}^{\tilde{W}}y^i > 0,\ {}^{\tilde{W}}z^i < 0 \end{cases} \qquad i = 1,2,3. \tag{4.88}$$

Note that these cases follow from similar considerations as those shown for ξ in Fig. 4.28. Figure 4.29 provides another detailed view on the angles and frames involved in inverse kinematics calculations.

The different angles can next be used to define finite orientations ${}^{W}\mathbf{R}^i_{B''}$ of the link K'' as ${}^{W}\mathbf{R}^i_{B''}(\phi_d^i) = {}^{W}\mathbf{R}_{\tilde{W}}\mathbf{R}_x(-\phi_d^i)$. This transformation rotates B'', such that its xz-plane is parallel to the plane spanned by $\hat{\mathbf{d}}$ and $\hat{\mathbf{c}}$. Hence, the next step towards defining the movement of $K2$ or $B2$ is another constant y-rotation by the angle β. This aligns the z-axis of $B2$ with $\hat{\mathbf{c}}$ and afterwards a final z-rotation by the angle ϕ_c defines the movement of $B2$. The constant angle β may be found for instance from

$$\beta = \arctan\left(\frac{^{\tilde{W}}x_c^1}{\sqrt{(^{\tilde{W}}y_c^1)^2 + {}^{\tilde{W}}z_c^1)^2}}\right). \tag{4.89}$$

Note that also ${}^{\tilde{W}}\mathbf{c}^2$ or ${}^{\tilde{W}}\mathbf{c}^3$ may be used to yield the same angle β. The angle ϕ_c^i can be specified by choosing three arbitrary angles. This is because no constraints are imposed to the previously determined spatial RR chain. The result is the following composition of rotations, that define the orientation of $B2$:

$${}^{W}\mathbf{R}^i_{B2}(\phi_d^i, \phi_c^i) = \mathbf{R}_y(-\xi)\mathbf{R}_z(\zeta)\mathbf{R}_x(-\phi_d^i)\mathbf{R}_y(\beta)\mathbf{R}_z(\phi_c^i), \quad i = 1,2,3. \tag{4.90}$$

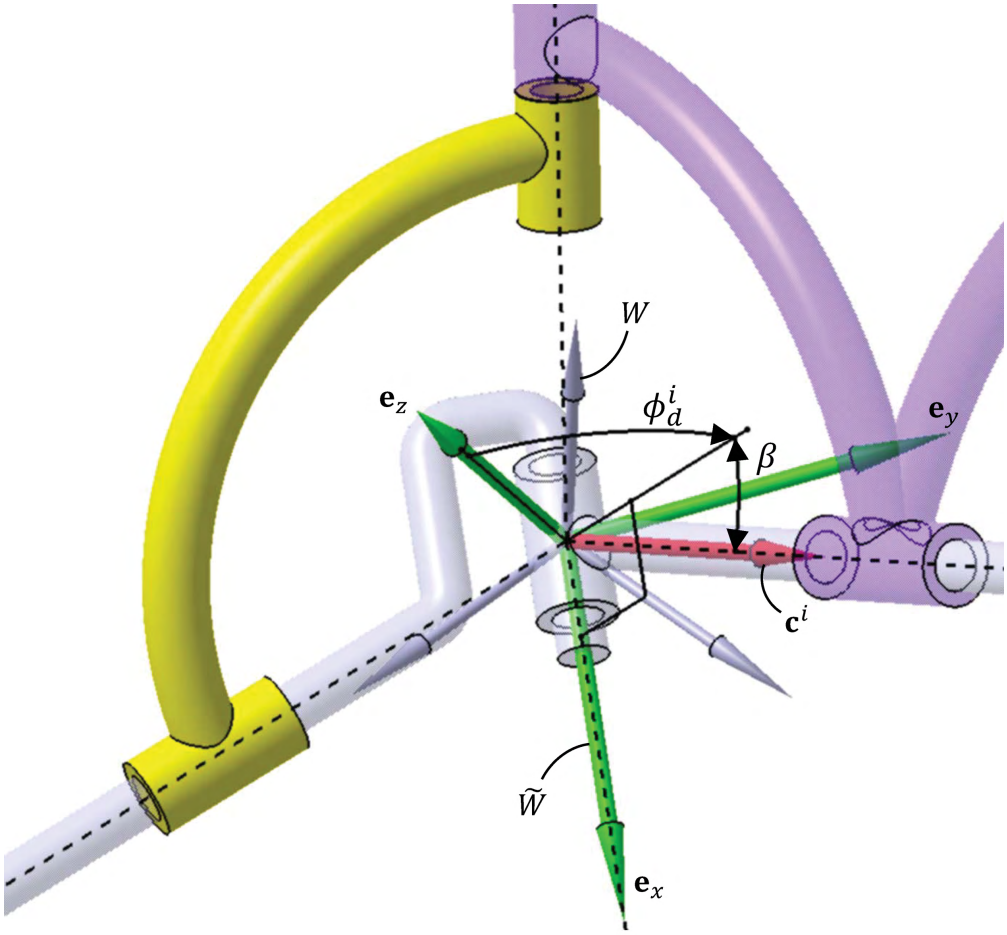

Figure 4.29.: The Frame $\tilde{W}$ as well as angles involved in the inverse kinematics calculations

The relative rotation is obtained as

$$\mathbf{R}_{B2}^{1i} = {}^{W}\mathbf{R}_{B2}^{i}({}^{W}\mathbf{R}_{B2}^{1})^{T}, \quad i = 2,3 \tag{4.91}$$

using Eq. (2.3). This includes the relative rotation $\mathbf{R}_z(\phi_c^{1i}) = \mathbf{R}_z(\phi_c^i)(\mathbf{R}_z(\phi_c^1))^T$, where $\phi_c^{1i} = \phi_c^i - \phi_c^1$.

Three-position synthesis of spherical RR chains

This section provides the final synthesis step in the three-position synthesis procedure of the spherically constrained spatial RR chain and is almost identical to the final step from sect. 4.3.3. Hence, the following text is partially identical to this section.

In order to complete the spherically constrained spatial RR chain the remaining links $K1$ and $K3$ must be found, such that the resulting linkage reaches the three poses of K'''. This is done using Eq. (2.52) and synthesizing two spherical RR chains. The first is formed by links K', $K1$ and $K2$, while the second one is formed by links $K2$, $K3$ and K'''. Because K' is a fixed link this yields $\mathbf{R}_W^{1i} = \mathbf{E}$ and $\mathbf{a}^1 = \mathbf{a}$ and the result are the following synthesis equations for the first RR chain

$$(\mathbf{b}^1)^T \cdot \mathbf{M}^{1i} \cdot \mathbf{a} = 0,\ i = 2,3, \quad \text{where} \quad \mathbf{M}^{1i} = \mathbf{E} - (\mathbf{R}_{B2}^{1i})^T. \tag{4.92}$$

Note, that $\mathbf{R}_{B2}^{1i}$ is given from the previous section, Eq. (4.91). The second spherical RR chain is

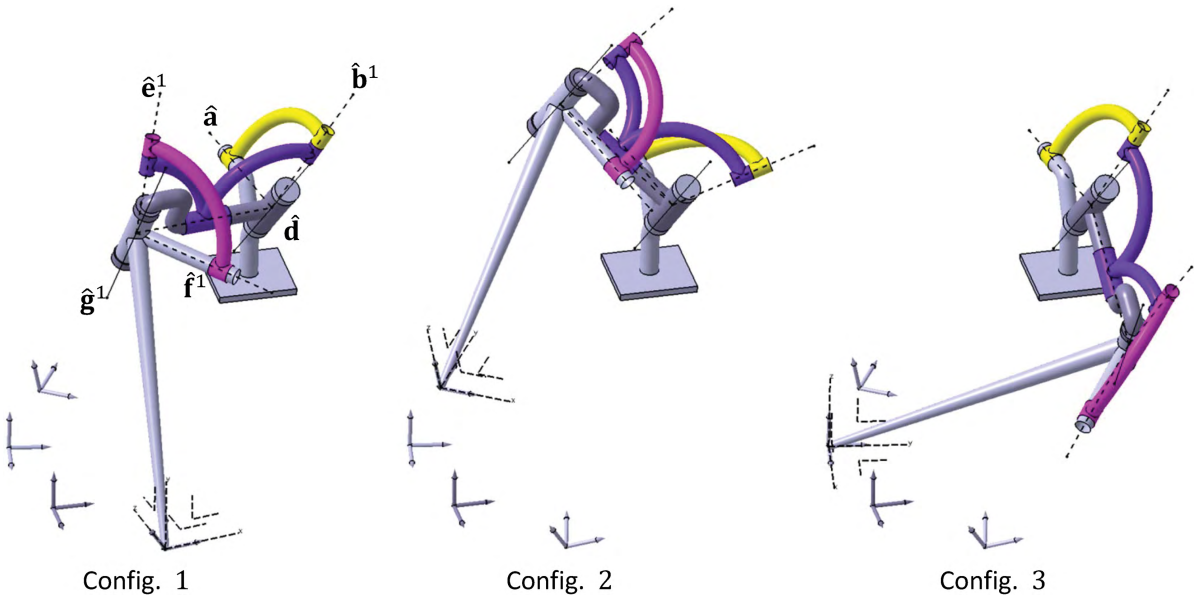

Figure 4.30.: Kinematic CAD-model reaching the three spatial poses of link K'''

defined by axes $\hat{\mathbf{e}}$ and $\hat{\mathbf{f}}$ and the corresponding synthesis equation may be written as

$$(\mathbf{f}^1)^T \cdot \mathbf{M}^{1i} \cdot \mathbf{e}^1 = 0,\ i = 2,3, \quad \text{where} \quad \mathbf{M}^{1i} = \mathbf{E} - (\mathbf{R}^{1i}_{B'''})^T \mathbf{R}^{1i}_{B2}, \tag{4.93}$$

where $\mathbf{R}^{1i}_{B'''} = {}^W\mathbf{R}^{i}_{B'''}({}^W\mathbf{R}^{1}_{B'''})^{-1}$ is the rotation matrix from Eq. (4.75), which contains the rotation data from table 4.9.

It's important to recall here, that the spherical synthesis problem only includes information about the orientation of frames, while their locations are not of interest. For this reason different locations do not affect the spherical RR synthesis problem.

The spherical algebraic three-position RR synthesis is an underspecified problem, simple to solve. To see this consider the general spherical RR synthesis equations (2.52) being written as

$$(a^i(\mathbf{b}^1)\ b^i(\mathbf{b}^1)\ c^i(\mathbf{b}^1)) \cdot \mathbf{a}^1 = 0, \quad i = 2,3, \tag{4.94}$$

where $(a^i(\mathbf{b}^1)\ b^i(\mathbf{b}^1)\ c^i(\mathbf{b}^1)) = (\mathbf{b}^1)^T \cdot \mathbf{M}^{1i}$. Equation (4.94) expresses the intersection of the two planes

$$\begin{aligned} a^2(\mathbf{b}^1) \cdot x_a + b^2(\mathbf{b}^1) \cdot y_a + c^2(\mathbf{b}^1) \cdot z_a &= 0 \\ a^3(\mathbf{b}^1) \cdot x_a + b^3(\mathbf{b}^1) \cdot y_a + c^3(\mathbf{b}^1) \cdot z_a &= 0. \end{aligned} \tag{4.95}$$

Of course these planes intersect in a common line (as far as they are not parallel). This line of intersection has the direction $\mathbf{a}$, which may be found simply as:

$$\mathbf{a} = \begin{pmatrix} a^2 \\ b^2 \\ c^2 \end{pmatrix} \times \begin{pmatrix} a^3 \\ b^3 \\ c^3 \end{pmatrix}. \tag{4.96}$$

Hence, choose an arbitrary $\mathbf{b}^1$ and solve Eq. (4.96) to obtain a spherical RR chain that can reach three prescribed orientations. Applying this procedure to Eq. (4.92) and (4.93) shows that one may specify one direction at each vertex of the spherically constrained spatial RR chain.

Table 4.11.: Orientation data for frame $B2$

$\{\xi,\ \zeta,\ \beta\}$	$\{-127.2971\text{ deg}, -10.001\text{ deg}, 0.0\text{ deg}\}$
$\{\phi_d^1,\ \phi_d^2,\ \phi_d^3\}$	$\{-82.5463\text{ deg}, -138.967\text{ deg}, 4.368\text{ deg}\}$
$\{\phi_c^1,\ \phi_c^2,\ \phi_c^3\}$	$\{50.0\text{ deg}, 85.0\text{ deg}, 0.0\text{ deg}\}$

Table 4.12.: Axis parameters of the spherically constrained spatial RR in configuration $i = 1$, measured in W

	Direction	Location
$\hat{\mathbf{c}}^1$	$(\ 0.2075 \quad -0.9765 \quad 0.0584\ )^T$	$\underbrace{(\ -98.2409 \quad 191.0778 \quad 182.6130\ )^T}_{\tilde{\mathbf{p}}_d=\mathbf{p}_d,\ \lambda_d=0}$
$\hat{\mathbf{a}}$	$(\ -0.9848 \quad -0.1736 \quad 0.0\ )^T$	$\tilde{\mathbf{p}}_d$
$\hat{\mathbf{b}}^1$	$(\ 0.0897 \quad 0.5082 \quad 0.8566\ )^T$	$\tilde{\mathbf{p}}_d$
$\hat{\mathbf{e}}^1$	$(\ -0.1093 \quad 0.1667 \quad 0.9799\ )^T$	$\underbrace{(\ -74.5438 \quad 79.5812 \quad 189.2786\ )^T}_{\tilde{\mathbf{p}}_g^1=\mathbf{p}_g^1,\ \lambda_g=0}$
$\hat{\mathbf{f}}^1$	$(\ 0.6330 \quad 0.7544 \quad -0.1736\ )^T$	$\tilde{\mathbf{p}}_g^1$

Example of a spherically constrained spatial RR chain

Figure 4.30 shows a CAD model of an example design of a complete spherically constrained spatial RR chain, which is based on the synthesis steps provided before, i.e. on the position data from table 4.9 as well as the spatial RR chain formed by axes $\hat{\mathbf{d}}$ and $\hat{\mathbf{g}}^1$. Results of the inverse kinematics part are listed in table 4.11. Table 4.12 on the other hand lists the axis parameters of the remaining axes. Note that $\lambda_d = \lambda_g = 0$ is selected here, which corresponds to $\beta = 0$ in table 4.11. As one can see, the previously determined spatial RR chain defined by $\hat{\mathbf{d}}$ and $\hat{\mathbf{g}}^1$ still reaches the three task poses. Recall from Fig. 4.27 that this represents one of the RR chains in a Bennett linkage. Even though the linkage determined here suffers from an assembly mode change, required to reach pose 3, the result is a design solution whose axes are located compactly along the spatial RR guiding chain.

4.4. Detecting the Intersections Between Joint Axes and Triangulated Surface Tesselations

The computer-aided kinematic design process from chapter 5 regards given space limits of a task by considering, whether solutions obtained from a certain synthesis procedure fit into a certain given envelope. This is done using the stl representation of the envelope, which provides a tesselation of triangles, see sect. 5.3. In particular the links of linkage may be designed such that they fit into the given envelope, if at least the joint axes intersect the triangulated surface. Hence, in order to check for existing intersections between the envelope and an axis of the linkage, the intersection between a line and a triangle must be considered. This problem refers to the ray tracing problem, also used in computer graphics to detect intersections between rays

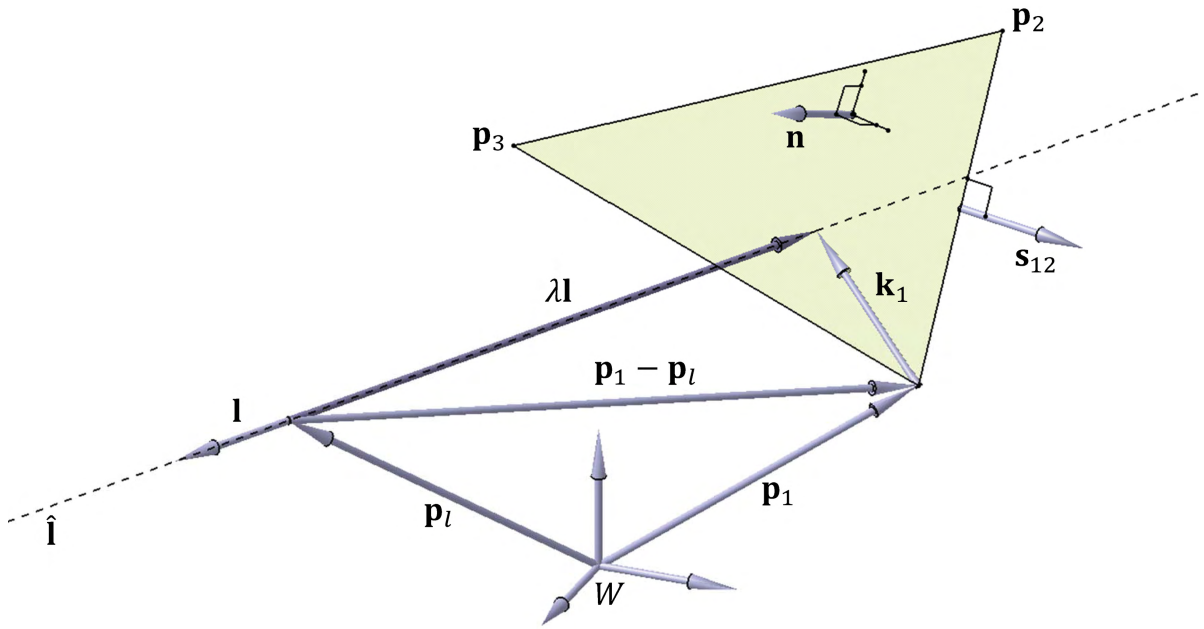

Figure 4.31.: Quantities that measure the intersection of ray and triangle

and bodies, see also [117].

In what follows a simple procedure is provided, which allows to detect the intersection between a line and a triangle and which is also part of [112]. The procedure has also been implemented and used in chapters 5 and 6 to check, whether the axes of a spatial RR chain, obtained from three-position synthesis pass through a given envelope.

If a line $\hat{\mathbf{l}}$ intersects the plane of a triangle, direction $\mathbf{l}$ and location $\mathbf{p}_l$ of $\hat{\mathbf{l}}$ satisfy:

$$\lambda = \frac{(\mathbf{n})^T \cdot (\mathbf{p}_1 - \mathbf{p}_l)}{(\mathbf{l})^T \cdot \mathbf{n}}, \tag{4.97}$$

where $\mathbf{n}$ is the normal of the plane and $\mathbf{p}_1$ represents one of the three vertices of the triangle (note that $\mathbf{n}$ and $\mathbf{p}_1$ are known for each triangle from the stl file, see also sect. 5.3 for details). The parameter λ is a real constant, so that $\mathbf{h} = \mathbf{p}_l + \lambda\mathbf{l}$ describes the point of intersection. Note that in order to have no intersections at infinity between line and plane it is required that $(\mathbf{l})^T \cdot \mathbf{n} \neq 0$. In order to have $\mathbf{h}$ furthermore being located inside the triangle also the following conditions must be satisfied:

$$(\mathbf{s}_{12})^T \cdot \mathbf{k}_1 < 0, \quad (\mathbf{s}_{32})^T \cdot \mathbf{k}_2 < 0, \quad (\mathbf{s}_{13})^T \cdot \mathbf{k}_3 < 0, \tag{4.98}$$

where for instance $\mathbf{s}_{12} = (\mathbf{p}_2 - \mathbf{p}_1) \times \mathbf{n}$ represents an outwards oriented normal direction at the edge of the triangle defined by $(\mathbf{p}_2 - \mathbf{p}_1)$, see Fig. 4.31. Vectors $\mathbf{k}_i$ are defined as $\mathbf{k}_i = \mathbf{h} - \mathbf{p}_i$, $i = 1,2,3$.

When Eq. (4.97) and (4.98) are evaluated for the joint axes of a spatial RR chain and each triangle of the tesselated representation of the envelope this yields each existing intersection between axes and envelope. In case of an arbitrarily shaped envelope with both convex and concave shape as well as several holes there may exist various points of intersection. However, if the envelope represents an approximately convex polyhedron, there are either 0, 1 or 2 points of intersection for an axis.

5. A Concept for Computer-Aided Kinematic Design (CAKD) of Linkages

This chapter presents a concept towards the *computer-aided kinematic design (CAKD) of linkages*, which aims at *quick evaluations of the feasibility*[1] *of a linkage*. The CAKD approach, couples linkage-specific kinematic synthesis calculations, performed in the *computing environment* MATLAB, with a corresponding *parametrized CAD model* in the *design environment* CATIA V5. Note that the concept is also applicable with eventual minor modifications using other computing environments such Mathematica or Maple, or also other design environments such as for instance SolidWorks, ProEngineer or Siemens NX.

The simplest approach couples the different software packages using simple design tables, which control the parameters of a CAD-model and allow a quick evaluation of changes of the kinematic dimensions of a linkage. Such changes may particularly affect the feasibility and occur from different linkage synthesis solutions, which result from a variation of a given motion task or either from a variation of of free kinematic design parameters. A more advanced CAKD approach additionally makes use of VBA programming capabilities provided by common CAD-systems. This allows for instance to control various synthesis solutions stored in a single design table or also to create individualized toolbars for CAKD within the CAD-environment.

The simple CAKD approach is discussed exemplarily using the three-position synthesis procedure of a spherically constrained spatial RR chain from sect. 4.3.4. Afterwards, examples of CAKD based on VBA programming are discussed using a spatial RR chain. However, the presented general methodology also holds for any other type of linkage, i.e. planar, spherical or spatial single or also multi-d.o.f. mechanisms and only requires an appropriate adoption of implemented kinematic synthesis calculations as well as a parametrized CAD-model.

5.1. The General CAKD Methodology

The general computer-aided kinematic design approach considers the *design engineer* as the central subject, that controls the different steps in a kinematic design process. These steps include *preprocessing*, *solving* and *postprocessing*, which may occur in the computing as well as in the design environment (see also Fig. 5.1) and which are defined here as follows:

1. *Preprocessing* begins by considering the motion task as well as given requirements. This particularly includes classification of the motion characteristics of the task, i.e. whether it requires planar, spherical or either spatial movement. In order to solve the given problem using linkage design theory the designer may consult or derive corresponding methods

[1] The feasibility of a linkage is always related to the requirements of a given task and must be considered individually by a designer. On the one hand it is determined by suitable kinematic dimensions that fit into a given allowed envelope as well as useful kinematic/kinetostatic transmission properties, which are obtained from synthesis and analysis procedures of specific linkage topologies (examples of such procedures are developed in chapter 4). On the other hand feasibility includes the design of links as well as collision-free movement within the workspace of the linkage.

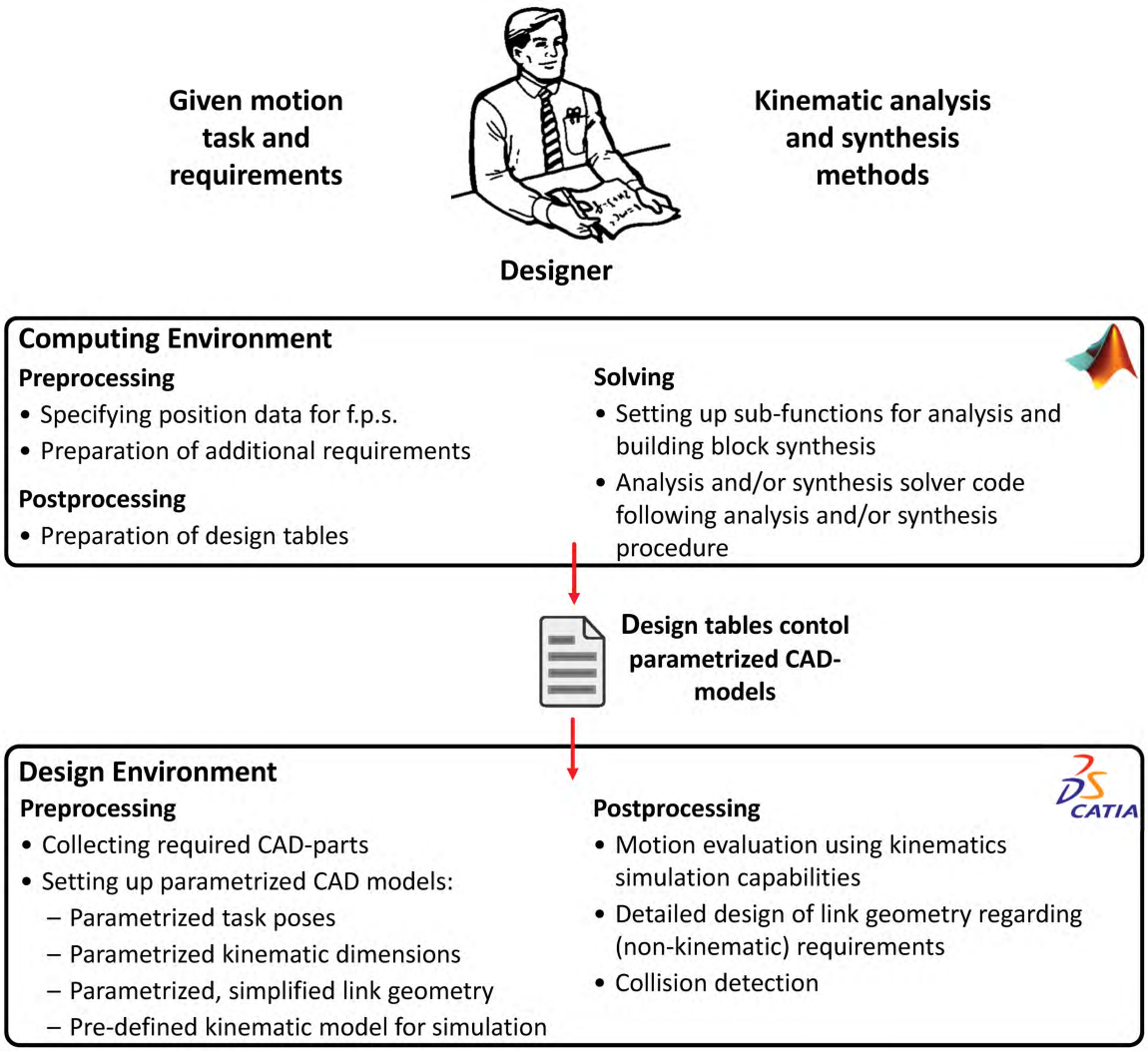

Figure 5.1.: Computer-aided kinematic design of a specific linkage topology based on parametrized CAD-models and kinematic solver code

or procedures for kinematic analysis and synthesis of either planar, spherical or spatial linkages.

Within the design environment, i.e. the CAD-system, the motion task as well as given requirements, such as for instance given space requirements, then must be specified by collecting and assembling required CAD-parts. This includes parts that define an envelope, where the linkage must fit in or wherein the linkage is allowed to move. CAD-integrated preprocessing parallels a preprocessing step within the computing environment, where the task as well as given requirements also need to be translated into a numerical set of position data. When a specific linkage topology is chosen to be evaluated for the given task the next preprocessing step is to set up a parametrized CAD-model of the desired structure. The CAD-model must include parameters that define task poses, kinematic dimensions, simplified link geometry and a kinematic model for simulation. Control of the parameters of the model will be achieved via design tables that are provided by a kinematic solver within the computing environment.

2. *Solving* represents any kinematics calculations performed within the computing environ-

ment. An efficient approach considers the implementation of universal analysis and synthesis solver modules, which are based on planar, spherical or either spatial linkage design theory. These must next be combined appropriately into a complete synthesis and/or analysis solver code, which is implemented with respect to a specific kinematic design procedure of the considered linkage topology. Input data such as task positions or free design parameters of this solver are conveniently amplified within allowed ranges during processing. This may be achieved through numerous iterative computations in order to provide various alternative solutions.

In the case of a pure synthesis solver, the calculation results include the kinematic dimensions of each linkage solution obtained from the variation of input data. However, this also includes solutions which suffer from weak kinematic or kinetostatic transmission properties or may even require an assembly mode change during the movement. Then, the non-feasible synthesis solutions occur for the first time in a simulation of CAD-integrated postprocessing. An opportunity to avoid such situations is to include analysis subroutines into solver code, which filter weak synthesis results.

3. *Postprocessing* is performed in both the computing as well as the design environment. After the solving process the calculated parameters defined above are assembled into a design table by a subroutine within the computing environment. This controls the parametrized CAD-model of the linkage and is considered here as an external document, which may also be used in environments other than the CAD-system. Based on that, the dimensions of the parametrized CAD-model are updated (automatically by the CAD-system) and CAD-integrated postprocessing begins. This includes simulation of the movement as well as detailed design of link geometry using design capabilities of the CAD-system. In fact these final design steps usually must be performed iteratively, since an appropriate detailed design of links in a reference configuration of the linkage may yield collisions in another configuration and hence a non-feasible design. However, collision detection is also a common functionality in current CAD-environments and may hence also be performed herein.

   A further important CAD-integrated postprocessing step consists in evaluating whether the resulting linkage design acually meets further given requirements of the whole product development process. An example is a given envelope, where the linkage must fit in or wherein the linkage is allowed to move. In fact, beside adequate kinematic/kinetostatic behavior this requirement represents a major feasibility aspect, which must be evaluated in regard of any given parts, that define or either affect the allowed envelope

5.2. The Parametrized Basis CAD-Model of a Linkage Topology

This section presents the step wise development of the parametrized *basis* CAD-model of a linkage topology. This denotes a *non-movable* CAD-part of the complete linkage in a *reference synthesis configuration* 1 and represents the basis for the parametrized *kinematic* CAD-model allowing for simulation of the movement, see sect. 5.4. A basis model includes parameters that define task poses, kinematic dimensions and link geometry, which are controlled via one or more design tables, which are provided by a kinematic solver.

The parametrized basis CAD-model shall enable studies of parameter variations in the kinematic solver and shall also be potentially reused for other tasks. Hence, the goal is a model

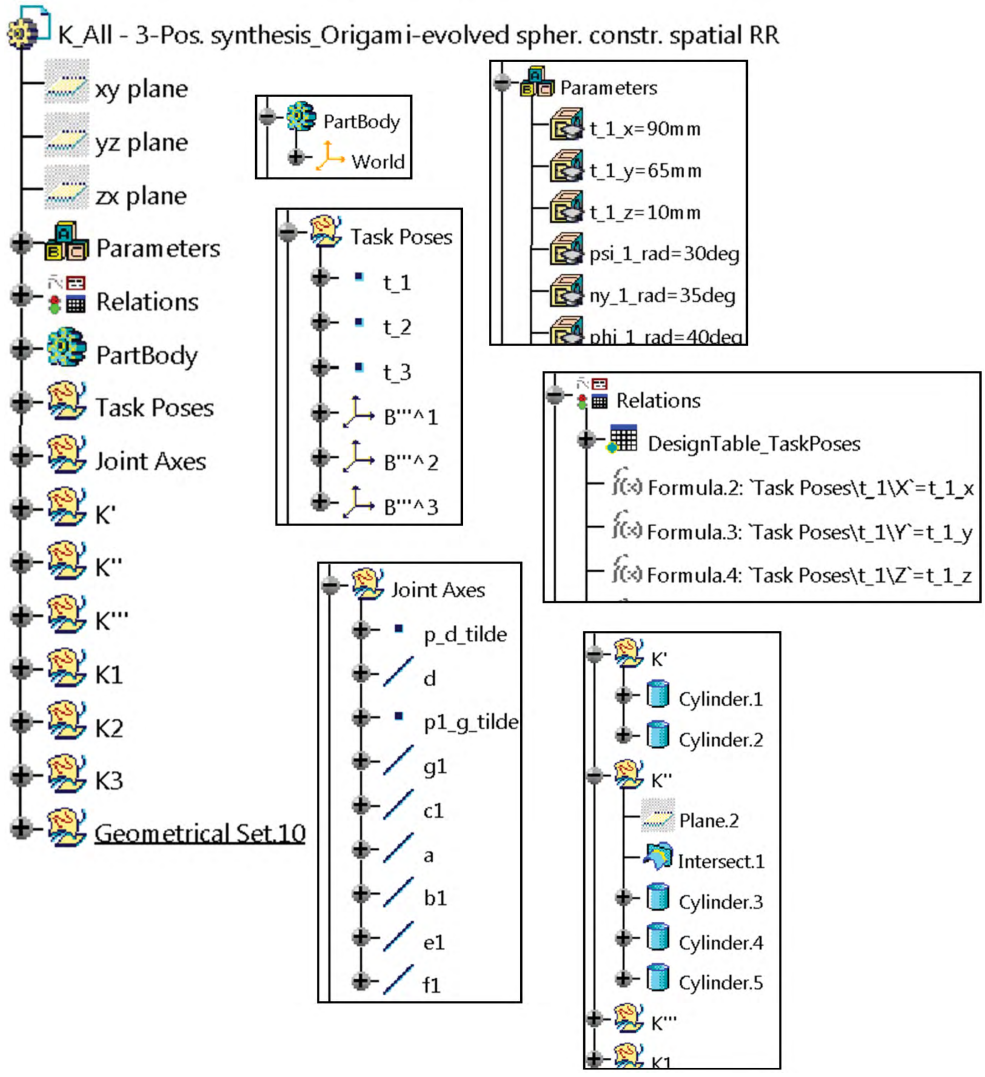

Figure 5.2.: Design tree of the pre-defined parametrized model for three-position synthesis procedure of a spherically constrained spatial RR chain

whose elements, such as coordinate frames, axes or link geometry may follow (almost) any possible shape changing induced by amplified design tables. This requires a well-organized CAD-tree with specific pre-defined folders, described in the following section, where the different elements are stored. The set or skeleton of axes essentially represents the kinematic topology as well as kinematic dimensions of the considered linkage and the parametrization of location and orientation of axes is presented afterwards. This is followed then by a discussion of simplified parametric link designs, which are based on the skeleton of axes.

The different key elements are discussed in the following using an example basis model for the three-position synthesis procedure of a spherically constrained spatial RR chain from sect. 4.3.4. However, due to a general methodology similar parametrized models may also be developed for other planar, spherical or spatial topologies and corresponding design procedures.

Editor - SPATIAL_RR_to_Origami_guided_3Poses_central.m | Variables - DesignTable_PoseData

DesignTable_PoseData

1x18 table

	1 t_1_x	2 t_1_y	3 t_1_z	4 psi_1_rad	5 ny_1_rad	6 phi_1_rad	7 t_2_x	8 t_2_y	9 t_2_z	10 psi_2
1	0.0900	0.0650	0.0100	0.5236	0.6109	0.6981	-0.0100	-0.0100	0.1000	
2										
3										

Figure 5.3.: Design table DesignTable_TaskPoses for three-position synthesis procedure of a spherically constrained spatial RR chain

5.2.1. Required Elements and the Design Tree

Figure 5.2 shows the design tree of a basis CAD-model for a three-position synthesis procedure of a spherically constrained spatial RR chain, which includes the complete linkage in a reference configuration 1, i.e. links K', K", ..., K3 and axes a, b1, ..., g1 (note that these are nothing but the mathematical quantities K', K'',...,$K3$ and $\hat{\mathbf{a}}$, $\hat{\mathbf{b}}^1$,...,$\hat{\mathbf{g}}^1$ from the synthesis procedure from sect. 4.3.4). Recall here for instance from Fig. 3.2 how links and axes are defined for a spherically constrained spatial RR chain. The different parametrized CAD-objects associated with axes and link geometry are stored into the corresponding folders of the tree and are discussed more detailed in sect. 5.2.2.

The desired parametrization of the CAD-model is introduced by defining different types of parameters for each geometric quantity that should be parametrized. This includes paramters of type 'length' and 'angle', which are shown exemplarily in Fig. 5.2 by parameters t_1_x, t_1_y and t_1_z defining x-, y- and z-translation values as well as by parameters psi_1_rad, ny_1_rad and phi_1_rad defining z-x-z Euler rotation angles. The different length parameters are defined with respect to the common reference coordinate frame World (cooresponds to frame W), which is stored in the folder PartBody.

The six parameters t_1_x, t_1_y, ..., phi_1_rad together define the location of a point t_1 and the orientation of coordinate frame B"'^1, stored in the folder Task Positions. B"'^1 is nothing but the frame defining the first task position and is located at t_1. In a similar fashion six further length parameters define points, i.e. translations t_2 and t_3, while six other angular parameters define the orientation of frames B"'^2 and B"'^3. Note that this defines the three-position synthesis task of the spherically constrained spatial RR chain and numerical values for this set of parameters are stored in the design table DesignTable_TaskPoses. An exemplary screen shot of the design table defining position data is shown in Fig. 5.3. Further parameters control the location, orientation and also the length of the axis skeleton of the linkage (discussed in detail in sect. 5.2.2) as well as specific dimensions of the simplified link geometry (discussed in detail in sect. 5.2.3). The total number of parameters of the CAD-model is summarized in sect. 5.2.4.

The connection between the different geometric quantities, i.e. points, frames, axes, etc. and the different parameters is provided by Relations, which map parameter values of design tables to the corresponding quantities. This is done using so called formulas, provided by the CAD-System and is shown exemplarily for the x-, y- and z-translations of task position 1.

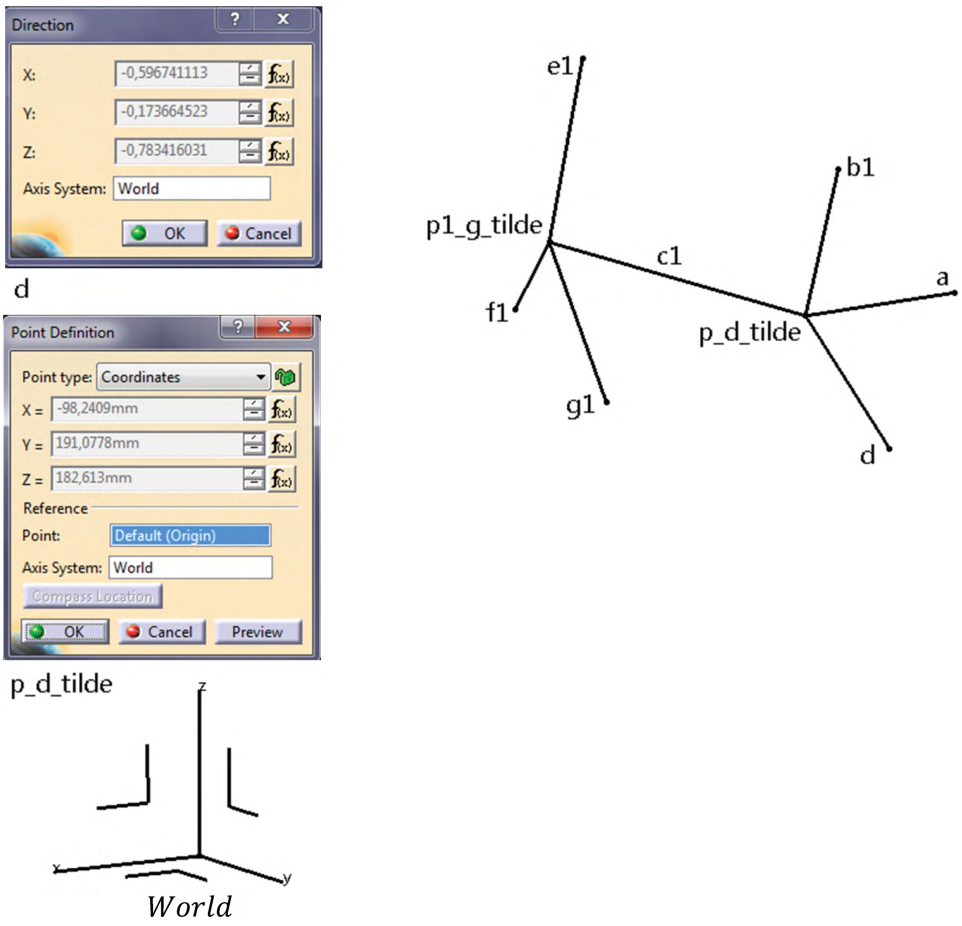

Figure 5.4.: Parametrized axis skeleton of a spherically constrained spatial RR chain in reference configuration 1

5.2.2. Parameterized Kinematic Dimensions

The kinematic dimensions of a linkage are represented by the joint axes determined from synthesis calculations in reference configuration 1 and with axis coordinates measured in frame World. Within the basic CAD-model the parametrized axis skeleton, formed by lines in the CAD-system, represents these kinematic dimensions.

Figure 5.4 shows the axis skeleton of a spherically constrained spatial RR chain, defined by axes a, b1, ..., g1. Since the link K' is considered as the fixed link in the synthesis procedure from sect. 4.3.4 axes a and d do not necessarily require the right superscript. The geometric CAD-objects of the different axes are lines, which are stored in a corresponding folder Joint Axes, see again Fig. 5.2. These objects accept numerical input data to define a direction and require a pre-defined point in order to define a location. Hence, additional points p_d_tilde and p1_g_tilde are included, which define the location of any axes of a spherically constrained RR chain. These represent nothing but the vectors $\tilde{\mathbf{p}}_d$ and $\tilde{\mathbf{p}}_g^1$ from sect. 4.3.4, which might be varied along the axes d and g1 of the spatial RR chain. Recall here that only these two points are required to define the location of any other axis in a spherically constrained RR chain.

The different CAD-objects are of course parametrized quantities, since they need to change as synthesized axis coordinates change. Parameters are controlled by a specific design table, which provides numeric values that define locations and orientations. This is shown exemplarily for

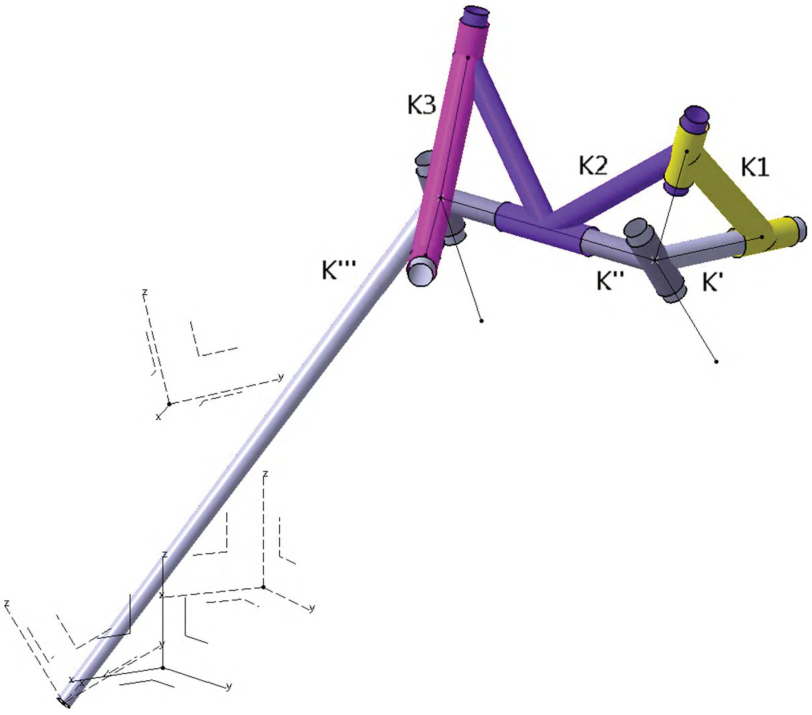

Figure 5.5.: Simple voluminous representation of the parametrized axis skeleton of a spherically constrained spatial RR chain in reference configuration 1

the locating point p_d_tilde and the direction of d in Fig. 5.4, where formulas f(x), provided by the CAD-system, are used to map numeric values from the design table to axis coordinates measured in World.

Axis c1 of the skeleton is defined between p_d_tilde and p1_g_tilde. However, this defines the length of c1 as the distance between p_d_tilde and p1_g_tilde. Since these points in fact result from the synthesis solver the considered length may be calculated as another parameter value and submitted to the CAD-model via the design table. This length also provides a suitable parameter to define the length of further axes and is used for the spherically constrained spatial RR chain to define a finite length of a, b1, d, e1, f1 and g1. Note from Fig. 5.4 that actually a scaled version of the distance between p_d_tilde and p1_g_tilde is used to define the length of these axes.

5.2.3. Standardized Shape of Building Block Parts

The geometric design of parts, i.e. links of a linkage turns the axis skeleton of the linkage into a more realistic voluminous object. This is oftentimes a creative process, with usually unbounded multifarious design possibilities. However, in order to have designs that are able to follow unpredictable strong changes of the kinematic dimensions (that result from different synthesis solutions) a robust and standardized design of parts is required.

The simplest standard shape of parts can be realized by simply defining cylinders as joint axes and also as connections between different axes at one specific link. This attributes a voluminous representation of the axis skeleton to the linkage, which, as a first rough approximation may represent the real dimensions of the structure. Even though this usually consists of various collisions between different links and is far from representing a final design, this representation is maximally able to follow changes of the kinematic dimensions. This allows for a quick

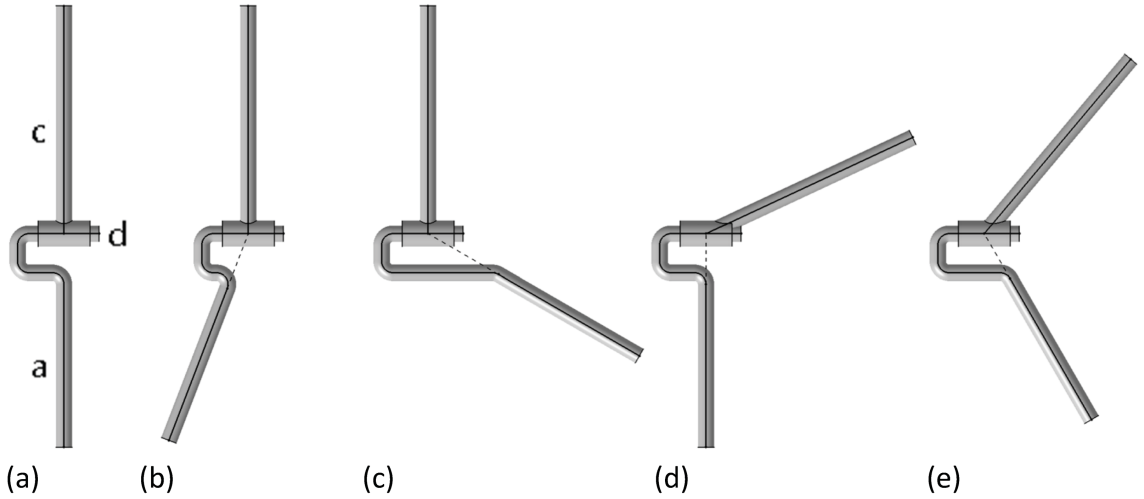

Figure 5.6.: Examples of more detailed standard geometries of two coupled links, where dramatic changes in the kinematic dimensions may yield unfeasible link designs or interference between links

evaluation of the impact of parameter studies on the geometric shape of the linkage. Examples of such parameter studies may be the changing of task poses or other free parameters of the synthesis procedure.

Figure 5.5 shows a particularly simple CAD-model of the spherically constrained spatial RR chain in a reference configuration. The structure was synthesized for three task poses, i.e. the three frames B‴^1, B‴^2 and B‴^3, simple cylinders provide a voluminous representation of the axis skeleton from Fig. 5.4 and also define connections between the different joints. A connection between frame B‴^1 and axis g1 is also provided by another connecting tube, whose length is automatically defined as the distance between the location of B‴^1 (i.e. t_1) and p1_g_tilde.

Standardized building block parts based on tube-like link geometry

Further other detailed standard geometries of links may of course be defined, which already take into account collision or more realistic designs of joints. However, due to a more detailed design, such links also may not follow dramatic changes of the axis skeleton.

An example showing this issue is provided in Fig. 5.6, which shows a kinematic pair based on the link design used several times in the context of spherical linkages throughout the work. Figure a) shows the case where axes a and d as well as c and d enclose an angle of 90 deg. A slight variation of 20 deg to the left between a and d as shown in figure b) is the maximum for the lower link (note that such angular changes may result from different synthesis solutions that define the direction of lines). This is because at that amount two radii at the center curve of the tube-like rib interfere and hence produce an error in the CAD-model. On the other hand the center curve of the tube-like rib allows a variation of at least 65 deg to the right. However, the result is a link geometry, which is also far from a final design because it obviously has weak structural mechanical properties.

Figure d) shows a variation of the upper link by an angle of 65 deg measured from the initial axis c in figure a). Instead of a single tube-like rib this link consist of a cylinder that defines axis c as a hull defining the joint connecting the two links, which, however, collides with the

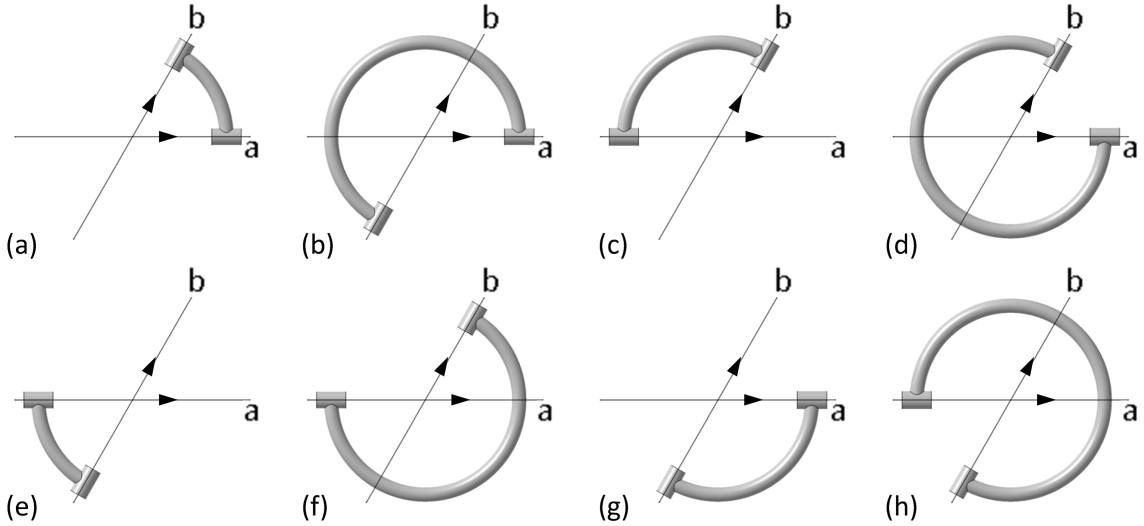

Figure 5.7.: Eight possible cases how to define a spherical tube-like ring connecting two axes in spherical binary link

lower link. Finally figure e) shows the case where axes a and c both enclose an angle other than 90 deg with d, which provides an non-colliding example.

Standardized spherical binary links

Another standard link geometry interesting to study is that of spherical binary links, which occur as the connecting link between the two R joints in a spherical RR chain. Figure 5.7 shows the eight possibilities how to define a spherical tube-like ring connecting two axes a and b with specified directions. In a CAKD process each of these cases may represent a first valid link geometry, which can provide insight into collision properties in a kinematic simulation. Based on that the designer can carry out a detailed, more complex design of a link.

From a structural mechanics point of view the 'shortest distance' between two axes in a spherical binary link may be seen as an indicator for high durability against deformations. Furthermore, when case b) provides collision-free movement, then also a), c) and e) do so. When, on the other hand d) or f) provide collision-free movement, then also c), e) and g) or a), e) and g) do so. Finally, if case h) provides collision-free movement, then also a), c) and g) do so. These considerations identify cases a), c), e) and g) as those, which may represent a first valid link geometry providing insight into collision properties.

Control of proportion using a minimum set of parameters

The dimensional synthesis computations can result in kinematic dimensions of particularly large and/or also small scale. Then the result is an axis skeleton of either particularly large and/or small distances measured between the joints in a link. However, when using appropriately parametrized standard link geometry, the shape of links in the CAD-model can automatically adapt to the scale of the axis skeleton. This conveniently only requires a minimum set of parameters defined in terms of available dimensions of the axis skeleton. This is called *the set of master parameters* here, whose specific numeric values are provided by a design table. Recall that design tables are generated by the kinematic solver or the computing environment, which also defines the kinematic dimensions of the axis skeleton of a linkage.

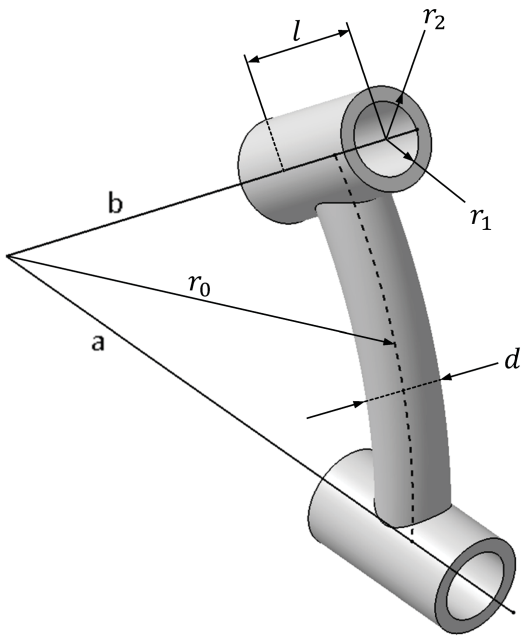

Figure 5.8.: Master and slave parameters that allow a proportional scaling of a spherical binary link

The master parameters of the CAD-model control another set of slave parameters, that define further scaleable link geometry. While master parameters occur explicitly in the folder Parameters of the design tree of a basis CAD-model (see again Fig. 5.2) slave parameters are defined as Formulas. These relate different angles or lengths and are stored in the folder Relations. An example is a slave parameter of type 'length', which controls the thickness of a certain rod connecting two joint axes with respect to the distance between these axes.

Another example of master and slave parameters is shown in Fig. 5.8 using the example of a spherical binary link. Herein the radius r_0 represents the master parameter that completely controls the link geometry of the crank. Note that axes a and b represent the axis skeleton of the link, whose directions are defined by coordinates provided by a design table. The parameters r_1, r_2, d and l are the slave parameters, that are defined as

$$r_1(r_0) = k_1 \cdot r_0, \qquad r_2(r_1(r_0)) = k_2 \cdot r_1, \qquad d(r_0) = r_1(r_0), \qquad l(r_0) = k_3 \cdot r_0. \tag{5.1}$$

Herein k_1, k_2 and k_3 are constant values defining the proportion of the binary crank, which can be defined directly in common CAD-systems. These were defined here as $k_1 = 0.0625$, $k_2 = 1.4$ and $k_3 = 0.3125$, which results in the geometric shape shown in Fig. 5.8.

5.2.4. The Number of Parameters

The number of parameters P in a basis CAD-model is considered here as corresponding to the parameters provided by one or more design tables. This number is determined by the number of task poses of a linkage synthesis procedure, the set of joint coordinates of a linkage topology and further parameters, such as master parameters defining scaleable link geometry.

In case of a spatial synthesis procedure there are six parameters for each of the n task positions. This yields the number of task position parameters as $P_{task} = 6 \cdot n$. The number of joint parameters P_{joint} differs for different joint types such as C, R, P or S joints. Let n_C, n_R, n_P and

n_S be the number of C, R, P or S joints then numbers of parameters defining their location and direction in a reference configuration of the linkage are

$$P_C = 6 \cdot n_C \qquad P_R = 6 \cdot n_R \qquad P_P = 6 \cdot n_P \qquad \text{and} \qquad P_S = 3 \cdot n_S. \tag{5.2}$$

This results from the fact that C, R and P joints are defined by a spatially located and directed line while S joints are defined only by their center points. Note that this is the general spatial case, where each joint axis must be defined independently by its own location and orientation. The total number of joint parameters is simply $P_{joint} = P_C + P_R + P_P + P_S$. Together with a total number of remaining parameters P_r the total number of parameters of a basis CAD-model is defined as

$$P = P_{task} + P_{joint} + P_r. \tag{5.3}$$

In case of a spherical linkage, where all revolute joint axes intersect at a common location, only one single set of three location parameters but $3 \cdot n_R$ direction parameters must be defined. The result is a set of $P_R = 3(1 + n_R)$ R joint parameters for a spherical linkage. Furthermore, task position parameters reduce to three orientation parameters for each of the n task positions: $P_{task} = 3 \cdot n$.

In case of a planar linkage design project, there are three parameters defining the planar pose of each of the n planar task poses, which yields $P_{task} = 3 \cdot n$. When the linkage consists of n_R R joints, their location may be defined by two different parameters in the plane where the motion takes place, which yields $P_R = 2 \cdot n_R$. Note that this can be extended to $P_R = 3 \cdot n_R$, if axes should be described explicitly by three-dimensional locations. The direction of R joints clearly remains oriented perpendicular to this plane, which can be defined directly in the CAD-system. When the linkage consists of n_P P joints lying in the plane where the motion takes place, there are two location and two orientation parameters required to define the joint, which yields $P_P = 4 \cdot n_P$. Hence, the total number of parameters for a planar linkage is $P = 3 \cdot n + 2 \cdot n_R + 4 \cdot n_P + P_r$.

Parameters in the CAD-system that are controlled via specific design tables are subject to a usually automated update process of the CAD-model, which is triggered as soon as at least one single parameter in a design table changes. Hence, a large number of parameters in a CAD-model will probably result in a time consuming update process. However, the example CAD-model from Fig. 5.5 based on the three-position synthesis procedure of spherically constrained spatial RR chains from sect. 4.3.4 with $P = 43$ parameters showed, that a model of that dimension updates in 1 - 2 seconds on a common intel CORE i7 PC, without any particular timer-based execution of the CAD-system.

Parameters of the basis CAD-model for three-position synthesis of spherically constrained spatial RR chains

The CAKD based on the three-position synthesis procedure of spherically constrained spatial RR chains from sect. 4.3.4 represents a spatial linkage design approach, which requires a particular set of parameters in the basis CAD-model. One the one hand three-position synthesis requires $P_{task} = 6 \cdot 3 = 18$ task parameters to define the three task poses. Next, in order to parametrize the axis skeleton from Fig. 5.4 six location parameters for p_d_tilde and p1_g_tilde are defined. These define the location of axes a, b1, d, e1, f1 and g1, whose directions are defined by $3 \cdot 6 = 18$ further parameters. Note that c1 does not require any particular parameter since it is defined as the line connecting p_d_tilde and p1_g_tilde. The resulting set of joint parameters counts $P_{joint} = 18 + 6 = 24$ that defines the location and direction of R joints in coordinate frame World.

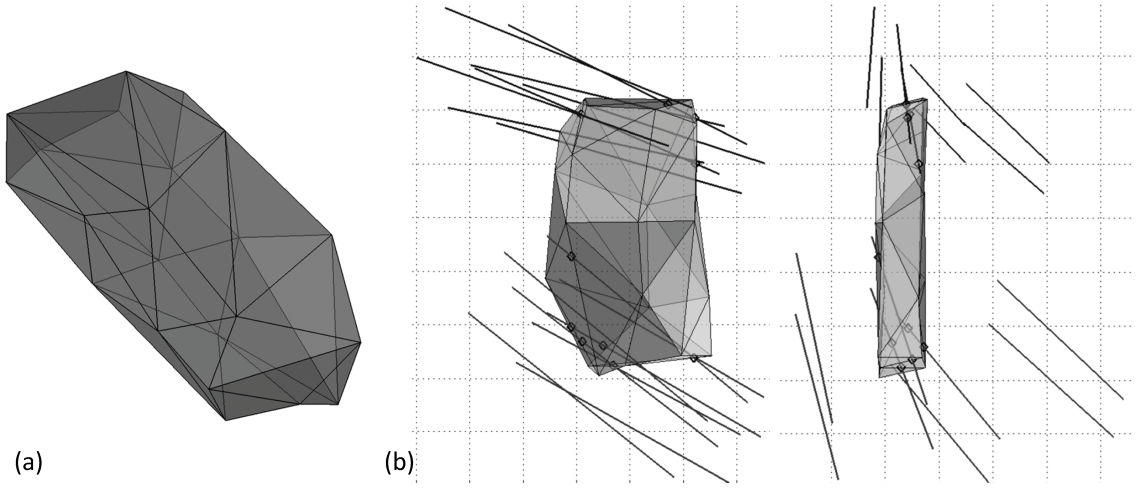

Figure 5.9.: Envelope as a triangulated surface defining the portion of space where axes of the spherically constrained spatial RR chain from sect. 6.1 must fit in. a) CAD-part of the envelope. b) Analysis of intersections between spatial RR axes and envelope performed in the computing environment

In order to define parametrized link geometry in a basis CAD-model of a synthesized spherically constrained spatial RR chain the distance between p_d_tilde and p1_g_tilde can be defined as master parameter in the kinematic solver. This is submitted via a design table and allows to control various further slave parameters in the CAD-model. These define the proportions of the links of the linkage as described in the previous section. This defines $P_r = 1$ here, so that the total number of parameters controlled via specific design tables is $P = 43$. However, also further controlled parameters may be defined, which allow to study various further quantities in a three-position synthesis procedure of a spherically constrained spatial RR chain. An example is the principal axis frame of a cylindroid (see, sect. 4.3.4), whose location and orientation can be defined in the CAD-model and controlled via corresponding parameters and design tables.

5.3. Definition of Envelopes Using the STL File Format

Based on the synthesis and design results defining the axis skeleton as well as the geometric shape of the basis CAD-model of a linkage in a reference configuration, an essential postprocessing step consists in evaluating whether the results fit into a given envelope.

A basic approach described in the following using the example of a spatial RR chain considers, whether the linkage fits into such an envelope in the synthesis reference configuration. Because a spatial RR chain represents a particular building block of a spherically constrained spatial RR chain, the approach was also used in the application scenario, described in chapter. 6. Furthermore, because of a general methodology, the approach may also be used for other linkage topologies. On the one hand, one may evaluate whether the axis skeleton of other linkage building blocks fits into a given envelope. On the other hand complete multilink mechanisms could directly be analyzed.

Since the spatial RR chain is made up from R joints it must be detected whether the lines associated with the different R joints intersect with the given envelope. On the one hand, this can be observed manually in the design environment by the designer from the visually available CAD-model of the linkage. On the other hand, in a computational approach, one may also detect

intersections within the kinematic solver code implemented in the computing environment. In any case a suitable representation of the considered envelope is required.

A suitable representation for an envelope is the stl representation of a surface. One available definition of 'stl' is *stereolithography* [118], which describes a surface as a triangulated tesselation. Each triangle of the tesselated surface is defined by an outwards oriented normal vector and three points defining the vertices of the triangle. This information is stored into a set of rows of a stl file which take the following exemplary form:

```
facet normal -9.424492e-001 -3.341834e-001  1.053194e-002
  outer loop
    vertex -4.680349e+001  1.379301e+002  1.554831e+001
    vertex -3.406774e+001  1.014916e+002 -1.005743e+000
    vertex -3.060530e+001  9.557938e+001  1.212320e+002
  endloop
endfacet
```

The complete stl file describing the complete envelope then consists of numerous sets of these rows defining a closed triangulated surface.

When the intersection between the axis skeleton and the envelope should be evaluated in a computational process within the computing environment, a stl file of the complete envelope must be available for the kinematic solver. This is easily arranged since actual CAD-systems provide the stl file format as an output format for an arbitrary CAD-part. Hence, a designer may specify the envelope during CAD-integrated preprocessing by considering a representative portion space where the linkage must fit into as a CAD-part. Afterwards a corresponding stl file may be derived, which is used to analyze intersections between axis skeleton and envelope in the computing environment. For this purpose a corresponding preprocessing step in the computing environment consists in storing and sorting the vertex and normal data from the stl file in the kinematic solver. A computational analysis of the intersection between axis skeleton and envelope can be done using ray tracing procedures as described in sect. 4.4.

Figure 5.9 shows the triangulated surface representation of an envelope that defines the portion of space, where the axes of a spatial RR chain must pass through. Figure a) shows the CAD-part of the envelope and figure b) shows intersection analysis results performed within the computing environment, which both belong to the application scenario described in detail in chapter 6. The sets of axes result from different synthesis solutions, which are obtained from a variation of task poses. The benefit of this intersection analysis is that synthesis solutions can be filtered before stored into design tables and submitted to the parametrized basis CAD-model of the linkage.

5.4. The Kinematic CAD-Model of a Linkage Topology

Based on a valid basis CAD-model of a linkage with useful kinematic dimensions that fit into a given envelope, the movement of the structure must be considered. This can be done using the *kinematic CAD-model of the linkage* and allows to study collision properties of the different links. These were considered in the previous sections as roughly designed parts, which can now be modified according to specific collisions. Afterwards the designer may carry out a detailed final design that can turn into a manufacturing process.

The kinematic model requires the different links as well as kinematic constraints that define the different joints of a linkage topology. Based on that, kinematic solver modules commonly available in actual CAD-systems allow to manipulate, i.e. to move the linkage with respect to

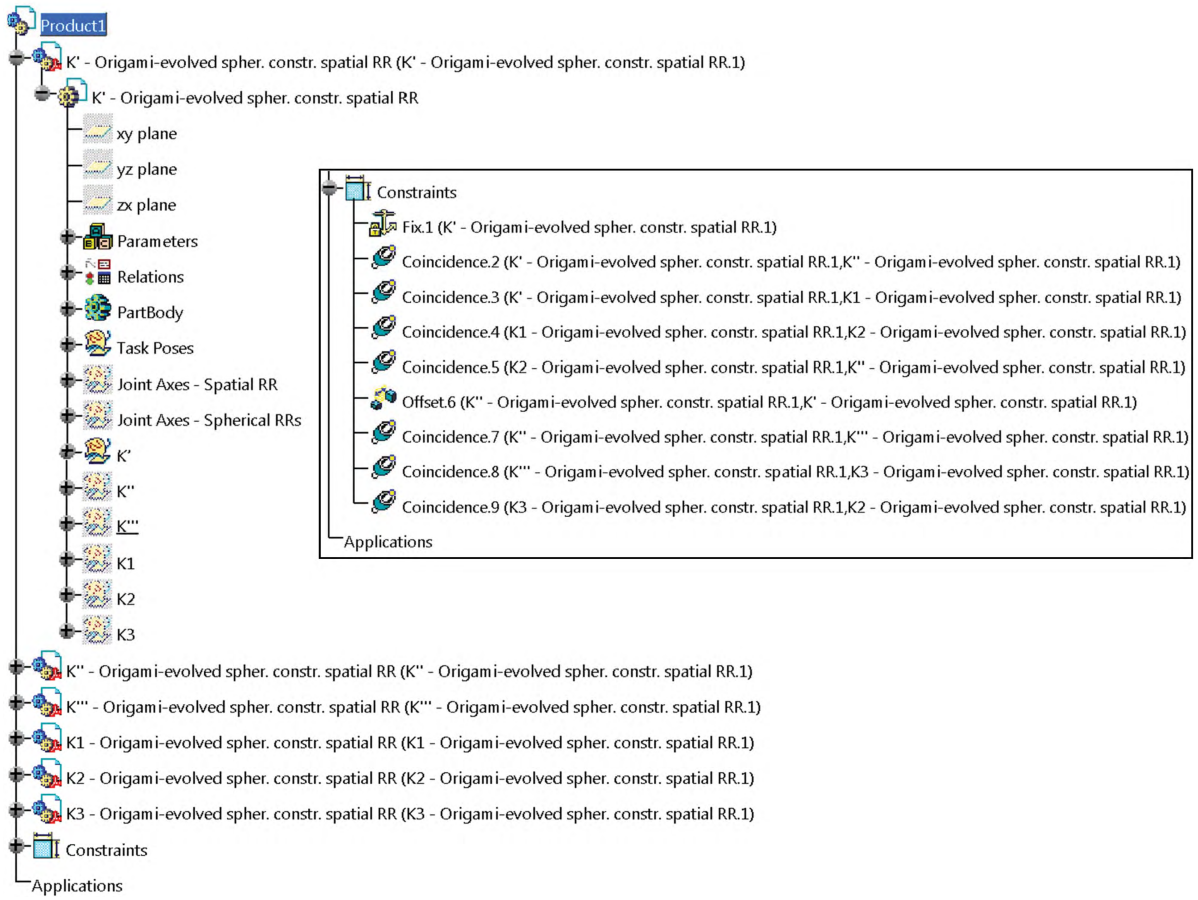

Figure 5.10.: The design tree of the kinematic model of a spherically constrained spatial RR chain

the joint constraints. Within the design environment CATIA V5 used here, such a kinematic model may simply be derived from a number of copies of the basis CAD-model described in the previous sections. The specific number of copies just matches the number of the different links of the linkage. Using the example of the basis CAD-model of the spherically constrained RR chain from Fig. 5.5 and with the design tree from Fig. 5.2 the number of copies is six. When a particular copy of this basis model should represent for instance the link K' in the kinematic CAD-model then each of the remaining folders K'',...,K3 with corresponding link geometry needs to be hidden. Similarly the copy representing K'' requires that each of the remaining folders are hidden. Repeating this procedure for each link constituting the structure yields the different parts that are required to complete the kinematic model.

Within the design environment CATIA V5 a kinematic model is represented as an assembly of the different links, which has another design tree [2]. Figure 5.10 shows the design tree of the kinematic model for the spherically constrained RR chain from Fig. 5.5. This includes the design tree from Fig. 5.2 as a sub-tree for each link of the structure. This is shown for K', where each of the remaining links are hidden objects in the kinematic model. Note that axes were stored here into two distinct folders.

[2]Note that this may not be the case in other CAD-systems. An example is the Siemens NX software, where kinematic CAD-models not require another design tree. Hence, when performing CAKD within such an environment, an extra kinematic model may not be necessary

In addition to the different links, the design tree includes the folder Constraints, where any kinematic constraint defined between the different axes is stored. Due to the fact, that a spherically constrained RR chain may also be considered as a RCC-C-CCC linkage (see sect. 3.2.1) this folder contains seven constraints of type Coincident between the different joint axes and a single additional Offset-constraint. While six Coincident constraints define C joints the seventh combines with the Offset constraint to yield the single R joint. The result is a kinematic model, that can be moved in order to study collision properties of the linkage.

Because each of the links is defined by the same basis CAD-model, whose parameters are controlled by the same design table(s), also the kinematic model is a parametrized model, that may follow changes in the design table(s). A kinematic model of the spherically constrained RR chain consists of six basis CAD-models each of which is parametrized by $P = 43$ parameters. Hence, an update process in the kinematic model updating changes in the design tables must evaluate $P_{Kin} = 6 \cdot P = 258$ parameters. Even though this seems as a particularly increased set of parameters update processes performed within specific design sessions yielded update times $t_{update} < 7s$ using a common intel CORE i7 PC. This particularly refers to the simple link geometry described in the previous sections, and finally yields a quick evaluation of changes in the geometric shape of the synthesized linkage.

5.5. VBA-Based Control of Parameters and Design Tables

Another possibility to further advance the CAKD of a certain linkage topology with corresponding synthesis procedure is to use CAD-automation approaches based on VBA-programming (Visual Basic for Applications). Note that VBA- or also VB-Net-programming is available in several actual CAD-systems. A first simple example is a VBA-code, which allows to switch between different synthesis solutions of a linkage, all together stored in a single design table. Recall here, that in the previously described CAKD approach the parameters of the CAD-model were controlled by a design table, which only included a single solution set obtained from the solver. Compared to that, the VBA-based approach completely decouples solving from CAD-integrated postprocessing and avoids performing another solving process each time another parameter setting should be evaluated. This and other VBA-codes can be made available to a designer in the graphical user interface of the CAD-system via specific toolbars and buttons that trigger the different VBA-codes.

In the following a VBA-based CAKD-specific toolbar is presented. The toolbar particularly supports the synthesis of a spatial RR chain, such that it intersects a given envelope. This requires a variation of three spatial task poses, which results in various sets of position data with corresponding RR joint axes denoted as d and g1. Due to the fact, that spatial RR chains occur as building blocks of different other linkages such as the spherically constrained spatial RR chain, the toolbar may also be used in CAKD of other linkage structures. The toolbar then allows to quickly switch between solutions and also to vary points p_d_tilde and p1_g_tilde that define the location of any axis of a spherically constrained RR chain (see, e.g. Fig. 5.4). The different implementations for this toolbar were done in a CAD-integrated VBA editor and were performed by Manuel Winkler who is gratefully acknowledged.

5.5.1. A VBA-Based Toolbar for CAKD of Spatial RR Chains

The VBA-based toolbar that allows an advanced CAKD approach considers a kinematic CAD-model of a spatial RR chain for three-position synthesis being given. This may be prepared

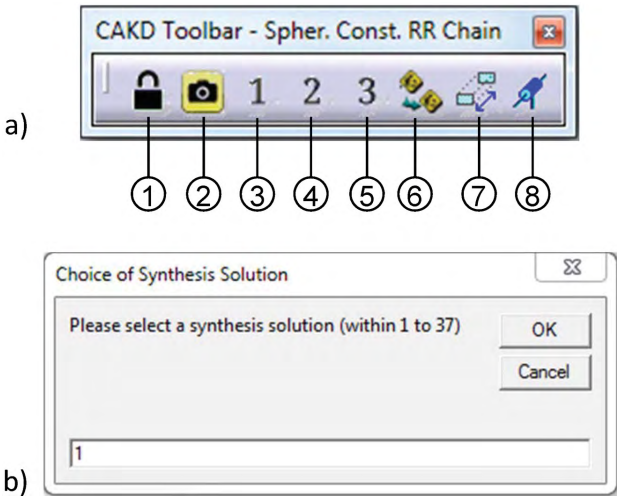

Figure 5.11.: A VBA-controlled toolbar for CAKD of spatial RR chains and a corresponding input box

and organized as shown for the more complex model of a spherically constrained spatial RR chain, see sect. 5.4. Herein a designer should have already specified three different spatial task poses of a certain part that later on will be associated with the end link of the spatial RR chain. Note that this link will be denoted as K''' here, since the spatial RR chain is considered as a building block of a spherically constrained spatial RR chain. Furthermore, a stl file providing numerical data that defines an envelope where synthesis solutions or the axis skeleton must fit in is considered to be available to the designer (see sect. 5.3). Based on these preliminaries the buttons ①,②,...,⑧ of the toolbar shown in Fig. 5.11a) provide support to the designer in the CAKD procedure. The different buttons trigger VBA programming code and are described as follows.

Button ② - The spatial position snap shot

Based on the three specified spatial task poses of the parts associated with link K''' the VBA triggered by this button extracts the location and orientation of each position. The CAD-system allows to extract directly 3×3 rotation matrices ${}^{W}\mathbf{R}^{i}_{B'''}$ as well as 3×1 translation vectors ${}^{W}\mathbf{t}^{i}_{B'''}$, $i = 1,2,3$ of a coordinate frame B''' associtated with link K'''. This position data is stored into a specific input file for the kinematic solver implemented in the computing environment, which can usually directly use vectors and matrices as input for synthesis calculations.

Synthesis calculations based on the three positions particularly include solving the design equations (2.55), (2.57) and (2.59) from sect. 2.3.5 for the unknown revolute joint axes of the spatial RR chains. In case of a spherically constrained spatial RR chain these are denoted as d and g1, which do not necessarily pass through the given envelope. Hence, the designer will probably vary the initial set of task poses within the kinematic solver. The result is a set of various three-position tasks with corresponding valid joint axes, which are stored into a corresponding design table (recall here that intersection between axes and the envelope is checked within the kinematic solver, see sect. 5.3, 4.4). The parameters of the kinematic model defining the frames B'''^1, B'''^2 and B'''^3 as well as the axis skeleton are controlled by these design tables. Based on that, the kinematic model is assembled in the first solution out of this set.

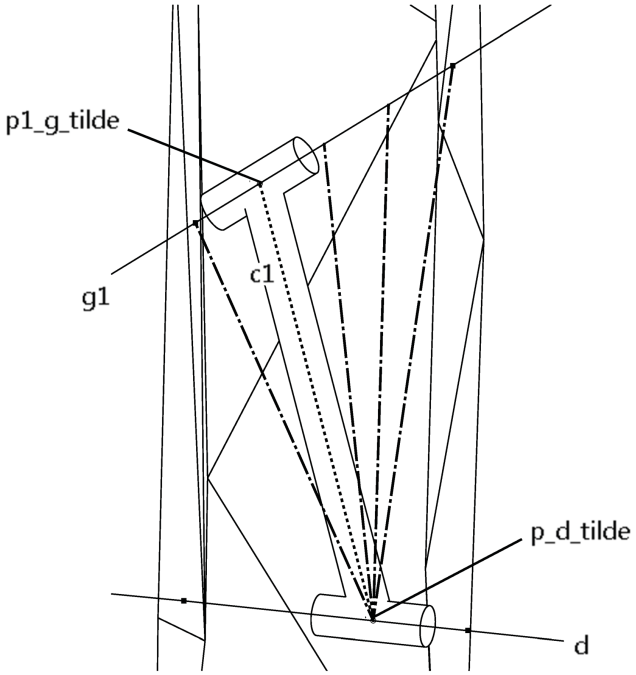

Figure 5.12.: Possible definition and variations of p_d_tilde and p1_g_tilde of a spatial RR chain within a given envelope, which are controlled via button ⑦ of the CAKD toolbar

Button ① - Automated adjusting of initial task poses

Since the variation of position data within the computing environment will usually yield task poses other than those initially defined in the CAD-system, a button is required, that adjusts the location and orientation of the three poses. This is achieved through button ①, which induces that the initial locations and orientations of K" swap to the first set of task poses. The first valid three task poses have two corresponding valid axes d and g1 passing through the envelope, which is also visualized in the CAD-system.

Button ⑥ - Switching between three-position tasks with corresponding valid joint axes

In order to allow a designer to switch between different three-position tasks with axes d and g1 passing through the envelope, button ⑥ can be used. This opens another input box (GUI)) where the designer may select one solution out of the set. Figure 5.11b) shows the input box of a design session, where the variation of task positions within the kinematic solver yielded 37 different three-position task with corresponding $2 \cdot 37 = 74$ RR joint axes in configuration 1 of the linkage.

Button ⑦ - Definition and variation of p_d_tilde and p1_g_tilde

The points p_d_tilde and p1_g_tilde defining, where the R joints shall be located along the axes are conveniently defined within the given envelope. Since the points of intersection between axes and the envelope as well as the location and orientation of axes were calculated within the kinematic solver, this may easily be arranged by providing adequate coordinates for p_d_tilde and p1_g_tilde in the design table. Based on that the voluminous representation of joints, such as given for instance by simple basic cylinders (see again sect. 5.2.3, Fig. 5.5) is generated automatically from the parameters of the CAD-system.

Because a cylinder defining a joint may usually be located at several different places along an axis among entrance and emersion point of an axis with the envelope, the designer may wish to vary this location. This possibility is provided by different discrete coordinates for p_d_tilde and p1_g_tilde along d and g1, which are available from another design table. The different alternative points can be evaluated using button ⑦, which automatically switches between different p_d_tilde and p1_g_tilde.

Figure 5.12 shows an exemplary spatial RR chain based on simple cylinders, which is defined using a specific p_d_tilde and p1_g_tilde within the envelope. In this example a design table also provides further valid p1_g_tilde along axis g1, which can be selected via button ⑦. Then the automated update procedure of the CAD-system yields other connecting rods between d and g1. When such a RR chain is used in a three-position synthesis procedure of spherically constrained spatial RR chains (see sect. 4.3.4) this yields different axes c1, which will have impact on the synthesis procedure. If only n different points p1_g_tilde along axis g1 are available, then there are also n different axes c1. However, if there are n different points p1_g_tilde and m different points p_d_tilde there is a total number of $n \cdot m$ different axes c1.

Buttons ③, ④ and ⑤ - Switching between linkage configurations of one specific three-position task

After the designer has chosen a suitable RR chain that fits appropriately into the given envelope he may evaluate location, size of the chain or also collision characteristics between links and other parts in the two other configurations, defined from the three-position task. This is enabled via buttons ④ and ⑤, which allow to assemble the synthesized RR chain, such that its end link K''' reaches task pose 2 and 3. Note that this is achieved by activating corresponding constraints of the CAD-model. By clicking ③ the RR chain swaps back to configuration 1.

Button ⑧ - Preparing coordinates of p_d_tilde and p1_g_tilde for further synthesis computations

In case that a useful spatial RR chain is found, whose links fit into the given envelope, it may represent the building block chain, required in further synthesis procedures of another linkage topology. Then the coordinates of the final selection of p_d_tilde and p1_g_tilde must be available in another kinematic solver, implemented using the computing environment. This is achieved via button ⑧, which triggers the generation of a corresponding input file for the kinematic solver. In fact, this is just the scenario of CAKD of spherically constrained spatial RR chains, where another spherical RR synthesis is performed based on the spatial RR synthesis results (see again sect. 4.3.4).

5.6. A Flowchart for CAKD of Spherically Constrained Spatial RR chains

The parametrized CAD-models of a linkage topology with corresponding synthesis procedure as well as envelopes defining allowed regions where a linkage must fit into may be used to define a CAKD flowchart. This provides an organized overview of the different linkage design steps performed in both the design as well as the computing environment and somehow summarizes the various facets of a CAKD process.

Figure 5.13 shows such a CAKD flowchart for three-position synthesis of spherically constrained spatial RR chains, where specific steps are also supported by the CAKD toolbar presented before. The different steps performed and implemented within the computing environment are those described in detail in sect. 2.3.4, 2.3.5, 4.1.2, 4.3.4 and 4.4. Furthermore, the flowchart directly applies to the application scenario from sect. 6.3.

In a similar fashion CAKD flowcharts for other linkage topologies with corresponding kinematic design procedures can be developed. Examples of such other procedures are provided along chapter 4 for linkage topologies such as spherical four-bars or spherically constrained planar RR chains.

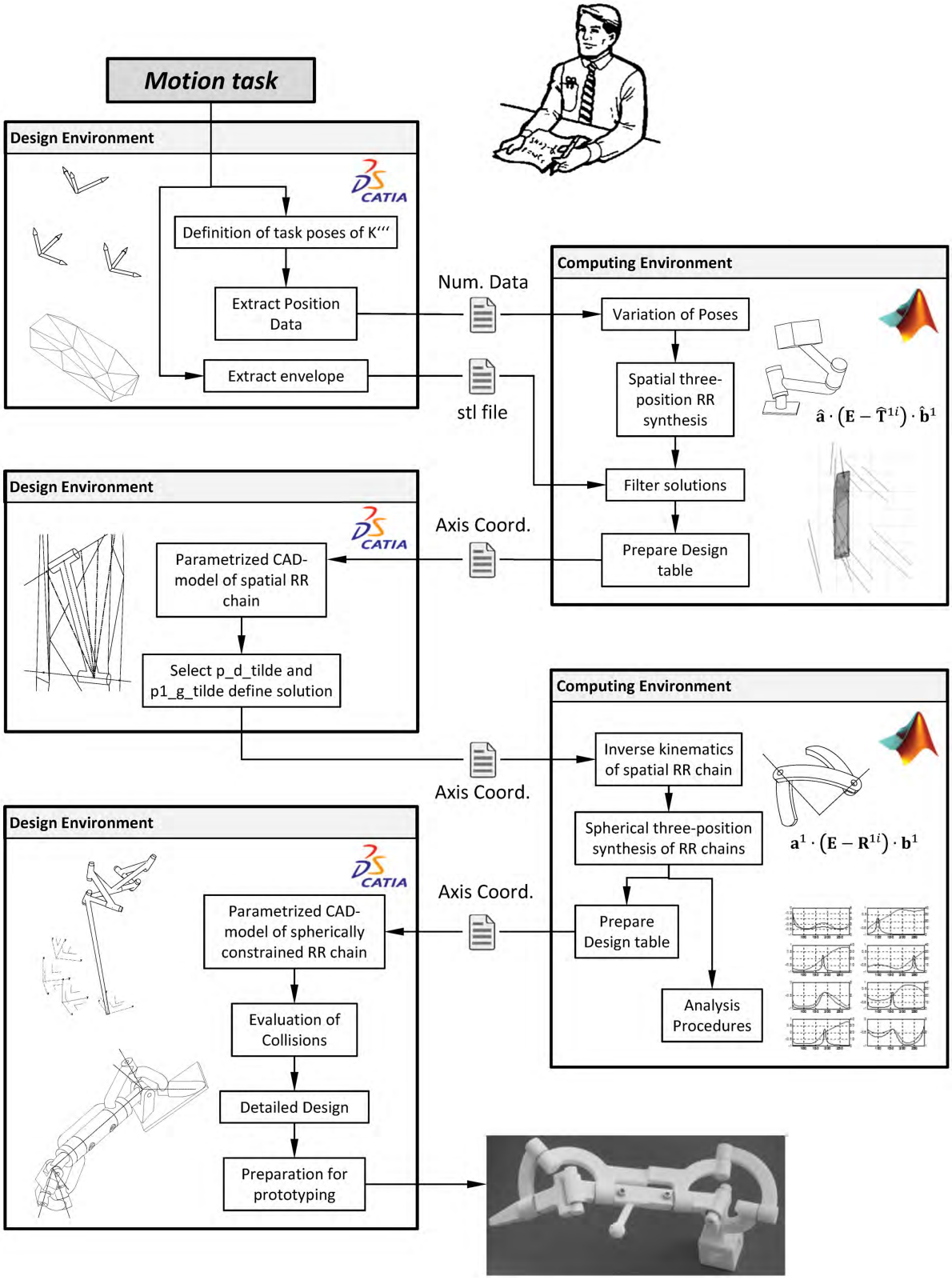

Figure 5.13.: A flowchart for CAKD of spherically constrained spatial RR chains

6. Application

The CAKD of linkages particularly described in chapter 5 includes CAD-integrated linkage design processes as well as kinematic synthesis and analysis procedures within the computing environment and is evaluated in this chapter using a specific engineering design example. The goal is the CAKD of a spherically constrained spatial RR chain, such that it guides a car door between two distinct spatial poses. A particular given requirement of the task is that synthesis results must be integrable into the given parts of a car. A linkage design solution for this motion task should significantly ease getting into a car in cramped parking spots. In fact, the approach is inspired from Sonawale and McCarthy [68], who solved a car door guidance task in a CAD-integrated five-position synthesis procedure using a spherical Watt-1 six-bar linkage and their MechGen linkage design software (see also sect. 2.4.3).

The problem of cramped parking spots has also been studied in [119] from a practical point of view, where a planar RR chain is considered for planar car door guidance. While planar car door guidance may easily be prescribed using a plane sketch, a spatial guidance problem requires more advanced approaches in order to be prescribed adequately. Here Richter et al. [120] developed the idea of a force controlled serial robot in order to guide a car door along a spatial task trajectory. Based on the inverse kinematics of the robot spatial positions of the door can then be used in a computer-aided linkage design process.

In order to solve the car door guidance task different solution approaches are discussed in the following. On the one hand the spatial RR chain guiding the car door is found following a two-configuration synthesis procedure (see sect. 4.2.3). This is demonstrated using the simplified geometry of links in a parametrized CAD-model, which was introduced in sect. 5.2. On the other hand the guiding spatial RR chain is found following the three-position synthesis procedure from sect. 4.3.4 in combination with particular space requirements for the linkage, see sect. 5.3. Additionally a singularity analysis based on sect. 4.1.3 is included in order to consider transmission properties. The three-position synthesis approach is discussed using a detailed design of the spherically constrained spatial RR chain, which appropriately fits into a given envelope obtained from CAD-parts of the car. The results of the three-position synthesis approach may also be found in [112] and have also been manufactured using rapid prototyping. As a final remark, the author gratefully acknowledges the support of BMW AG for providing CAD-parts of the car.

6.1. A Car Door Guidance Task for the Spherically Constrained Spatial RR Chain

A first preprocessing step of the CAKD procedure consist in collecting different CAD-parts of the car including the car door as well as additional parts, that define the space requirements for the linkage. The different parts are shown in Fig. 6.1. On the one hand, the car door is shown, which only provides a slim region where the linkage is allowed to be connected. Note that this is usually also the valid region for simple R joints commonly used to realize the connection. On the other hand, the side panel of the car must be available for the designer, since this represents

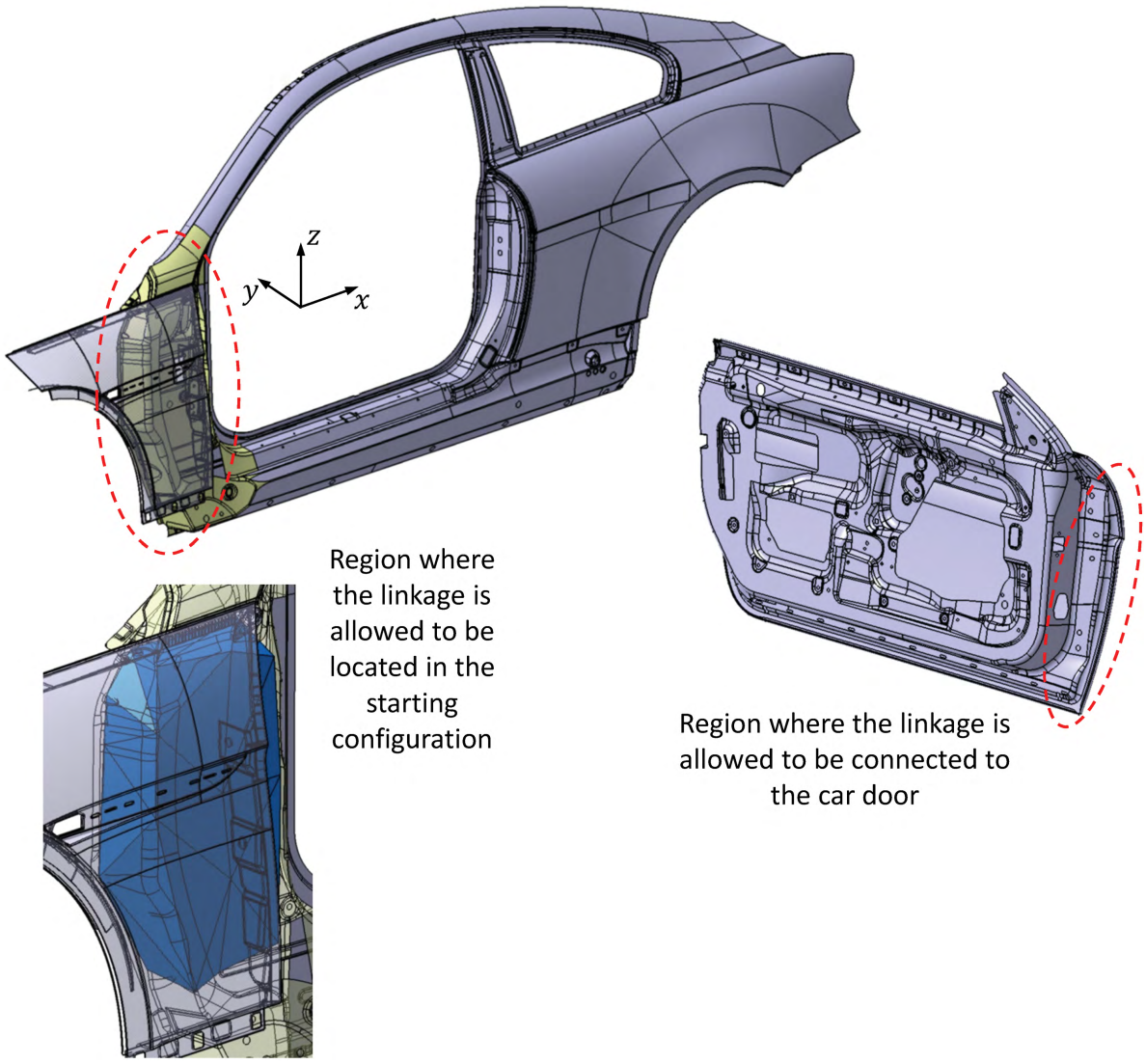

Figure 6.1.: CAD-parts required to define the spatial motion task of a car door with allowed regions for the linkage (courtesy of BMW AG)

the fixed reference link of the linkage. Since car doors are commonly connected in the front part of the car right behind the front wheel, this region is also the allowed volume, where the linkage must fit into when the door is closed.

In order to evaluate this region within the computing environment, i.e. in order to filter synthesis solutions, the portion of space is modelled as an approximately convex polyhedron, which can be saved using the stl file format. Note that this is just the envelope already shown in Fig. 5.9, which will be used for three-position synthesis of the spatial RR chain in sect. 6.3.

Based on the preliminary steps the designer may begin defining task poses of the car door. Note that this is done separately for the two distinct CAKD approaches described in the following in sect. 6.2 and 6.3.

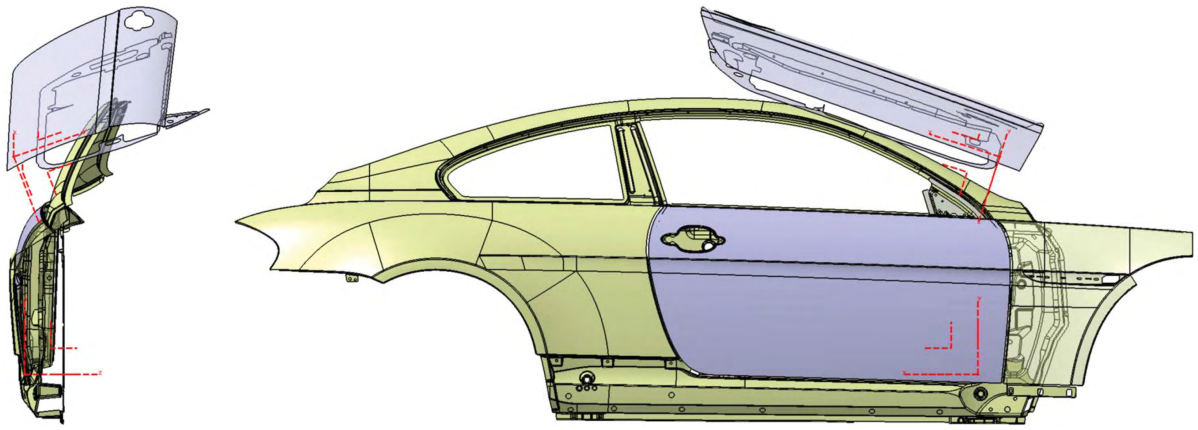

Figure 6.2.: Two task positions of the car door for two-configuration synthesis of a spatial RR chain

6.2. A Linkage Obtained From a Transformation of a GS Chain

In this section a two-configuration synthesis approach is chosen in order to find an appropriate spherically constrained spatial RR chain that solves the car door guidance task. This is particularly based on a transformation of a spatial GS chain into a spatial RR chain using the procedure from sect. 4.2.3. The CAKD procedure towards a final design of a kinematic CAD-model with simple link geometry as shown in Fig. 5.5 requires the following essential steps:

1. Based on the CAD-parts of the side panel as well as the car door two task positions of the door are defined by a designer. While the initial position clearly cannot be varied, since it is the closed door configuration, the second position can be specified arbitrarily. However, because the goal is to ease getting into the car in cramped parking spots, the second pose shall be defined, such that the door is located appropriately upon the car top.

2. The two finitely separated spatial task positions are next used in a two position synthesis of a GS chain using Eq. (4.54). Because of two-position synthesis five of the six joint coordinates can be selected with respect to the given space requirements discussed in the previous section.

3. Following sect. 4.2.3 and applying two-configuration synthesis allows to transform the GS chain into a spatial RR chain, that reaches the two positions of the car door. Recall that this also includes inverse kinematic calculations of the GS chain.

4. Since the spatial RR chain next must be constrained using spherical RR chains as described in sect. 4.3.2 it is convenient to define another intermediate position of the door. This yields a more precise approximation of the movement between the two initially defined task poses. However, note that this is clearly only possible respecting the already existing RR guiding chain. This means that the two independent d.o.f. of the chain must be used to define the intermediate spatial position.

5. Since now there are three positions of the door but corresponding unknown configurations of the spatial RR chain the next step is to enter into sect. 4.3.2 and continue with step 3. The

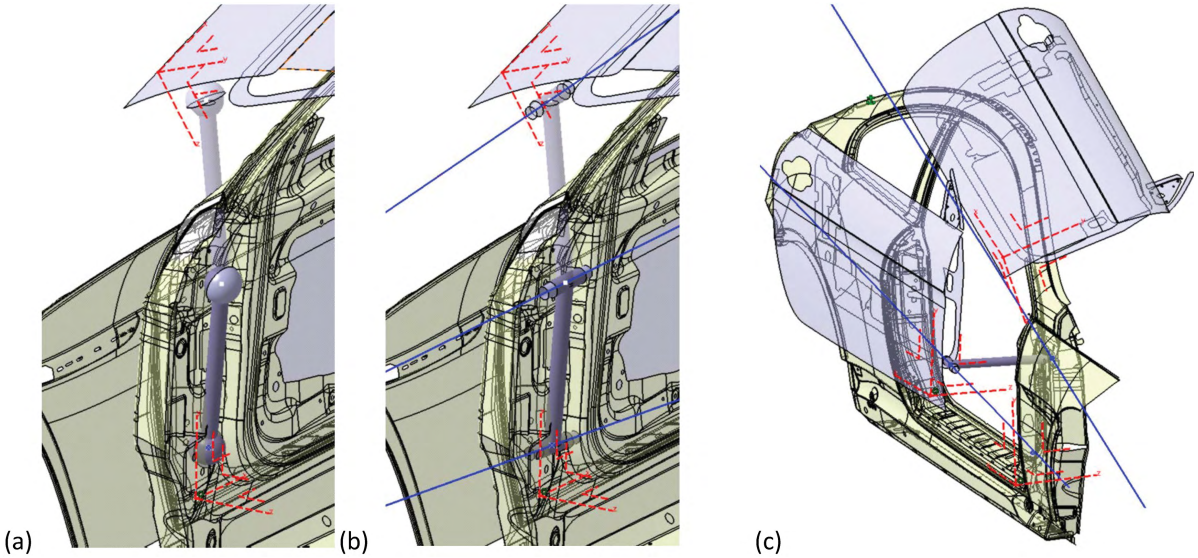

Figure 6.3.: Design results from steps 2, 3 and 4: a) A spatial GS chain and b) a spatial RR chain obtained from two-configuration synthesis both reaching the two task positions of the car door. c) An intermediate position of the door defined by the RR chain obtained from two-configuration synthesis

result are the inverse kinematics that define the configurations of the spatial RR chain. For details about the inverse kinematics calculations, see the corresponding subsection of sect. 4.3.4.

6. The final synthesis step consists in continuing with step 4 from sect. 4.3.2. This consists in performing three-position spherical RR synthesis in order to constrain the movement of the spatial RR chain. Details about the corresponding synthesis calculations are found from the final subsection of sect. 4.3.4.

The result of these steps is a spherically constrained spatial RR chain that reaches two 'real' task positions and another intermediate one, which was restricted to be defined by the spatial RR chain. In this context the procedure performed here could also be termed as 2.5-position synthesis.

The particular benefit of the approach is represented by step 2, where five of the six joint coordinates of a GS chain can be defined with respect to the challenging space requirements. This strongly increases the chances to obtain a useful GS chain located inside the given envelope, since only one single joint coordinate must be calculated, while the remaining ones can be selected appropriately. However, when step 2 yields a valid GS chain also the axes of the spatial RR chain will pass through the allowed regions, because the joint axes will always include the previously determined center points of the G and S joint (see sect. 4.2.3, Fig. 4.13).

6.2.1. Design Results

Following step 1 two spatial task positions of the car door were specified as shown in Fig. 6.2. Recall here that this is also the first step in the flowchart from Fig. 5.13 and note that in contrast to Fig. 6.1 mirrored parts of side panel and car door were considered (which, however, clearly do not change the motion task). Based on position data extracted from coordinate frames

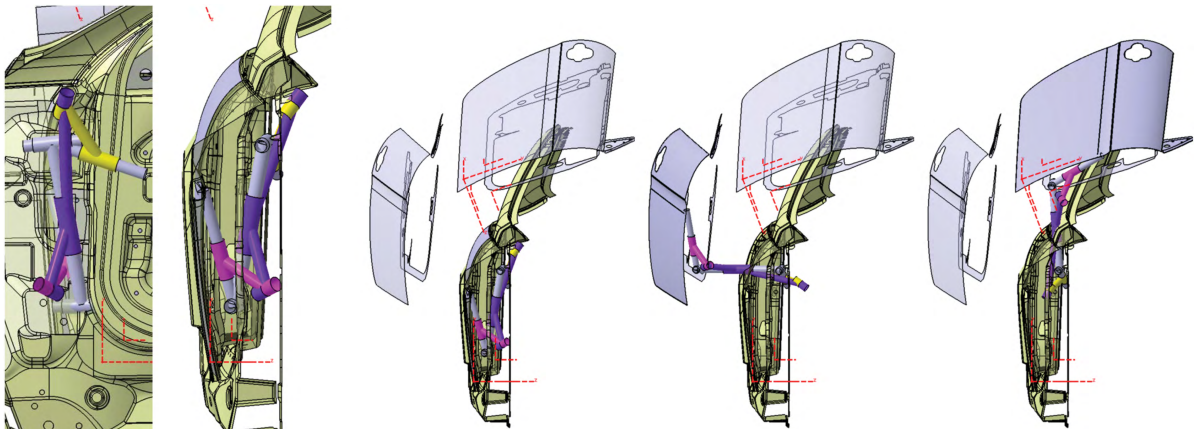

Figure 6.4.: Final result of the simple parametrized CAD-model of the spherically constrained spatial RR chain

rigidly attached to the door two-position synthesis calculations implemented in the computing environment yielded the spatial GS chain in step 2, which is shown in Fig. 6.3 a). Note that the three coordinates defining the moving S joint in configuration 1 as well as two of the three coordinates for the fixed G joint were the selected as free design parameters.

In order to obtain the spatial RR chain two-configuration synthesis as well as inverse kinematics calculations of the GS chain were performed using the computing environment. The result is shown in Fig. 6.3 b), which allowed the intermediate postprocessing step of evaluating the feasibility of the spatial RR design results. On the one hand, based on the simple parametrized CAD-model of the chain it could be verified that at least the simple parts fit into the given envelope. On the other hand an intermediate task position could be defined using the RR chain (step 4), which was useful, see Fig. 6.3 c).

In order to constrain the RR chain such that it becomes a spherically constrained spatial RR chain step 5 was performed, which was nothing but step 3 from sect. 4.3.2. In fact this is nothing but the first computational step in the second computing-environment-block of flowchart from Fig. 5.13). Based on the results spherical three-position synthesis (step 4 from sect. 4.3.2 was performed within the computing environment, which yielded the remaining axes of the spherically constrained spatial RR chain. These were submitted to the parametrized kinematic CAD-model with simple geometric shape, which is shown in Fig. 6.4.

Even though the resulting linkage has roughly designed parts it could be considered for further detailed design, because it provides a compact stowed configuration when the door is closed. On the other hand it provides another slim ending configuration when the door is stored upon the car top. While collision issues might be solved by appropriately shaped links another important aspect are the transmission properties of the structure. On the one hand, the line-based analysis from sect. 4.1.4 could be evaluated, which however was not done in this example (see next section). On the other hand, also the kinetostatic properties must be evaluated since a car door usually represents a particularly heavy part. However, kinetostatics is beyond the scope of this work and should be part of future research on the class of spherically constrained linkages.

6.3. A Linkage Obtained From Three-Position Synthesis of a Spatial RR Chain

Compared to the previous example in this section a 'real' three-position synthesis procedure is applied in order to solve the car door guidance task. This means that the designer can directly follow the flowchart shown in Fig. 5.13, which includes the following steps:

1. Based on the CAD-parts of the side panel as well as the car door three finitely separated task positions of the door are defined by the designer. As it was the case in the previous design session the first position clearly is uniquely given, since it is the configuration of the closed door. However, now the second position - which shall represent the intermediate pose - as well as the third position can be specified arbitrarily. Because the goal is to ease getting into the car in cramped parking spots, the second pose should be defined in a similar fashion as shown in Fig. 6.3c), while the third one locates the door appropriately upon the car top. In contrast to sect. 6.2, where five of the six design parameters of the GS chain could be specified directly inside the given envelope the next step in this scenario is to extract an stl-file of the given envelope. This is because it must be evaluated within the computing environment, whether spatial RR synthesis results actually intersect the given envelope.

2. Based on the previous CAD-integrated preprocessing steps spatial RR three-position synthesis is performed (sect. 2.3.5, the corresponding subsection of 4.3.4 or either C.3 for details). This yields two distinct spatial RR chains, which can reach the initially prescribed task positions but, however, will probably not intersect the given envelope. Hence, a variation of task poses 2 and 3 probably needs to be performed in order to obtain RR synthesis solutions, which intersect the envelope. Note that the detection of intersections is performed by implementation of the method from sect. 4.4 using the computing environment.

3. After the first solving step the designer evaluates the synthesized joint axes using the simple CAD-model of the spatial RR chain and can define joints at the axes, that are located inside the given envelope. Recall from chapter 5, that this can be done via parameters and design tables at the CAD-model, which are controlled via the computing environment.

4. Based on a desired spatial RR chain the second solving procedure begins within the computing environment, which includes the corresponding steps of the procedure from sect. 4.3.4. This is the calculation of the inverse kinematics of the spatial RR chain, which allows to perform spherical RR synthesis in order to obtain the complete set of kinematic dimensions of the spherically constrained spatial RR chain. Implementation of the position analysis as well as of line-based analysis procedures from sect. 4.1.2, 4.1.3 and 4.1.4 then allows to evaluate kinematic transmission properties, which particularly decide whether a spherically constrained spatial RR chain can be considered for detailed design.

5. Based on a useful synthesis solution the final step consists in CAD-integrated postprocessing, i.e. the simulation of the mechanism's movement in combination with an analysis of collisions among the different parts of the parametrized kinematic CAD-model (see again sect. 5.4). Based on that a detailed design of the spherically constrained spatial RR chain for car door guidance is carried out.

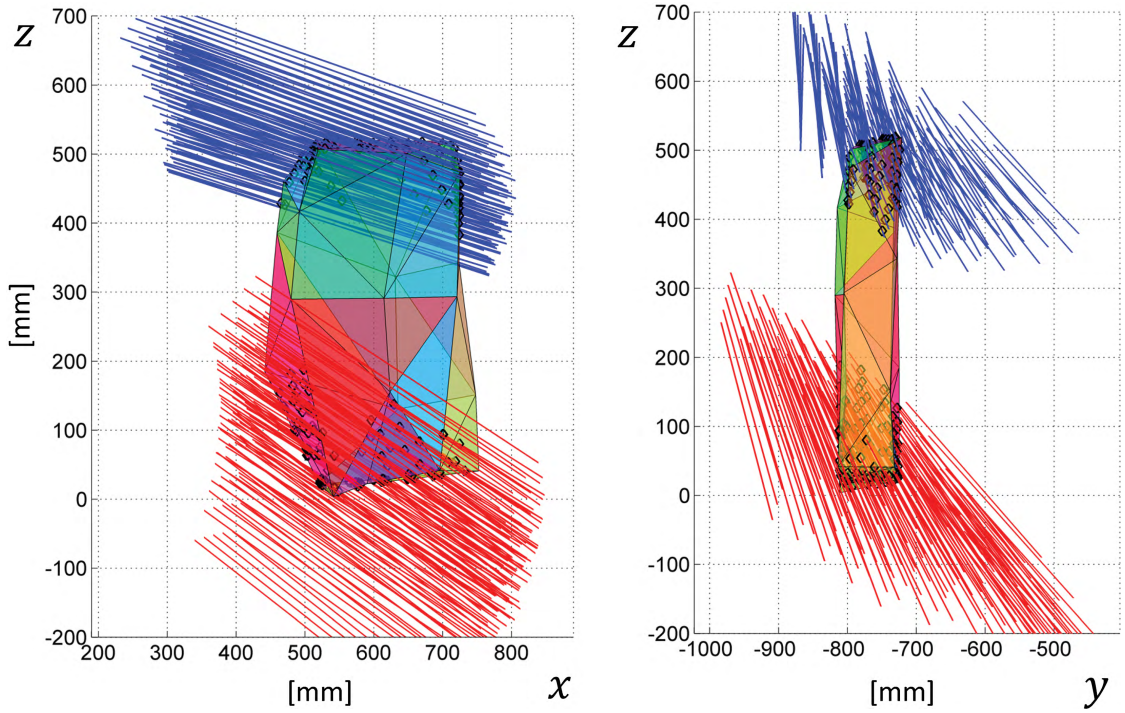

Figure 6.5.: Intersections between joint axes of the spatial RR chain and the given envelope, which are obtained from varied task position data

6.3.1. Design Results

Following step 1 three initial spatial task positions of the car door were specified. Based on that variations of poses yielded spatial RR synthesis results whose axes intersected the given envelope, see Fig. 6.5. In fact a few of these joint axes were already shown in Fig. 5.9. Out of this set of valid RR chains a suitable one was chosen, which has the corresponding set of three task positions shown in Fig. 6.6.

Following the further different design steps the parametrized basis CAD-model of a spherically constrained spatial RR chain from Fig. 6.7 was found, which can reach each of the three poses on a continuous motion path. In fact this synthesis result was considered as a useful design because of adequate singularity analysis results described in the following section. This motivated a detailed CAD-model of the spherically constrained spatial RR chain, which is described afterwards.

Discussion of line-based analysis results of transmission properties

The continuous movement of the car door along the three task positions is achieved via actuation of the fixed R joint of the spatial RR chain. Recall from Fig. 4.2 that this axis was denoted as $\hat{\mathbf{d}}$, so that the input angle is denoted as ϕ_d. This allows to perform the line-based analysis of transmission properties by simply following the procedures from sect. 4.1.3 and 4.1.4. This yielded the determinants as well as the weighted Frobenius condition numbers of the car door guidance linkage, which characterize the transmission properties. The determinants and conditions numbers are shown in Fig. 6.8 over an input range of $\Delta\phi_d = \phi_{d,end} - \phi_{d,start} = 150$ deg and corresponding graphical depictions of the configurations where $det(\mathbf{J}) = 0$ or $\kappa(\mathbf{J}) >> 1$ are shown in Fig. 6.9. However, before analyzing the different configurations, it is important to

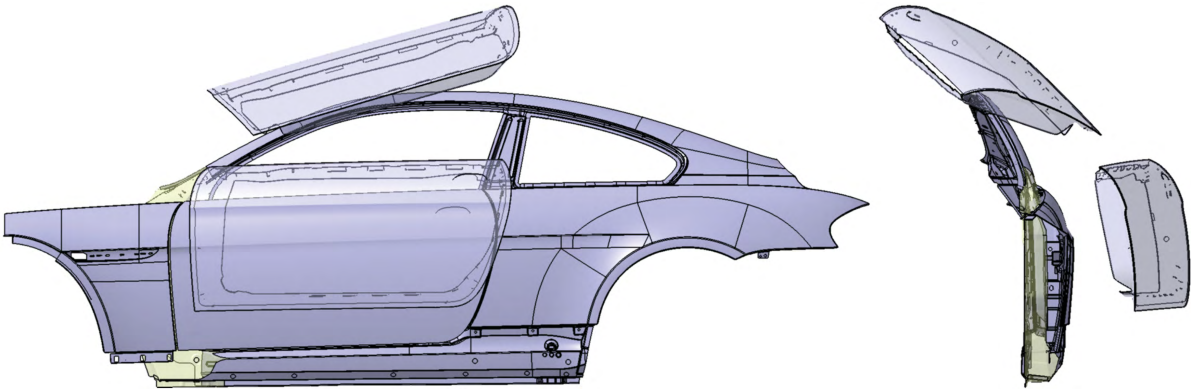

Figure 6.6.: Three task positions of the car door obtained from a variation of initial position data

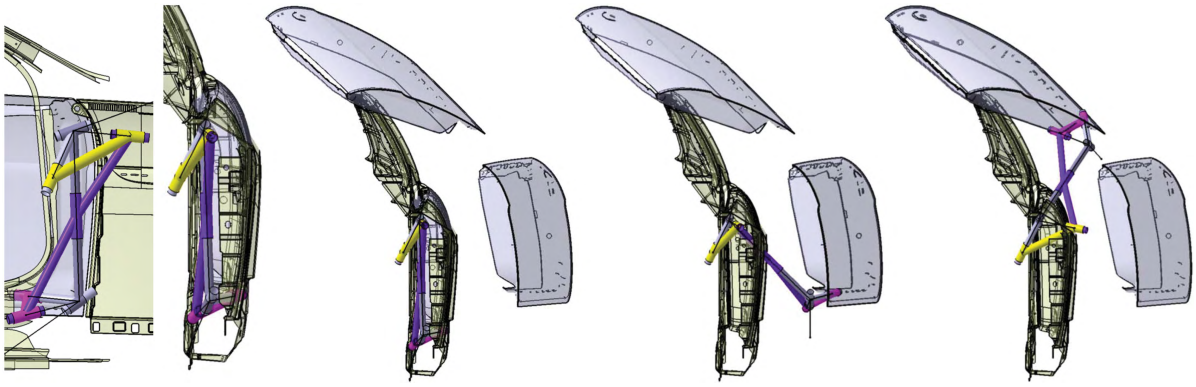

Figure 6.7.: Parametrized simple kinematic CAD-model which can reach each of the three poses without a change of the assembly mode

clearly define the desired operation mode of the linkage. This may be formulated as follows:

In order to precisely control the movement of the car door between the initial and ending configuration without weak transmission properties, the two coupled four-bars in the spherically constrained RR chain must satisfy the following:

1. *The input range of the driving angle ϕ_d of the 'first' four-bar formed by the axes $\hat{\mathbf{a}}$, $\hat{\mathbf{b}}$, $\hat{\mathbf{c}}$ and $\hat{\mathbf{d}}$ must not include any limits on the input. This is because those were the configurations, where the input cannot resist (small) changes of the output angles.*

2. *In order to provide a homogeneous input for the 'second' four-bar formed by the axes $\hat{\mathbf{c}}$, $\hat{\mathbf{e}}$, $\hat{\mathbf{f}}$ and $\hat{\mathbf{g}}$, the output angle ϕ_c of the 'first' four-bar should not reach any limit within the input range of ϕ_d. (Recall from sect. 4.1.2 or 4.1.4 that $\phi_c(\phi_d)$ was the input of the second four-bar)*

3. *In order to sufficiently resist changes of the output angles ϕ_e, ϕ_f and ϕ_g of the 'second' four-bar, the input range of angle $\phi_c(\phi_d)$ of the second four-bar must not include any limits.*

4. *Limits on the output angles ϕ_a, ϕ_b, ϕ_e, ϕ_f and ϕ_g at the starting or either ending configuration are welcome because those provide particular stability in the considered configurations.*

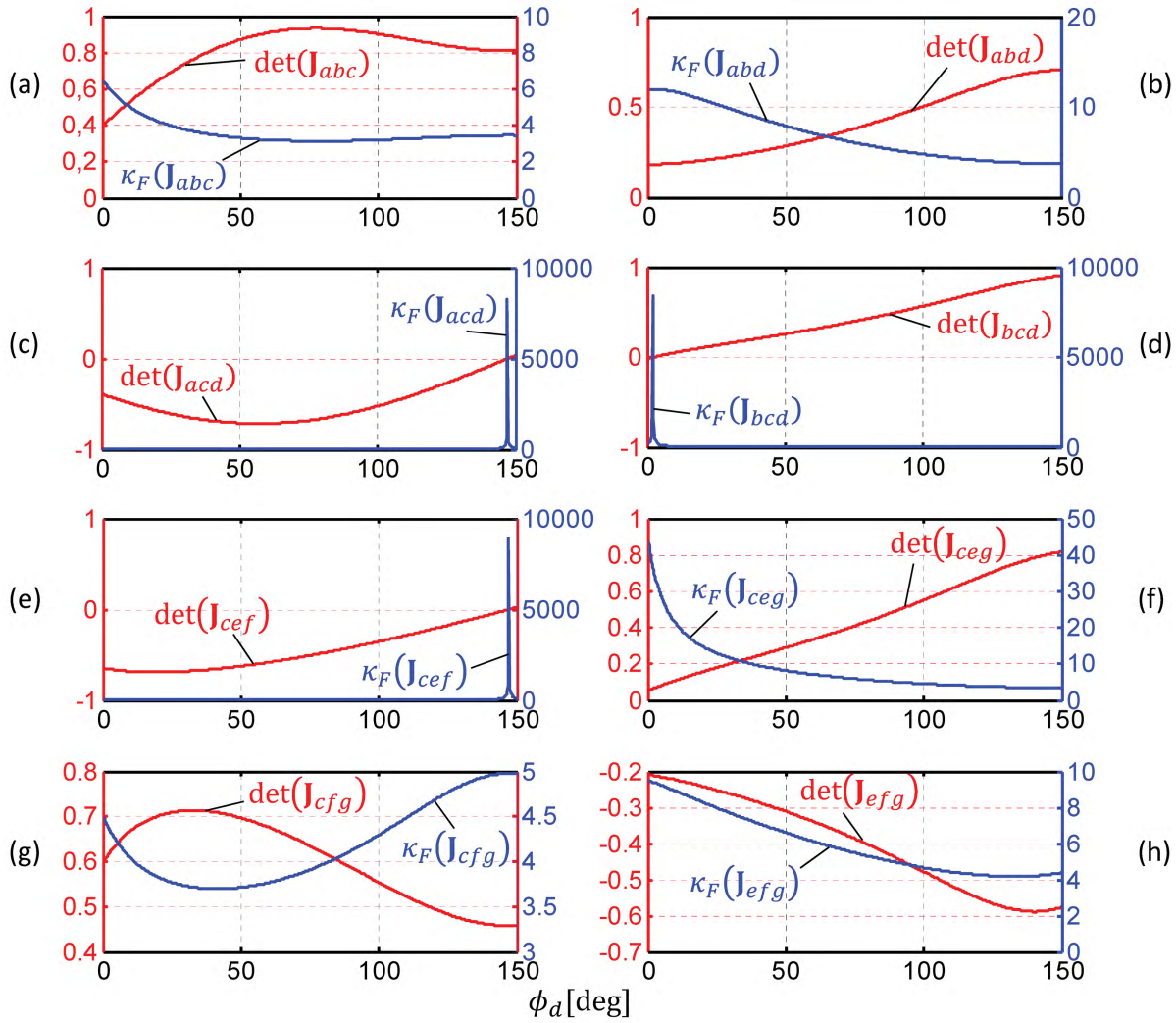

Figure 6.8.: Determinants and weighted Frobenius condition numbers within an input range $\Delta\phi_d = \phi_{d,end} - \phi_{d,start} = 150$ deg in order to detect singular configurations of the car door guidance linkage

The case shown in Fig. 6.8 a) corresponds to the the Jacobian $\mathbf{J}_{abc}$, which can be used to identify limits on the input angle ϕ_d. However, this doesn't show dramatically increased condition numbers or determinants close to zero and hence not directly indicate a limit on the input. In fact, it could be shown that a first limit is reached at $\phi_d \approx \phi_{d,start} - 17.8$ deg, which was considered to be 'far away enough' from the evaluated input range. In a similar fashion figure b) doesn't represent any significant limit on the output angle ϕ_c which meets the second point in the list from above.

The configurations shown in Fig. 6.8 c) and d) correspond to rank-deficiencies of the Jacobians $\mathbf{J}_{acd}$ and $\mathbf{J}_{bcd}$ of axes that form the 'first' four-bar and hence correspond to limits of the output angles ϕ_b and ϕ_a respectively. However, since these angles do not represent any input angles the configurations (which are particularly close to the starting and ending configuration) don't lead to any weak transmission properties.

Fig. 6.8 e) shows a rank-deficient configuration of $\mathbf{J}_{cef}$, which corresponds to a limit on the output angle ϕ_g. Note that this is measured about axis $\hat{\mathbf{g}}$, which represents the output angle of the 'second' four-bar. In fact, since this axis controls the orientation of the car door with respect to

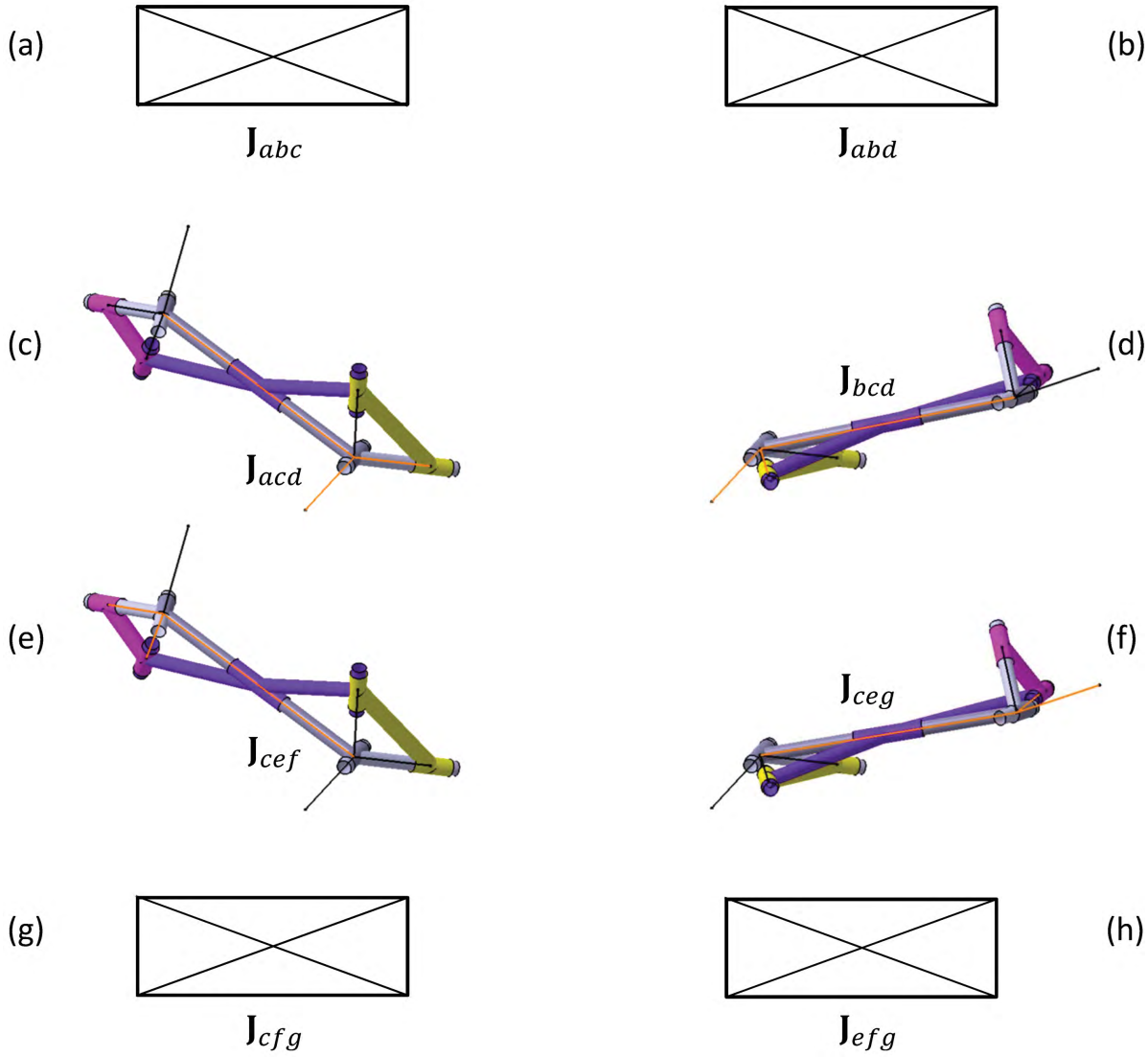

Figure 6.9.: Graphical depiction of the singular configurations within an input range $\Delta\phi_d = \phi_{d,end} - \phi_{d,start} = 150$ deg

the complete linkage, the limit on the output angle ϕ_g in the ending configuration indicates high stability. This corresponds to the fourth point in the above mentioned list, which also holds for the singularity shown in figure f). This corresponds to a rank-deficient Jacobian $\mathbf{J}_{ceg}$ and stands for a limit of angle ϕ_f.

While Fig. 6.8 g) doesn't indicate any specific limits on the output angle ϕ_e, figure h) provides inside on the limit of input angle $\phi_c(\phi_d)$ of the second four-bar. After point three from above, this must not include any limits, which is considered here to be satisfied, because it could be verified, that $\det(\mathbf{J}_{efg})$ as well as $\kappa_F(\mathbf{J}_{efg})$ do not tend even to zero or to infinity for the limit of the input ϕ_d, which was $\phi_d \approx \phi_{d,start} - 17.8$ deg. Hence, ultimately the different requirements from the list could be reached, which motivated a detailed design as well as a corresponding rapid prototyping model described in the following.

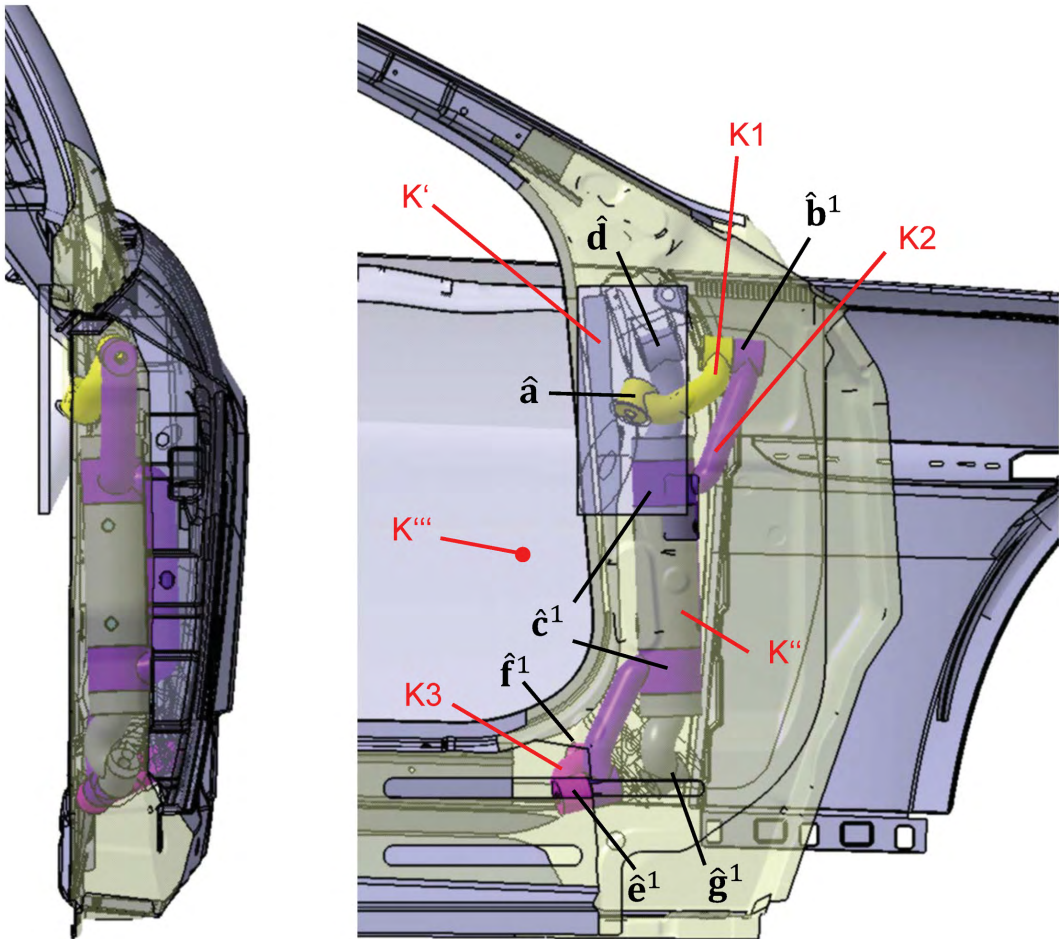

Figure 6.10.: Detailed CAD-model of a spherically constrained spatial RR chain, that is free from collisions and which matches the given space requirements

Discussion of link design

Based on the kinematic analysis results a detailed design of the simple kinematic CAD-model was carried out (see Fig. 6.10). This appropriately matches the given space requirements, since it can be stowed compactly right behind the front wheel. Note that each of the links K1, K2,...,K‘‘‘ already introduced in chapter 3 also occur in the final design. The different links shown in detail in Fig. 6.11 actually perform collision-free movement, which is particularly important in the beginning of the movement, where the linkage leaves the chassis through a particularly slim chamber, see Fig. 6.12 a). The sequence in Fig. 6.12 b) shows how the linkage also reaches the two remaining task positions of the door from Fig. 6.6.

The different links represent particularly complex CAD-parts, which, however, require this unique shape in order to fit into the given envelope and to provide collision-free movement. Furthermore, in order to allow assembly of the linkage the link K“ must be removable. The connection between the car door (link K‘‘‘) and other adjacent links could be realized within a given allowed region (see again Fig. 6.1) via an appropriate adapter located at the lower part of the door.

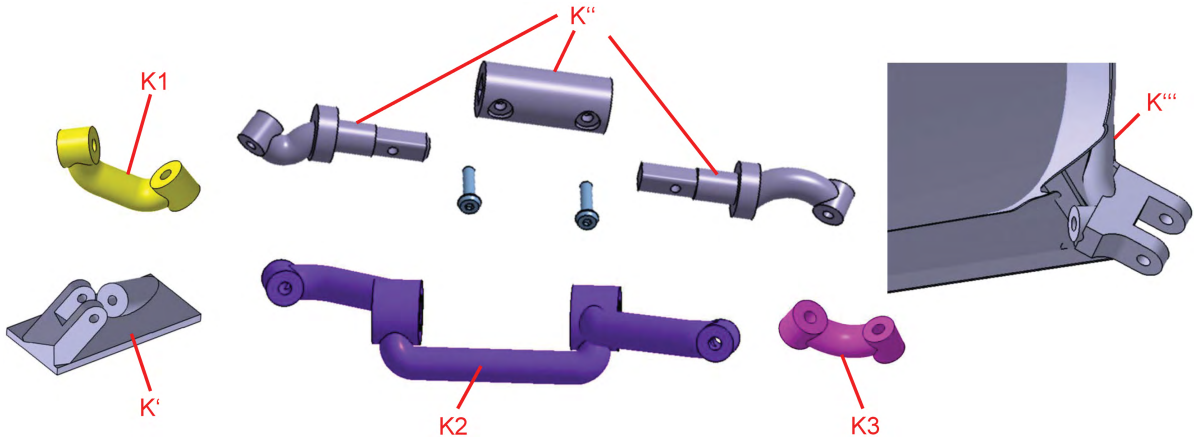

Figure 6.11.: Detailed designs of links allowing assembly and collision-free movement of the spatial linkage topology

Discussion of a scaled rapid prototyping function model

It is clear that the considered complex part design would require particular extensive manufacturing effort. However, in view of contemporary manufacturing techniques such as the selective laser sintering rapid manufacturing technique such link designs are easily fabricable. This was evaluated for a scaled function model of the spherically constrained spatial RR chain, which is shown in Fig. 6.13. In fact, this prototype was manufactured based on the analysis of transmission properties from the previous section in order to validate the analysis.

In the ending configuration, i.e. when the door is stored upon the car top, the rapid prototyping model reflects the predicted stability of the linkage. Recall from the previous section, that this was because the ending configuration actually coincides with a limit of the output angle ϕ_g. The stability characteristics are indicated by a particularly stiff mechanism, which has very little shakiness although there is a little joint clearance as well as structural deformations from polyamide material properties.

Unfortunately, in the starting configuration of the linkage suffers from weak transmission properties. This is characterized by a noteworthy shakiness of the door, even if the input is blocked, see Fig. 6.13d). One reason for this behavior surely relies on the mentioned joint clearance in combination with structural elasticity of the model. However, precise study and observation of the model indicates that the starting configuration of the 'first' four-bar in fact is 'closer' to a limit of the input ϕ_d as it was suggested in the previous section.

As a first guess towards a more useful linkage, another variation of the free selectable design parameters could be evaluated. On the one hand task positions of the door could be varied again. On the other hand free parameters of the underspecified spherical synthesis problem could be varied again. Another idea towards a useful linkage could also be building a more precise model, consisting of metal materials and bearings.

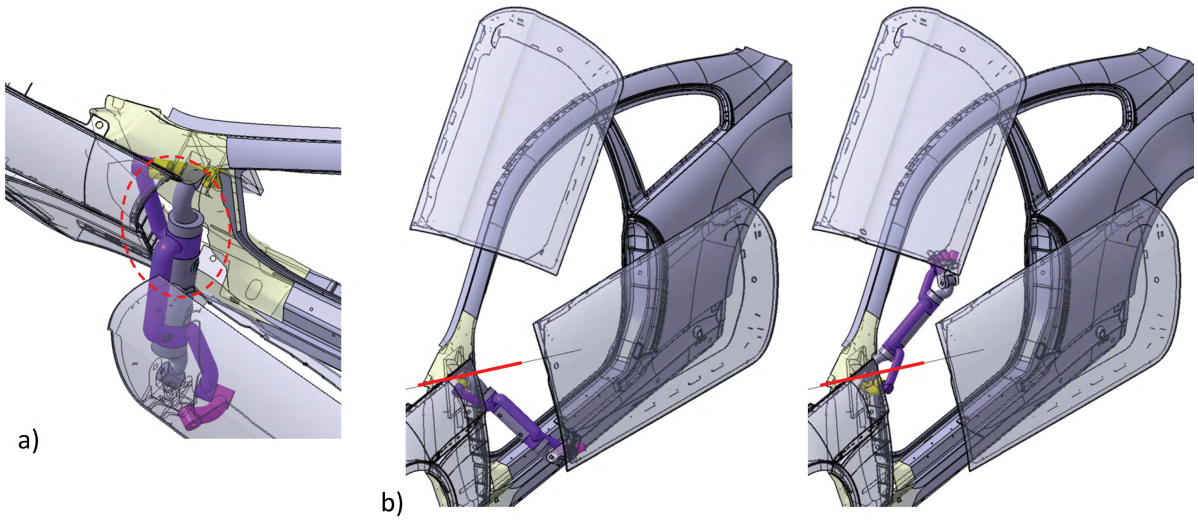

Figure 6.12.: Motion sequences of the car door guidance linkage: a) Linkage leaves the chassis through a particularly slim chamber. b) Linkage reaching the two further task positions of the car by actuating the fixed R joint of the spatial RR chain.

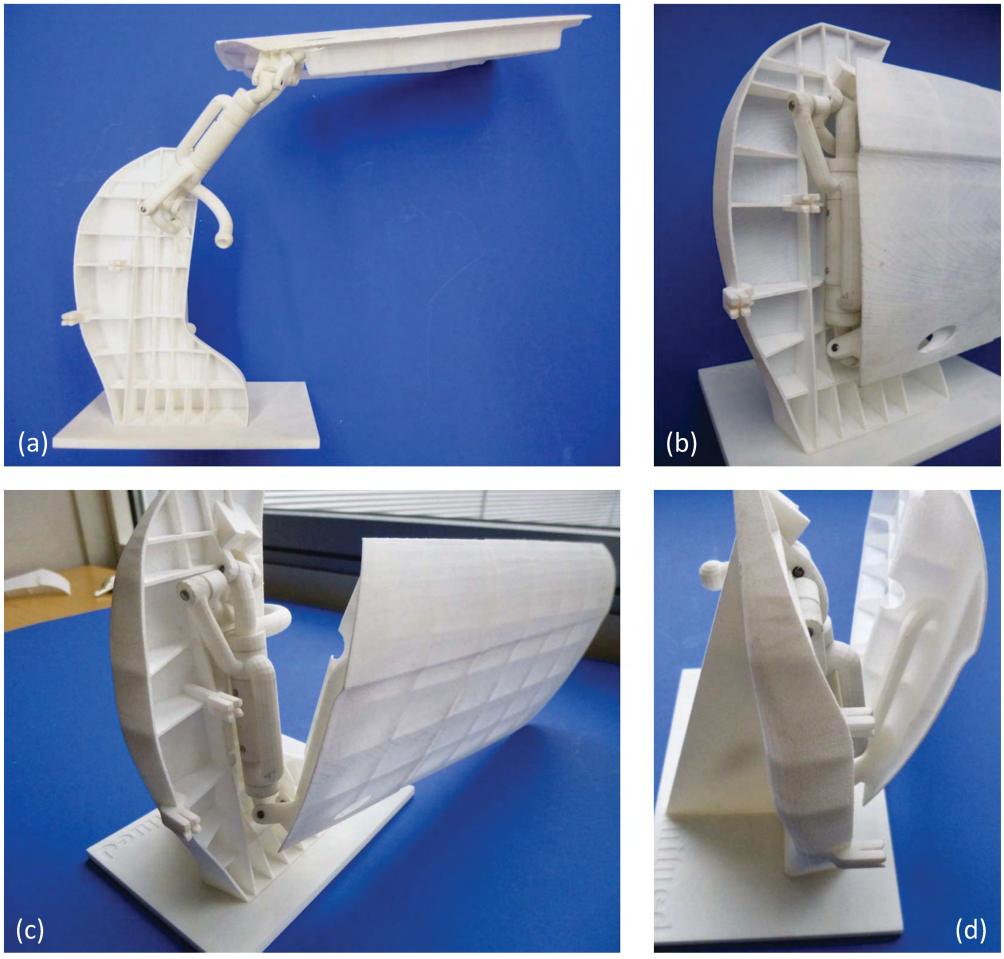

Figure 6.13.: Scaled function prototype manufactured using selective laser sintering technique

7. Summary and Conclusions

This work provides a contribution towards computer-aided kinematic design of spatially moveable low-d.o.f. linkage structures. The specific characteristic is, that task-based design is under consideration, where engineering motion problems should be solved. This means, that the design goal is to calculate the dimensions of a linkage, such that it provides a desired movement. Furthermore, also given space requirements are considered in this work, which represent additional requirements of the task.

However, because the desired movement is given as a spatial path of a rigid body, the dimensions that are of major importance are kinematic dimensions measured as angles and distances between the different axes of linkage. Roughly spoken, those dimensions represent a finite number of unknowns of the design problem, which only allow to define a corresponding finite number of task poses of the rigid link instead of a continuous motion path. Formulated that way, the calculation process can be solved algebraically, which leads to what is known as the finite position synthesis (denoted here as f.p.s.) of linkages.

F.p.s. represents the major part of this work where several results have been produced. Aside linkage synthesis the work also provides some results on kinematic linkage analysis, which represents the second big part involved in task-based kinematic design and which considers feasibility aspects of synthesized linkages. In order to make practical use of these computational procedures, also a computer-aided kinematic design methodology (denote here as 'CAKD') has been developed

The overall results are the following:

1. In order to provide a supporting introduction to kinematic analysis and synthesis, a detailed but compact excerpt of essential information on more and less known kinematic theory is given. This covers displacement equations, homogeneous transforms, velocity twists, line screws and dual screw algebra. Based on that Denavit-Hartenberg kinematics equations are introduced, which are used throughout the work in order to perform position and velocity analysis. Furthermore, introduction of algebraic finite position synthesis of linkage building blocks benefits from the introductory part on kinematic theory. On this journey it was also tried to introduce a convenient nomenclature that appropriately describes the mathematical quantities. These are the results of chapter 2, which are actually presented in a way, that readers might be familiar with from books on kinematic design theory. This is because a lot of the content is also part of a lecture on kinematic design (see [52]), the author has created during his phd position at the institute of micro technology and medical device technology.

2. Since it was the goal to provide design methodologies for compact spatial linkages, such a class of linkages is developed and presented in chapter 3. The topologies evolve from origami folding and are denoted as spherically constrained linkage topologies here. Initial studies of the author on these structures date back to 2010, [103]. However, now a new and precise classification has been developed, which systematically considers single- and also multi-d.o.f. structures that have the property of a naturally given slim shape. In fact any structure under consideration represents a system of specifically coupled spherical

four-bars. The structures can be categorized following the common distinction of planar, spherical and spatial structures and hence represent a family of linkages.

3. Chapter 4 represents the major part of the work and includes several kinematic analysis and f.p.s. procedures that apply to the spherically constrained structures from chapter 3. Parts of the results may also be found in [104], [105], [111] and [112], which have been developed and published during the author's phd position.

The results include position analysis as well as a line-based analysis of transmission properties of one single and two specifically coupled spherical four-bar linkages. F.p.s. results include a two-configuration synthesis method that allows to prescribe two planar, spherical or either spatial positions (also denoted as poses) of each link that make up a linkage. Initial studies of the author on this method also date back to 2010, [103]. However, now this method has been specified precisely in the sense, that most compact formulations are available, which apply to planar, spherical and spatial linkages in general. Examples are provided adressing two-configuration synthesis of spherically constrained structures as well as origami structures.

Aside, two-configuration synthesis also three- and four-position synthesis procedures are developed for spherically constrained single-d.o.f. structures, where task positions can be prescribed only for one single link. However, the procedures represent stepwise design methodologies, which follow the approach of mechanically constraining serial kinematic chains to obtain the well-known Watt linkage topologies. The stepwise synthesis uses the algebraic f.p.s. results of planar, spherical and spatial revolute-revolute (RR) chains, which are developed in chapter 2 as well as in the appendix. Furthermore f.p.s. results of spatial GS chains are included and used in an approach that combines two-configuration synthesis with spherical RR synthesis. In order to check whether synthesis results fit into a given envelope, that represents a region where a linkage is allowed to be located, another approach is developed. This detects intersections between synthesized joint axes and the given envelope (given as a stl-file) and makes use of a ray tracing method.

4. The different procedures developed in chapter 4 represent the computational part in a computer-aided kinematic design process (CAKD), which is developed in chapter 5. The CAKD process aims at providing a general design methodology that combines a computing environment and a design environment (CAD-system). The particular feature is that a designer is the central subject in the process, who interacts with computing and design environment. Based on a systematically developed parametrized CAD-model of a linkage with simple link geometry it is shown how to control parameters of the model using simple design tables and the computing environment. This allows quick evaluations of the synthesis results at the design environment.

A CAD-system is used here as the design environment, because it allows to perform kinematic design with regard to various CAD-parts that define requirements of a given task. Furthermore, beneficial functionalities of the CAD-system can be used to support the designer in evaluating synthesis results or also in creating a detailed design. An example of such functionalities for instance is VBA programming, which allows to define automated procedures. Here, a VBA-based toolbar for CAKD is developed and described. The methodology is described using the example of spherically constrained kinematic chains but the basic approach also applies to other linkage topologies.

5. In order to evaluate the computational procedures from chapter 4 as well as the CAKD

methodology from chapter 5 an application scenario from automotive engineering with particularly challenging space requirements is described and performed in chapter 6. This includes f.p.s. and analysis of a spherically constrained spatial RR linkage topology. The result is a car door guidance linkage, that can reach three spatially displaced task positions of the door and that regards the given space requirements. Kinematic analysis results indicated that the structure has useful transmission properties, which motivated it to build a rapid prototyping function model using a polymer and selective laser sintering technique. However, the result showed, that the structure suffers from weak transmission properties, that might result from filigree parts of the scaled polymer prototype. However, this and further aspects should be part of further research on task-based kinematic design of the spherically constrained linkage topologies.

7.1. Future Research

Through the application scenario a task-based CAKD of a spatial linkage topology could be performed successfully. A particular benefit of finite position synthesis and kinematic analysis in combination with computing and design environments could be shown, when motion design problems in engineering are a concern. However, there are still a variety of topics, which define the scope of future research and which should aim at improving results in CAKD processes. A brief sketch of these topics is given as follows.

7.1.1. Kinetostatic Analysis

In order to support the area of linkage analysis for spherically constrained chains also spatial kinetostatic analysis procedures are required. These may regard static and kinetic forces, that of course are always involved in the linkage design process. An example is given by the car door guidance task studied in chapter 6, where particularly heavy parts (such as the door) are involved in the task.

7.1.2. Analysis and Synthesis of Multi-D.o.F. Spherically Constrained Chains

This work has mainly focused on kinematic design procedures for single-d.o.f. spherically constrained structures. However, as derived in chapter 3 also multi-d.o.f. spherically constrained chains can be found, which may be designed in a compact or slim way and may hence be used in robotic devices in a variety of applications. However, these require particular analysis and synthesis procedures.

7.1.3. Matching Space Requirements

A particular issue regarded in this work is that of given space requirements of a task. This was defined as the problem of finding spatial synthesis solutions (locations and directions of joint axes), such that these fit into a given envelope. This was solved here by simply varying task positions. However, what would be beneficial here are more systematic methodologies. An example is given here by Mlinar and Erdman [11], who introduced Burmester field theory for planar synthesis. However, (to the author's best knowledge) there is little theory on such a rectification of spatial synthesis results in regard to given space limits.

7.1.4. Actuation Principles for Spherically Constrained Chains

In order to make use of spherically constrained spatial linkages in real applications advanced actuation principles must be developed. Actuation may be realized using classical dc motors or also gas springs but may also be defined using cables, which are stringed along the chain. Furthermore, mechanical springs or dampers could also be included in a detailed linkage design in order to improve mechanical advantage.

7.1.5. Applications

Last but of course not least spherically constrained kinematic chains should be used to solve application-driven motion design problems. Due to the fact that the joint axes of the structures are located relative to each other, such that a detailed design may have particularly slim shape, spherically constrained linkages may be used especially in applications with challenging space requirements.

A. More Rigid Body Kinematics!

A.1. Rotations and Skew Symmetric Matrices

A possibility to describe the spatial orientation of a frame B with respect to another frame W other than using the composition of coordinate rotations (Eq. (2.7)) is to define a rotation matrix in terms of a given rotation angle and rotation axis. In order to derive a corresponding formula one can use the Cayley map (also known as Cayley's formula), which represents a fundamental relationship between rotation matrices and skew symmetric matrices (for a detailed derivation see e.g. [34], pp. 14-15):

$$\begin{aligned} {}^{W}\mathbf{R}_{B} &= (\mathbf{E}-\mathbf{H})^{-1}(\mathbf{E}+\mathbf{H}) = \\ &= \frac{1}{k}\begin{pmatrix} {x_h}^2-{y_h}^2-{z_h}^2+1 & -2\,(z_h-x_h\,y_h) & 2\,(y_h+x_h\,z_h) \\ 2\,(z_h+x_h\,y_h) & -{x_h}^2+{y_h}^2-{z_h}^2+1 & -2\,(x_h-y_h\,z_h) \\ -2\,(y_h-x_h\,z_h) & 2\,(x_h+y_h\,z_h) & -{x_h}^2-{y_h}^2+{z_h}^2+1 \end{pmatrix}. \end{aligned} \tag{A.1}$$

Herein $k = {x_h}^2+{y_h}^2+{z_h}^2+1$ and $\mathbf{H}$ is a skew symmetric matrix assembled from parameters x_h, y_h and z_h measured in W. By rearranging Eq. (A.1) can also be solved for $\mathbf{H}$, such that

$$\mathbf{H} = ({}^{W}\mathbf{R}_{B}-\mathbf{E})({}^{W}\mathbf{R}_{B}+\mathbf{E})^{-1}, \tag{A.2}$$

which means that for any given rotation matrix one may find a corresponding skew symmetric matrix.

In fact the vector $\mathbf{h} = (x_h,\, y_h,\, z_h)^T$, also known as the *Rodrigues vector*, represents a direction of the rotation axis, which will be retraced in brief in section A.4. A detailed study on $\mathbf{h}$, that can be found e.g. in [33] pp. 189-190, then yields the important result that $|\mathbf{h}| = \tan\frac{\phi}{2}$, where ϕ is the rotation angle about $\mathbf{h}$. Hence, one may write Rodrigues' vector using a normalized direction $\mathbf{s}$: $\mathbf{h} = \tan\frac{\phi}{2}\mathbf{s}$, which allows to rewrite Eq. (A.1) in terms of the parameters of the rotation axis and ϕ:

$${}^{W}\mathbf{R}_{B}(\phi,\mathbf{s}) = (\mathbf{E}-\tan\frac{\phi}{2}\mathbf{S})^{-1}(\mathbf{E}+\tan\frac{\phi}{2}\mathbf{S}), \tag{A.3}$$

where $\mathbf{S}$ is a skew symmetric matrix assembled from parameters x_s, y_s, z_s. However, retrace that Eq. (A.3) acually requires $\phi \neq \pm\pi$. Following [34], p. 18, Eq. (A.3) may be then expanded to yield *Rodrigues' rotation formula* in terms of a given angle and axis:

$${}^{W}\mathbf{R}_{B}(\phi,\mathbf{s}) = \mathbf{E}+\sin\phi\mathbf{S}+(1-\cos\phi)(\mathbf{S})^2. \tag{A.4}$$

The Cayley map also holds for relative rotations that relates two finitely separated orientations of frame B. In this case one may write: $\mathbf{R}_{B}^{ij} = (\mathbf{E}-\mathbf{H})^{-1}(\mathbf{E}+\mathbf{H})$, where the right superscript at $\mathbf{H}$ can be ignored, because $\mathbf{h}$ actually represents a fixed axis. Using the notation for relative transformations introduced in Eq. (2.4), (A.4) may then be written as

$$\mathbf{R}_{B}^{ij}(\phi^{ij},\mathbf{s}) = \mathbf{E}+\sin\phi^{ij}\mathbf{S}+(1-\cos\phi^{ij})(\mathbf{S})^2, \quad \text{where} \quad \phi^{ij} = \phi^{j}-\phi^{i}. \tag{A.5}$$

A.2. The Standard Form of a Screw

The six-vector representation of the tangent operator introduced in Eq. (2.12), i.e. the velocity of a rigid body, can also be written only in terms of the components of a specific line $\hat{\nu} = (\vec{\nu},\ \mathbf{p}_\nu \times \vec{\nu})^T$, also known as the *instantaneous screw axis*, e.g. [34] pp. 39-40. To see this, decompose the linear velocity $\mathbf{v}$ from Eq. (2.12) into components perpendicular and parallel to $\vec{\omega}$. Letting $\mathbf{v}^\perp$ and $\mathbf{v}^\parallel$ be this perpendicular and parallel component one may write $\mathbf{v} = \mathbf{v}^\perp + \mathbf{v}^\parallel$, where $\mathbf{v}^\parallel$ is easily constructed for any given $\mathbf{v}$ and $\vec{\omega}$ as

$$\mathbf{v}^\parallel = k\vec{\omega}, \quad \text{where} \quad k = \frac{(\mathbf{v})^T \vec{\omega}}{(\vec{\omega})^T \vec{\omega}}. \tag{A.6}$$

Next one may rearrange such that $\mathbf{v}^\perp = \mathbf{v} - k\vec{\omega}$. However, this result for $\mathbf{v}^\perp$ also satisfies the moment $\mathbf{p}_\nu \times \vec{\omega}$, because a point $\mathbf{p}_\nu$ actually exists. To see this, multiply $\mathbf{p}_\nu \times \vec{\omega} = \mathbf{v} - k\vec{\omega}$ on both sides by $\vec{\omega}\times$, apply Grassmanns' identity to the vector triple product on the left hand side and rearrange to obtain

$$\mathbf{p}_\nu = \frac{\vec{\omega} \times \mathbf{v}}{(\vec{\omega})^T \cdot \vec{\omega}}. \tag{A.7}$$

Note, that $\mathbf{p}_\nu$ was taken here directly as a vector perpendicular to $\vec{\omega}$ since this doesn't change the moment. The result is that the linear velocity $\mathbf{v} = \mathbf{t} \times \vec{\omega} + \dot{\mathbf{t}}$ from sect. 2.1.2 may also always be written as $\mathbf{v} = \mathbf{p}_\nu \times \vec{\omega} + k\vec{\omega}$. Substituting this into Eq. (2.12) yields

$$\hat{\mathbf{v}} = (\vec{\omega},\ \mathbf{p}_\nu \times \vec{\omega} + k\vec{\omega})^T = \omega(\vec{\nu},\ \mathbf{p}_\nu \times \vec{\nu} + k\vec{\nu})^T, \tag{A.8}$$

which is known as the *standard form of a screw*. A benefit of this expression is that the tangent operator is written only in terms of the essential screw parameters, $\vec{\omega}$ and $\mathbf{p}_\nu$ as well as the so called pitch k of the screw, which provides a convenient way to introduce screw systems.

A.3. Screw Systems

The standard form of a screw provides a convenient way to introduce screw systems, which are defined as linear combinations of independent screws. Given for instance two screws $\hat{\mathbf{v}}_1$ and $\hat{\mathbf{v}}_2$ the linear combination

$$\hat{\mathbf{v}} = \hat{\mathbf{v}}_1 + \hat{\mathbf{v}}_2 = \omega_1 \begin{pmatrix} \vec{\nu}_1 \\ \mathbf{p}_{\nu_1} \times \vec{\nu}_1 + k_1 \vec{\nu}_1 \end{pmatrix} + \omega_2 \begin{pmatrix} \vec{\nu}_2 \\ \mathbf{p}_{\nu_2} \times \vec{\nu}_2 + k_2 \vec{\nu}_2 \end{pmatrix} \tag{A.9}$$

is called a *two-system*. Similarly three-, four- or five-systems are defined, which are of importance in the kinematic analysis of linkage structures, see sect. 2.2.4. A precise study and classification of screw systems has been provided by Hunt [115].

A.4. The Screw Axis of a Relative Displacement

As already mentioned in the previous sections, rigid displacements in three space may be represented as screw motions, defined by rotation around and a translation along a specific invariant line, called the screw axis. This is retraced in this section for the case of relative displacements, where two spatial poses i and j of a frame B are under consideration. The result is a line, computed from the parameters of such a relative displacement, that is measured in another frame W.

An invariant line $\hat{\mathbf{s}} = (\mathbf{s},\ \mathbf{p}_s \times \mathbf{s})^T$, which is not affected by a spatial displacement of a line, satisfies

$$\hat{\mathbf{s}} = \hat{\mathbf{T}}_B^{ij} \cdot \hat{\mathbf{s}} \qquad \Leftrightarrow \qquad \left(\hat{\mathbf{E}} - \hat{\mathbf{T}}_B^{ij}\right) \cdot \hat{\mathbf{s}} = \hat{\mathbf{0}}, \tag{A.10}$$

where $\hat{\mathbf{E}}$ is a 6×6 identity matrix and $\hat{\mathbf{0}}$ is a 6×1 vector equal to zero. Note that the right superscript at $\hat{\mathbf{s}}$ vanishes because 'not affected' means, that the line remains fixed. The rearranged equation is called the *equation of the screw axis*, which can be expanded into two equations:

$$\left(\mathbf{E} - \mathbf{R}_B^{ij}\right) \cdot \mathbf{s} = \mathbf{0} \quad \text{and} \quad \left(\mathbf{E} - \mathbf{R}_B^{ij}\right) \cdot (\mathbf{p}_s \times \mathbf{s}) - \tilde{\mathbf{t}}_B^{ij} \mathbf{R}_B^{ij} \cdot \mathbf{s} = \mathbf{0}. \tag{A.11}$$

Substituting Cayley's formula for a relative rotation (see sect. A.1) into the first equation simplifies after some rearranging to $\mathbf{H} \cdot \mathbf{s} = \mathbf{0}$, which is clearly satisfied for $\mathbf{s} = \mathbf{h}$, since $\mathbf{H}$ is a skew symmetric matrix. Hence, one can find the direction of the screw axis from the rotational part of the given relative displacement by applying the relative displacement form of Eq. (A.2). Substituting this result into the second equation in (A.11) and taking into account that $\mathbf{R}_B^{ij} \cdot \mathbf{s} = \mathbf{s}$ from the first equation in (A.11) yields

$$\left(\mathbf{E} - \mathbf{R}_B^{ij}\right) \cdot (\mathbf{p}_s \times \mathbf{h}) = \tilde{\mathbf{t}}_B^{ij} \cdot \mathbf{h} =: \mathbf{t}^{\perp}. \tag{A.12}$$

Even though $\det(\mathbf{E} - \mathbf{R}_B^{ij}) = 0$ from the first equation of (A.11) a unique solution for $\mathbf{p}_s \times \mathbf{h}$ exists. This is because the vector $\mathbf{t}^{\perp}$, perpendicular to $\mathbf{h}$ does not have a component in the direction of the null space of $(\mathbf{E} - \mathbf{R}_B^{ij})$. Again substituting Cayley's formula into Eq. (A.12) yields after some rearranging

$$\mathbf{H} \cdot (\mathbf{p}_s \times \mathbf{h}) = \frac{1}{2} (\mathbf{H} - \mathbf{E}) \cdot \mathbf{t}^{\perp} \quad \text{or using vectors} \quad \mathbf{h} \times (\mathbf{p}_s \times \mathbf{h}) = \frac{1}{2} \left(\mathbf{h} \times \mathbf{t}^{\perp} - \mathbf{t}^{\perp}\right). \tag{A.13}$$

Since in fact $\mathbf{p}_s$, locating the screw axis in space, is of rather interest than $\mathbf{p}_s \times \mathbf{h}$ here, one may apply Grassmanns' identity to the vector triple product on the left hand side to solve for $\mathbf{p}_s$:

$$\mathbf{p}_s = \frac{1}{2(\mathbf{h})^T \cdot \mathbf{h}} \left(\mathbf{h} \times \mathbf{t}^{\perp} - \mathbf{t}^{\perp}\right). \tag{A.14}$$

Note that it was forced here, that $\mathbf{p}_s$ is perpendicular to $\mathbf{h}$, i.e. $(\mathbf{p}_s)^T \cdot \mathbf{h} = 0$, which is valid since this does not change the moment of a line. The final result is the screw axis $\hat{\mathbf{s}} = (\mathbf{s},\ \mathbf{p}_s \times \mathbf{s})^T$, where $\mathbf{s} = \mathbf{h}$ for the given rotational part of a spatial displacement. For convenience this is normalized such that $\mathbf{s} = \frac{\mathbf{h}}{|\mathbf{h}|}$ in order to derive a relative displacement in terms of screw parameters.

A.5. Relative Displacements in Terms of Screw Parameters

An important condition for the right hand side of Eq. (A.12) is obtained if one asks directly for the point $\mathbf{p}_s$ instead of the moment $\mathbf{p}_s \times \mathbf{h}$. This amounts to searching for the fixed points of the relative displacement equation (2.5):

$$\left(\mathbf{E} - \mathbf{R}_B^{ij}\right) \cdot \mathbf{p}_s = \grave{\mathbf{t}}^{\perp}. \tag{A.15}$$

The vector $\grave{\mathbf{t}}^{\perp}$ satisfies the following condition:

$$\grave{\mathbf{t}}^{\perp} = -\frac{1}{(\mathbf{h})^T \cdot \mathbf{h}} \mathbf{h} \times \mathbf{h} \times \mathbf{t}_B^{ij} = -\mathbf{s} \times \mathbf{s} \times \mathbf{t}_B^{ij}, \tag{A.16}$$

where $\mathbf{s}$ represents the normalized direction of the screw axis. Eq. (A.16) is easily obtained after substituting Eq. (A.14) and Cayley's formula for $\mathbf{R}_B^{ij}$ into Eq. (A.15) and replacing the skew symmetric matrix $\mathbf{H}$ by $\mathbf{h}\times$. Next, applying Grassmanns' identity to the vector triple product on the right hand side yields

$$\grave{\mathbf{t}}^{\perp} = \mathbf{t}_B^{ij} - s^{ij}\mathbf{s}, \quad \text{, where} \quad s^{ij} = (\mathbf{t}_B^{ij})^T \cdot \mathbf{s}. \tag{A.17}$$

The parameter s^{ij} is called the *slide* of frame B along the screw axis from configuration i to j. It determines the length of a vector $\mathbf{t}^{\parallel} = s^{ij}\mathbf{s}$ parallel to $\mathbf{s}$ and allows a particular classification of a given displacement:

1. A slide $s^{ij} \neq 0$ means a spatial motion and allows it to produce the movement $\mathbf{T}_B^{ij}$ by a rotation around and the slide along $\hat{\mathbf{s}}$.

2. $s^{ij} = 0$ means a non-spatial motion and allows it to produce $\mathbf{T}_B^{ij}$ by a pure rotation about $\hat{\mathbf{s}}$.

Beside this classification, Eq. (A.17) furthermore provides a convenient way to express the translation vector as $\mathbf{t}_B^{ij} = (\mathbf{E} - \mathbf{R}_B^{ij}) \cdot \mathbf{p}_s + s^{ij}\mathbf{s}$, which in turn allows to express a relative displacement in terms of the screw parameters. Together with the angle-axis representation of a rotation matrix, Eq. (A.5), the homogeneous transform in Eq. (2.4) then takes the form:

$$\mathbf{T}_B^{ij}\left(\phi^{ij}, s^{ij}, \hat{\mathbf{s}}\right) = \begin{pmatrix} \mathbf{R}_B^{ij}(\phi^{ij}, \mathbf{s}) & (\mathbf{E} - \mathbf{R}_B^{ij}) \cdot \mathbf{p}_s + s^{ij}\mathbf{s} \\ \mathbf{0}^T & 1 \end{pmatrix}. \tag{A.18}$$

Since now it is clear that the parameters forming the screw axis are actually transforming quantities, it may also be convenient to denote them as $\hat{\mathbf{s}}^{ij} = (\mathbf{s}^{ij},\ \mathbf{p}_s^{ij} \times \mathbf{s}^{ij})^T$ if required. This is particularly the case in sect. 2.3.5 and 4.3.4, where it is necessary to distinguish different relative displacements.

Remark: The fundamental properties of a screw motion actually only differ for the particular cases of *planar*, *spherical* and *spatial motion* and yield the well-known *pole*, the *rotation axis* and the general *screw axis* as the corresponding invariant.

B. Kinematics Equations of Spatial RR Chains

The general spatial 2R serial chain consists of two revolute joints whose joint axes are skew. Hence, its kinematics equations are given by an appropriately modified version of Eq. (2.29). This is obtained by cutting off joints $\hat{\mathbf{c}}$ to $\hat{\mathbf{f}}$ from the general 6R chain in Fig. 2.2 and considering frames W and B being located somewhere in the fixed and in the new end link, connected to the revolute axis $\hat{\mathbf{b}}$, results in

$$ {}^{W}\mathbf{T}_{B} = {}^{W}\mathbf{T}_{1,z}\,{}^{1}\mathbf{T}_{2,x}\,{}^{2}\mathbf{T}_{3,z}\,{}^{3}\mathbf{T}_{4,x}\,{}^{4}\mathbf{T}_{5,z}\,{}^{5}\mathbf{T}_{6,x}\,{}^{6}\mathbf{T}_{B,z}, \tag{B.1} $$

where matrices ${}^{W}\mathbf{T}_{2} = {}^{W}\mathbf{T}_{1,z}\,{}^{1}\mathbf{T}_{2,x}$, ${}^{3}\mathbf{T}_{4,x}$ and ${}^{5}\mathbf{T}_{B} = {}^{5}\mathbf{T}_{6,x}\,{}^{6}\mathbf{T}_{B,z}$ define structural dimensions of the chain.

B.1. Relative Kinematics Equations of Spatial RR Chains

A particularly simplified version of the kinematics equations of a spatial RR chain is required for synthesis (sect. 2.3.5, 4.3 and C.3) and is obtained by introducing relative displacements derived in section 2.1.1, Eq. (2.3). To see this compute $\mathbf{T}_{B}^{ij} = {}^{W}\mathbf{T}_{B}^{j}({}^{W}\mathbf{T}_{B}^{i})^{-1}$ using Eq. (B.1), which yields

$$ \begin{aligned} \mathbf{T}_{B}^{ij} &= ({}^{W}\mathbf{T}_{2}\,{}^{2}\mathbf{T}_{3,z}^{j}\,{}^{3}\mathbf{T}_{4,x}\,{}^{4}\mathbf{T}_{5,z}^{j}\,{}^{5}\mathbf{T}_{B})({}^{W}\mathbf{T}_{2}\,{}^{2}\mathbf{T}_{3,z}^{i}\,{}^{3}\mathbf{T}_{4,x}\,{}^{4}\mathbf{T}_{5,z}^{i}\,{}^{5}\mathbf{T}_{B})^{-1} = \\ &= ({}^{W}\mathbf{T}_{2}\,{}^{2}\mathbf{T}_{3,z}^{j}\,{}^{3}\mathbf{T}_{4,x}\,{}^{4}\mathbf{T}_{5,z}^{j}\,{}^{5}\mathbf{T}_{B})({}^{B}\mathbf{T}_{5}\,{}^{5}\mathbf{T}_{4,z}^{i}\,{}^{4}\mathbf{T}_{3,x}\,{}^{3}\mathbf{T}_{2,z}^{i}\,{}^{2}\mathbf{T}_{W}) = \\ &= {}^{W}\mathbf{T}_{2}\,{}^{2}\mathbf{T}_{3,z}^{j}\,{}^{3}\mathbf{T}_{4,x}\,{}^{4}\mathbf{T}_{5,z}^{j}\,{}^{5}\mathbf{T}_{4,z}^{i}\,{}^{4}\mathbf{T}_{3,x}\,{}^{3}\mathbf{T}_{2,z}^{i}\,{}^{2}\mathbf{T}_{W} = \\ &= {}^{W}\mathbf{T}_{2}\,{}^{2}\mathbf{T}_{3,z}^{j}\,{}^{3}\mathbf{T}_{4,x}\mathbf{T}_{5,z}^{ij}(\phi_{b}^{ij})\,{}^{4}\mathbf{T}_{3,x}\,{}^{3}\mathbf{T}_{2,z}^{i}\,{}^{2}\mathbf{T}_{W}. \end{aligned} \tag{B.2} $$

The homogeneous transform $\mathbf{T}_{5,z}^{ij}(\phi_{b}^{ij})$ has entries measured in frame 4 and describes a relative rotation by an angle ϕ_{b}^{ij} about axis $\hat{\mathbf{b}}$. Recall from Fig. 2.2, that $\hat{\mathbf{b}}$ is nothing but the z-axis of frames 4 and 5. Note that the right superscripts i and j only occur at matrices that describe the joint movement. Next introduce the 4×4 identity $\mathbf{I} = ({}^{2}\mathbf{T}_{3,z}^{i})^{-1}({}^{W}\mathbf{T}_{2})^{-1}{}^{W}\mathbf{T}_{2}\,{}^{2}\mathbf{T}_{3,z}^{i}$ right after the matrix ${}^{2}\mathbf{T}_{3,z}^{j}$ to obtain

$$ \begin{aligned} \mathbf{T}_{B}^{ij} &= {}^{W}\mathbf{T}_{2}\,{}^{2}\mathbf{T}_{3,z}^{j}({}^{2}\mathbf{T}_{3,z}^{i})^{-1}({}^{W}\mathbf{T}_{2})^{-1}{}^{W}\mathbf{T}_{2}\,{}^{2}\mathbf{T}_{3,z}^{i}\,{}^{3}\mathbf{T}_{4,x}\mathbf{T}_{5,z}^{ij}(\phi_{b}^{ij})\,{}^{4}\mathbf{T}_{3,x}\,{}^{3}\mathbf{T}_{2,z}^{i}\,{}^{2}\mathbf{T}_{W} = \\ &= ({}^{W}\mathbf{T}_{2}\mathbf{T}_{3,z}^{ij}(\phi_{a}^{ij})({}^{W}\mathbf{T}_{2})^{-1})({}^{W}\mathbf{T}_{2}\,{}^{2}\mathbf{T}_{3,z}^{i}\,{}^{3}\mathbf{T}_{4,x}\mathbf{T}_{5,z}^{ij}(\phi_{b}^{ij})\,{}^{4}\mathbf{T}_{3,x}\,{}^{3}\mathbf{T}_{2,z}^{i}\,{}^{2}\mathbf{T}_{W}) = \\ &= ({}^{W}\mathbf{T}_{2}\mathbf{T}_{3,z}^{ij}(\phi_{a}^{ij})\,{}^{2}\mathbf{T}_{W})({}^{W}\mathbf{T}_{4}^{i}\mathbf{T}_{5,z}^{ij}(\phi_{b}^{ij})\,{}^{4}\mathbf{T}_{W}^{i}). \end{aligned} \tag{B.3} $$

Expanding the transformation ${}^{W}\mathbf{T}_{2}\mathbf{T}_{3,z}^{ij}(\phi_{a}^{ij})\,{}^{2}\mathbf{T}_{W}$ yields

$$ {}^{W}\mathbf{T}_{2}\mathbf{T}_{3,z}^{ij}(\phi_{a}^{ij})\,{}^{2}\mathbf{T}_{W} = \begin{pmatrix} {}^{W}\mathbf{R}_{2}\mathbf{R}_{3,z}^{ij}(\phi_{a}^{ij})\,{}^{2}\mathbf{R}_{W} & (\mathbf{E} - {}^{W}\mathbf{R}_{2}\mathbf{R}_{3,z}^{ij}(\phi_{a}^{ij})\,{}^{2}\mathbf{R}_{W})\cdot{}^{W}\mathbf{t}_{2} \\ \mathbf{0}^{T} & 1 \end{pmatrix}, \tag{B.4} $$

where the composition ${}^{W}\mathbf{R}_2\mathbf{R}^{ij}_{3,z}(\phi^{ij}_a)^2\mathbf{R}_W$ represents a coordinate transformation of a rotation about the z-axis of frames 2 and 3 (see again Fig. 2.2). When $\mathbf{R}^{ij}_{3,z}$ is written in angle-axis-representation (see Eq. (A.5)) it's easy to see that this transformation only acts on the direction of the rotation axis and yields its coordinates measured in W. Here this is nothing but the direction $\mathbf{a}$ of the fixed axis $\hat{\mathbf{a}} = (\mathbf{a},\ \mathbf{p}_a \times \mathbf{a})^T$, which allows to write Eq. (B.4) as

$$ {}^{W}\mathbf{T}_2\mathbf{T}^{ij}_{3,z}(\phi^{ij}_a)^2\mathbf{T}_W = \mathbf{T}^{ij}_3(\phi^{ij}_a,\hat{\mathbf{a}}) = \begin{pmatrix} \mathbf{R}^{ij}_3(\phi^{ij}_a,\mathbf{a}) & (\mathbf{E}-\mathbf{R}^{ij}_3)\cdot {}^{W}\mathbf{t}_2 \\ \mathbf{0}^T & 1 \end{pmatrix}. \tag{B.5} $$

The translation vector locates $\hat{\mathbf{a}}$ in space and may be written as ${}^{W}\mathbf{t}_2 = \mathbf{p}_a + \lambda\mathbf{a}$, which yields

$$ (\mathbf{E}-\mathbf{R}^{ij}_3)\cdot {}^{W}\mathbf{t}_2 = (\mathbf{E}-\mathbf{R}^{ij}_3)\cdot\mathbf{p}_a + \lambda(\mathbf{E}-\mathbf{R}^{ij}_3)\cdot\mathbf{a}. \tag{B.6} $$

However, the last term satisfies $(\mathbf{E}-\mathbf{R}^{ij}_3)\cdot\mathbf{a} = \mathbf{0}$, since $\mathbf{a}$ represents the rotation axis of $\mathbf{R}^{ij}_3$. Hence, one may simply replace ${}^{W}\mathbf{t}_2$ by $\mathbf{p}_a$ in Eq. (B.5) and compare with Eq. (A.18) to see that this is nothing but a relative displacement in terms of the parameters of the fixed axis of the RR chain.

A similar result is obtained for the second matrix ${}^{W}\mathbf{T}^{i}_4\mathbf{T}^{ij}_{5,z}(\phi^{ij}_b)^4\mathbf{T}^{i}_W$ in Eq. (B.3), which shows that this is nothing but a relative displacement in terms of the parameters of the moving axis of the RR chain in configuration i:

$$ \mathbf{T}^{ij}_5(\phi^{ij}_b,\hat{\mathbf{b}}^i) = \begin{pmatrix} \mathbf{R}^{ij}_5(\phi^{ij}_b,\mathbf{b}^i) & (\mathbf{E}-\mathbf{R}^{ij}_5)\mathbf{p}^i_b \\ \mathbf{0}^T & 1 \end{pmatrix}. \tag{B.7} $$

Using this the relative displacement form of the kinematics equations of a general RR chain take the simple form:

$$ \mathbf{T}^{ij}_B = \mathbf{T}^{ij}_3(\phi^{ij}_a,\hat{\mathbf{a}})\mathbf{T}^{ij}_5(\phi^{ij}_b,\hat{\mathbf{b}}^i). \tag{B.8} $$

Eq. (B.8) can be used to describe the movement of the end effector of a RR chain with respect to a reference configuration i and will be used in sect. C.3. By straight forward extending the approach shown here also relative kinematics equations of chains with more than two joints can be derived.

C. Algebraic Solutions of Finite Position RR Synthesis

This chapter provides specific algebraic solution procedures that are particularly required in sect. 4.3.3 and 4.3.4. The procedures correspond to the four-position synthesis problem of planar and spherical RR chains as well as the three-position synthesis of spatial RR chains. However, due to the fact that the spatial synthesis solution procedure is more extensive and complex than the planar and spherical counterparts this problem is only considered roughly in the corresponding section. More detailed derivations may be found in [30]. A fundamental reference providing a unified treatment of the algebraic finite position synthesis theory is [33].

C.1. Four-Position Synthesis of Planar RR Chains

The synthesis of a planar RR chain whose end links may reach four arbitrarily prescribed (planar) poses requires the solution of a set of three bilinear design equations (2.47):

$$(\mathbf{p}_b^1)^T \cdot \mathbf{M}^{1i} \cdot \mathbf{p}_a^1 + (\vec{\lambda}^{1i})^T \cdot \mathbf{p}_b^1 + (\vec{\mu}^{1i})^T \cdot \mathbf{p}_a^1 + \delta^{1i} = 0, \quad i = 2,3,4. \tag{C.1}$$

Recall from sect. 2.3.2 that (i) 2×1 vectors $\mathbf{p}_b^1$ and $\mathbf{p}_a^1$ are the unknown W-frame coordinates that define the location of the two R joints in configuration 1 of the chain and (ii) the parameters $\mathbf{M}^{1i}$, $\vec{\lambda}^{1i}$, $\vec{\mu}^{1i}$ and δ^{1i} are given in terms of position data.

In order to solve Eq. (C.1) for the unknowns it is convenient to rearrange, such that

$$\underbrace{\left((\mathbf{p}_b^1)^T \cdot \mathbf{M}^{1i} + (\vec{\mu}^{1i})^T\right)}_{\left((a^i(\mathbf{p}_b^1)\ b^i(\mathbf{p}_b^1)\right)} \cdot \mathbf{p}_a^1 = \underbrace{-\left((\vec{\lambda}^{1i})^T \cdot \mathbf{p}_b^1 + \delta^{1i}\right)}_{r^i(\mathbf{p}_b^1)}, \quad i = 2,3,4. \tag{C.2}$$

This is a linear system of equation, which may also be written as

$$\underbrace{\begin{pmatrix} a^2(\mathbf{p}_b^1) & b^2(\mathbf{p}_b^1) \\ a^3(\mathbf{p}_b^1) & b^4(\mathbf{p}_b^1) \\ a^4(\mathbf{p}_b^1) & b^4(\mathbf{p}_b^1) \end{pmatrix}}_{\mathbf{K}} \cdot \underbrace{\begin{pmatrix} x_{p_a}^1 \\ y_{p_a}^1 \end{pmatrix}}_{\mathbf{p}_a^1} = \underbrace{\begin{pmatrix} r^2(\mathbf{p}_b^1) \\ r^3(\mathbf{p}_b^1) \\ r^4(\mathbf{p}_b^1) \end{pmatrix}}_{\mathbf{v}}. \tag{C.3}$$

For this linear system to have a solution the augmented coefficient matrix $(\mathbf{K}|\mathbf{v})$ must satisfy $\mathrm{Rg}(\mathbf{K}|\mathbf{v}) \leq 2$. Another way of saying this is that the determinant of $(\mathbf{K}|\mathbf{v})$ must satisfy

$$\det(\mathbf{K}|\mathbf{v}) = 0. \tag{C.4}$$

This yields a cubic polynomial in the W-frame coordinates $\mathbf{p}_b^1$, which may be written as

$$\begin{aligned} \det(\mathbf{K}|\mathbf{v}) \quad = \quad & k_1 \cdot \left(y_{p_b}^1\right)^3 + \left(k_2 \cdot x_{p_b}^1 + k_3\right) \cdot \left(y_{p_b}^1\right)^2 + \left(k_4 \cdot \left(x_{p_b}^1\right)^2 + k_5 \cdot x_{p_b}^1 + k_6\right) \cdot y_{p_b}^1 + \\ & + k_7 \cdot \left(x_{p_b}^1\right)^3 + k_8 \cdot \left(x_{p_b}^1\right)^2 + k_9 \cdot x_{p_b}^1 + k_{10} = 0. \end{aligned} \tag{C.5}$$

Any point $\mathbf{p}_b^1$ on this cubic curve may be chosen as a R joint of the planar RR chain. This may be done by selecting an arbitrary $x_{p_b}^1$ and afterwards solving the polynomial for $y_{p_b}^1$. The result may be as many as three real solutions, since the polynomial is of order three. Substituting a resulting $\mathbf{p}_b^1$ into Eq. (C.3) allows to solve for the remaining $\mathbf{p}_a^1$, which describes the second R joint of the planar RR chain that can reach the four initially prescribed planar poses.

Remark: In the case of five given planar poses of the end links of a planar RR chain there are four design equations, which can be reduced to a single univariate polynomial of order four, see e.g. [33], pp. 108-109. This may have zero, two or either four real solutions, which correspond to either zero, two or four different planar RR chains that can reach the given set of poses.

C.2. Four-Position Synthesis of Spherical RR Chains

The synthesis of a spherical RR chain whose end links may reach four arbitrarily prescribed spatial orientations requires the solution of a set of three bilinear design equations (2.52):

$$(\mathbf{b}^1)^T \cdot \mathbf{M}^{1i} \cdot \mathbf{a}^1 = 0, \quad i = 2,3,4. \tag{C.6}$$

Recall from sect.2.3.4 that (i) 3×1 vectors $\mathbf{a}^1 = (x_a^1, y_a^1, z_a^1)^T$ and $\mathbf{b}^1 = (x_b^1, y_b^1, z_b^1)^T$ are the unknown W-frame coordinates that define the orientation of the two R joints in configuration 1 of the chain and (ii) the matrices $\mathbf{M}^{1i}$ are given in terms of position data.

For convenience Eq. (C.6) is rewritten as

$$(a^i(\mathbf{b}^1)\; b^i(\mathbf{b}^1)\; c^i(\mathbf{b}^1)) \cdot \mathbf{a}^1 = 0, \quad i = 2,3,4, \tag{C.7}$$

where $(a^i(\mathbf{b}^1)\; b^i(\mathbf{b}^1)\; c^i(\mathbf{b}^1)) = (\mathbf{b}^1)^T \cdot \mathbf{M}^{1i}$. This is a linear homogeneous system of equations, which may also be written as

$$\underbrace{\begin{pmatrix} a^2(\mathbf{b}^1) & b^2(\mathbf{b}^1) & c^2(\mathbf{b}^1) \\ a^3(\mathbf{b}^1) & b^3(\mathbf{b}^1) & c^3(\mathbf{b}^1) \\ a^4(\mathbf{b}^1) & b^4(\mathbf{b}^1) & c^4(\mathbf{b}^1) \end{pmatrix}}_{\mathbf{K}} \cdot \underbrace{\begin{pmatrix} x_a^1 \\ y_a^1 \\ z_a^1 \end{pmatrix}}_{\mathbf{a}^1} = \begin{pmatrix} 0 \\ 0 \\ 0 \end{pmatrix}. \tag{C.8}$$

For this to have a solution other than $\mathbf{a}^1 = \mathbf{0}$ the matrix $\mathbf{K}$ must satisfy $\mathrm{Rg}(\mathbf{K}) \leq 2$, which is equivalent to saying that the determinant of $\mathbf{K}$ must satisfy

$$\det(\mathbf{K}) = 0. \tag{C.9}$$

This yields a cubic polynomial in the coordinates of $\mathbf{b}^1$, which is the equation of a surface through the origin of W. The polynomial is furthermore homogeneous, because each monomial is of order three:

$$\begin{aligned} \det(\mathbf{K}) \;=\; & k_1 \cdot \left(y_b^1\right)^3 + \left(k_2 \cdot x_b^1 + k_3 \cdot z_b^1\right) \cdot \left(y_b^1\right)^2 + \left(k_4 \cdot \left(x_b^1\right)^2 + k_5 \cdot x_b^1 \cdot z_b^1 + k_6 \cdot \left(z_b^1\right)^2\right) \cdot y_b^1 + \\ & + k_7 \cdot \left(x_b^1\right)^3 + k_8 \cdot \left(x_b^1\right)^2 \cdot z_b^1 + k_9 \cdot x_b^1 \cdot \left(z_b^1\right)^2 + k_{10} \cdot \left(z_b^1\right)^3 = 0. \end{aligned} \tag{C.10}$$

However, homogeneity means that if a certain $\mathbf{b}^1$ solves Eq. (C.10), then $\lambda \mathbf{b}^1$, $\lambda \in \mathbb{R}$, is a solution as well. This identifies Eq. (C.10) as the equation of a ruled surface through the origin of W - a cubic cone.

In order to find coordinates $\mathbf{b}^1$ that solve Eq. (C.10) one may set $z_b^1 = 1$, which yields the equation of a cubic curve similar to that, obtained from four-position synthesis of planar RR

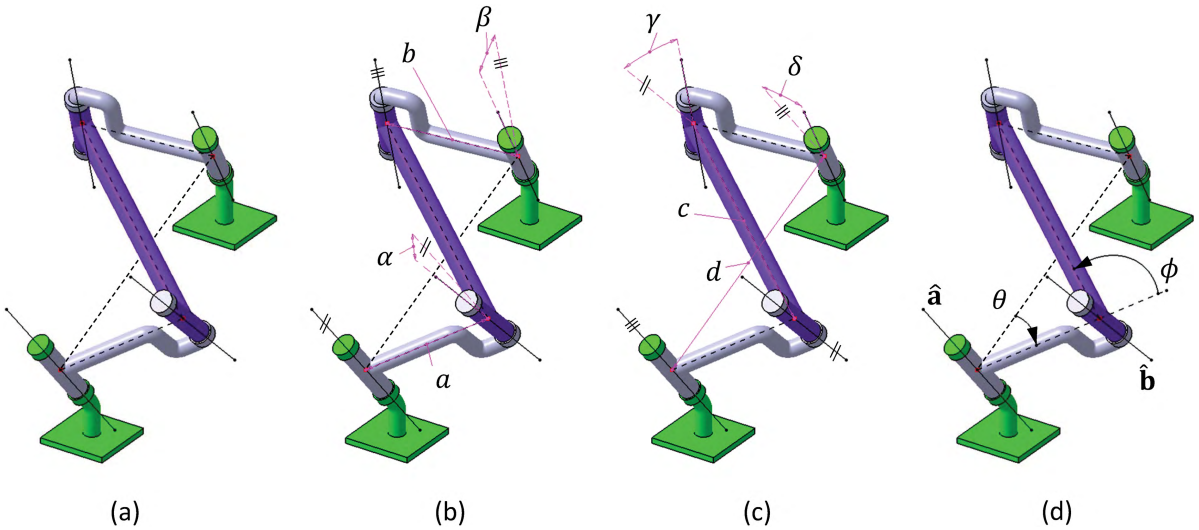

Figure C.1.: Properties of the Bennett Linkage: (a) four revolute joint axes with intersecting adjacent common normals (b), (c) opposite sides as well as opposite twist angles measured between the different joint axes must be equal (d) Angles that describe the joint movement and which are measured among normals

chains. In fact this is the curve of intersection between a plane through $z_b^1 = 1$ and the cubic cone Next, selecting an arbitrary x_b^1 and afterwards solving the polynomial for y_b^1 may yield as many as three real solutions for $\mathbf{b}^1$. Substituting a resulting $\mathbf{b}^1$ into Eq. (C.8) allows to solve for the remaining $\mathbf{a}^1$, which describes the second R joint of the spherical RR chain that can reach the four initially prescribed spatial orientations.

Remark: In the case of five given orientations of the end links of a spherical RR chain there are four design equations, which can be reduced to a single univariate polynomial of order six, see e.g. [33], pp. 221-222. This may have zero, two, four or either six real solutions, which correspond to either zero, two, four or six different spherical RR chains that can reach the given set of orientations.

C.3. Bennett's Spatial Four-Bar Linkage and the Cylindroid

As already mentioned in the introduction of sect. 2.3.5 an algebraic solution procedure of the polynomial design equations (2.55), (2.57) and (2.59) yields that there exist two spatial RR chains for three specified task poses of frame B, which together form a Bennett four-bar linkage. Figure C.1 shows a Bennett linkage, which in fact is just the one determined in sect. 4.3.4 and which satisfies several geometric conditions in order to provide single-d.o.f. movement [13].

As shown in Fig. C.1a) the consecutive common normals between the joint axes intersect. Next, opposite sides as well as opposite twist angles measured between the different joint axes must be equal, i.e. $a = b$, $c = d$, $\alpha = \beta$ and $\gamma = \delta$ (Fig. C.1 b) and c)). Furthermore, these parameters satisfy

$$\frac{\sin\alpha}{a} = \frac{\sin\gamma}{c} \qquad \text{or} \qquad \frac{\sin\beta}{b} = \frac{\sin\delta}{d}. \tag{C.11}$$

Through these conditions it can be shown that a Bennett linkage moves with mobility 1. Based on the parameters it can be shown that the linkage satisfies the following angular relationship

between the angles θ and ϕ (Fig. C.1 d)), [115]:

$$\tan\frac{\phi}{2} = k\tan\frac{\theta}{2}, \qquad \text{where} \qquad k = \frac{\sin\frac{\alpha+\gamma}{2}}{\sin\frac{\alpha-\gamma}{2}}. \tag{C.12}$$

A single spatial RR chain with axes $\hat{\mathbf{a}}$ and $\hat{\mathbf{b}}$ whose joint movement is constrained to follow this relationship is also called a mechanically constrained spatial RR chain since its movement is determined by a mechanical transmission relationship. In the case of a given angle θ this means that the rotation around $\hat{\mathbf{b}}$ is determined as $\phi(\theta)$ obtained from Eq. (C.12). For relative rotations with respect to a specific reference configuration 1 this yields $\theta^{1i} = \theta^i - \theta^1$ and $\phi^{1i} = \phi^i(\theta^i) - \phi^1(\theta^1)$. The relative kinematics equations of the mechanically constrained spatial RR chain may then be written in terms of the fixed and moving axis as

$$\begin{aligned} \mathbf{T}_B^{1i} &= \mathbf{T}^{1i}\left(\theta^{1i}, \hat{\mathbf{a}}\right)\mathbf{T}^{1i}\left(\phi^{1i}, \hat{\mathbf{b}}^1\right) = \\ &= \begin{pmatrix} \mathbf{R}^{1i}(\theta^{1i}, \mathbf{a}) & (\mathbf{E} - \mathbf{R}^{1i})\mathbf{p}_a \\ \mathbf{0}^T & 1 \end{pmatrix} \begin{pmatrix} \mathbf{R}^{1i}(\phi^{1i}, \mathbf{b}^1) & (\mathbf{E} - \mathbf{R}^{1i})\mathbf{p}_b^1 \\ \mathbf{0}^T & 1 \end{pmatrix}, \end{aligned} \tag{C.13}$$

where $i = 2, \ldots, n$. (See section B.1 , Eq. (B.2) to (B.8) for a detailed derivation of these equations). Recall here, that positions of B are measured with respect to a given world frame W.

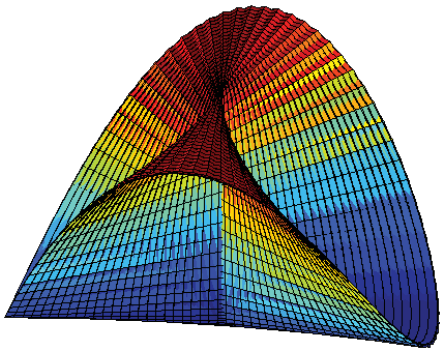

Figure C.2.: Qualitative example of a cylindroid

For given line screws $\hat{\mathbf{a}}$ and $\hat{\mathbf{b}}^1$ as well as a given and calculated set of angles θ^{1i} and ϕ^{1i} Eq. (C.13) results in a set of matrices with numerical values on the left hand side. Using the procedure from sect. A.4 yields a corresponding set of screw axes $\hat{\mathbf{s}}^{1i}$, which, due to relation (C.12), form a cylindroid, [116]. Figure C.2 provides an example of this ruled surface, which can be obtained by rotating and translating a line around and along another perpendicular line. A particular feature of this surface is that two generators intersect at right angles just in the middle of the perpendicular line, which allows the definition of a specific coordinate frame known as the *principal axis frame*.

The fundamental property of a principal axis frame H of a cylindroid, generated from the relative screw axes of Bennett's linkage, is, that joint axes $\hat{\mathbf{a}}$ and $\hat{\mathbf{b}}^1$ in a RR chain can be described using four parameters, measured in H, [30]. In the case of a three-position synthesis of a RR chain these parameters are unknown and the reduction of the number of unknowns from ten to four synthesis parameters corresponds to the fact that the six normal constraints from Eq. (2.59) are identically satisfied. However, since H is not a priori given, the key step for synthesis is to find the location and orientation of this frame relative to W, based on the given three positions of frame B. This can be done following Hunt [115], who derives that a cylindroid can be seen as any possible linear combination of two screws (a two-system) and who shows how to obtain H for two such given screws. In fact, because two screws can be associated with the the relative transform $\mathbf{T}_B^{12}$ and $\mathbf{T}_B^{13}$ of the three task poses of the spatial RR synthesis problem one may find H.

In order to solve the four design equations (2.55) and (2.57), measured in H, the motion parameters $\mathbf{R}_B^{1i}$ and $\mathbf{s}^{1i}$, originally measured in W, need to be transformed, such that they correspond to the movement of B measured in H. Assuming that the location and orientation of

principal axis frame H with respect to W is known this is easily done using the composition

$$ {}^{H}\mathbf{T}_{B}^{i} = \left({}^{W}\mathbf{T}_{H}\right)^{-1} {}^{W}\mathbf{T}_{B}^{i}, \quad i = 1,2,3 \tag{C.14} $$

Note that ${}^{W}\mathbf{T}_{H}$ has no right superscript since W and H are fixed. Afterwards computing the relative displacement using Eq. (2.4) yields $\mathbf{T}_{B}^{1i}$, $i = 2,3$, measured in H. The rotational submatrix of this homogeneous transform can then be substituted into Eq. (2.55). Next, computing the Rodriguez vectors $\mathbf{h}^{12}$ and $\mathbf{h}^{12}$ from this rotation using Eq. (A.2) allows to compute $\mathbf{s}^{12} = \frac{\mathbf{h}^{12}}{|\mathbf{h}^{12}|}$ and $\mathbf{s}^{13} = \frac{\mathbf{h}^{13}}{|\mathbf{h}^{13}|}$ measured in H. $\mathbf{s}^{1i}$ can then be substituted into Eq. (2.57). This together with Eq. (2.55) can then be solved for the four independent design parameters of the spatial RR chain chain.

The cylindroid-based three-position synthesis can be found in detail in [30], where also an algebraic elimination procedure is presented that reduces the four design equations to an univariate polynomial of order 3. This has only one single real root, which corresponds to two four-parameter sets, which represent two different spatial RR chains. These together form a Bennett linkage that can reach the three task positions The approach with corresponding screw axes $\hat{\mathbf{s}}^{12}$ and $\hat{\mathbf{s}}^{13}$, principal axis frame H and one of the RR solutions are required in the synthesis procedure of a spherically constrained spatial RR chain in sect. 4.3.4.

Bibliography

[1] Reuleaux, F. *Lehrbuch der Kinematik, Erster Band: Theoretische Kinematik. Grundzüge einer Theorie des Maschinenwesens*. Braunschweig: Vieweg und Sohn, 1875, p. 38.

[2] Reuleaux, F. *The Kinematics of Machinery - Outlines of a Theory of Machines*. London: Macmillan and Co., 1876, p. 35.

[3] Joskowitz, L. and McCarthy, J. M. *Formal Engineering Design Synthesis, Chapter 8: Kinematic Synthesis*. Cambridge: Cambridge University Press, 2005.

[4] Luck, K. and Modler, K.-H. *Getriebetechnik - Analyse, Synthese, Optimierung, 2. Auflage*. Berlin Heidelberg: Springer, 1995.

[5] Sandor, G. N. and Erdman, A. G. *Advanced Mechanism Design: Analysis and Synthesis, Vol. 2*. New Jersey: Prentice Hall, Inc., Englewood Cliffs, 1987.

[6] Kerle, H., Pittschellis, R., and Corves, B. *Einführung in die Getriebelehre*. Wiesbaden: Teubner, 2007.

[7] Uicker, J. J., Pennock, G. R., and Shigley, J. E. *Theory of Machines and Mechanisms*. Oxford: Oxford University Press, 2003.

[8] Hosemann, W.-G. *Minimally Invasive Endonasal Sinus Surgery*. Stuttgart, Germany: Thieme, 2000.

[9] Krinninger, M. et al. "The Kinematic Design of a new Endoscope Manipulator System (EMS) for Functional Endoscopic Sinus Surgery and Familiar Techniques in ENT Surgery". In: *IFMBE Proceedings 25/VI*. Ed. by O. Doessel and W. Schlegel. Springer, London, 2009, pp. 267–270.

[10] Corves, B. and Niggemann, H. "CAD-gestützte, grafische Maßsynthese sphärischer und räumlicher Übertragungskurvengetriebe mit dem Programm CADiS". In: *VDI Bewegungstechnik Berichte Nr. 1845*. VDI-Verlag, Duesseldorf, 2004, pp. 145–167.

[11] Mlinar, J. R. and Erdman, A. G. "An Introduction to Burmester Field Theory". In: *ASME Journal of Mechanical Design* 122 (2000), pp. 25–30.

[12] Mavroidis, C. and Roth, B. "Analysis of Overconstrained Mechanisms". In: *ASME Journal of Mechanical Design* 117.1 (1995), pp. 69–74.

[13] Bennett, G. T. "The Skew Isogram-Mechanism". In: *Proceedings of the London Mathematical Society* 13 (1913), pp. 151–173.

[14] Delassus, E. "Les chaînes articulées fermées et déformables à quatre membres". In: *Bulletin des Sciences Mathématiques, 2nd series* 46 (1922), pp. 283–304.

[15] Bricard, R. *Leçons de cinématique, Vol. 2*. Paris: Gauthier-Villars, 1927.

[16] Myard, F. E. "Contribution à la géométrie des systèmes articulés". In: *Bulletin de la Société Mathématique de France* 59 (1931), pp. 183–210.

[17] Goldberg, M. "New Five-Bar and Six-Bar Linkages in Three Dimensions". In: *Transactions of the ASME* 65 (1943), pp. 649–661.

[18] Sarrus, P. T. “Note sur la transformation des mouvements rectilignes alternatifs, en mouvements circulaires; et réciproquement”. In: *Comptes Rendus Hebdomadaires des Séances de I’Académie des Sciences, Paris* 36 (1853), pp. 1036–1038.

[19] Tachi, T. “Geometric Considerations for the Design of Rigid Origami Structures”. In: *Proc. of the int. assoc. for shell and spatial struct.* 2010.

[20] Stavric, M. and Wiltsche, A. “Investigations on Quadrilateral Patterns for Rigid Folding Structures”. In: *Open Systems: Proceedings of the 18th International Conference on Computer-Aided Architectural Design Research in Asia (CAADRIA 2013)*. Ed. by R. Stouffs et al. CAADRIA, 2013, pp. 893–902.

[21] Miura, K. and Natori, M. “2-D Array Experiment on Board a Space Flyer Unit”. In: *Space Solar Power Rev.* 5 (1985), pp. 345–356.

[22] Greenberg, H. C. et al. “Identifying Links Between Origami and Compliant Mechanisms”. In: *Mechanical Sciences open access* 2 (2011), pp. 217–225.

[23] Schenk, M. and Guest, S. D. “Geometry of Miura-folded meta materials”. In: *Proceedings of the National Academy of Sciences of the United States of America* 110.9 (2013), pp. 3276–3281.

[24] Su, H.-J. et al. “Design and Fabrication of DNA Origami Mechanisms and Machines”. In: *Advances in Reconfigurable Mechanisms and Robots I*. Ed. by J. S. Dai, M. Zoppi, and X. Kong. Springer, 2012, pp. 487–500.

[25] You, Z. and Kuribayashi, K. “A Novel Origami Stent”. In: *Proceedings of the 2003 Summer Bioengineering Conference*. 2003, pp. 257–258.

[26] Lee, D.-Y. et al. “The Deformable Wheel Robot Using Magic-Ball Origami Structure”. In: *ASME 2013 International Design Engineering Technical Conferences, 37th Mechanisms and Robotics Conference, Parts A and B*. ASME, 2013, p. 9.

[27] Felton, S. et al. “A Method for Building Self-Folding Machines”. In: *Science* 345.6197 (2014), pp. 644–646.

[28] Tachi, T. “Generalization of Rigid Foldable Quadrilateral Mesh Origami”. In: *Proc. of the int. assoc. for shell and spatial struct.* Ed. by A. Domingo and C. Lazaro. 2009.

[29] Tsai, L.-W. and Roth, B. “A Note on the Design of Revolute-Revolute Cranks”. In: *Mechanism and Machine Theory* 8.1 (1973), pp. 23–31.

[30] Perez, A. and McCarthy, J. M. “Dimensional Synthesis of Bennett Linkages”. In: *ASME Journal of Mechanical Design* 125.1 (2003), pp. 98–104.

[31] Brunnthaler, K., Schröcker, H.-P., and Husty, M. “A New Method for the Synthesis of Bennett Mechanisms”. In: *Proc. of CK2005, Int. Workshop on Computational Kinematics*. Cassino, 2005.

[32] Hegedüs, G., Schicho, J., and Schröcker, H.-P. “Four-Pose Synthesis of Angle-Symmetric 6R Linkages - Accepted Manuscript”. In: *ASME Journal of Mechanisms and Robotics* (2015).

[33] McCarthy, J. M. and Soh, G. S. *Geometric design of linkages, 2nd edition*. New York: Springer Interdisciplinary Applied Mathematics, 2010.

[34] McCarthy, J. M. *An Introduction to Theoretical Kinematics*. Cambridge, Massachusetts London, England: The MIT Press, 1990.

[35] Beyer, R. *Technische Raumkinematik, Lehr- Hand- und Übungsbuch zur Analyse räumlicher Getriebe*. Berlin Göttingen Heidelberg: Springer Verlag, 1963.

[36] Ball, R. S. *The Theory of Screws: A study in the dynamics of a rigid body*. Dublin, Ireland: Dublin Hodges, 1876.

[37] Dimentberg, F. M. *The Screw Calculus and Its Applications in Mechanics*. Virginia, US: English trans. AD680993,Clearing House for Federal Technical and Scientific Information, 1965.

[38] Davies, T. H. "Kirchhoff's Circulation Law Applied to Multi-Loop Kinematic Chains". In: *Mechanism and Machine Theory* 16.3 (1981), pp. 171–183.

[39] Backer, J. E. "On Mobility and Relative Freedoms in Multiloop Linkages and Structures". In: *Mechanism and Machine Theory* 16.6 (1981), pp. 583–597.

[40] Kong, X. and Gosselin, C. *Type Synthesis of Parallel Mechanisms*. New York: Springer, 2007.

[41] Wohlhart, K. "Screw Spaces and Connectivities in Multiloop Linkages". In: *On Advances in Robot Kinematics*. Ed. by J. Lenarčič and C. Galletti. Kluwer Academic Publishers, Netherlands, 2004, pp. 97–104.

[42] Gogu, G. *Structural Synthesis of Parallel Robots, Part 1: Methodology*. New York: Springer, 2008.

[43] Stachel, H. "On the Flexibility and Symmetry of Overconstrained Mechanisms". In: *Philos Trans R. Soc. A* 372.2008 (2013).

[44] Husty, M. "An Algorithm for Solving the Direct Kinematics of General Steward-Gough Platforms". In: *Mechanism and Machine Theory* 31.4 (1996), pp. 365–380.

[45] Wampler, C. W. "Displacement Analysis of Spherical Mechanisms Having Three or Fewer Loops". In: *ASME Journal of Mechanical Design* 1.126 (2004), pp. 93–100.

[46] Denavit, J. and Hartenberg, R. S. *Kinematic Synthesis of Linkages*. New York: McGraw Hill, 1964.

[47] Hao, F. and McCarthy, J. M. "Conditions for Line-Based Singularities in Spatial Platfrom Manipulators". In: *Journal of Robotics Systems* 15.1 (1998), pp. 43–55.

[48] Dandurand, A. "The Rigidity of Compound Spatial Grids". In: *Structural Topology* 10 (1984), pp. 43–55.

[49] Merlet, J. P. "Singular Configurations of Parallel Manipulators and Grassmann Geometry". In: *The International Journal of Robotics Research* 8.5 (1989), pp. 45–56.

[50] Roth, B. "Finite-Position Theory Applied to Mechanism Synthesis". In: *ASME Journal of Applied Mechanics* 34.3 (1967), pp. 599–605.

[51] Suh, C. H. and Radcliff, C. W. *Kinematics and Mechanism Design*. New York: John Wiley and Sons, 1978.

[52] Abdul-Sater, K., Lueth, T. C., and Irlinger, F. "Computer-Aided, Task-Based Kinematic Design of Linkages - A New Lecture for Engineering Students". In: *New Trends in Mechanism and Machine Science*. Ed. by P. Flores and F. Viadero. Springer, 2014, pp. 891–899.

[53] Freudenstein, F. and Sandor, G. "Synthesis of a Path Generating Mechanism by Means of a Programmed Digital Computer". In: *ASME Journal of Engineering for Industry* 81 (1956), pp. 159–168.

[54] McLarnan, C. W. “Synthesis of Six-Link Plane Mechanisms by Numerical Analysis”. In: *ASME Journal of Engineering for Industry* 85.1 (1963), pp. 5–10.

[55] Plecnik, M. M. and McCarthy, J. M. “Numerical Synthesis of Six-Bar Linkages for Mechanical Computation”. In: *ASME Journal of Mechanisms and Robotics* 6.3 (2014), p. 12.

[56] Plecnik, M. M., McCarthy, J. M., and Wampler, C. W. “Kinematic Synthesis of a Watt 1 Six-Bar Linkage for Body Guidance”. In: *Advances in Robot Kinematics*. Ed. by J. Lenarčič and O. Khatib. Springer International Publishing, Switzerland, 2014, pp. 317–325.

[57] Perez, A. and McCarthy, J. M. “Dual Quaternion Synthesis of Constrained Robotic Sytems”. In: *ASME Journal of Mechanical Design* 126.3 (2004), pp. 425–435.

[58] Perez, A. and McCarthy, J. M. “Geometric Design of RRP, RPR and PRR Serial Chains”. In: *Mechanism and Machine Theory* 40.11 (2005), pp. 1294–1311.

[59] Innocenti, C. “Polynomial Solution of the Spatial Burmester Problem”. In: *ASME Journal of Mechanical Design* 70 (1994), pp. 161 –166.

[60] Veldkamp, G. R. “Canonical Systems and Instantaneous Invariants in Spatial Kinematics”. In: *Mechanism and Machine Theory* 2.3 (1967), pp. 329–388.

[61] Suh, C. H. “On the Duality in the Existence of R-R Links for Three Positions”. In: *ASME Journal of Manufacturing Science and Engineering* 91.1 (1969), pp. 129–134.

[62] Huang, C. “The Cylindroid Assciated with Finite Motions of the Bennett Mechanism”. In: *ASME Journal of Mechanical Design* 119.4 (1997), pp. 521–524.

[63] Tsai, L.-W. and Roth, B. “Design of Dyads with Helical, Cylindrical, Spherical, Revolute, and Prismatic Joints”. In: *Mechanism and Machine Theory* 7.1 (1972), pp. 85–102.

[64] Plecnik, M. M. and McCarthy, J. M. “Design of a 5-SS Spatial Steering Linkage”. In: *ASME 2012 International Design Engineering Technical Conferences, 36th Mechanisms and Robotics Conference, Parts A and B*. ASME, 2012, pp. 725–735.

[65] Soh, G. S. and McCarthy, J. M. “The Synthesis of Six-bar Linkages as Constrained Planar 3R Chains”. In: *Mechanism and Machine Theory* 40.2 (2008), pp. 160–170.

[66] Soh, G. S., Ying, F., and McCarthy, J. M. “Dimensional Synthesis of Planar Six-Bar Linkages by Mechanically Constrain a PRR Serial Chain”. In: *ASME 2012 International Design Engineering Technical Conferences, 36th Mechanisms and Robotics Conference, Parts A and B*. ASME, 2012, pp. 551–557.

[67] Plecnik, M. M. and McCarthy, J. M. “Dimensional Synthesis of Six-Bar Linkage as a Constrained RPR Chain”. In: *New Trends in Mechanism and Machine Science, Theory and Applications in Engineering*. Ed. by F. Viadero and M. Ceccarelli. Springer, 2013, pp. 273–280.

[68] Sonawale, K. H., Arredondo, A., and McCarthy, J. M. “Computer-Aided Design of Useful Spherical Watt 1 Six-Bar Linkages”. In: *ASME 2013 International Design Engineering Technical Conferences, 37th Mechanisms and Robotics Conference, Parts A and B*. ASME, 2013, p. 7.

[69] Soh, G. S. and McCarthy, J. M. “Seven-Position Synthesis of a Spatial Eight-Bar Linkage by Constraining a TRS Serial Chain”. In: *ASME 2009 International Design Engineering Technical Conferences, 33th Mechanisms and Robotics Conference*. ASME, 2009, pp. 577–584.

[70] Krovi, V., Ananthasuresh, G. K., and Kumar, V. “Kinematic and Kinetostatic Synthesis of Planar Coupled Serial Chain Mechanisms”. In: *ASME Journal of Mechanical Design* 124.2 (2002), pp. 301–312.

[71] Soh, G. S. and Ying, F. “Dimensional Synthesis of Planar Eight-Bar Linkages Based on a Parallel Robot With a Prismatic Base Joint”. In: *ASME 2013 International Design Engineering Technical Conferences, 37th Mechanisms and Robotics Conference, Parts A and B*. ASME, 2013, p. 8.

[72] Soh, G. S. and McCarthy, J. M. “Parametric Design of a Spherical Eight-Bar Linkage Based on a Spherical Parallel Manipulator”. In: *ASME Journal of Mechanisms and Robotics* 43.2 (2008), pp. 160–170.

[73] Larochelle, P. “Synthesis of Spatial CC Dyads and 4C Mechanisms for Pick-and-Place Tasks with Guiding Locations”. In: *Latest Advances in Robot Kinematics*. Ed. by J. Lenarčič and M. Husty. Springer, Netherlands, 2012, pp. 437–444.

[74] Bai, S. and Angeles, J. “Synthesis of RCCC Linkages to Visit Four Given Poses”. In: *ASME Journal of Mechanisms and Robotics* 7.3 (2015), p. 9.

[75] Waldron, K. J. “Overconstrained Linkage Geometry by Solution of Closure Equations - Part 1. Method of Study”. In: *Mechanism and Machine Theory* 8.1 (1973), pp. 94–104.

[76] Baker, J. E. “An Analysis of the Bricard Linkages”. In: *Mechanism and Machine Theory* 15.4 (1980), pp. 267–286.

[77] Baker, J. E. “On 5-Revolute Linkages with Parallel Adjacent Joint Axes”. In: *Mechanism and Machine Theory* 19.6 (1984), pp. 467–475.

[78] Deng, Z. et al. “Synthesis of Deployable/Foldable Single Loop Mechanisms With Revolute Joints”. In: *ASME Journal of Mechanisms and Robotics* 3.3 (2011), p. 12.

[79] Viquerat, A. D., Hutt, T., and Guest, S. D. “A Plane Symmetric 6R Foldable Ring”. In: *Mechanism and Machine Theory* 63.1 (2013), pp. 73–88.

[80] Baker, J. E. “A Collapsible Network of Similar Pairs of Nested Bennett Linkages”. In: *Mechanism and Machine Theory* 59.1 (2013), pp. 119–124.

[81] Wei, G. and Dai, J. S. “Reconfigurable and Deployable Platonic Mechanisms with a Variable Revolute Joint”. In: *Latest Advances in Robot Kinematics*. Ed. by J. Lenarčič and O. Khatib. Springer International Publishing, Switzerland, 2014, pp. 485–495.

[82] Tachi, T. “Freeform Variations of Origami”. In: *Journal for Geometry and Graphics* 14.2 (2010), pp. 203–215.

[83] Perez-Gracia, A. “Synthesis of Spatial RPRP Closed Linkages for a Given Screw System”. In: *ASME Journal of Mechanisms and Robotics* 2.3 (2011), p. 8.

[84] Batbold, B. et al. “Exact Workspace Synthesis for RCCR Linkages”. In: *Computational Kinematics*. Ed. by F. Thomas and A. Perez-Gracia. Springer, Netherlands, 2013, pp. 349–357.

[85] Stolle, G. and Corves, B. “Maßsynthese mehrgliedriger ebener Drehgelenkgetriebe durch Kreispunktsuche und Homotopieverfahren”. In: *VDI Bewegungstechnik Berichte Nr. 1707*. VDI-Verlag, Düsseldorf, 2002, pp. 101–121.

[86] Breitfeld, C. *GENESYS - Architektur und Kernrealisierung eines Softwaresystems zur Entwicklung ungleichmäßig übersetzender Getriebe, Nr. 257*. Düsseldorf: Fortschritt-Berichte VDI, 1995.

[87] Hüsing, M., Braune, R., and Corves, B. “Dimensional Synthesis with Mechanism Processing Strategy”. In: *New Trends in Mechanism and Machine Science*. Ed. by P. Flores and F. Viadero. Springer, 2014, pp. 139–146.

[88] Brix, T., Döring, U., and Reeßing, M. “DMG-Lib - A New Knowledge Base in Mechanism Theory to Support the Design Process”. In: *19th International Congress of Mechanical Engineering, COBEM 2007*. ABCM, 2007, p. 10.

[89] Ruth, D. A. and McCarthy, J. M. “SphinxPC: An implementation of four position synthesis for planar and spherical 4R linkages”. In: *CD-ROM Proceedings of the ASME DETC’97*. ASME, 1997.

[90] Larochelle, P. “SPADES: Software for Synthesizing Spatial 4C Mechanisms”. In: *1998 ASME Design Engineering Technical Conferences DETC98*. ASME, 1998, p. 10.

[91] Perez, A., Su, H.-J., and McCarthy, J. M. “SYNTHETICA 2.0: Software for the Synthesis of Constrained Serial Chains”. In: *2004 ASME Design Engineering Technical Conferences DETC04*. ASME, 2004, pp. 1363–1369.

[92] Leger, C. *DARWIN2K An Evolutionary Approach to Automated Design for Robotics*. New York: Springer Science+Business Media, LLC, 2000.

[93] Prause, I. et al. “Vergleich von dynamisch-interaktiver Geometriesoftware für die Maßsynthese von ebenen Getrieben”. In: *10. Getriebekolloquium*. Ed. by L. Zentner. ISBN 987-3-86360-065-5, 2013, pp. 39–56.

[94] Su, H.-J., McCarthy, J. M., and Watson, L. T. “Generalized Linear Product Homotopy Algorithms and the Computation of Reachable Surfaces”. In: *ASME Journal of Computers and Information Science and Engineering* 4.3 (2004), pp. 226–234.

[95] Sommese, A. J. and Wampler, C. W. *The Numerical Solution of Systems of Polynomials Arising in Engineering and Science*. Singapore: World Scientific, 2005.

[96] Guan, Y. and Verschelde, J. “PHClab: A MATLAB/Octave interface to PHCpack”. In: *IMA Volume 148: Software for Algebraic Geometry*. Ed. by M. E. Stillman, N. Takayama, and J. Verschelde. Springer, 2008, pp. 15–32.

[97] Nefzi, M., Riedel, M., and Corves, B. “Towards an Automated and Optimal Design of Parallel Manipulators, ISBN 978-3-902613-41-7”. In: *InTech* (2008), p. 15.

[98] Scherer, T. et al. “Einsatzmöglichkeiten der 3D-CAD-Systeme CATIA V5 und Pro-Engineer Wildfire in der Getriebetechnik”. In: *9. Getriebekolloquium*. Ed. by M. Berger. Universitätsverlag Chemnitz, 2011, pp. 171–188.

[99] Berger, M. et al. “Syntheseverfahren zur Auslegung von Übertragungsgetrieben mit Hilfe parametrischer CAD-Systeme”. In: *VDI Bewegungstechnik*. VDI Verlag, 2012, pp. 243–259.

[100] Berger, M. and Matthes, J. “Implementierung und Anwendung klassischer Syntheseverfahren zur Entwicklung neuer Antriebssysteme im Umfeld von CAD und MKS”. In: *VDI Bewegungstechnik*. VDI Verlag, 2010, pp. 149–160.

[101] Klein, J. *A CAD Add-in for Synthesis of RSSR Function Generators*. Project report. Robotics and Automation Laboratory, University of California Irvine, 2005.

[102] Abdul-Sater, K., Irlinger, F., and Lueth, T. C. "CAD-integrierte kinematische Auslegung ebener Gelenkgetriebe". In: *VDI Bewegungstechnik*. VDI Verlag, 2012, pp. 225–241.

[103] Abdul-Sater, K. "Analysis and Design of Spatial Folding Linkages and Membrane Folding Patterns Based on Origami (Semester work - unpublished)". In: *Institute of Lightweight Structures, Technische Universität München* (2010), p. 129.

[104] Abdul-Sater, K., Irlinger, F., and Lueth, T. C. "Two-Configuration Synthesis of Origami-Guided Planar, Spherical and Spatial Revolute-Revolute Chains". In: *ASME Journal of Mechanisms and Robotics* 5.3 (2013), p. 10.

[105] Abdul-Sater, K., Irlinger, F., and Lueth, T. C. "Four-Position Synthesis of Origami-Evolved, Spherically Constrained Planar RR Chains". In: *Interdisciplinary Applications of Kinematics*. Ed. by A. Kecskeméthy and F. Geu Flores. Springer International Publishing, Switzerland, 2014, pp. 63–71.

[106] Bowen, L. A. et al. "A Classification of Action Origami as Systems of Spherical Mechanisms". In: *ASME Journal of Mechanical Design* 135.11 (2013), p. 7.

[107] Wei, G. and Dai, J. S. "Geometry and Kinematic Analysis of an Origami-Evolved Mechanism Based on Artmimetics". In: *ASME/IFToMM Int. Conference on Reconfigurable Mechanisms and Robots*. Ed. by J.S. Dai, M. Zoppi, and X. Kong. IEEE, 2009, pp. 450–455.

[108] Alizade, R. I. et al. "Function Synthesis of Bennett 6R Mechanisms Using Chebyshev Approximation". In: *Mechanism and Machine Theory* 81 (2014), pp. 62–78.

[109] Chiang, C. H. *Kinematics of Spherical Mechanisms*. Cambridge, UK: Cambridge University Press, 1988.

[110] Kiper, G. and Bagdadioglu, B. "Function Generation Synthesis with a 2-DoF Overconstrained Double-Spherical 7R Mechanism Using the Method of Decomposition and Least Squares Approximation". In: *New Trends in Mechanism and Machine Science*. Ed. by P. Flores and F. Viadero. Springer, 2014, pp. 175–183.

[111] Abdul-Sater, K., Lueth, T. C., and Irlinger, F. "Kinematic Design of Miura-Ori-Based Folding Structures Using the Screw Axis of a Relative Displacement". In: *Advances in Robot Kinematics*. Ed. by J. Lenarčič and O. Khatib. Springer International Publishing, Switzerland, 2014, pp. 233–241.

[112] Abdul-Sater, K. et al. "Three-Position Synthesis of Origami-Evolved, Spherically Constrained Spatial RR Chains (Accepted Manuscript)". In: *ASME Journal of Mechanisms and Robotics* (2015), p. 14.

[113] Siciliano, B. and Khatib, O. *Handbook of Robotics, Chapter 10 Performance Evaluation and Design Criteria*. New York: Springer, 2008.

[114] Kahn, W. A. and Angeles, J. "The Kinetostatic Optimization of Robotic Manipulators: The Inverse and Direct Problems". In: *ASME Journal of Mechanical Design* 128.1 (2005), pp. 168–178.

[115] Hunt, K. H. *Kinematic Geometry of Mechanisms*. Oxford, UK: Claredon, Oxford University Press, 1978.

[116] Perez, A. and McCarthy, J. M. “Bennett’s Linkage and the Cylindroid”. In: *Mechanism and Machine Theory* 37.11 (2002), pp. 1245–1260.

[117] O’Rourke, J. *Computational Geometry in C, 2nd edition*. Cambridge, UK: Cambridge University Press, 1998.

[118] Grimm, T. *A User’s Guide to Rapid Protyping*. USA: Society of Manufacturing Engineers, 2004.

[119] Fischer, M. et al. “Reduktion des Tür-Diskomforts beim Ein- und Ausstieg in engen Parksituationen”. In: *Automobiltechnische Zeitschrift* 9.109 (2007), pp. 820–829.

[120] Richter, C. et al. “A Spatial Path Specification System for Mechanism Development”. In: *IEEE International Conference on Human System Interaction (HSI) 2009*. Ed. by H. Krawczyk and T. Pomianek. IEEE, 2009, pp. 236 –241.